



TARGET CLASSIFICATION OF CANONICAL
SCATTERERS USING CLASSICAL ESTIMATION AND
DICTIONARY BASED TECHNIQUES

THESIS

G. Barry Hammond II, Captain, USAF

AFIT/GE/ENG/12-19

DEPARTMENT OF THE AIR FORCE
AIR UNIVERSITY

AIR FORCE INSTITUTE OF TECHNOLOGY

Wright-Patterson Air Force Base, Ohio

APPROVED FOR PUBLIC RELEASE; DISTRIBUTION UNLIMITED

The views expressed in this thesis are those of the author and do not reflect the official policy or position of the United States Air Force, Department of Defense, or the United States Government. This material is declared a work of the U.S. Government and is not subject to copyright protection in the United States.

TARGET CLASSIFICATION OF CANONICAL SCATTERERS USING
CLASSICAL ESTIMATION AND DICTIONARY BASED TECHNIQUES

THESIS

Presented to the Faculty
Department of Electrical Engineering
Graduate School of Engineering and Management
Air Force Institute of Technology
Air University
Air Education and Training Command
In Partial Fulfillment of the Requirements for the
Degree of Master of Science in Electrical Engineering

G. Barry Hammond II, B.S. Electrical and Computer Engineering
Captain, USAF

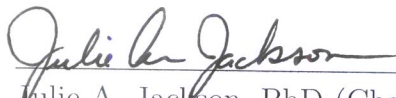
March 2012

AFIT/GE/ENG/12-19

TARGET CLASSIFICATION OF CANONICAL SCATTERERS USING CLASSICAL
ESTIMATION AND DICTIONARY BASED TECHNIQUES

G. Barry Hammond II, B.S. Electrical and Computer Engineering
Captain, USAF

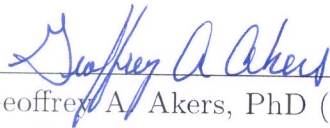
Approved:



Julie A. Jackson, PhD (Chairman)

29 Feb 2012

Date



Geoffrey A. Akers, PhD (Member)

29 Feb 2012

Date



Richard K. Martin, PhD (Member)

29 Feb 2012

Date

Abstract

This research effort will utilize a hierarchical dictionary-based approach for canonical shape classification within measured synthetic aperture radar (SAR) phase history data. This primary goal of this research is to develop an efficient framework for dictionary based SAR feature extraction using modified 3-D radar scattering models derived by Jackson. Previous work in this area relies on maximum likelihood (ML) estimation and similar approaches to extract shapes using 2-D signal models presented in previous literature. In support of the primary goal, we include characterizations of shape model redundancies caused by similar shape scattering responses. A Gram-Matrix is used to identify these highly correlated dictionary columns (atoms) which are “confuser” shape configurations that lead to poor feature identifiability. Simulated SAR collection methods, including frequency, elevation aspect, and polarization diversities, are modeled to show reductions in inter-atom correlation. A “molecule” clustering method is used to combine highly correlated atoms to support a basis pursuit (BP) method of feature identification. Finally, a Bayesian approach is used to determine a maximum *a posteriori* (MAP) estimate for each atom, leading to feature classification and parameter identification. This approach lies the foundation for future research on estimation of a posterior PDF for determining confidence within classification results.

Acknowledgements

I would like to first and foremost thank my wonderful wife! You been there every step of the way supporting me through all of the stressful times and motivating me to do my best. Thank you for being my best friend throughout all of the adventures we've experienced in our time here. Secondly, I would like to thank my advisor, Dr. Julie Jackson. Your expertise, knowledge, and guidance significantly helped in the completion of this thesis. Also, I would like to thank my close friends that I've gained throughout this program. You have helped out tremendously in both academic and personal life. Finally, I would like to thank my parents for always caring and teaching me from the start that success is always an option that one must work for.

G. Barry Hammond II

Table of Contents

	Page
Abstract	iv
Acknowledgements	v
List of Figures	ix
List of Tables	xiii
I. Introduction	1
1.1 Problem Description	1
1.2 Research Goals and Methodology	3
1.3 Thesis Organization	4
II. Background	5
2.1 Chapter Overview	5
2.2 Estimation Theory	5
2.2.1 Classical Estimation	5
2.2.2 Bayesian Estimation	6
2.2.3 Posterior Probability Estimation	8
2.3 Hypothesis Testing and Detection Theory	8
2.4 3-D SAR Scattering Models	11
2.4.1 Rectangular Plate	14
2.4.2 Dihedral	14
2.4.3 Trihedral	15
2.4.4 Cylinder	15
2.4.5 Tophat	15
2.4.6 Sphere	16
2.4.7 Differential Range	16
III. Model Development and Methodology	18
3.1 Chapter Overview	18
3.2 Dictionary Setup	18
3.3 Dictionary Based Classification	20
3.3.1 Feature Extraction	20
3.3.2 Dictionary Analysis and Reduction	21
3.4 Dictionary Reduction	22
3.4.1 Correlation Reduction Through Diversity	23
3.4.2 Coherence Reduction Via Molecules	25

	Page
3.5 Dictionary Reduction Results	25
3.5.1 Coherence Reduction Via Diversity	25
3.5.2 Coherence Reduction Via Molecules	29
3.5.3 Coherence Reduction Summary	30
3.6 Feature Classification Using Reduced Dictionary	32
3.6.1 Molecule Selection via Basis Pursuit	33
3.6.2 Atom Selection via Probability	34
3.6.3 Multiple Shapes	36
IV. Results	38
4.1 Chapter Overview	38
4.2 Scenario 1 Results	38
4.2.1 Dihedral Target	39
4.2.2 Cylinder Target	41
4.3 Scenario 2 Results	50
4.3.1 X Parameter	51
4.3.2 Y Parameter	55
4.3.3 Z Parameter	58
4.3.4 RCS Parameters	61
4.4 Scenario 3 Results	66
4.5 Comprehensive Results	72
4.5.1 SNR versus RCS	72
4.5.2 Feature Extraction Scenario Summary	75
V. Conclusions and Future Work	82
5.1 Chapter Overview	82
5.2 Review of Objectives and Methodology	82
5.3 Conclusions	83
5.4 Future Development and Research	83
Appendix A. Dictionary Coherence Reduction	85
A.1 Plate Dictionary	85
A.2 Sphere Dictionary	88
A.3 Top-Hat Dictionary	91
A.4 Trihedral Dictionary	94
A.5 Cylinder Dictionary	97
Appendix B. Scenario 1 Results	102
B.1 Plate Target	102
B.2 Sphere Target	104
B.3 Top-hat Target	107
B.4 Trihedral Target	110

	Page
Appendix C. Scenario 2 Results	115
C.1 Dihedral Results	115
C.1.1 X Parameter	115
C.1.2 Y Parameter	116
C.1.3 Z Parameter	117
C.1.4 RCS Parameters	118
C.2 Sphere Results	120
C.2.1 X Parameter	120
C.2.2 Y Parameter	133
C.2.3 Z Parameter	136
C.2.4 RCS Parameters	139
C.3 Top-Hat Results	141
C.3.1 X Parameter	141
C.3.2 Y Parameter	144
C.3.3 Z Parameter	147
C.3.4 RCS Parameters	151
C.4 Trihedral Results	156
C.4.1 X Parameter	156
C.4.2 Y Parameter	159
C.4.3 Z Parameter	165
C.4.4 RCS Parameters	170
C.5 Cylinder Results	172
C.5.1 X Parameter	172
C.5.2 Y Parameter	174
C.5.3 Z Parameter	177
C.5.4 RCS Parameters	182
Appendix D. Scenario 3 Results	188
D.1 Dihedral, Trihedral, and Top-hat Target Scene	188
D.2 Sphere, Top-hat, and Cylinder Target Scene	193
Bibliography	200

List of Figures

Figure		Page
2.1	Canonical scattering primitives for target shapes re-used with permission from [1].	12
3.1	Correlation map corresponding to $\mathbf{D}_{\Gamma_{\text{dihedral}}}$ generated using a linear flight path, HH polarization, and 1 frequency.	23
3.2	Non-linear flight path elevation	24
3.3	Reduction in correlation due to increased aspect and frequency diversity for $\mathbf{D}_{\Gamma_{\text{dihedral}}}$	27
3.4	Coherence reduction using molecule method (dihedral)	29
3.5	Coherence reduction using modified molecule method (cylinder)	31
3.6	Overview of main algorithm.	33
4.1	BP results for scenario 1, dihedral example	40
4.2	Posterior log-likelihood, scenario 1, dihedral example	42
4.3	BP results for scenario 1, cylinder example	44
4.4	BP results for scenario 1, cylinder example (zoomed)	46
4.5	Posterior log-likelihood, scenario 1, cylinder example	47
4.6	BP results for scenario 1, modified cylinder example	48
4.7	BP results for scenario 1, modified cylinder example (zoomed)	50
4.8	Posterior log-likelihood, scenario 1, modified cylinder example	51
4.9	BP results for scenario 2, plate example 1	52
4.10	Range profile for the true, extracted, and close simulated plate targets.	54
4.11	BP results for scenario 2, plate example 2	56
4.12	Posterior log-likelihood plot, scenario 2, plate example 2	58
4.13	BP results for scenario 2, plate example 3	60
4.14	BP results for scenario 2, plate example 4	63
4.15	BP results for scenario 2, plate example 5	64
4.16	BP results for scenario 3, example 1 (iteration 1)	68
4.17	BP results for scenario 3, example 1 (iteration 2)	69

Figure		Page
4.18	BP results for scenario 3, example 1 (iteration 3)	70
4.19	Posterior log-likelihood plot, scenario 3, plate example 1	73
4.20	SNR versus RCS	74
A.1	Correlation map corresponding to $\mathbf{D}_{\Gamma_{\text{plate}}}$ generated using a linear flight path, HH polarization, and 1 frequency.	86
A.2	Reduction in correlation due to increased aspect and frequency diversity for $\mathbf{D}_{\Gamma_{\text{plate}}}$	87
A.3	Coherence reduction using molecule method (plate)	88
A.4	Correlation map corresponding to $\mathbf{D}_{\Gamma_{\text{sphere}}}$ generated using a linear flight path, HH polarization, and 1 frequency.	89
A.5	Reduction in correlation due to increased aspect and frequency diversity for $\mathbf{D}_{\Gamma_{\text{sphere}}}$	90
A.6	Coherence reduction using molecule method (sphere)	91
A.7	Correlation map corresponding to $\mathbf{D}_{\Gamma_{\text{top-hat}}}$ generated using a linear flight path, HH polarization, and 1 frequency.	92
A.8	Reduction in correlation due to increased aspect and frequency diversity for $\mathbf{D}_{\Gamma_{\text{top-hat}}}$	93
A.9	Coherence reduction using molecule method (top-hat)	94
A.10	Correlation map corresponding to $\mathbf{D}_{\Gamma_{\text{triangular}}}$ generated using a linear flight path, HH polarization, and 1 frequency.	95
A.11	Reduction in correlation due to increased aspect and frequency diversity for $\mathbf{D}_{\Gamma_{\text{triangular}}}$	96
A.12	Coherence reduction using molecule method (triangular)	97
A.13	Correlation map corresponding to $\mathbf{D}_{\Gamma_{\text{cylinder}}}$ generated using a linear flight path, HH polarization, and 1 frequency.	98
A.14	Reduction in correlation due to increased aspect and frequency diversity for $\mathbf{D}_{\Gamma_{\text{cylinder}}}$	99
A.15	Coherence reduction using molecule method (cylinder)	100
A.16	Coherence reduction using modified molecule method (cylinder)	101
B.1	BP results for scenario 1, plate example	103

Figure		Page
B.2	Posterior log-likelihood plot, scenario 1, plate example	105
B.3	BP results for scenario 1, sphere example	106
B.4	BP results for scenario 1, top-hat example	109
B.5	Posterior log-likelihood plot, scenario 1, top-hat example	111
B.6	BP results for scenario 1, trihedral example	112
B.7	Posterior log-likelihood plot, scenario 1, trihedral example	114
C.1	BP results for scenario 2, dihedral example 1	122
C.2	Range profile for the true, extracted, and close simulated dihedral targets.	123
C.3	BP results for scenario 2, dihedral example 2	124
C.4	BP results for scenario 2, dihedral example 3 (iteration 1)	125
C.5	BP results for scenario 2, dihedral example 3 (iteration 2)	126
C.6	BP results for scenario 2, dihedral example 4	127
C.7	BP results for scenario 2, dihedral example 5 (iteration 1)	128
C.8	BP results for scenario 2, dihedral example 5 (iteration 2)	129
C.9	BP results for scenario 2, sphere example 1 (iteration 1)	130
C.10	BP results for scenario 2, sphere example 1 (iteration 2)	131
C.11	BP results for scenario 2, sphere example 2	134
C.12	BP results for scenario 2, sphere example 3	137
C.13	BP results for scenario 2, sphere example 4	140
C.14	BP results for scenario 2, top-hat example 1	142
C.15	BP results for scenario 2, top-hat example 2	145
C.16	BP results for scenario 2, top-hat example 3 (iteration 1)	148
C.17	BP results for scenario 2, top-hat example 3 (iteration 2)	149
C.18	BP results for scenario 2, top-hat example 4	152
C.19	BP results for scenario 2, top-hat example 5 (iteration 1)	153
C.20	BP results for scenario 2, top-hat example 5 (iteration 2)	154
C.21	BP results for scenario 2, trihedral example 1 (iteration 1)	157

Figure		Page
C.22	BP results for scenario 2, trihedral example 1 (iteration 2)	158
C.23	BP results for scenario 2, trihedral example 2 (iteration 1)	161
C.24	BP results for scenario 2, trihedral example 2 (iteration 2)	162
C.25	BP results for scenario 2, trihedral example 2 (iteration 3)	163
C.26	BP results for scenario 2, trihedral example 3 (iteration 1)	166
C.27	BP results for scenario 2, trihedral example 3 (iteration 2)	167
C.28	BP results for scenario 2, trihedral example 3 (iteration 3)	168
C.29	BP results for scenario 2, trihedral example 4	171
C.30	BP results for scenario 2, cylinder example 1	173
C.31	BP results for scenario 2, cylinder example 2	176
C.32	BP results for scenario 2, cylinder example 3 (iteration 1)	179
C.33	BP results for scenario 2, cylinder example 3 (iteration 2)	180
C.34	BP results for scenario 2, cylinder example 4	183
C.35	BP results for scenario 2, cylinder example 5 (iteration 1)	184
C.36	BP results for scenario 2, cylinder example 5 (iteration 2)	185
D.1	BP results for scenario 3, example 2 (iteration 1)	189
D.2	BP results for scenario 3, example 2 (iteration 2)	190
D.3	BP results for scenario 3, example 2 (iteration 3)	191
D.4	Posterior log-likelihood plot for scenario 3, plate example 2	193
D.5	BP results for scenario 3, example 3 (iteration 1)	195
D.6	BP results for scenario 3, example 3 (iteration 2)	196
D.7	BP results for scenario 3, example 3 (iteration 3)	197
D.8	Posterior log-likelihood plot for scenario 3, plate example 3	199

List of Tables

Table		Page
2.1	Shape parameters	17
3.1	Coherence reduction results due to increased radar collection diversity.	28
3.2	Coherence reduction results for molecule cluster method.	30
4.1	Dihedral parameters for scenario 1	39
4.2	Atom correspondence for scenario 1, dihedral example	39
4.3	Coefficients and ℓ^1 norms for scenario 1, dihedral example	41
4.4	Estimated versus true parameters for scenario 1, dihedral example.	42
4.5	Cylinder parameters for scenario 1	43
4.6	Atom correspondence for scenario 1, cylinder example	43
4.7	Coefficients and ℓ_1 norms for scenario 1, cylinder example 1	45
4.8	Estimated versus true parameters for scenario 1 using original reduced cylinder dictionary.	45
4.9	Coefficients and ℓ_1 norms for scenario 1, cylinder example 2	49
4.10	Estimated versus true parameters for scenario 1 using modified reduced cylinder dictionary.	49
4.11	Plate parameters for scenario 2, example 1	51
4.12	Coefficients and ℓ_1 norms for scenario 2, plate example 1	53
4.13	Estimated versus true parameters for scenario 2, plate example 1.	53
4.14	LS errors for scenario 2, plate example 1	53
4.15	Plate parameters for scenario 2, example 2	55
4.16	Coefficients and ℓ_1 norms for scenario 2, plate example 2	57
4.17	Estimated versus true parameters for scenario 2, plate example 2.	57
4.18	LS errors for scenario 2, plate example 2	58
4.19	Plate parameters for scenario 2, example 3	59
4.20	Coefficients and ℓ_1 norms for scenario 2, plate example 3	61
4.21	Estimated versus true parameters for scenario 2, plate example 3.	61

Table		Page
4.22	LS errors for scenario 2, plate example 3	62
4.23	Plate parameters for scenario 2, examples 4 and 5	62
4.24	Coefficients and ℓ_1 norms for scenario 2, plate example 4	65
4.25	Coefficients and ℓ_1 norms for scenario 2, plate example 5	65
4.26	Estimated versus true parameters for scenario 2, plate example 4. .	65
4.27	Estimated versus true parameters for scenario 2, plate example 5. .	66
4.28	The parameters used to create scene 3, example 1.	66
4.29	Atom correspondence for scenario 3, example 1	66
4.30	Coefficients and ℓ^1 norms for scenario 3, example 1	71
4.31	Extracted parameter sets for each shape compared to truth for scenario 3, example 1.	72
4.32	Coefficients and ℓ_1 norms for scenario 2, plate example 3	76
4.33	Coefficients and ℓ_1 norms for scenario 2, plate example 3, post thresholding	76
4.34	Estimated versus true parameters for scenario 2, plate example 2. .	77
4.35	LS errors for scenario 2, plate example 2	77
4.36	Comprehensive results for scenario 2, off-dictionary X examples . .	78
4.37	Comprehensive results for scenario 2, off-dictionary Y examples . .	79
4.38	Comprehensive results for scenario 2, off-dictionary Z examples . .	79
4.39	Comprehensive results for scenario 2, off-dictionary RCS examples	80
B.1	Plate parameters for scenario 1	102
B.2	Atom correspondence for scenario 1, plate example	102
B.3	Coefficients and ℓ_1 norms for scenario 1, plate example	104
B.4	Estimated versus true parameters for scenario 1, plate example. . .	104
B.5	Sphere parameters for scenario 1	105
B.6	Coefficients and ℓ_1 norms for scenario 1, sphere example	107
B.7	Estimated versus true parameters for scenario 1, sphere example. .	107
B.8	Top-hat parameters for scenario 1	107

Table		Page
B.9	Atom correspondence for scenario 1, top-hat example	108
B.10	Coefficients and ℓ_1 norms for scenario 1, top-hat example	110
B.11	Estimated versus true parameters for scenario 1, top-hat example.	110
B.12	Trihedral parameters for scenario 1	111
B.13	Atom correspondence for scenario 1, trihedral example	111
B.14	Coefficients and ℓ_1 norms for scenario 1, trihedral example	113
B.15	Estimated versus true parameters for scenario 1, trihedral example.	113
C.1	Dihedral parameters for scenario 2, example 1	115
C.2	Coefficients and ℓ^1 norms for scenario 2, dihedral example 1	115
C.3	Estimated versus true parameters for scenario 2, dihedral example 1.	115
C.4	LS errors for scenario 2, dihedral example 1	116
C.5	Dihedral parameters for scenario 2, example 2	116
C.6	Coefficients and ℓ_1 norms for scenario 2, dihedral example 2	117
C.7	Estimated versus true parameters for scenario 2, dihedral example 2.	117
C.8	LS errors for scenario 2, dihedral example 2	117
C.9	Dihedral parameters for scenario 2, example 3	118
C.10	Coefficients and ℓ_1 norms for scenario 2, dihedral example 3	118
C.11	Estimated versus true parameters for scenario 2, dihedral example 3.	118
C.12	LS errors for scenario 2, dihedral example 3	119
C.13	Dihedral parameters for scenario 2, examples 4 and 5	119
C.14	Coefficients and ℓ_1 norms for scenario 2, dihedral example 4	119
C.15	Coefficients and ℓ_1 norms for scenario 2, dihedral example 5	120
C.16	Estimated versus true parameters for scenario 2, dihedral example 4.	120
C.17	Estimated versus true parameters for scenario 2, dihedral example 5.	120
C.18	Sphere parameters for scenario 2, example 1	121
C.19	Coefficients and ℓ_1 norms for scenario 2, sphere example 1	132
C.20	Estimated versus true parameters for scenario 2, sphere example 1.	132
C.21	LS errors for scenario 2, sphere example 1	132

Table		Page
C.22	Sphere parameters for scenario 2, example 2	133
C.23	Coefficients and ℓ_1 norms for scenario 2, sphere example 2	135
C.24	Estimated versus true parameters for scenario 2, sphere example 2.	135
C.25	LS errors for scenario 2, sphere example 2	135
C.26	Sphere parameters for scenario 2, example 3	136
C.27	Coefficients and ℓ_1 norms for scenario 2, sphere example 3	138
C.28	Estimated versus true parameters for scenario 2, sphere example 3.	138
C.29	LS errors for scenario 2, sphere example 3	138
C.30	Sphere parameters for scenario 2, example 4	139
C.31	Coefficients and ℓ_1 norms for scenario 2, sphere example 4	141
C.32	Estimated versus true parameters for scenario 2, sphere example 4.	141
C.33	Top-hat parameters for scenario 2, example 1	141
C.34	Coefficients and ℓ_1 norms for scenario 2, top-hat example 1	143
C.35	Estimated versus true parameters for scenario 2, top-hat example 1.	143
C.36	LS errors for scenario 2, top-hat example 1	143
C.37	Top-hat parameters for scenario 2, example 2	144
C.38	Coefficients and ℓ_1 norms for scenario 2, top-hat example 2	146
C.39	Estimated versus true parameters for scenario 2, top-hat example 2.	146
C.40	LS errors for scenario 2, top-hat example 2	146
C.41	Top-hat parameters for scenario 2, example 3	147
C.42	Coefficients and ℓ_1 norms for scenario 2, top-hat example 3	150
C.43	Estimated versus true parameters for scenario 2, top-hat example 3.	150
C.44	LS errors for scenario 2, top-hat example 3	151
C.45	Top-hat parameters for scenario 2, examples 4 and 5	151
C.46	Coefficients and ℓ_1 norms for scenario 2, top-hat example 4	155
C.47	Coefficients and ℓ_1 norms for scenario 2, top-hat example 5	155
C.48	Estimated versus true parameters for scenario 2, top-hat example 4.	156
C.49	Estimated versus true parameters for scenario 2, top-hat example 5.	156

Table		Page
C.50	Trihedral parameters for scenario 2, example 1	156
C.51	Coefficients and ℓ_1 norms for scenario 2, trihedral example 1	159
C.52	Estimated versus true parameters for scenario 2, trihedral example 1.	159
C.53	LS errors for scenario 2, trihedral example 1	160
C.54	Trihedral parameters for scenario 2, example 2	160
C.55	Coefficients and ℓ_1 norms for scenario 2, trihedral example 2	164
C.56	Estimated versus true parameters for scenario 2, trihedral example 2.	164
C.57	LS errors for scenario 2, trihedral example 2	165
C.58	Trihedral parameters for scenario 2, example 3	165
C.59	Coefficients and ℓ_1 norms for scenario 2, trihedral example 3	169
C.60	Estimated versus true parameters for scenario 2, trihedral example 3.	169
C.61	LS errors for scenario 2, trihedral example 3	170
C.62	Trihedral parameters for scenario 2, example 4	170
C.63	Coefficients and ℓ_1 norms for scenario 2, trihedral example 4	172
C.64	Estimated versus true parameters for scenario 2, trihedral example 4.	172
C.65	Cylinder parameters for scenario 2, example 1	172
C.66	Coefficients and ℓ_1 norms for scenario 2, cylinder example 1	174
C.67	Estimated versus true parameters for scenario 2, cylinder example 1.	174
C.68	LS errors for scenario 2, cylinder example 1	174
C.69	Cylinder parameters for scenario 2, example 2	175
C.70	Coefficients and ℓ_1 norms for scenario 2, cylinder example 2	177
C.71	Estimated versus true parameters for scenario 2, cylinder example 2.	177
C.72	LS errors for scenario 2, cylinder example 2	177
C.73	Cylinder parameters for scenario 2, example 3	178
C.74	Coefficients and ℓ_1 norms for scenario 2, cylinder example 3	181
C.75	Estimated versus true parameters for scenario 2, cylinder example 3.	181
C.76	LS errors for scenario 2, cylinder example 3	181
C.77	Cylinder parameters for scenario 2, examples 4 and 5	182

Table		Page
C.78	Coefficients and ℓ_1 norms for scenario 2, cylinder example 4	186
C.79	Coefficients and ℓ_1 norms for scenario 2, cylinder example 5	186
C.80	Estimated versus true parameters for scenario 2, cylinder example 4.	187
C.81	Estimated versus true parameters for scenario 2, cylinder example 5.	187
D.1	The parameters used to create scene 3, example 2.	188
D.2	Atom correspondence for scenario 3, example 2	188
D.3	Coefficients and ℓ_1 norms for scenario 3, example 2	192
D.4	Extracted parameter sets for each shape compared to truth for scenario 3, example 2.	193
D.5	The parameters used to create scene 3, example 3.	194
D.6	Atom correspondence for scenario 3, example 3	194
D.7	Coefficients and ℓ_1 norms for scenario 3, example 3	198
D.8	Extracted parameter sets for each shape compared to truth for scenario 3, example 3.	199

TARGET CLASSIFICATION OF CANONICAL SCATTERERS USING CLASSICAL ESTIMATION AND DICTIONARY BASED TECHNIQUES

I. Introduction

1.1 *Problem Description*

Synthetic aperture radar (SAR) remote sensing provides an all-weather capable means to collect data sets used to generate high-resolution imagery. The data is comprised of electromagnetic scattering returns from scatterers in a scene and includes both amplitude and phase history. These data sets include target information that, if extracted, can provide important information for use in automatic target recognition (ATR) models. Specifically, detection and estimation of features that describe canonical shape scatterers can be fit to models that describe real-world scenes of interest. These geometric features have been used to create 2-D and 3-D simulations for computer-aided target identification.

The phase history data used in SAR signal processing has been used in previous research efforts [1] and [2], for extraction, recognition and classification of canonical shapes within a target scene of interest. The algorithms proposed in these efforts rely on classical least squares estimation and non-convex optimization algorithms to estimate parameters within a signal model. This method proves computationally cumbersome and relies on accurate initial shape parameter estimates due to the inherent multi-modal cost surface. The accuracy of these parameters relies on prior knowledge of the target scene of interest which is usually not available. Incorrect initialization may lead to incorrect classification.

In [1], Jackson derives 3-D scattering models for six canonical shapes improving on the previously utilized 2-D models introduced in [2]. The shapes include a plate, dihedral, sphere, top-hat, cylinder, and trihedral. The proposed approach in this thesis relies on a hierarchical, sparsity-based, dictionary methodology, similar to efforts

described in [3–7] to extract each of these shapes and associated physical parameters from a target scene. This method utilizes a set of shape dictionaries which contain simulated phase histories for various combinations of physical shape and radar collection parameters. Dictionaries are created for each of the six shape hypotheses using the 3-D shape models from [1]. A hierarchical approach is used to narrow down atoms to find each shape and associated parameter set.

The dictionary data are first analyzed to describe possible “confuser” configurations. These confuser parameter combinations are highly correlated and lead to an over-complete and redundant dictionary. These redundancies lead to misclassifications when using matching pursuit algorithms such as basis pursuit (BP). A Gram-Matrix is computed for each of the dictionaries and used to identify redundancies based on correlations between dictionary columns (atoms). Intensity maps, or “confuser maps,” are visual representations of these matrices. The confuser shape configurations lead to poor feature identifiability.

To reduce atom redundancies we characterize the effects of radar collection diversity and introduce a clustering method for combining correlated atoms. Simulated SAR collection methods, including frequency, elevation aspect, and polarization diversities, are modeled to show reductions in inter-atom correlation. Also, a method similar to the molecule method described in [7] is used to cluster atoms to reduce overall dictionary coherence. The reduced dictionaries support the use of a BP method of feature identification. The BP principle has been used in many research efforts and in the linear programming (LP) world to find optimized solutions in quadratic, non-convex optimization problems. The BP method is described in detail in [8], [9], and many others. This clustering method alone reduces the possible number of solution atoms from several thousand to less than a hundred, in most cases. We then utilize posterior log-likelihoods and a maximum *a posteriori* estimation framework to select the final solution.

1.2 Research Goals and Methodology

The primary goal of this research effort is to develop a hierarchical, dictionary-based, canonical shape classification and parameter estimation algorithm framework utilizing the 3-D radar scattering models presented in [1]. This framework will provide a baseline for future work aimed at improving extraction efficiency and accuracy over previous least squares estimation schemes used in [10]. This research will be the first to use the 3-D scattering models from [1] in a dictionary based feature extraction scheme. A characterization and identification of confuser configurations amongst shape hypotheses and parameter combinations is provided as a supporting objective. Collection methods are also addressed to promote reduction in inter-atom correlations within the dictionaries. A sparsity-based, basis pursuit de-noising (BPDN) algorithm is chosen to perform extraction due to inherent efficiency and error tolerance.

Multiple shape dictionaries containing sets of simulated SAR phase history data are generated for many combinations of shape parameters and radar collection methods, such as flight profile, polarization, and frequency diversity. Each column within a dictionary corresponds to a specific set of shape and radar parameters and is referred to throughout this discussion as an ‘atom’. Each atom is a simulated phase history data vector that is created using the 3-D signal models described in [1].

Each of the shape dictionaries is over-complete and contains many redundant atoms which, when normalized, are perfectly correlated. These correlations must be minimized for accurate feature extraction using sparse reconstruction methods, as shown in [6, 7]. Each dictionary is reduced by combining redundant atoms into molecules, or sub-dictionaries, and a BPDN algorithm is used to select the “best” molecule corresponding to a set of noisy measured data. The *spgl1* BPDN optimization algorithm described in [11] is used throughout this research for molecule identification. The molecule contains many highly correlated atoms. Bayes rule is used to derive and estimate the posterior log-likelihoods for each of these atoms. The

atom corresponding to the largest probability is selected and provided as the extracted shape and parameter set.

1.3 Thesis Organization

Chapter II provides background information applicable to this research. Classical maximum likelihood (ML) and Bayesian estimation and detection theory is presented from [12–14]. The algorithms and scattering model equations provided by [1] and [2] are then presented. Chapter III presents the development and methodology of the dictionary based feature extraction algorithm presented in this thesis. A brief background of dictionary based approaches and optimization schemes for wavelet matching is presented and a summary of literature regarding these algorithms is included. Computational memory requirements and methods for the creation of the dictionaries are introduced. Chapter IV presents the results of this research. Finally, Chapter V is a summary of the conclusions made throughout the research, and provides recommendation for future work.

II. Background

2.1 Chapter Overview

This chapter presents the background information used to facilitate the understanding of shape extraction and SAR data modeling. Several key foundational elements will be discussed. These include classical ML estimation, Bayesian maximum *a posteriori* (MAP) estimation and hypothesis testing theory. A discussion of dictionary approaches and correlation mapping will follow.

The first portion of this chapter will concentrate on building a theoretical foundation for classical and Bayesian estimation and hypothesis testing. Theory will be presented from [12–14]. Then, we present the 3-D radar scattering models derived by Jackson in [10].

2.2 Estimation Theory

2.2.1 Classical Estimation. In most situations, *a priori* knowledge of a target or scene of interest is not available. In these cases, classical estimation techniques such as ML estimation algorithms are used to find the most likely parameter estimates. The ML estimation principle is the most popular estimation approach [12].

The ML estimate is defined as the parameter set Θ that maximizes the likelihood function. Take, for example, a system modeled by

$$\mathbf{x} = \mathbf{s}(\Theta) + \mathbf{w} \quad (2.1)$$

where $\mathbf{s}(\Theta)$ represents the signal model data vector based on the parameter set Θ and \mathbf{w} is white Gaussian noise (WGN), $\mathbf{w} \sim \mathcal{CN}(0, \sigma^2 \mathbf{I})$.

The ML estimate is given by

$$\hat{\Theta}_{ML} = \arg \max_{\Theta} p(\mathbf{x}|\Theta) \quad (2.2)$$

where

$$\mathbf{x}|\Theta \sim \mathcal{N}(\mathbf{s}(\Theta), \mathbf{C}_{\mathbf{x}|\Theta}) \quad (2.3)$$

and $p(\mathbf{x}|\Theta)$ represents the multivariate Gaussian PDF [12]

$$p(\mathbf{x}|\Theta) = \frac{\exp(-\frac{1}{2}(\mathbf{x} - \mathbf{s}(\Theta))^T \mathbf{C}_{\mathbf{x}|\Theta} (\mathbf{x} - \mathbf{s}(\Theta)))}{(2\pi)^{\frac{N}{2}} \det^{\frac{1}{2}}(\mathbf{C}_{\mathbf{x}|\Theta})} \quad (2.4)$$

for an $N \times 1$ measured data set \mathbf{x} given a parameter set Θ . If the covariance $\mathbf{C}_{\mathbf{x}|\Theta} = \sigma^2 \mathbf{I}$ for variance σ^2 and $N \times N$ identity matrix \mathbf{I} , we can rewrite the PDF as

$$p(\mathbf{x}|\Theta) = \frac{\exp(-\frac{1}{2\sigma^2}(\mathbf{x} - \mathbf{s}(\Theta))^T (\mathbf{x} - \mathbf{s}(\Theta)))}{(2\pi)^{\frac{N}{2}} \sigma^2}. \quad (2.5)$$

For simplicity, we may write (2.5) as the log-likelihood function

$$\ln p(\mathbf{x}|\Theta) = -\frac{N}{2} \ln(2\pi) - \ln(\sigma^2) - \frac{1}{2\sigma^2}(\mathbf{x} - \mathbf{s}(\Theta))^T (\mathbf{x} - \mathbf{s}(\Theta)) \quad (2.6)$$

since the log operation does not change the location of the maximum. The ML estimate may then be written as

$$\hat{\Theta}_{ML} = \arg \min_{\Theta} (\mathbf{x} - \mathbf{s}(\Theta))^T (\mathbf{x} - \mathbf{s}(\Theta)) \quad (2.7)$$

or equivalently as the non-linear least squares (LS) problem

$$\hat{\Theta}_{LS} = \arg \min_{\Theta} \|\mathbf{x} - \mathbf{s}(\Theta)\|_2^2 \quad (2.8)$$

where $\|\cdot\|_2$ represents the ℓ_2 norm. The LS approach was used in [1] for feature extraction and parameter estimation.

2.2.2 Bayesian Estimation. A Bayesian MAP technique may be used to estimate a set of parameters Θ by maximizing the posterior probability over Θ when

the prior probability $p(\Theta)$ is assumed or known. This is shown by

$$\hat{\Theta}_{MAP} = \arg \max_{\Theta} p(\Theta | \mathbf{x}). \quad (2.9)$$

Once again, we assume the overall system model can be represented by (2.1). The parameters in $\Theta = [\Theta_1, \dots, \Theta_N]^T$ are each assigned a user-defined prior probability. These probabilities should be chosen based on any *a priori* knowledge of the target scene and user expertise.

Assuming independence between all parameters, the prior probability becomes

$$p(\Theta_{p \times 1}) = \prod_{i=1}^N p(\Theta_i). \quad (2.10)$$

Bayes rule can be used to compute the posterior probabilities based on the conditional probability given by $p(\mathbf{x} | \Theta)$ and the prior given by (2.10). Bayes rule states the following relationship:

$$p(\Theta | \mathbf{x}) = \frac{p(\mathbf{x} | \Theta)p(\Theta)}{p(\mathbf{x})}. \quad (2.11)$$

To find the MAP estimate of Θ , the numerator of (2.11) must be maximized. The denominator may be dropped as it does not depend on Θ and will not affect the position of the maximum. The numerator of (2.11) is simplified and expanded by first taking the natural logarithm as shown by

$$\ln p(\Theta | \mathbf{x}) \propto \ln p(\mathbf{x} | \Theta) + \sum_{i=1}^N \ln p(\Theta_i). \quad (2.12)$$

Finally, the MAP estimate $\hat{\Theta}_{MAP}$ is given by

$$\hat{\Theta}_{MAP} = \arg \min_{\Theta} \left(\|\mathbf{x} - \mathbf{s}(\Theta)\|_2^2 - \sum_{i=1}^N \ln p(\Theta_i) \right). \quad (2.13)$$

2.2.3 Posterior Probability Estimation. Although the MAP estimate $\hat{\Theta}_{\text{MAP}}$ may provide the “best” solution for Θ , we may want to associate a probability with this estimate. This posterior probability may be used as a metric to derive confidence for the estimate. The posterior, in many cases, may be difficult to compute due to intractable integration of the denominator $p(\mathbf{x})$.

Using Bayes Rule we identify the posterior probability as

$$p(\Theta|\mathbf{x}) = \frac{p(\mathbf{x}|\Theta)p(\Theta)}{p(\mathbf{x})}. \quad (2.14)$$

The denominator in (2.14) is given by

$$p(\mathbf{x}) = \int p(\mathbf{x}|\Theta)p(\Theta)d\Theta. \quad (2.15)$$

The final posterior $p(\Theta|\mathbf{x})$ is given by

$$p(\Theta|\mathbf{x}) = \frac{p(\mathbf{x}|\Theta)p(\Theta)}{\int p(\mathbf{x}|\Theta)p(\Theta)d\Theta}. \quad (2.16)$$

Further analysis of (2.16) requires intelligent selection of the prior $p(\Theta)$. The selection of this prior continues to be a topic of high interest in the research community. For this research we will introduce, in Chapter 3, a popular selection that has been proposed for similar extraction efforts. In this thesis, we will only use the MAP estimator to determine the final solutions. Future work should include the derivation of $p(\Theta|\mathbf{x})$. The decision to use the MAP estimator is supported by the M-ary hypothesis test derivation shown in the next section.

2.3 Hypothesis Testing and Detection Theory

An M-ary hypotheses test using Bayes criterion is used to make a decision between M hypotheses. The Bayes criterion assigns risk to each of the alternatives, assumes a set of *a priori* probabilities for the parameter set, and attempts to minimize

the risk. The resulting decision criterion, assuming uniform costs, leads to the MAP estimator described previously. This derivation is summarized and presented directly from [13].

The risk is determined by

$$\mathfrak{R} = \sum_{i=0}^{M-1} \sum_{j=0}^{M-1} P_j C_{ij} \int_{z_i} p_{\mathbf{r}|H_j}(\mathbf{R}|H_j) d\mathbf{R} \quad (2.17)$$

where z is the observation space, \mathbf{R} is a point in the observation space, P_j represents the priori probability for the j th hypothesis, and C_{ij} represents the cost for the ij th course of action. To find the optimum Bayes test we vary z_i to minimize \mathfrak{R} over all hypotheses H . The subscript (i) represents each specific hypothesis. For example, if there are three hypotheses to choose from ($M = 3$), $z = z_0 \cup z_1 \cup z_2$, the risk

$$\mathfrak{R} = P_0 C_{00} + P_1 C_{11} + P_2 C_{22} + I_0(\mathbf{R}) + I_1(\mathbf{R}) + I_2(\mathbf{R}) \quad (2.18)$$

where,

$$\begin{aligned} I_0(\mathbf{R}) = \int_{z_0} [P_2(C_{02} - C_{22})p_{r|H_2}(\mathbf{R}|H_2) \\ + P_1(C_{01} - C_{11})p_{r|H_1}(\mathbf{R}|H_1)] d\mathbf{R} \end{aligned} \quad (2.19)$$

$$\begin{aligned} I_1(\mathbf{R}) = \int_{z_1} [P_0(C_{10} - C_{00})p_{r|H_0}(\mathbf{R}|H_0) \\ + P_2(C_{12} - C_{22})p_{r|H_2}(\mathbf{R}|H_2)] d\mathbf{R} \end{aligned} \quad (2.20)$$

$$\begin{aligned} I_2(\mathbf{R}) = \int_{z_2} [P_0(C_{20} - C_{00})p_{r|H_0}(\mathbf{R}|H_0) \\ + P_1(C_{21} - C_{11})p_{r|H_1}(\mathbf{R}|H_1)] d\mathbf{R} \end{aligned} \quad (2.21)$$

The first three terms in \mathfrak{R} represent fixed costs and the integrands $I_i(\mathbf{R})$ represent variable costs over z_i . If we choose the appropriate points \mathbf{R} for each region z_i that minimize each integrand, the minimum risk \mathfrak{R} is determined by the smallest integrand. Therefore, appropriate decision rules may be written as,

If $I_0(\mathbf{R}) < I_1(\mathbf{R})$ and $I_2(\mathbf{R})$, choose H_0

If $I_1(\mathbf{R}) < I_0(\mathbf{R})$ and $I_2(\mathbf{R})$, choose H_1

If $I_2(\mathbf{R}) < I_0(\mathbf{R})$ and $I_1(\mathbf{R})$, choose H_2

or equivalently,

$$I_0(\mathbf{R}) \underset{H_0 \text{ or } H_2}{\overset{H_1 \text{ or } H_2}{\geq}} I_1(\mathbf{R}) \quad (2.22)$$

$$I_1(\mathbf{R}) \underset{H_0 \text{ or } H_1}{\overset{H_0 \text{ or } H_2}{\geq}} I_2(\mathbf{R}) \quad (2.23)$$

$$I_0(\mathbf{R}) \underset{H_0 \text{ or } H_1}{\overset{H_1 \text{ or } H_2}{\geq}} I_2(\mathbf{R}) \quad (2.24)$$

By defining likelihood ratios

$$\Lambda_1(\mathbf{R}) \triangleq \frac{p_{r|H_1}(\mathbf{R}|H_1)}{p_{r|H_0}(\mathbf{R}|H_0)} \quad (2.25)$$

$$\Lambda_2(\mathbf{R}) \triangleq \frac{p_{r|H_2}(\mathbf{R}|H_2)}{p_{r|H_0}(\mathbf{R}|H_0)} \quad (2.26)$$

and manipulating (2.19)-(2.24), we have

$$P_1(C_{01} - C_{11}) \Lambda_1(\mathbf{R}) \underset{H_0 \text{ or } H_2}{\overset{H_1 \text{ or } H_2}{\geq}} P_0(C_{10} - C_{00}) + P_2(C_{12} - C_{02}) \Lambda_2(\mathbf{R}) \quad (2.27)$$

$$P_2(C_{02} - C_{22}) \Lambda_2(\mathbf{R}) \underset{H_0 \text{ or } H_1}{\overset{H_2 \text{ or } H_1}{\geq}} P_0(C_{20} - C_{00}) + P_1(C_{21} - C_{01}) \Lambda_1(\mathbf{R}) \quad (2.28)$$

$$P_2(C_{12} - C_{22}) \Lambda_2(\mathbf{R}) \underset{H_1 \text{ or } H_0}{\overset{H_2 \text{ or } H_0}{\geq}} P_0(C_{20} - C_{10}) + P_1(C_{21} - C_{11}) \Lambda_1(\mathbf{R}) \quad (2.29)$$

These rules can be simplified by assigning uniform costs, $C_{00} = C_{11} = C_{22} = 0$ and $C_{ij} = 1$ for $i \neq j$. This assumption means that there is no cost for choosing the correct hypothesis and equal cost for choosing the wrong hypothesis. Using this assumption and manipulating (2.27)-(2.29), we have

$$P_1 p_{r|H_1}(\mathbf{R}|H_1) \underset{H_0 \text{ or } H_2}{\overset{H_1 \text{ or } H_2}{\geq}} P_0 p_{r|H_0}(\mathbf{R}|H_0) \quad (2.30)$$

$$P_2 p_{r|H_2}(\mathbf{R}|H_2) \underset{H_0 \text{ or } H_1}{\overset{H_2 \text{ or } H_1}{\geq}} P_0 p_{r|H_0}(\mathbf{R}|H_0) \quad (2.31)$$

$$P_2 p_{r|H_2}(\mathbf{R}|H_2) \underset{H_1 \text{ or } H_0}{\overset{H_2 \text{ or } H_0}{\geq}} P_1 p_{r|H_1}(\mathbf{R}|H_1) \quad (2.32)$$

These are equivalent to comparing the posterior probabilities for each hypothesis and choosing the largest, which is equivalent to the MAP estimate.

2.4 3-D SAR Scattering Models

The least squares estimation approach, described in both [1] and [2], provides a framework for estimating model parameters and classifying shapes based on collected SAR phase history data. The results from [1] conclude that shape classification between several similar shapes proves difficult, due to the inherent multi-modal cost surface. Incorrect initialization results in incorrect extraction in many cases.

In [1], shapes are distinguished by their associated physical characteristics, described by a concise set of parameters. The parameters are represented by $\Theta = [X, Y, Z, H, L, r, \tilde{\gamma}, \tilde{\theta}, \tilde{\phi}]$, where X , Y , and Z are the scatterer locations in 3-D cartesian space, H is the height of the scatterer, L is the length of the scatterer, r is the radius of the shape, and $\tilde{\gamma}, \tilde{\theta}, \tilde{\phi}$ are the scatterer's roll, pitch, and yaw aspect with respect to the radar.

The six shapes utilized in this research are provided in Figure 2.1 along with their respective orientations, parameter definitions, and scattering primitives [1].

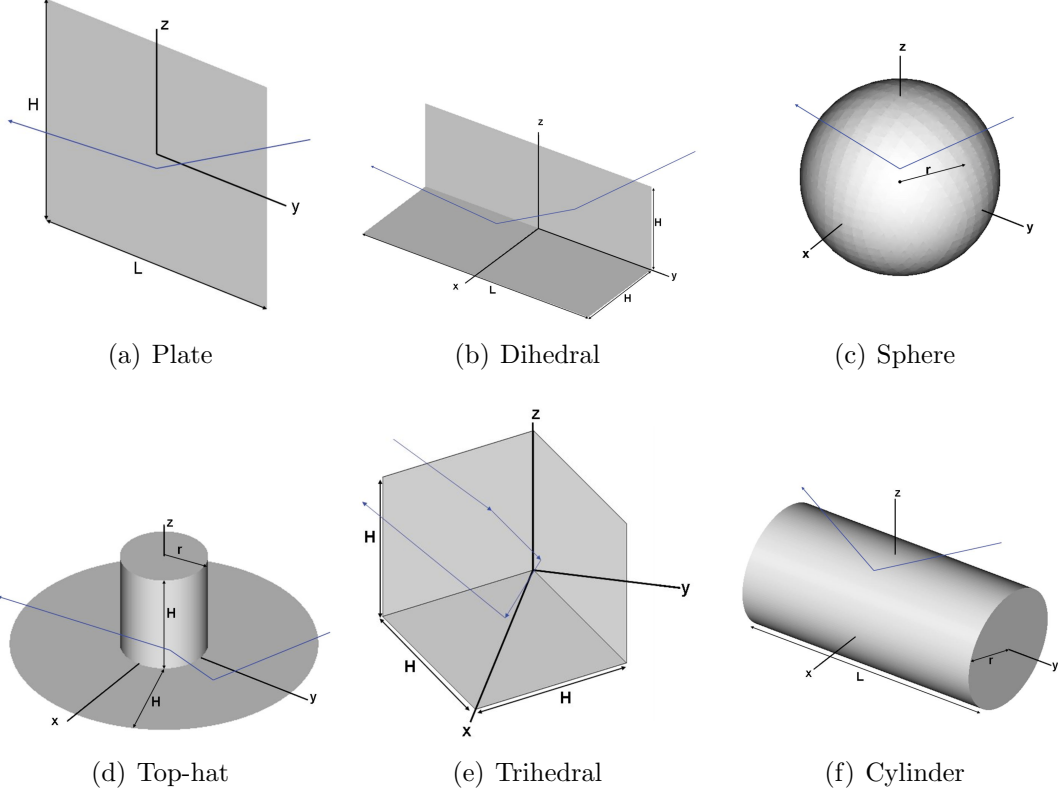


Figure 2.1: Canonical scattering primitives for target shapes re-used with permission from [1].

The received radar signal is modeled as a sum of scatterers in both [1, 2]. The 2-D SAR scattering model shown in [2], is given by

$$s(\omega, \phi; \theta) = \sum_{k=1}^N A_k \left(j \frac{\omega}{\omega_c} \right)^{\alpha_k} \text{sinc} \left(\frac{\omega}{c} L_k \sin(\phi - \bar{\phi}_k) \right) e^{(-\omega \gamma_k \sin \phi)} \cdot e^{(j \frac{\omega}{c^2} (x_k \cos \phi + y_k \sin \phi))} \quad (2.33)$$

where the frequency $w = 2\pi f$, w_c is the center frequency of the radar bandwidth, c is the speed of light, and ϕ is the aspect angle. Each of the N scatterers is defined by the parameter set given by $\Theta = [x, y, A, \alpha, L, \phi, \gamma]$, where (x, y) represents the scattering center location on the (x, y) -plane, A is a relative amplitude, L is the length of the scattering center, $\bar{\phi}$ is the scatterer's orientation angle, α characterizes

frequency dependence of the scattering center, and γ models the aspect dependence of scattering center cross-section.

This model was modified by Jackson in [1] to include an extended parameter set for a 3-D space and radar collection parameters Λ . The new model is given by

$$S(k, \Lambda; \Theta, \Gamma) = \sum_{q=1}^Q P_{\beta_q}(\Lambda; \Theta_q) M_{\Gamma_q}(k, \Lambda; \Theta_q) e^{jk\Delta R(\Lambda; \Theta_q)} \quad (2.34)$$

where $k \triangleq \frac{2\pi f}{c}$ is the wavenumber for frequency f and speed of light c . We use $\Lambda = (\phi_t, \theta_t, \phi_r, \theta_r)$ to represent the scattered signal dependence on transmitter (subscript t) and receiver (subscript r) azimuth (ϕ) and elevation (θ) locations. In this research we assume a monostatic radar ($\phi_t = \phi_r, \theta_t = \theta_r$). The shape ($\Gamma = [\text{plate, dihedral, sphere, top-hat, trihedral, cylinder}]$) parameter sets are denoted by the parameter vector Θ . For further details see [10].

The model is parameterized based on each specific shape hypothesis. This increases computational efficiency by eliminating the estimation of nuisance parameters that are not required for certain shapes. The signal model (2.34) may be represented by

$$S(k, \Lambda; \Theta, \Gamma) = \sum_{q=1}^Q S(k, \Lambda; \Theta_q, \Gamma_q) \quad (2.35)$$

for Q scatterers within a target scene. The polarization response $\mathbf{P}_{\beta(m)}$ is, in general, a 2×2 matrix that represents the polarization dependence for a specific shape described by the subscript $\beta(m)$. Specifically, \mathbf{P}_{β} is defined by

$$\mathbf{P}_{\beta}(\Lambda; \Theta_m) = \begin{bmatrix} P_{\beta}^{vv} & P_{\beta}^{vh} \\ P_{\beta}^{hv} & P_{\beta}^{hh} \end{bmatrix} \quad (2.36)$$

where the superscripts denote vertical and horizontal receiver and transmitter polarizations. For the monostatic case, as described in this research, $\mathbf{P}_{\beta(m)}$ is symmetric.

Each shape is characterized by the number of reflections and is separated into either an “odd-bounce” or “even-bounce” category. The polarization dependence for an odd-bounce perfect electrical conductor (PEC) is

$$\mathbf{P}_{\text{odd}} = \begin{bmatrix} -1 & 0 \\ 0 & 1 \end{bmatrix} \quad (2.37)$$

The polarization response for even-bounce scatterers must account for antenna line of sight (LOS) and the object’s rotation ζ about that LOS. The matrix \mathbf{P}_{even} is given by

$$\mathbf{P}_{\text{even}} = \begin{bmatrix} -\cos \zeta & \sin \zeta \\ \sin \zeta & \cos \zeta \end{bmatrix} \quad (2.38)$$

The derivation of ζ is provided in [1].

The next several subsections provide a summary of the scattering response, $M_{\Gamma_q}(k, \Lambda; \Theta_q)$, for each shape from [1].

2.4.1 Rectangular Plate. The plate is characterized by the parameter set $\Theta_{\text{plate}} = [X, Y, Z, H, L, \tilde{\gamma}, \tilde{\theta}, \tilde{\phi}]$. The amplitude scale factor is defined as $A = LH$ for a calibrated radar.

The shape response for the plate is given by

$$M_{\Gamma_{\text{plate}}}(k, \Lambda; \Theta_{\text{plate}}) = \frac{jk}{\sqrt{\pi}} A \text{sinc}[kL \sin \phi \cos \theta] \times \text{sinc}[kH \sin \theta], \quad (2.39)$$

$$\phi \in \left[-\frac{\pi}{2}, \frac{\pi}{2}\right], \quad \theta \in \left[-\frac{\pi}{2}, \frac{\pi}{2}\right]$$

2.4.2 Dihedral. The dihedral has the parameter set $\Theta_{\text{dihedral}} = [X, Y, Z, H, L, \tilde{\gamma}, \tilde{\theta}, \tilde{\phi}]$. The amplitude scale factor is defined as $A = 2LH$ for a calibrated radar.

The shape response for the dihedral is given by

$$M_{\Gamma_{dihedral}}(k, \Lambda; \Theta_{dihedral}) = \frac{jk}{\sqrt{\pi}} A \text{sinc}[kL \sin \phi \cos \theta] \times \begin{cases} \sin(\theta), & \theta \in [0, \frac{\pi}{4}] \\ \cos(\theta), & \theta \in [\frac{\pi}{4}, \frac{\pi}{2}] \end{cases}, \phi \in [-\frac{\pi}{2}, \frac{\pi}{2}] \quad (2.40)$$

2.4.3 Trihedral. The trihedral has the parameter set

$\Theta_{trihedral} = [X, Y, Z, H, \tilde{\gamma}, \tilde{\theta}, \tilde{\phi}]$. The amplitude scale factor is defined as $A = 2\sqrt{3}H^2$ for a calibrated radar.

The shape response for the trihedral is given by

$$M_{\Gamma_{trihedral}}(k, \Lambda; \Theta_{trihedral}) = \frac{jk}{\sqrt{\pi}} A \times \begin{cases} \sin(\theta + \frac{\pi}{4} - \tan^{-1}(\frac{1}{\sqrt{2}})), & \theta \in [0, \tan^{-1}(\frac{1}{\sqrt{2}})] \\ \cos(\theta + \frac{\pi}{4} - \tan^{-1}(\frac{1}{\sqrt{2}})), & \theta \in [\tan^{-1}(\frac{1}{\sqrt{2}}), \frac{\pi}{2}] \end{cases} \times \begin{cases} -\cos(\phi - \frac{\pi}{4}), & \phi \in [-\frac{\pi}{4}, 0] \\ \sin(\phi - \frac{\pi}{4}), & \phi \in [0, \frac{\pi}{4}] \end{cases} \quad (2.41)$$

2.4.4 Cylinder. The cylinder has the parameter set

$\Theta_{cylinder} = [X, Y, Z, L, r, \tilde{\gamma}, \tilde{\theta}, \tilde{\phi}]$. The amplitude scale factor is defined as $A = L\sqrt{r}$ for a calibrated radar. We assume the cylinder is centered on the y -axis.

The shape response for the cylinder is given by

$$M_{\Gamma_{cylinder}}(k, \Lambda; \Theta_{cylinder}) = \sqrt{\frac{jk}{\cos \phi}} A \cos \phi \text{sinc}[kL \sin \phi \cos \theta] \quad (2.42)$$

$$\phi \in [-\frac{\pi}{2}, \frac{\pi}{2}]$$

2.4.5 Tophat.

The tophat is a cylinder with a wide circular base that forms a right angle with the cylinder. The tophat has the parameter set $\Theta_{tophat} =$

$[X, Y, Z, H, r, \tilde{\gamma}, \tilde{\theta}, \tilde{\phi}]$. The amplitude scale factor is defined as $A = \sqrt{\frac{8r}{\sqrt{2}}}H$ for a calibrated radar.

The shape response for the tophat is given by

$$M_{\Gamma_{\text{tophat}}}(k, \Lambda; \Theta_{\text{tophat}}) = A\sqrt{jk} \times \begin{cases} \sin(\theta), & \theta \in [0, \frac{\pi}{4}] \\ \cos(\theta), & \theta \in [\frac{\pi}{4}, \frac{\pi}{2}] \end{cases} \quad (2.43)$$

2.4.6 Sphere. The final shape included in this research is the sphere. The sphere has the parameter set $\Theta_{\text{sphere}} = [X, Y, Z, r]$. The amplitude scale factor is defined as $A = r$ for a calibrated radar.

The shape response for the sphere is given by

$$M_{\Gamma_{\text{sphere}}}(k, \Lambda; \Theta_{\text{sphere}}) = A\sqrt{\pi} \quad (2.44)$$

The final piece of the 3-D model is the differential range ΔR .

2.4.7 Differential Range. The differential range term ΔR accounts for the phase changes caused by the non-zero range extent of an object and the object's range from scene center. This range may be written as the sum of the range to the scattering center location R_0 and the range due to non-zero object extent R_r , given by

$$\Delta R(\mathbf{\Lambda}(\tau); \mathbf{\Theta}_m) = \Delta R_0(\mathbf{\Lambda}(\tau); \mathbf{\Theta}_m) + \Delta R_r(\mathbf{\Lambda}(\tau); \mathbf{\Theta}_m) \quad (2.45)$$

These ranges are approximated in [1] as

$$\Delta R_0(\mathbf{\Lambda}(\tau); \mathbf{\Theta}_m) \approx 2x_0 \cos \phi(\tau) \cos \theta(\tau) + 2y_0 \sin \phi(\tau) \cos \theta(\tau) + 2z_0 \sin \theta(\tau) \quad (2.46)$$

and

$$\Delta R_r(\mathbf{\Lambda}(\tau); \mathbf{\Theta}_m) \approx 2x_r \cos \phi(\tau) \cos \theta(\tau) + 2y_r \sin \phi(\tau) \cos \theta(\tau) + 2z_r \sin \theta(\tau) \quad (2.47)$$

where τ represents time. Further details concerning these derivations are provided in [1]. The parameters to be estimated for each of the shapes are shown in Table 2.1.

Table 2.1: The parameters to be estimated for each shape.

Shape	X	Y	Z	H	L	r	$\tilde{\gamma}$	$\tilde{\theta}$	$\tilde{\phi}$
plate	x	x	x	x	x		x	x	x
dihedral	x	x	x	x	x		x	x	x
trihedral	x	x	x	x	x		x	x	x
cylinder	x	x	x			x	x	x	x
top-hat	x	x	x	x		x	x	x	x
sphere	x	x	x			x			

The derivations of each of the signal models are provided in [1].

In the next chapter, we will utilize the models developed in this section to build dictionaries of sample data. These dictionaries form the basis for the feature extraction algorithm proposed in this thesis.

III. Model Development and Methodology

3.1 Chapter Overview

This chapter presents the development and methodology of the dictionary based feature classification and parameter estimation algorithm proposed in this thesis. This algorithm will utilize all of the theory presented in Chapter II.

First, we will step through the creation of the shape dictionaries. Specifically, we will use the radar signal models developed in [1] to simulate radar phase history data for many combinations of physical shape parameters. We also describe the memory requirements and present a generic equation to determine the approximate size (in bytes) of a dictionary. Second, we will describe the shape classification and parameter estimation algorithm using the dictionaries. The algorithm requires a set of non-redundant dictionary columns, or ‘atoms’, to provide accurate solutions. Therefore, we discuss dictionary analysis used to ensure low redundancy. Third, we present several techniques to lower overall dictionary coherence. Finally, we discuss classification and estimation techniques using the reduced dictionaries.

3.2 Dictionary Setup

Each dictionary is populated using the 3-D scattering model given by

$$S(k, \Lambda; \Theta, \Gamma) = \sum_{q=1}^Q \mathbf{P}_{\beta_q}(\Lambda; \Theta_q) M_{\Gamma_q}(k, \Lambda; \Theta_q) e^{jk\Delta R(\Lambda; \Theta_q)} \quad (3.1)$$

developed by Jackson in [1] and provided in Section 2.4.

Dictionaries for each shape Γ_j are populated with data generated using (3.1) by varying Θ over many combinations of parameters for a specific radar collection setup Λ . The number of combinations is only limited by available computational memory and time required for correlation in within signal processor. The changes in all parameters are based on the range resolution of the radar system of interest. For example, the location (x, y, z) will be varied by a step-size of at least 0.5m for a

radar system with a range resolution of 0.5m. Smaller step-sizes lead to undesirable increases in atom redundancy, limiting atom selection accuracy.

The bulk of the computational requirements for the dictionary approach are required for the construction and storage of the model dictionaries. The resolution of the dictionary drives the memory and processing requirements of the system.

Generating the required feature dictionaries requires large amounts of computer memory, even for a coarsely-sampled parameter space. Each canonical shape response is represented by four to nine size, location, and orientation parameters depending on the shape type. The dictionary \mathbf{D} contains $N_T = \sum_{j=1}^J \prod_{q=1}^Q L_{jq}$ atoms, where L_{jq} represents the number of samples for the q th parameter in the j th dictionary parameter vector Θ_j . In addition, each atom has $2 \cdot K$ elements, including both real and complex values of radar returns associated with multiple frequencies, aspects, and polarizations. Specifically, $K = \# \text{ azimuths} \times \# \text{ polarizations} \times \# \text{ frequencies}$. Assuming each element is 64 bits or 8 bytes, the memory requirement for each atom is $16 \cdot K$ bytes. Therefore,

$$\text{memory required} = 16 \cdot K \cdot \sum_{j=1}^J \prod_{q=1}^Q L_{jq} \text{ bytes.} \quad (3.2)$$

The shape dictionaries used in this research are comprised of $2K = 113250$ element long atoms, each consuming 906 kilo-bytes (KB) of memory. There are six dictionaries used in the simulations presented, each of which contains 750 or 4500 atoms. The total memory needed to house these dictionaries is almost 18 giga-bytes (GB).

In the next section we will describe the use of these dictionaries in the proposed shape classification scheme.

3.3 Dictionary Based Classification

A dictionary based feature extraction algorithm is a fundamentally different approach than the estimation techniques in [2, 10]. This section will describe the use of a dictionary method for classifying measured data with models that cover a wide variety of parameter sets Θ for multiple shape hypotheses within the set Γ and various collection profiles described by Λ . For simplicity, all radar collection parameters, including the flight profile, frequencies, and polarizations, are combined into the parameter vector Λ . The non-convex optimization method used in the gradient descent for a least-squares cost surface optimization proves computationally inefficient when attempting to minimize the error of a high-dimensional, non-linear model.

As described in Section 3.2, each dictionary is populated with many atoms that are each comprised of simulated phase history data for a specific set of parameters $S(\Lambda; \Theta, \Gamma_j)$. Each atom is generated using the 3-D SAR scattering models developed in [1]. The simulated phase histories are columnized, with the real and imaginary pieces separated and stacked, and stored in a large dictionary matrix \mathbf{D}_{Γ_j} . Dictionaries are created for each shape hypothesis Γ .

We denote a dictionary representing the j th canonical shape as a matrix

$$\mathbf{D}_{\Gamma_j} = \begin{bmatrix} \text{Re}\{S(\Lambda_1; \Theta_1, \Gamma_j)\} & \cdots & \text{Re}\{S(\Lambda_1; \Theta_N, \Gamma_j)\} \\ \vdots & \vdots & \vdots \\ \text{Re}\{S(\Lambda_K; \Theta_1, \Gamma_j)\} & \cdots & \text{Re}\{S(\Lambda_K; \Theta_N, \Gamma_j)\} \\ \text{Im}\{S(\Lambda_1; \Theta_1, \Gamma_j)\} & \cdots & \text{Im}\{S(\Lambda_1; \Theta_N, \Gamma_j)\} \\ \vdots & \vdots & \vdots \\ \text{Im}\{S(\Lambda_K; \Theta_1, \Gamma_j)\} & \cdots & \text{Im}\{S(\Lambda_K; \Theta_N, \Gamma_j)\} \end{bmatrix} \quad (3.3)$$

where each column corresponds to an evaluation of the shape model function at one of N samples of the parameter vector Θ .

3.3.1 Feature Extraction. As described in [10], the feature extraction problem for a noisy set of radar measurements $\mathbf{Y}(\Lambda)$, may be posed as the least-squares

problem

$$\min_{\mathbf{\Theta}, \mathbf{\Gamma}} \|\mathbf{Y}(\mathbf{\Lambda}) - \mathbf{S}(\mathbf{\Lambda}; \mathbf{\Theta}_n, \mathbf{\Gamma}_j)\|_2^2 \quad (3.4)$$

The problem in (3.4) includes model order selection, feature classification, and parameter estimation. Assuming $2 \cdot K$ samples in the measurement vector and model order $M \ll N_T$ dictionary atoms, we can recast (3.4) as a sparse signal recovery problem [8, 15, 16]

$$\min \|\mathbf{x}\|_0 \quad \text{s.t.} \quad \|\mathbf{Y}(\mathbf{\Lambda}) - \mathbf{D}_{\mathbf{\Gamma}_j} \mathbf{x}\|_2^2 < \epsilon \quad (3.5)$$

for coefficients $\mathbf{x} = [x_1, \dots, x_{N_T}]^T$. By relaxing the ℓ_0 norm to the ℓ_1 norm, (3.5) becomes a convex problem [15]

$$\min \|\mathbf{x}\|_1 \quad \text{s.t.} \quad \|\mathbf{Y}(\mathbf{\Lambda}) - \mathbf{D}_{\mathbf{\Gamma}_j} \mathbf{x}\|_2^2 < \epsilon \quad (3.6)$$

Fine sampling of parameters is generally desired to achieve a good representation of the received signal. In general fine sampling results in an over-complete dictionary with highly correlated columns. In this problem, high column correlation also occurs for coarse parameter sampling due to similarity in the scattering response of different shapes for various parameter choices.

The problem statement provided in (3.6) is known as the basis pursuit de-noising (BPDN) principle which may be solved by a variety of algorithms. These algorithms have been shown to produce inaccurate sparse solutions when there is high inter-column correlation, or inter-atom redundancies [15]. To attempt to reduce redundancies between parameter combinations we analyze each dictionary over various $\mathbf{\Lambda}$. We also explore the use of a “molecule” clustering approach similar to [7], which groups correlated atoms.

3.3.2 Dictionary Analysis and Reduction. The most fundamental quantity used to describe a dictionary is *coherence* [9]. The peak dictionary coherence is defined

as

$$\mu = \max_{m \neq n} |\langle S(\Theta_m, \Gamma_j), S(\Theta_n, \Gamma_j) \rangle| \quad (3.7)$$

where $\langle S_m, S_n \rangle \equiv S_m^H S_n$ is the correlation between dictionary \mathbf{D} atoms $S(\Theta_m, \Gamma_j)$ and $S(\Theta_n, \Gamma_j)$ [9]. An incoherent dictionary (μ small) is required to meet the restricted isometry property (RIP) needed to find a “good” sparse solution using BP optimization [7].

The Gram-Matrix $\mathbf{G} \equiv (\bar{\mathbf{D}}^T \bar{\mathbf{D}})$, where $\bar{\mathbf{D}}$ is \mathbf{D} with normalized columns, describes the coherence within \mathbf{D} by computing correlation between all combinations of atoms. We plot \mathbf{G} as an intensity map with values in $[0, 1]$, which we refer to as a *correlation map* or *confuser map*. The confuser map visually depicts which features are similar and which are identifiable. We present several methods for reducing inter-atom correlation in the next section.

3.4 Dictionary Reduction

As mentioned previously, many popular dictionary based sparse signal recovery problems rely on the BP principle. Determining a good sparse approximation using a redundant dictionary is of combinatorial complexity and even a non-deterministic polynomial-time hard (NP-hard) problem [6, 7].

In this section we step through the correlation reduction process to support accurate BP optimizations. We will explore the effects of increasing radar collection diversity, including frequencies, flight profile, and polarizations. We then explore a modified version of the molecule method described in [7] to minimize dictionary coherence. For simplicity, confuser maps for only the dihedral dictionary are provided within this section. Maps for the other five shapes are included in Appendix A. The correlation reductions will be summarized for all shapes in Table 3.1.

The baseline correlation map, provided in Figure 3.1, is created for the dihedral dictionary generated with a linear flight profile, a single frequency, and HH polariza-

tion. This map contains many off-diagonal (inter-column) correlations which imply coherence within \mathbf{D} and violation of the RIP [6].

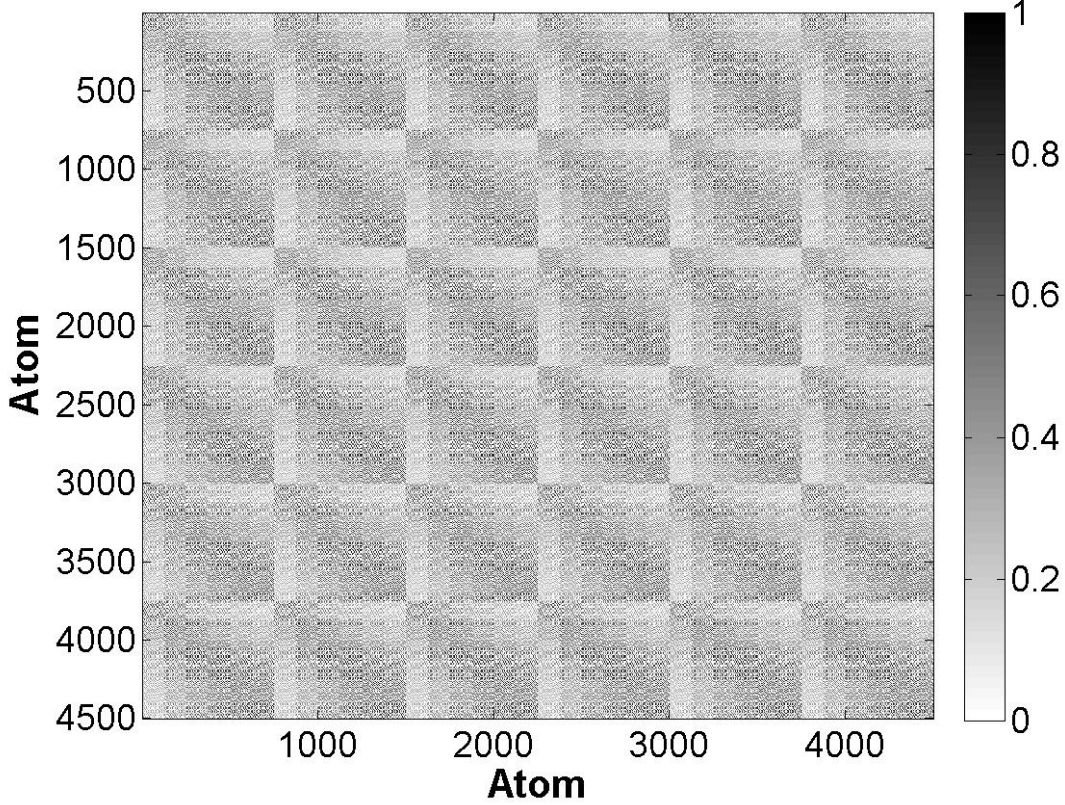


Figure 3.1: Correlation map corresponding to $\mathbf{D}_{\Gamma_{\text{dihedral}}}$ generated using a linear flight path, HH polarization, and 1 frequency.

3.4.1 Correlation Reduction Through Diversity. We first attempt to reduce these correlations by exploring the effects of varying radar collection parameters $\mathbf{\Lambda}$. We investigate the role of frequency diversity by creating dictionaries for 1 frequency and 256 frequencies and compare the confuser maps. We also create dictionaries for linear and non-linear flight paths where the radar elevation is varied. Confuser maps are then generated for dictionaries containing multiple polarizations. The overarching hypothesis for the effects of diversity is that greater diversity will reduce inter-atom correlation and redundancy by increasing resolution of each phase history vector.

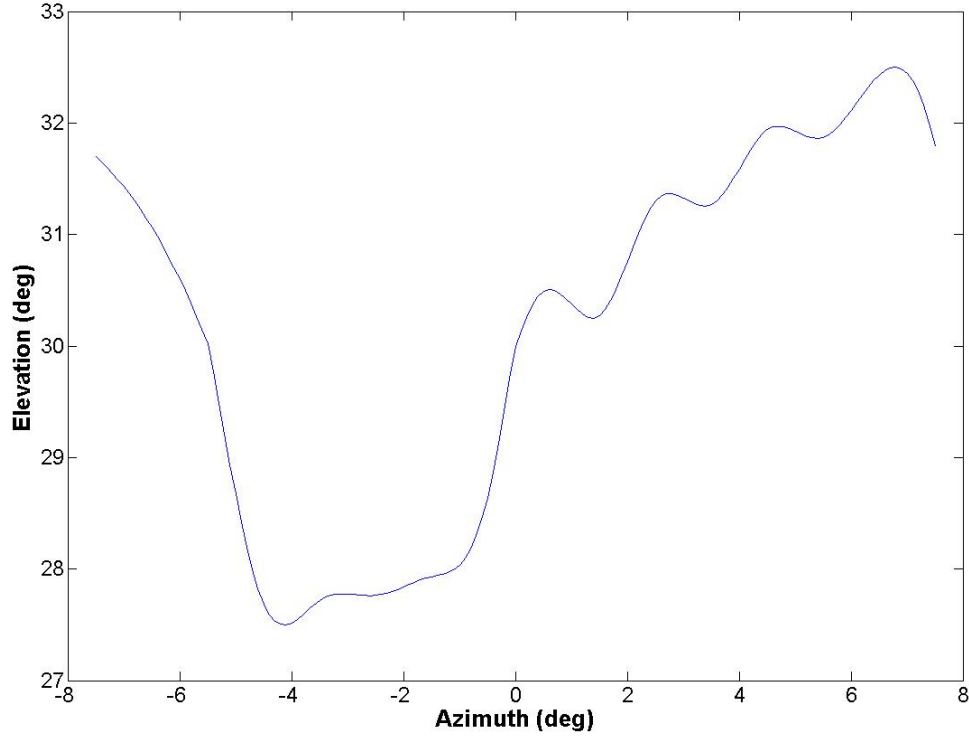


Figure 3.2: Example of non-linear flight path used for simulated SAR data collection.

Greater elevation aspect diversity is simulated by varying the flight elevation profile for the simulated SAR data collection. The initial collection path utilizes a constant radar elevation of 30° . Subsequent data correspond to non-linear flight paths where azimuth varies linearly and elevation varies along a non-linear path, varying between 25° and 35° . An example of the non-linear elevation collection path is shown in Figure 3.2. The increased elevation aspect diversity provides the angular resolution needed to separate shapes that provide similar scattering responses at specific angles. Varying the collection angle is the same as changing the pitch of the shape target.

Multiple collection polarizations are also simulated to attempt to lower correlation between similar shape scattering responses. The initial collection is performed using a HH polarization. Subsequent collections are simulated using HV and VV polarizations.

3.4.2 Coherence Reduction Via Molecules. The final method for reducing inter-atom correlation relies on a clustering method that groups similar atoms to minimize dictionary coherence. High inter-column coherency described by the off-diagonal intensities within the confuser maps refers to redundant atoms within the dictionaries. Redundancies may occur due to parameter insensitivity of the scattering models and may represent very different physical geometries. Nonetheless, the resulting signal response represented by correlated atoms is non-unique and must be accounted for. We cluster correlated atoms to create “molecules,” as described in [7]. The collection of non-redundant atoms and molecules form a new minimized dictionary $\hat{\mathbf{D}}$.

Each molecule may be represented as a sub-dictionary $\hat{\mathbf{D}}_m \in \mathbf{D}$, where the subscript m represents the molecule index. Each $\hat{\mathbf{D}}_m$ contains highly-correlated atoms $\hat{\mathbf{S}}$ which exceed a user-defined coherence threshold $|\langle \hat{\mathbf{S}}_i, \hat{\mathbf{S}}_j \rangle| \geq \eta$. Each molecule sub-dictionary is replaced in the overall dictionary by a single representative atom, given by the average across the molecule $\mathbf{d}_m = \frac{1}{N_m} \sum_{i=1}^{N_m} \hat{\mathbf{S}}_i$ to form a reduced dictionary $\hat{\mathbf{D}}$.

The new dictionary $\hat{\mathbf{D}}$ is considered minimized once it is no longer reducible, meaning the off-diagonal correlations in the Gram-Matrix and coherence μ are less than the user-defined threshold η . This is represented graphically by a diagonalized confuser map.

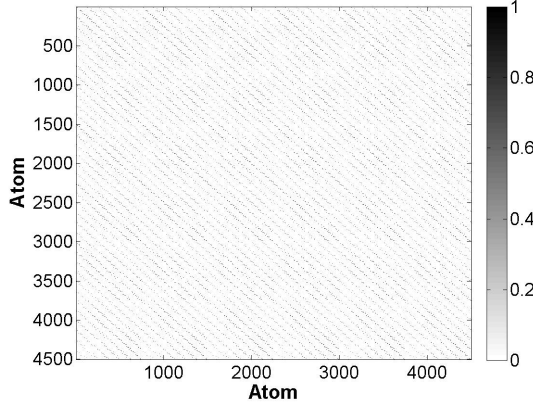
The results from each of the coherence reduction steps discussed are presented in Section 3.5.1 and Section 3.5.2.

3.5 Dictionary Reduction Results

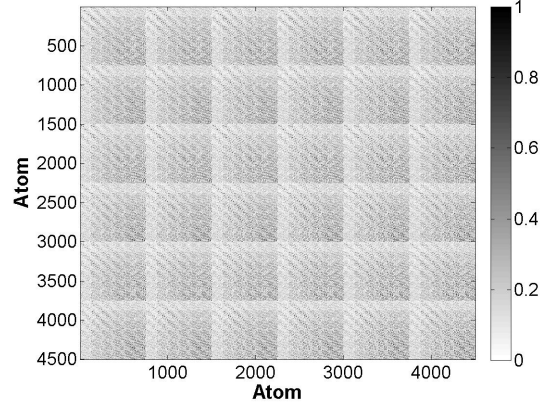
In this section we present the coherence reductions gained by the methods described in Section 3.4.

3.5.1 Coherence Reduction Via Diversity. The first reduction step is based on increasing radar collection diversity. Specifically, we examine the effects of increasing frequency, as well as, aspect and polarization diversity on the overall dictionary coherence. Frequency diversity is increased by simulating collection data over a range

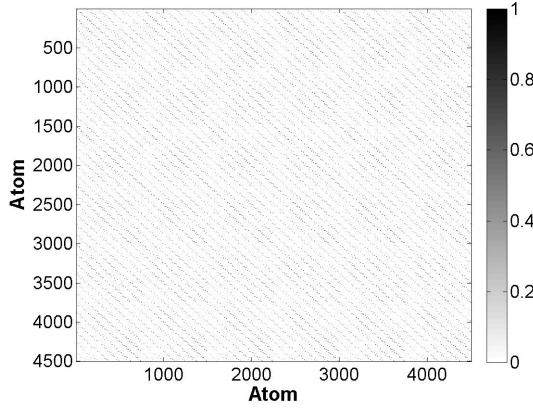
of radar frequencies. For this example, we increase the number of collection frequencies from 1 to 125, centered around a center frequency of 10 GHz with a bandwidth (BW) of 300 MHz, determined by a user specified range resolution of 0.5 m. Aspect diversity is increased by changing the simulated collection flight path from a linear, constant 30° collection elevation, to a non-linear path where the radar elevation is $30^\circ \pm 5^\circ$. The non-linear flight path used in all simulations is shown in Figure 3.2. Finally, the polarization diversity is increased by including HV and VV polarization responses in the simulated data. The coherence reductions from each of these diversity increases are shown in Figure 3.3 and summarized in Table 3.1.



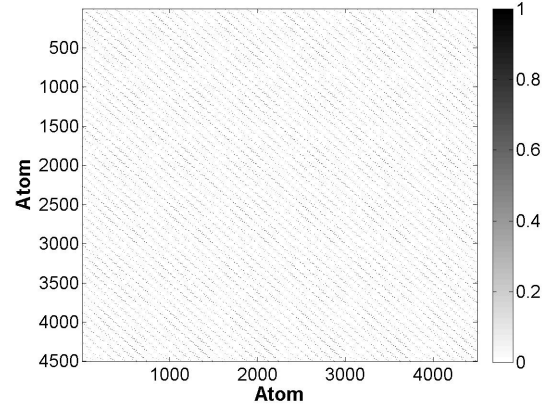
(a) Correlation map corresponding to $\mathbf{D}_{\Gamma_{\text{dihedral}}}$ generated using a linear flight path, HH polarization, and 125 frequencies.



(b) Correlation map corresponding to $\mathbf{D}_{\Gamma_{\text{dihedral}}}$ generated using a non-linear flight path, HH polarization, and 1 frequency.



(c) Correlation map corresponding to $\mathbf{D}_{\Gamma_{\text{dihedral}}}$ generated using a linear flight path, HH, HV, and VV polarizations, and 125 frequencies.



(d) Correlation map corresponding to $\mathbf{D}_{\Gamma_{\text{dihedral}}}$ generated using a non-linear flight path, HH, HV, and VV polarizations, and 125 frequencies.

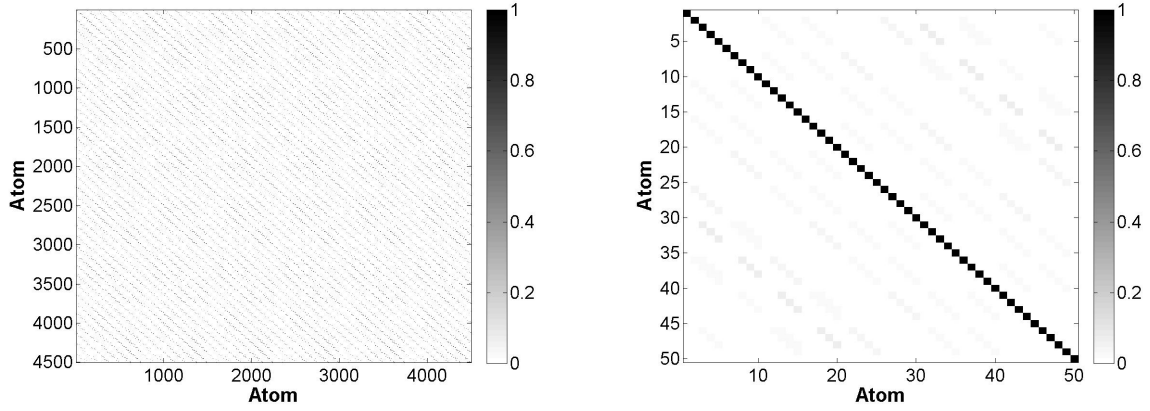
Figure 3.3: Reduction in correlation due to increased aspect and frequency diversity for $\mathbf{D}_{\Gamma_{\text{dihedral}}}$.

Table 3.1: Coherence reduction results due to increased radar collection diversity.

Shape	Scenario	Coherence		
		Peak	Mean	St. Dev.
plate	Linear path, 1 freq., single pol.	1	0.2441	0.3007
	Linear path, 125 freqs., single pol.	1	0.0212	0.1072
	Non-linear path, 1 freq., single pol.	0.9993	0.3220	0.2385
	Linear path, 125 freqs., multi-pol.	1	0.0212	0.1072
	Non-linear path, 125 freqs., multi-pol.	0.9988	0.0282	0.1217
dihedral	Linear path, 1 freq., single pol.	1	0.2437	0.3002
	Linear path, 125 freqs., single pol.	1	0.0211	0.1071
	Non-linear path, 1 freq., single pol.	1	0.1878	0.1600
	Linear path, 125 freqs., multi-pol.	1	0.0211	0.1071
	Non-linear path, 125 freqs., multi-pol.	1	0.0194	0.1065
sphere	Linear path, 1 freq., single pol.	1	0.0749	0.1415
	Linear path, 125 freqs., single pol.	1	0.0046	0.0277
	Non-linear path, 1 freq., single pol.	0.9069	0.0522	0.0628
	Linear path, 125 freqs., multi-pol.	1	0.0046	0.0277
	Non-linear path, 125 freqs., multi-pol.	0.1344	0.0030	0.0095
top-hat	Linear path, 1 freq., single pol.	1	0.0758	0.1448
	Linear path, 125 freqs., single pol.	1	0.0064	0.0395
	Non-linear path, 1 freq., single pol.	1	0.0486	0.0536
	Linear path, 125 freqs., multi-pol.	1	0.0064	0.0395
	Non-linear path, 125 freqs., multi-pol.	1	0.0047	0.0352
trihedral	Linear path, 1 freq., single pol.	1	0.0777	0.1458
	Linear path, 125 freqs., single pol.	1	0.0116	0.0851
	Non-linear path, 1 freq., single pol.	1	0.0508	0.0860
	Linear path, 125 freqs., multi-pol.	1	0.0116	0.0851
	Non-linear path, 125 freqs., multi-pol.	1	0.0105	0.0828
cylinder	Linear path, 1 freq., single pol.	0.9962	0.2445	0.2992
	Linear path, 125 freqs., single pol.	0.9877	0.0115	0.0577
	Non-linear path, 1 freq., single pol.	0.9616	0.1744	0.1506
	Linear path, 125 freqs., multi-pol.	0.9877	0.0115	0.0577
	Non-linear path, 125 freqs., multi-pol.	0.9556	0.0088	0.0479

These results are dependent on the specified parameter space defined for the shape locations, RCS, and orientations. These results will also change if the parameter space resolutions are changed.

Although the overall coherence has been reduced, the Gram-Matrix still includes many non-negligible off-diagonal values. Therefore, the molecule clustering method



(a) Correlation map corresponding to $\mathbf{D}_{\Gamma_{\text{dihedral}}}$ generated using a non-linear flight path, HH, HV, and VV polarizations, and 125 frequencies before clustering.

(b) Correlation map corresponding to $\mathbf{D}_{\Gamma_{\text{dihedral}}}$ generated using a non-linear flight path, HH, HV, and VV polarizations, and 125 frequencies after implementing molecule method.

Figure 3.4: Reduction in correlation due to molecule clustering algorithm.

introduced and described in [7] is implemented as a hierarchical approach for further reduction.

3.5.2 Coherence Reduction Via Molecules. The dictionary's coherence is minimized when the Gram-Matrix has been diagonalized. As seen in Figure 3.3(d), the confuser map still includes many off-diagonal components. These off-diagonal correlations represent atom redundancy. The clustering method described in [7] combines redundant atoms based on a user defined coherence threshold η and replaces them with a representative atom. In our case, this atom is the sample mean of the redundant atoms. The final reduced dictionary should contain only non-redundant atoms ($|\langle \hat{\mathbf{S}}_i, \hat{\mathbf{S}}_j \rangle| < \eta$).

For this discussion we set the coherence threshold to $\eta = 0.2$. The resulting reduction in coherence and dictionary size is shown in Figure 3.4 and summarized in Table 3.2.

The dictionary has now been minimized, as shown by the diagonalized Gram-Matrix in Figure 3.4(b). The total size of $\mathbf{D}_{\Gamma_{\text{dihedral}}}$ has also been reduced from 4500

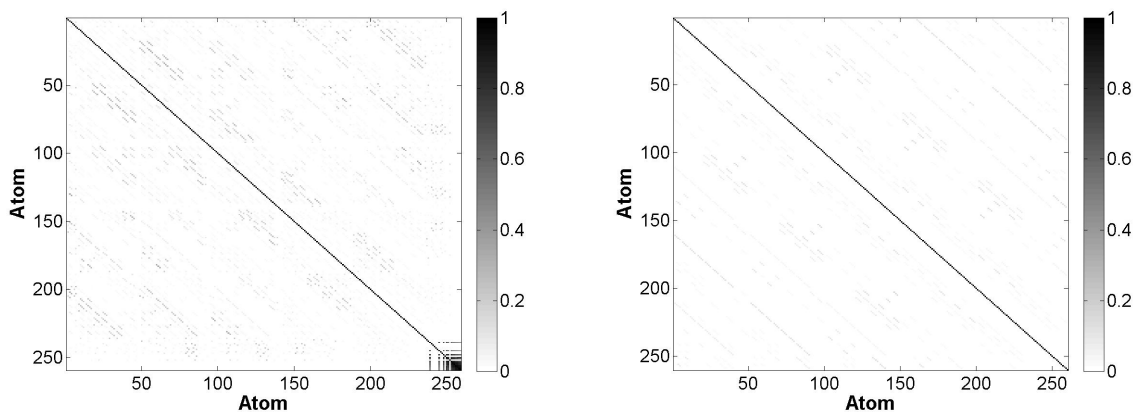
Table 3.2: Coherence reduction results for molecule cluster method.

Shape	Scenario	Coherence		
		Peak	Mean	St. Dev.
plate	Non-linear, 125 freqs, multi-pol	0.9988	0.0282	0.1217
	Non-linear, 125 freqs, multi-pol, clustered	0.2620	0.0158	0.0396
dihedral	Non-linear, 125 freqs, multi-pol	1	0.0194	0.1065
	Non-linear, 125 freqs, multi-pol, clustered	0.0642	0.0060	0.0091
sphere	Non-linear, 125 freqs, multi-pol	0.1344	0.0030	0.0095
	Non-linear, 125 freqs, multi-pol, clustered	0.1344	0.0030	0.0095
top-hat	Non-linear, 125 freqs, multi-pol	1	0.0047	0.0352
	Non-linear, 125 freqs, multi-pol, clustered	0.1402	0.0036	0.0118
trihedral	Non-linear, 125 freqs, multi-pol	1	0.0105	0.0828
	Non-linear, 125 freqs, multi-pol, clustered	0.1548	0.0039	0.0166
cylinder	Non-linear, 125 freqs, multi-pol	0.9556	0.0088	0.0479
	Non-linear, 125 freqs, multi-pol, clustered	0.9556	0.0092	0.0406

atoms to 50 molecules, each of which containing 70 to 100 atoms. The BP algorithm may now be implemented on the reduced dictionary $\hat{\mathbf{D}}_{\Gamma_{\text{dihedral}}}$.

3.5.3 Coherence Reduction Summary. From Tables 3.1 and 3.2 we can make several observations concerning shape responses and atom redundancy. The greatest reductions in inter-column correlations prior to clustering are due to increasing frequency and aspect diversity. Increasing polarization diversity alone did not change single shape dictionary coherence. However, polarization diversity may reduce coherence in dictionaries containing multiple shapes. For this research we use data simulated utilizing all three polarizations (HH, HV, VV) to support separation between shape dictionaries when performing the classification and estimation steps.

All shape confuser matrices, with the exception of the sphere, contain large off-diagonal correlations prior to clustering, shown by the large peak coherency listed in Table 3.1. All shape dictionaries were successfully minimized (diagonalized confuser map) after implementation of the molecule clustering method, except for the cylinder and sphere dictionaries. The sphere dictionary was already minimized due to the increased frequency and aspect diversities. The clustering method used for each of the other shapes did not minimize the cylinder dictionary. Further investigation shows



(a) Correlation map corresponding to $\mathbf{D}_{\Gamma_{\text{cylinder}}}$ generated using a non-linear flight path, HH, HV, and VV polarizations, 125 frequencies, and original clustering method.

(b) Correlation map corresponding to $\mathbf{D}_{\Gamma_{\text{cylinder}}}$ generated using a non-linear flight path, HH, HV, and VV polarizations, 125 frequencies, and modified clustering method.

Figure 3.5: Reduction in correlation due to modified molecule clustering algorithm for dihedral dictionary.

that the representative atoms for the cylinder dictionary, created using the means of each molecule, become highly correlated with each other; therefore, negating the successful minimization of previous correlations. This result may be due to several reasons, including model similarities and radial parameter insensitivity. The sphere may have led to the same results if the sphere dictionary had not been fully reduced from increased diversity.

A modified clustering method is implemented to alleviate this issue. This method simply replaces the mean representative atom with the atom corresponding to the current molecule index. As shown in Figure 3.5, this modified method successfully minimizes the off-diagonal correlations.

This method also works for minimizing the other dictionaries. The method improves estimation for the cylinder, but simulations show that the modified method leads to incorrect shape classifications and parameter estimations with the other five shapes.

The BP algorithm determines an appropriate coefficient vector ψ for each reduced dictionary $\hat{\mathbf{D}}$. This vector identifies the molecule for each shape that contains the most representative data. This solution is still ambiguous since the correct atom could be any one of the atoms contained within any of the selected molecules for any shape. The BP principle cannot be used to select the final solution, since it relies on low inter-atom correlation. Instead, log-likelihoods for the posterior probabilities of each of the atoms within each molecule are calculated and used to choose the most representative atom. This process is described in further detail in the next section.

3.6 Feature Classification Using Reduced Dictionary

Shape classification and parameter estimation is accomplished using the reduced shape dictionaries. The first step involves selecting the appropriate molecule contained within $\hat{\mathbf{D}}$ that contains the most representative data. This step relies on the BP principle. The second step uses Bayes rule to derive and compute posterior log-likelihoods for each atom within the selected molecule. The atom corresponding to the largest log-likelihood is selected as the solution along with its corresponding parameter set. An overview of the algorithm proposed is provided in Figure 3.6.

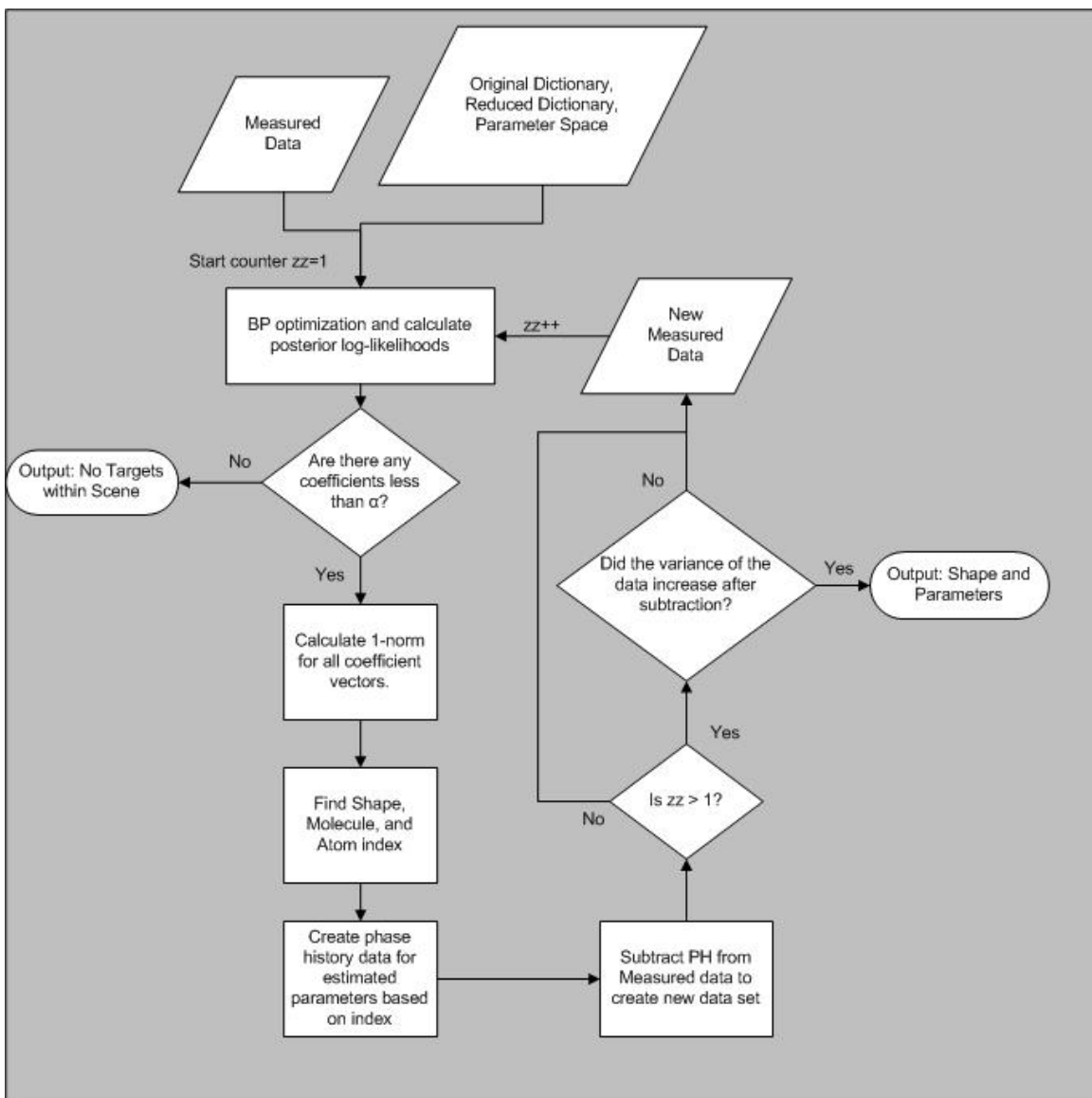


Figure 3.6: Overview of main algorithm.

3.6.1 Molecule Selection via Basis Pursuit. Once the dictionary has been reduced to $\hat{\mathbf{D}}$, the BP principle is used to estimate the molecule $\hat{\mathbf{D}}_m$ or set of molecules $\hat{\mathbf{D}}_1, \dots, \hat{\mathbf{D}}_M \in \hat{\mathbf{D}}$ that best represent the noisy phase history measurement signal $\mathbf{Y}(\Lambda)$.

Specifically, a Matlab[®] based algorithm called *spgl1* [11] is used to solve the BPDN problem

$$\min \|\psi\|_1 \quad \text{s.t.} \quad \left\| \mathbf{Y}(\mathbf{\Lambda}) - \hat{\mathbf{D}}_{\Gamma_j} \psi \right\|_2^2 < \epsilon \quad (3.8)$$

where $\|\cdot\|_1$ represents the ℓ_1 norm and the coefficient vector $\psi_{P \times 1}$ identifies the molecules that form the sparsest representation of $\mathbf{Y}(\mathbf{\Lambda})$. The *spgl1* algorithm reduces this problem to a linear program and solves using a spectral projected-gradient (SPG) algorithm. This SPG algorithm is described in detail in [11].

The output of this algorithm is a set of six coefficient vectors ψ each corresponding to a shape dictionary. Each of these vectors contains widely varying levels of sparseness and maximum values. The desired solution to the BP optimization corresponds to the sparsest vector containing the largest coefficient. However, many of the coefficients greatly exceed the optimum value of 1. Therefore, a user defined sparsity constraint λ along with a user defined coefficient ceiling α are used to select the appropriate solution vector. Specifically, the shape of the scatterer is classified by,

$$\max_{\mathbf{r}} (\max(\psi) - \lambda \cdot \|\psi\|_1) \quad \text{s.t.} \quad 0 \leq \max(\psi) \leq \alpha \quad (3.9)$$

which provides the index to the appropriate shape dictionary. The method of using a sparsity constraint λ and associated ℓ_1 norms is derived from the regularized LS cost function used in [6] and the ℓ_1 -regularized formulation in [17, 18].

The index of the maximum coefficient in the selected ψ is then used to identify the molecule $\hat{\mathbf{D}}_m$ containing the most representative data. Section 3.6.2 describes the process of determining the index pertaining to the solution atom within the selected $\hat{\mathbf{D}}_m$.

3.6.2 Atom Selection via Probability. The BP selected molecule $\hat{\mathbf{D}}_m$ contains highly correlated atoms, $\left| \langle \hat{\mathbf{S}}_i, \hat{\mathbf{S}}_j \rangle \right| \geq \eta$. For this research, where $\eta = 0.2$, these correlations are greater than 0.2. The BP algorithm requires a set of non-redundant, or uncorrelated atoms to accurately estimate the sparsest solution ψ_m [7].

Therefore, Bayes rule is used instead to derive an estimate via the posterior log-likelihoods $\ln p(\psi_m|\mathbf{Y})$ for each atom for the system described by,

$$\mathbf{Y} = \sum_m \hat{\mathbf{D}}_m \psi_m + \mathbf{w} \quad (3.10)$$

where

$$\mathbf{w} \sim \mathcal{N}(0, \sigma^2 \mathbf{I}) \quad (3.11)$$

The selected $N \times p$ matrix molecule is $\hat{\mathbf{D}}_m$ and ψ_m is the coefficient vector pertaining to that molecule indexed by m .

The conditional probability on measured data \mathbf{Y} is given by

$$p(\mathbf{Y}|\psi_m) = \frac{\exp(-\frac{1}{2\sigma^2}\mathbf{Q})}{(2\pi)^{N/2}\sigma^2} \quad (3.12)$$

where $\mathbf{Q} = (\mathbf{Y} - \hat{\mathbf{D}}_m \psi_m)^T (\mathbf{Y} - \hat{\mathbf{D}}_m \psi_m)$. Using Bayes rule we identify the posterior probability as

$$p(\psi_m|\mathbf{Y}) = \frac{p(\mathbf{Y}|\psi_m)p(\psi_m)}{p(\mathbf{Y})} \quad (3.13)$$

The denominator in (3.13) is given by,

$$p(\mathbf{Y}) = \int p(\mathbf{Y}|\psi_m)p(\psi_m)d\psi_m \quad (3.14)$$

The integral in (3.14) may become intractable depending on the selection of $p(\psi_m)$ as described in [18]. The numerical evaluation or approximation of $p(\mathbf{Y})$ utilizing the hierarchical prior derived in [18] is a future goal for this research. For now, we will only present a MAP estimate for ψ_m . Therefore, we consider the posterior log-likelihood given by

$$\ln p(\psi_m|\mathbf{Y}) \propto -\frac{1}{2\sigma^2}\mathbf{Q} + \ln p(\psi_m) + \text{const.} \quad (3.15)$$

For simplicity, we assume uniform costs $C_{00} = C_{11} = 0$, $C_{10} = C_{01} = 1$ and equal prior probabilities, $p(\psi_1) = p(\psi_2) = \dots = p(\psi_M)$ and $p(\psi_m) = \frac{1}{\# \text{ of atoms within molecule}} =$

$\frac{1}{M}$. These assumptions reduce (3.15) to

$$\ln p(\psi_m|\mathbf{Y}) \propto -\frac{1}{2\sigma^2}\mathbf{Q} + \text{const.} \quad (3.16)$$

The ML estimate is given by

$$\hat{\psi}_m = \arg \max_{\psi_m} (-(\mathbf{Y} - \hat{\mathbf{D}}_m \psi_m)^T (\mathbf{Y} - \hat{\mathbf{D}}_m \psi_m)) \quad (3.17)$$

For this specific case of uniform priors the MAP estimate is equal to the ML estimate. Referring back to the Bayes M-ary detection criteria derived in Section 2.3, we select $\hat{\psi}_m$ as the index for classification and the solution parameter set.

3.6.3 Multiple Shapes. The previous steps discussed in Section 3.6.1 and Section 3.6.2 work well for scenes containing only a single shape. To extract multiple features from a scene, a modification must be made to the algorithm.

An iterative phase history subtraction process is used to separate shapes from the measured data. The BP and probability methods will always extract the one feature in the scene that contributes the most significant radar scattering return. Once this feature is identified, the corresponding phase history within the appropriate dictionary is subtracted from the measured data. This method is applicable in the radar case since the scattering return from a scene is modeled as the sum of scatterers within the scene, given by

$$S(k, \Lambda; \Theta, \Gamma) = \sum_{q=1}^Q P_{\beta_q}(\Lambda; \Theta_q) M_{\Gamma_q}(k, \Lambda; \Theta_q) e^{jk\Delta R(\Lambda; \Theta_q)} \quad (3.18)$$

Once the extracted return is subtracted, the variance of the remaining measured data is used to determine whether all shapes within the scene have been accounted for. Specifically, the variance of the new data is compared to the variance of the previous data. If the variance has decreased, the extraction algorithm is repeated for

the new set of data. Otherwise, the extraction is halted and the previous extraction results are presented.

IV. Results

4.1 Chapter Overview

This chapter presents the results for the extraction steps presented in Chapter III. Three scenarios are set up to test the algorithm. The first scenario provides a baseline test. Feature extraction and parameter estimation are applied to a target scene containing a single shape, which directly corresponds to an atom within a dictionary. The second scenario tests the algorithm against target scenes comprised of a single shape with parameters outside of the defined dictionary parameter space. We will methodically step through each location and RCS parameter to present the level of instability for each parameter. The final scenario tests the algorithm’s ability to extract and estimate parameters for multiple shapes within a target scene. Specifically, this will test the algorithm’s iterative phase history subtraction process. The scenes will be comprised of three shapes of various combinations, each of which will directly correspond to a dictionary atom. We will conclude this chapter with a comprehensive results section. This section presents results of multiple Monte Carlo simulations used to characterize the effects of RCS and signal-to-noise ratio (SNR) on the algorithm. All target scenes are generated using 125 frequencies, HH, HV, and VV polarizations, and the non-linear flight path, shown in Figure 3.2.

4.2 Scenario 1 Results

In the first scenario, we attempt to extract a single canonical shape from a target scene. We will present only the dihedral and cylinder scenes as examples in this section. The results for the other 4 shapes are provided in Appendix B. For the cylinder scene example we will present the results from both molecule clustering methods. All other shapes rely on only the original clustering method, which replaces correlated atoms with a single representative atom equivalent to the mean of the grouped atoms within each molecule.

4.2.1 Dihedral Target. The dihedral target scene is simulated using atom 2473 from the dihedral dictionary. Random WGN is added to the dictionary atom to create the set of simulated measured data with an SNR of 30 dB. The specific parameters used to create the dihedral are shown in Table 4.1. The atom and molecule

Table 4.1: The parameters used to create the dihedral for scenario 1.

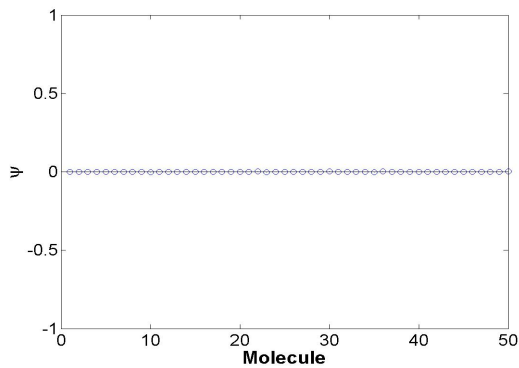
Shape	X	Y	Z	H	L	r	$\tilde{\gamma}$	$\tilde{\theta}$	$\tilde{\phi}$
dihedral	0	10	5	2	1	-	0	0	0

correspondences are provided in Table 4.2. Note that the “Molecule Atom” refers to the atom index within the molecule. The indexes are redefined within each molecule.

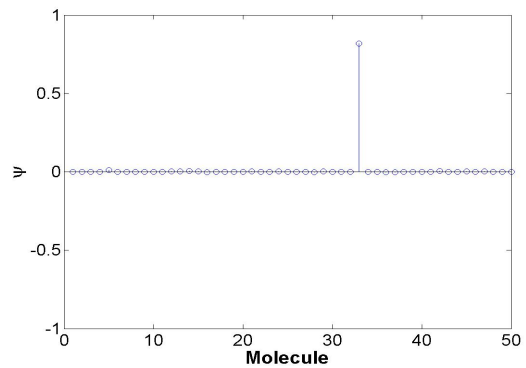
Table 4.2: Atom correspondence for measured shape.

Shape	Orig. Dict. Atom	Molecule	Molecule Atom
dihedral	2473	33	60

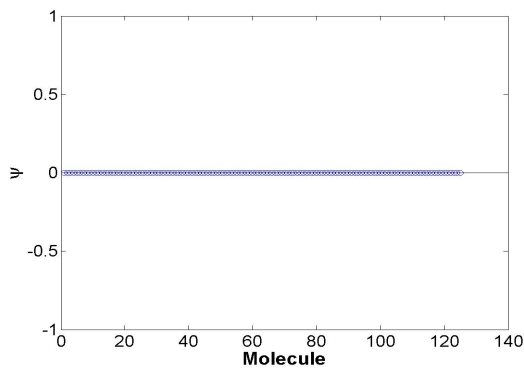
The BP algorithm described in Section 3.6.1 is used to search through each of the reduced shape dictionaries to identify the correct molecule which contains the best representation of the measured data. The six resulting coefficient plots, separated by shape, are provided in Figure 4.1.



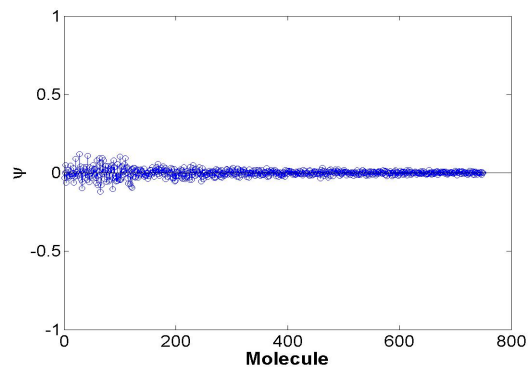
(a) BP result using the reduced plate dictionary.



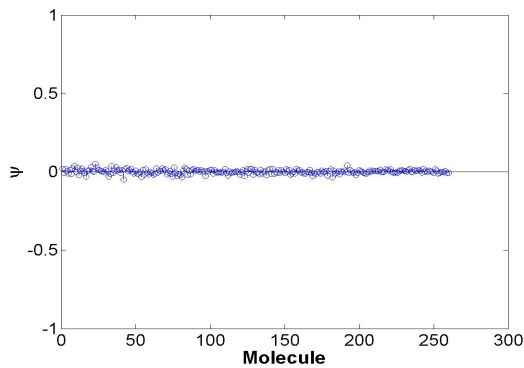
(b) BP result using the reduced dihedral dictionary.



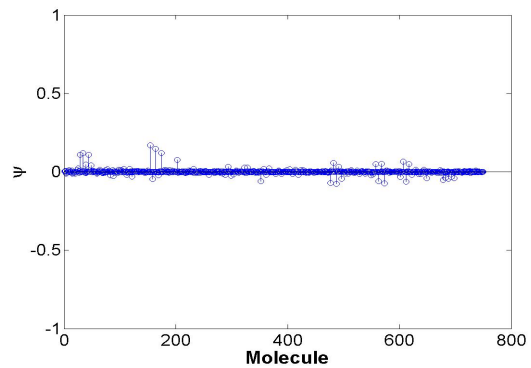
(c) BP result using the reduced trihedral dictionary.



(d) BP result using the reduced sphere dictionary.



(e) BP result using the reduced cylinder dictionary.



(f) BP result using the reduced top-hat dictionary.

Figure 4.1: BP results for each of the reduced shape dictionaries used in the feature extraction problem in scenario 1, dihedral example.

The shape is classified based on the largest coefficient value and a user defined sparsity constraint, $\lambda = 0.2$. The maximum coefficient returned by the BP algorithm for each of the shape dictionaries and the sparsities, described by $\|\psi\|_1$, are provided in Table 4.3. The sparsest solution that corresponds to the maximum coefficient $\hat{\psi}$,

Table 4.3: Maximum coefficients from each shape dictionary along with the ℓ_1 norm (sparsity descriptor).

Shape	$\max(\psi)$	$\ \psi\ _1$	$(\max(\psi) - \lambda \cdot \ \psi\ _1)$
plate	0.0018	0.0348	-0.0052
dihedral	0.8172	0.8910	0.6390
sphere	0.1205	11.2907	-2.1376
top-hat	0.1689	4.2640	-0.6839
trihedral	1.4897×10^{-4}	0.0065	-0.0011
cylinder	0.0516	2.8059	-0.5096

falling between the values of 0 and α is chosen. For the examples presented in this research, α is set to 3. This value is chosen to allow some variance around the optimum value of 1 due to added noise. Specifically, the shape dictionary $\hat{\mathbf{D}}$ is chosen by

$$\max(\max(\psi) - \lambda \cdot \|\psi\|_1) \quad \text{s.t. } 0 \leq \max(\psi) \leq 3 \quad (4.1)$$

This method correctly leads to a dihedral classification. The dihedral dictionary molecule corresponding to the largest coefficient within ψ is chosen as the “sub-dictionary” used for parameter estimation via the MAP estimator. The largest coefficient correctly corresponds to molecule 33.

Estimates of the posterior log-likelihoods are calculated for each atom within this molecule. These estimates are plotted and provided in Figure 4.2. The largest log-likelihood corresponds to the correct atom (atom 60) as shown by the associated parameters provided in Table 4.4. The algorithm successfully chose the correct feature and parameters for the dihedral scene.

4.2.2 Cylinder Target. In this example, we present two sets of results from the target scene containing a single cylinder. The first set of results is achieved using

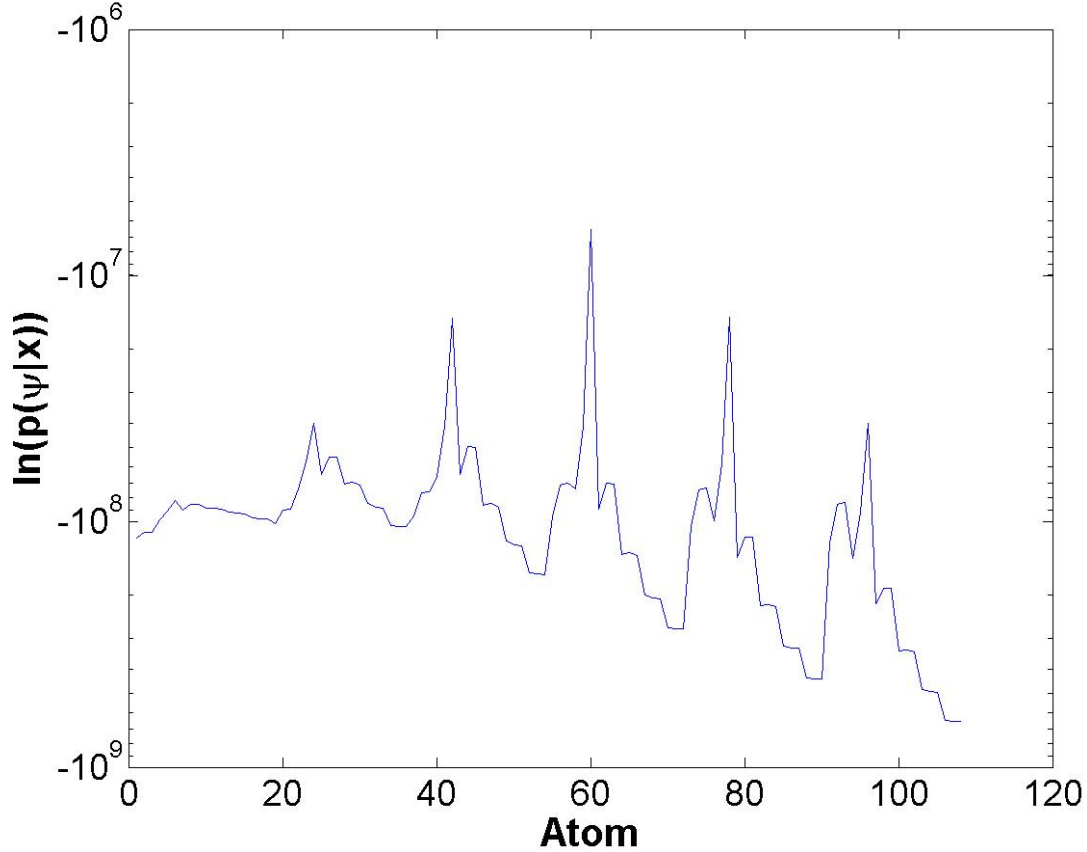


Figure 4.2: Posterior log-likelihood estimates associated with each atom within the selected dihedral molecule (True Atom = 60).

the reduced cylinder dictionary created using the original molecule method. The second set of results is achieved using the second reduced cylinder dictionary created using the modified molecule method.

The cylinder within the target scene corresponds to atom 10 from the cylinder dictionary. Again, we add WGN to the atom to achieve a measured SNR of 30 dB. The specific parameters used to create the cylinder are shown in Table 4.5. The atom and molecule correspondences are provided in Table 4.6.

Table 4.4: Estimated versus true parameters for scenario 1, dihedral example.

Shape	X	Y	Z	H	L	r	$\tilde{\gamma}$	$\tilde{\theta}$	$\tilde{\phi}$
True dihedral	0	10	5	2	1	-	0	0	0
Estimated dihedral	0	10	5	2	1	-	0	0	0

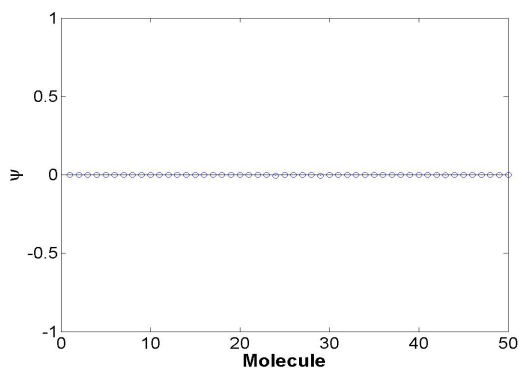
Table 4.5: Parameters used to create the cylinder for scenario 1.

Shape	X	Y	Z	H	L	r	$\tilde{\gamma}$	$\tilde{\theta}$	$\tilde{\phi}$
cylinder	10	-5	-10	-	0.5	0.5	0	0	0

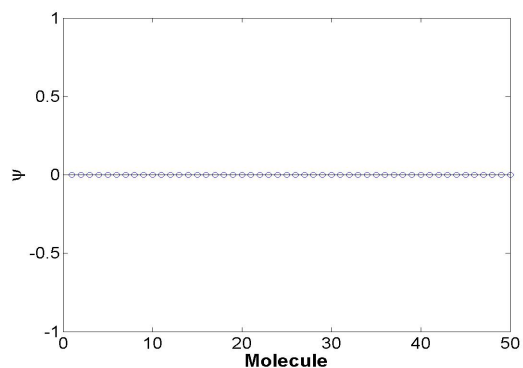
Table 4.6: Atom correspondence for measured shape.

Shape	Orig. Dict. Atom	Molecule	Molecule Atom
cylinder	10	10	1

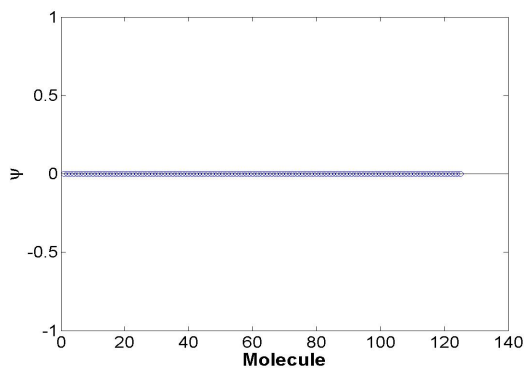
In the first attempt for extraction and parameter estimation, we use the reduced cylinder dictionary, created using the mean atom replacements in the original molecule grouping algorithm. The BP and log-likelihood plots for the extraction attempt using the original reduced cylinder dictionary are provided in Figure 4.3 and Figure 4.5.



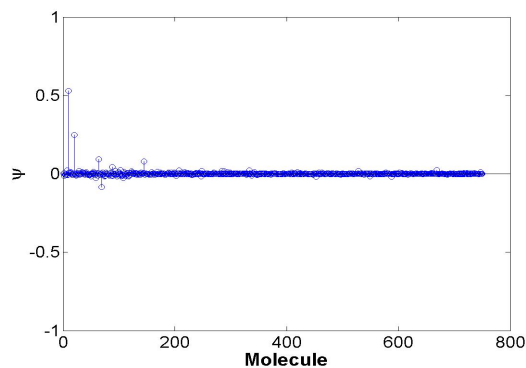
(a) BP result using the reduced plate dictionary.



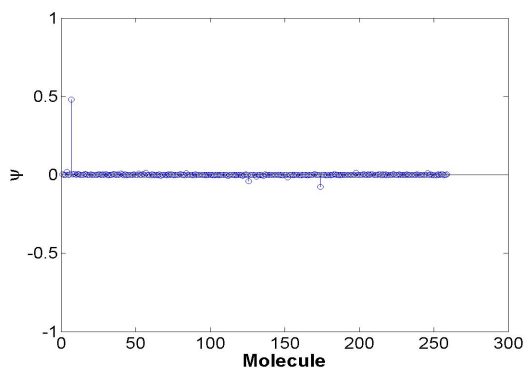
(b) BP result using the reduced dihedral dictionary.



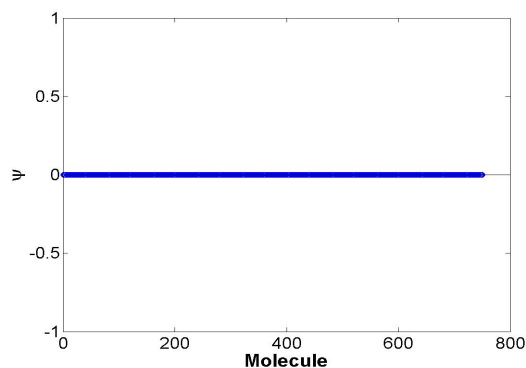
(c) BP result using the reduced trihedral dictionary.



(d) BP result using the reduced sphere dictionary.



(e) BP result using the reduced cylinder dictionary (original molecule clustering).



(f) BP result using the reduced top-hat dictionary.

Figure 4.3: BP results for each of the reduced shape dictionaries used in the feature extraction problem for the cylinder target scene in scenario 1. The reduced cylinder dictionary used for these results is generated using the original molecule method.

The shape is classified based on the largest coefficient value and the user defined sparsity constraint. The maximum coefficient returned by the BP algorithm for each of the shape dictionaries and the sparsities, described by $\|\psi\|_1$, are provided in Table 4.7.

Table 4.7: Maximum coefficients from each shape dictionary along with the ℓ_1 norm (sparsity descriptor) for scenario 1, cylinder example 1, using original molecule method.

Shape	$\max(\psi)$	$\ \psi\ _1$	$(\max(\psi) - \lambda \cdot \ \psi\ _1)$
plate	8.2595×10^{-4}	0.0176	-0.0027
dihedral	2.5545×10^{-5}	6.8228×10^{-4}	-1.1091×10^{-4}
sphere	0.5220	2.4421	0.0336
top-hat	8.7002×10^{-5}	0.0143	-0.0028
triangular	8.7963×10^{-5}	0.0012	-1.5810×10^{-4}
cylinder	0.4779	0.9161	0.2910

The sparsities and coefficients provided in Table 4.7 correctly lead to a cylinder classification. However, a zoomed-in version of the cylinder BP coefficient plot, shown in Figure 4.4, reveals that the largest coefficient corresponds to molecule 7 instead of the correct molecule 10. Therefore, the atom corresponding to the largest log-likelihood, shown in Figure 4.5, does not correspond to the correct cylinder parameter set, leading to incorrect parameter estimation, shown in Table 4.8.

Table 4.8: Estimated versus true parameters for scenario 1 using original reduced cylinder dictionary.

Shape	X	Y	Z	H	L	r	$\tilde{\gamma}$	$\tilde{\theta}$	$\tilde{\phi}$
True cylinder	10	-5	-10	-	0.5	0.5	0	0	0
Estimated cylinder	-5	-5	-10	-	0.5	0.5	0	0	0

In the next attempt, we use the reduced cylinder dictionary, created using the modified molecule algorithm. This method minimizes all of the off-diagonal correlations within the cylinder dictionary, which the original method failed to accomplish. The BP and log-likelihood plots are provided in Figure 4.6 and Figure 4.8.

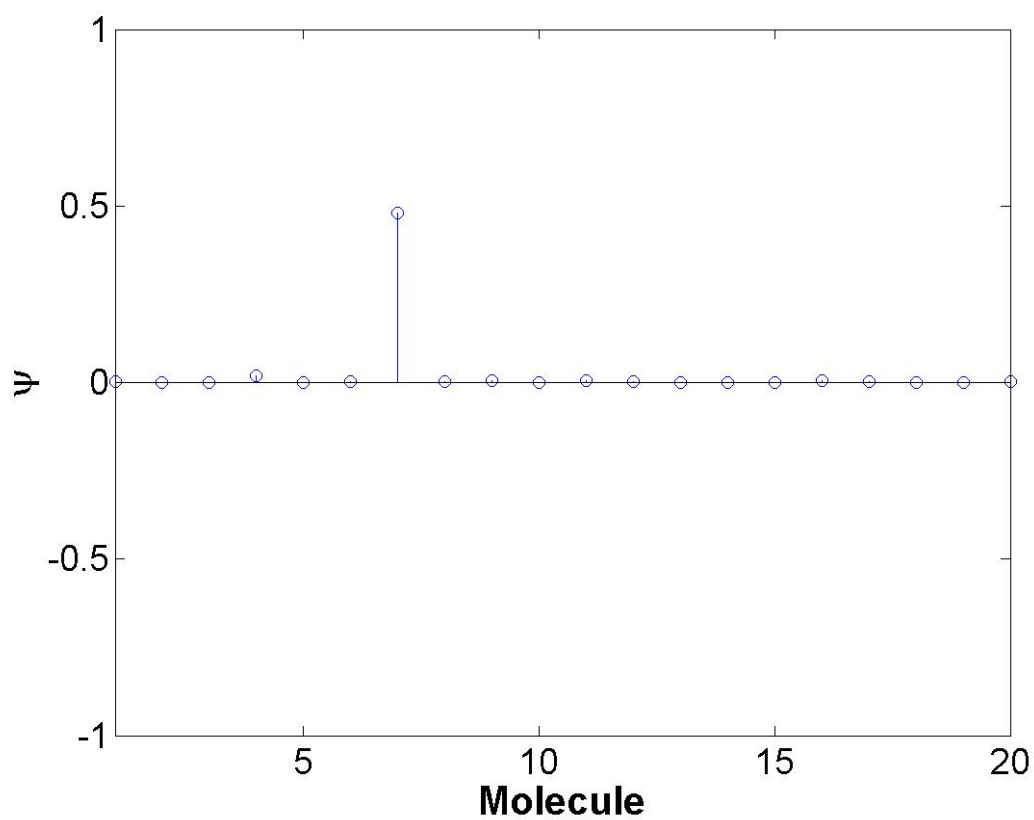


Figure 4.4: Zoomed in BP result for the reduced cylinder dictionary created using the original molecule method.

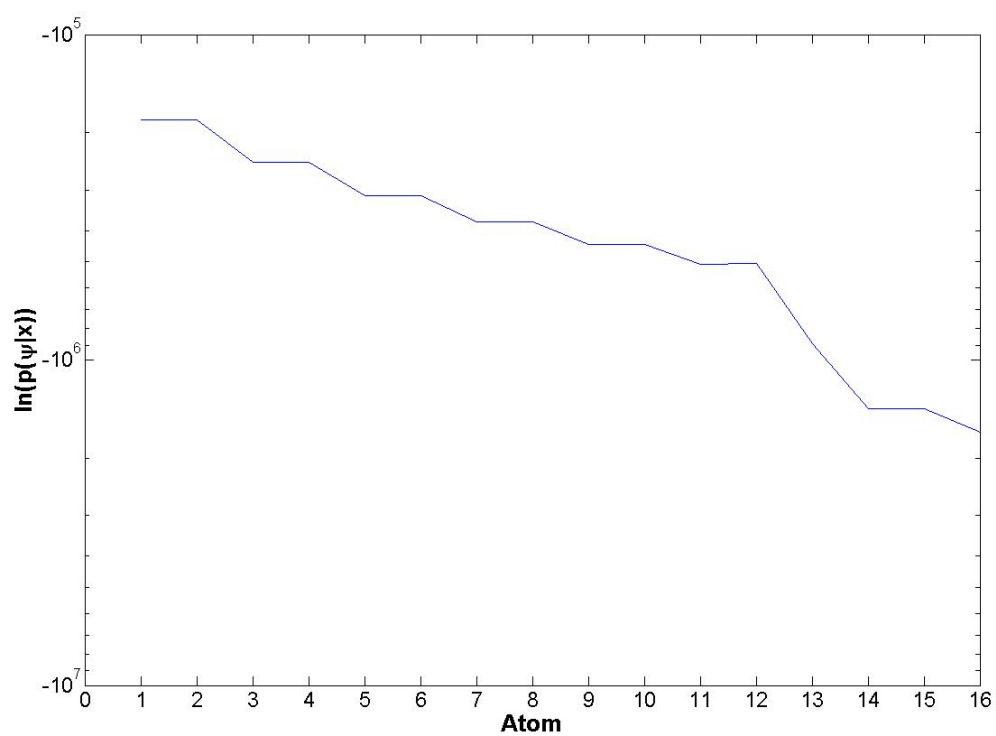
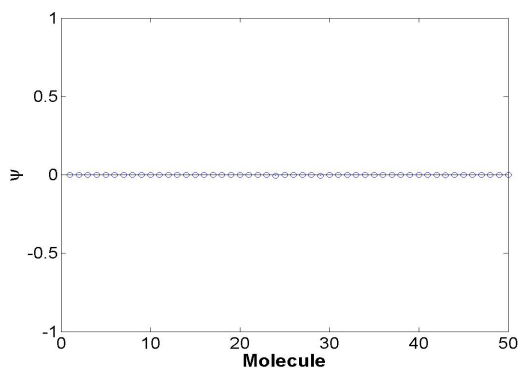
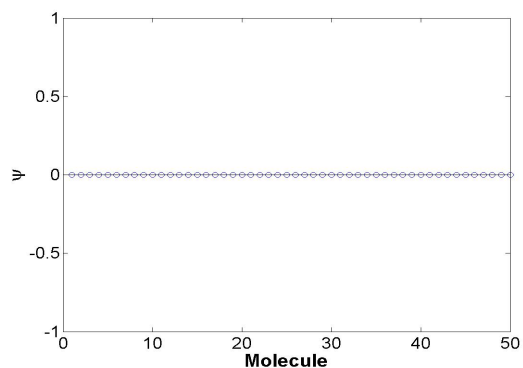


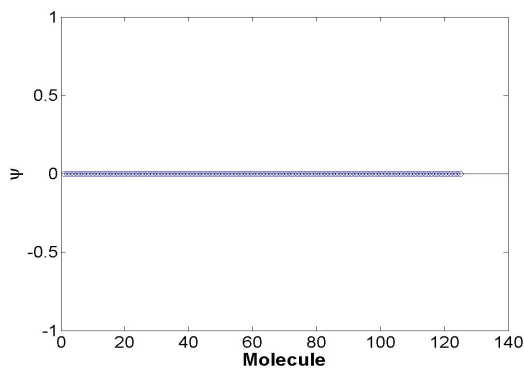
Figure 4.5: Posterior log-likelihood estimates associated with each atom within the selected cylinder molecule.



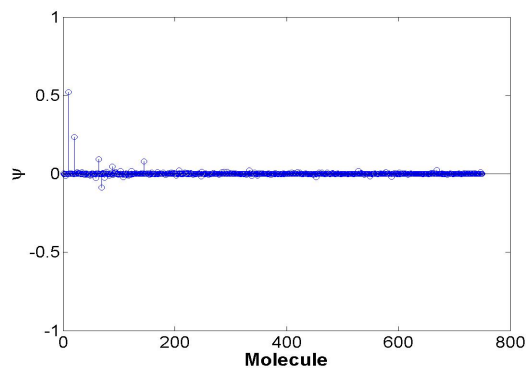
(a) BP result using the reduced plate dictionary.



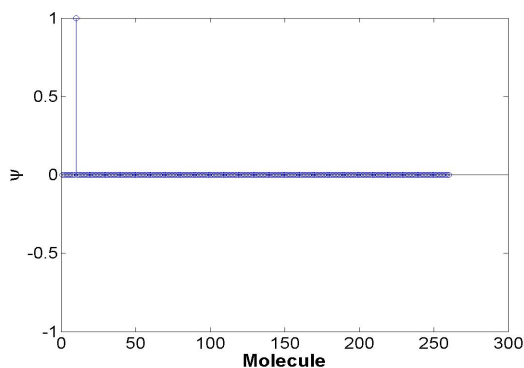
(b) BP result using the reduced dihedral dictionary.



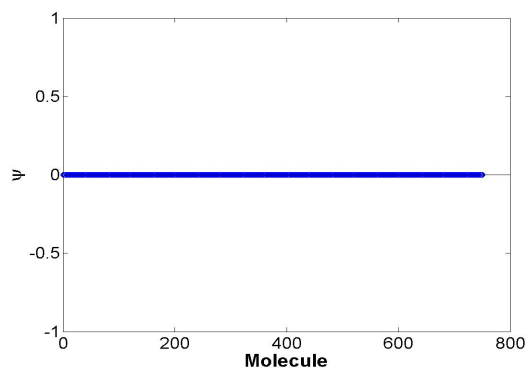
(c) BP result using the reduced trihedral dictionary.



(d) BP result using the reduced sphere dictionary.



(e) BP result using the reduced cylinder dictionary (modified molecule clustering).



(f) BP result using the reduced top-hat dictionary.

Figure 4.6: BP results for each of the reduced shape dictionaries used in the feature extraction problem for the cylinder target scene in scenario 1. The reduced cylinder dictionary used for these results is generated using the modified molecule method.

The maximum coefficient returned by the BP algorithm for each of the shape dictionaries and the sparsities, described by $\|\psi\|_1$, are provided in Table 4.9.

Table 4.9: Maximum coefficients from each shape dictionary along with the ℓ_1 norm (sparsity descriptor) for scenario 1, cylinder example 2, using modified molecule method.

Shape	$\max(\psi)$	$\ \psi\ _1$	$(\max(\psi) - \lambda \cdot \ \psi\ _1)$
plate	8.2595×10^{-4}	0.0176	-0.0027
dihedral	2.5545×10^{-5}	6.8228×10^{-4}	-1.1091×10^{-4}
sphere	0.5220	2.4421	0.0336
top-hat	8.7002×10^{-5}	0.0143	-0.0028
trihedral	8.7963×10^{-5}	0.0012	-1.5810×10^{-4}
cylinder	1.0000	1.0581	0.7884

Again, the sparsities and coefficients provided in Table 4.9 correctly lead to a cylinder classification. The zoomed-in version of the cylinder BP coefficient plot, shown in Figure 4.7, reveals that the largest coefficient corresponds to the correct molecule (molecule 10). The atom corresponding to the largest log-likelihood, shown in Figure 4.8, corresponds to the correct cylinder parameter set, leading to correct parameter estimation, shown in Table 4.10.

Table 4.10: Estimated versus true parameters for scenario 1 using modified reduced cylinder dictionary.

Shape	X	Y	Z	H	L	r	$\tilde{\gamma}$	$\tilde{\theta}$	$\tilde{\phi}$
True cylinder	10	-5	-10	-	0.5	0.5	0	0	0
Estimated cylinder	10	-5	-10	-	0.5	0.5	0	0	0

Based on these results, we use only the modified reduced dictionary for the cylinder for all other scenarios. This method was attempted with all other shapes, but led to incorrect classifications. Therefore, all other shapes utilize the original reduced dictionaries. The next scenario will test the ability of the algorithm to estimate shape configurations that do not directly correspond to a specific atom.

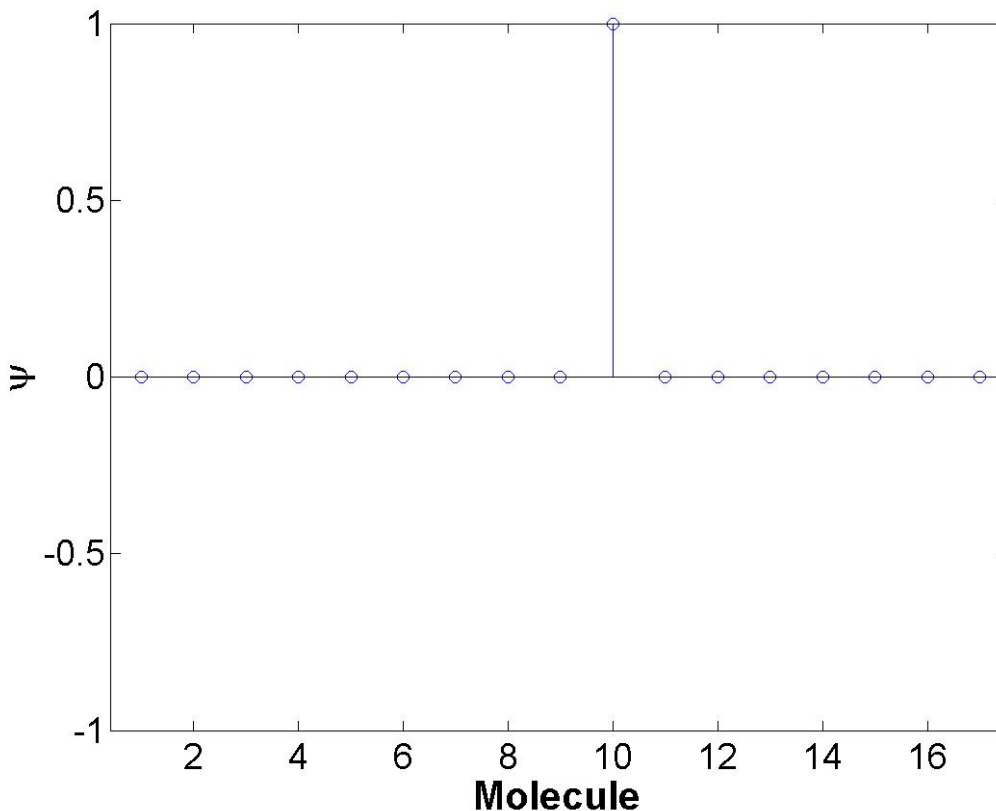


Figure 4.7: Zoomed in BP result for the reduced cylinder dictionary created using the modified molecule method.

4.3 Scenario 2 Results

The target scenes used in scenario 2 contain only a single shape, as in scenario 1; however, each shape corresponds to a parameter set that does not directly relate to a specific dictionary atom. For each of the six shapes we will choose one parameter at a time to fall between two atoms. We will step through each of the variable parameters ($\Theta = [x, y, z, H, L, r]$), each time holding all other parameters to a dictionary contained set. This approach methodically identifies the parameters for each shape that lead to misclassifications when not directly represented within a dictionary.

In this section we present only the results for the plate target example with five variations of parameters. The results for the other five shapes are contained in Appendix C.

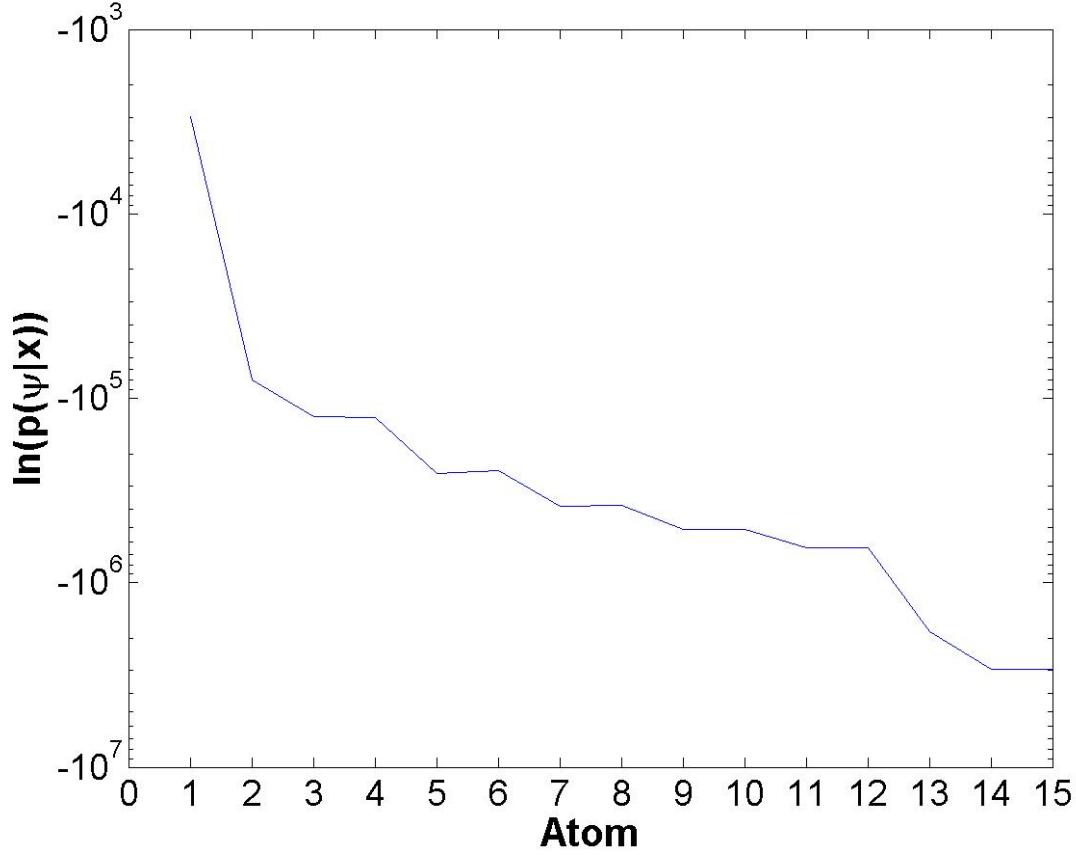


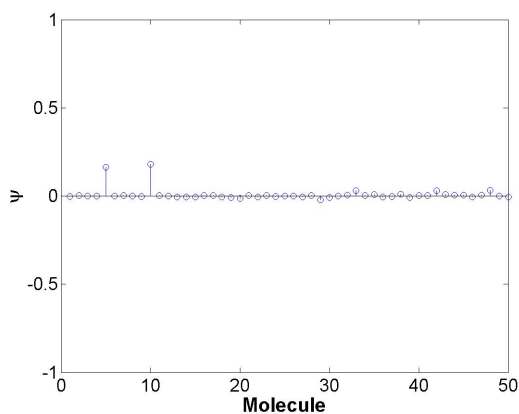
Figure 4.8: Posterior log-likelihood estimates associated with each atom within the selected cylinder molecule.

4.3.1 X Parameter. In the first example, we generate a plate target located at $x = 4$ m with an SNR of 30 dB. The dictionary parameter space used for the location parameters x, y, z is defined from -10 m to 10 m at 5 m increments. Therefore, the location used does not correspond directly to a dictionary entry. The plate target is simulated using the parameters listed in Table 4.11.

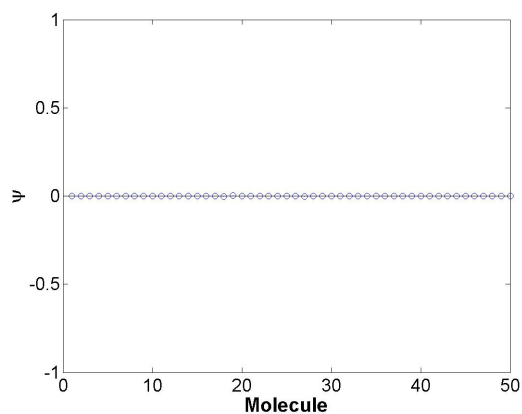
Table 4.11: The parameters used to create the plate target for scenario 2, example 1.

Shape	X	Y	Z	H	L	r	$\tilde{\gamma}$	$\tilde{\theta}$	$\tilde{\phi}$
plate	4	0	0	2	1	-	0	-30	0

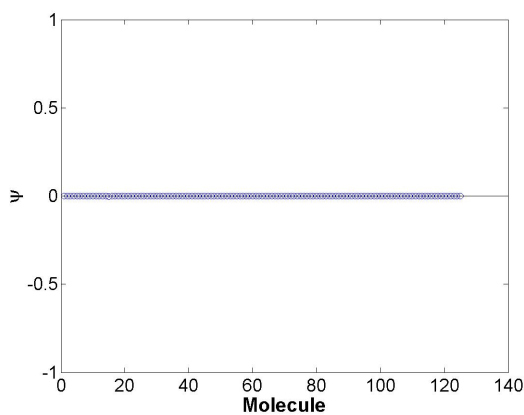
Once again, the extraction and estimation algorithm is implemented on the target scene. The BP results for each shape are provided in Figure 4.9.



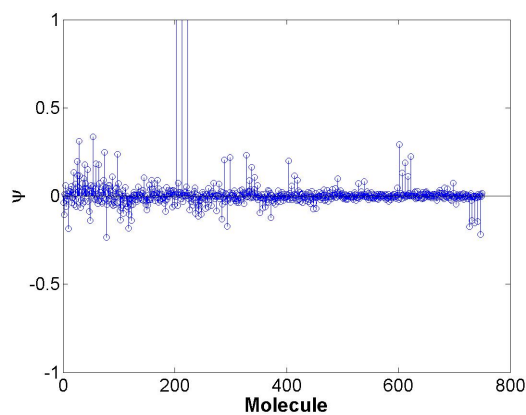
(a) BP result using the reduced plate dictionary.



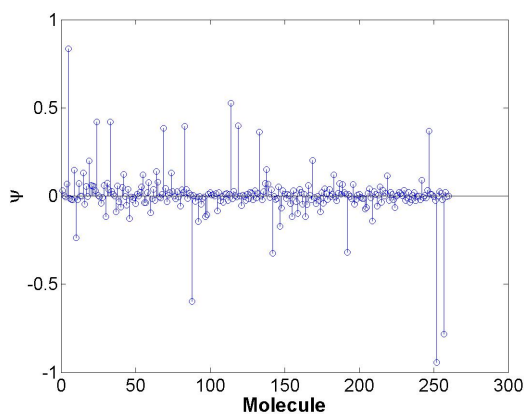
(b) BP result using the reduced dihedral dictionary.



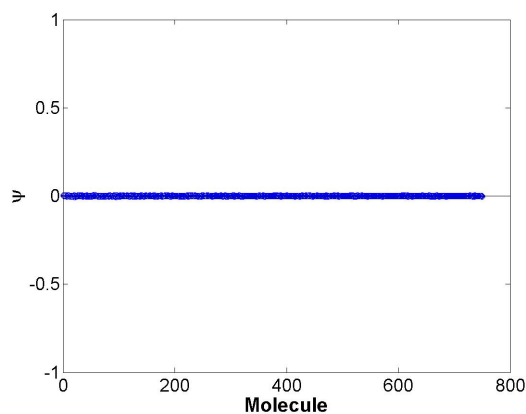
(c) BP result using the reduced trihedral dictionary.



(d) BP result using the reduced sphere dictionary.



(e) BP result using the reduced cylinder dictionary.



(f) BP result using the reduced top-hat dictionary.

Figure 4.9: BP results for each of the reduced shape dictionaries used in the feature extraction problem in scenario 2, plate example 1.

The maximum coefficient returned by the BP algorithm for each of the shape dictionaries and the sparsities, described by $\|\psi\|_1$, are provided in Table 4.12. This

Table 4.12: Maximum coefficients from each shape dictionary along with the ℓ_1 norm (sparsity descriptor) for scenario 2, plate example 1.

Shape	$\max(\psi)$	$\ \psi\ _1$	$(\max(\psi) - \lambda \cdot \ \psi\ _1)$
plate	0.1789	0.6361	0.0517
dihedral	0.0014	0.0301	-0.0046
sphere	1.4350	25.2137	-3.6077
top-hat	0.0058	0.7022	-0.1347
trihedral	2.0788×10^{-4}	0.0130	-0.0024
cylinder	0.8354	15.7779	-2.3202

method correctly leads to a plate classification. However, the algorithm incorrectly estimates both the size and location parameters, as shown in Table 4.13.

Table 4.13: Estimated versus true parameters for scenario 2, plate example 1.

Shape	X	Y	Z	H	L	r	$\tilde{\gamma}$	$\tilde{\theta}$	$\tilde{\phi}$
True plate	4	0	0	2	1	-	0	-30	0
Expected plate	5	0	0	2	1	-	0	-30	0
Estimated plate	10	5	-10	3	0.5	-	0	-30	0

Initially, we make the hypothesis that the parameter set extracted should be the closest dictionary contained representative parameter set, $\Theta = [5, 0, 0, 2, 1, 0, 0, -30, 0]$ (atom 2439). Although this atom seems closer, the range profile provided in Figure 4.10 shows that the extracted parameter set, $\Theta = [10, 5, -10, 3, 0.5, 0, 0, -30, 0]$ (atom 3770) is more representative in the range, or X , dimension. This range error may have led to a larger LS error and the incorrect parameter set estimation. The LS errors given by $\|\mathbf{x} - \mathbf{s}(\Theta_n)\|_2^2$, for $n = [3770, 2439]$ are provided in Table 4.14. The

Table 4.14: LS errors for the extracted and hypothesized data sets for scenario 2, plate example 1.

Data	$\ \mathbf{x} - \mathbf{s}(\Theta_n)\ _2^2$
Extracted	3.9014×10^7
Closest	7.4880×10^7

minimum LS error is equivalent to the MAP estimate, as described in Chapter II.

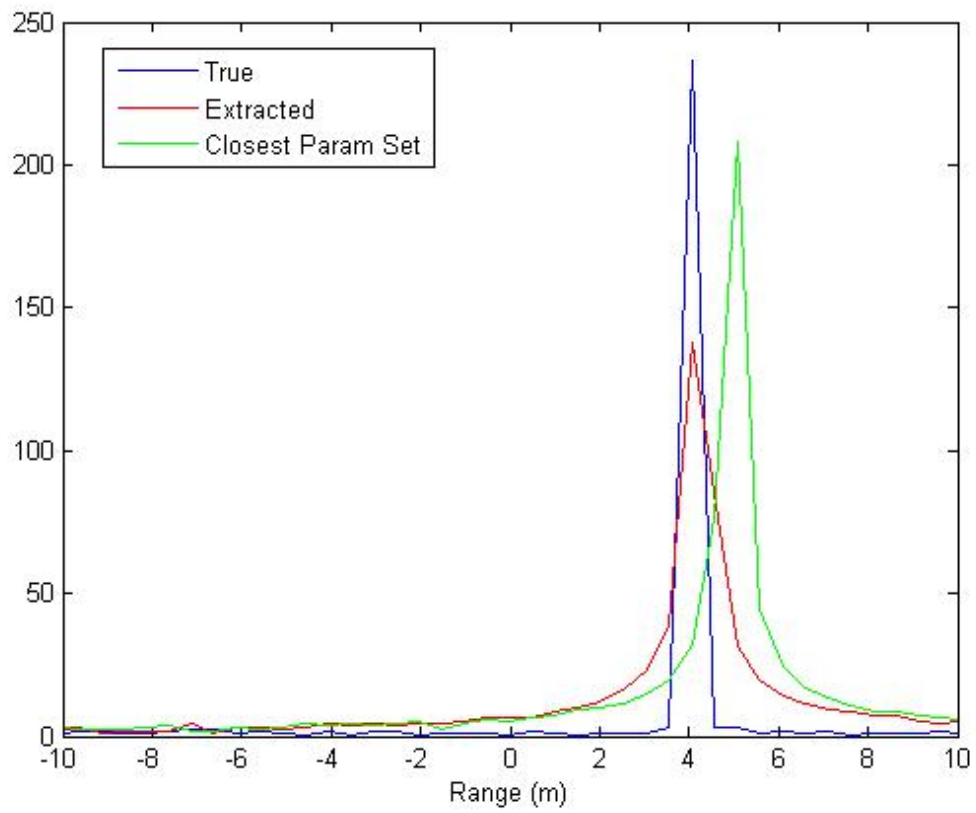


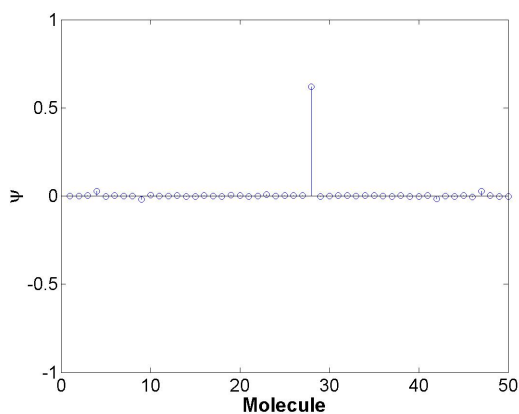
Figure 4.10: Range profile for the true, extracted, and close simulated plate targets.

4.3.2 *Y Parameter.* In this example, we generate a plate target located at $y = 4$ m with an SNR of 30 dB. Again, this location falls outside of the parameter space defined for the dictionary. We set the other parameters within the defined dictionary sample space. The plate target is simulated using the parameters listed in Table 4.15.

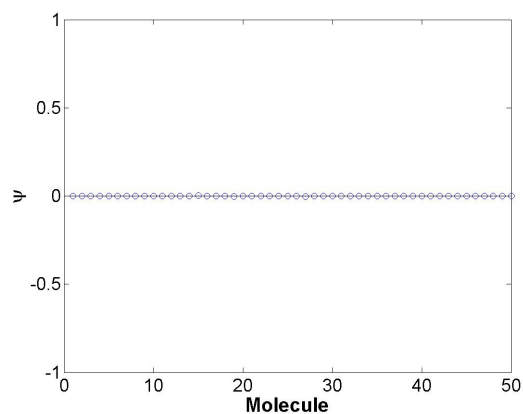
Table 4.15: The parameters used to create the plate target for scenario 2, example 2.

Shape	X	Y	Z	H	L	r	$\tilde{\gamma}$	$\tilde{\theta}$	$\tilde{\phi}$
plate	0	4	0	2	1	-	0	-30	0

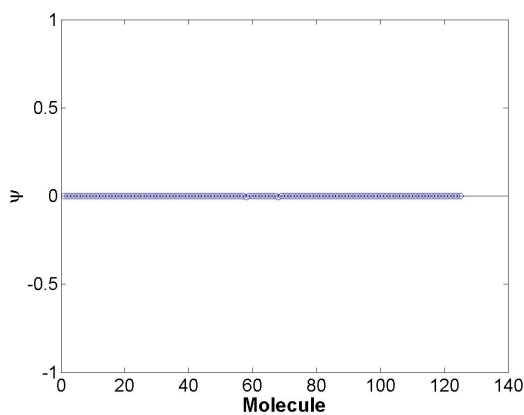
The BP results for each shape are provided in Figure 4.11.



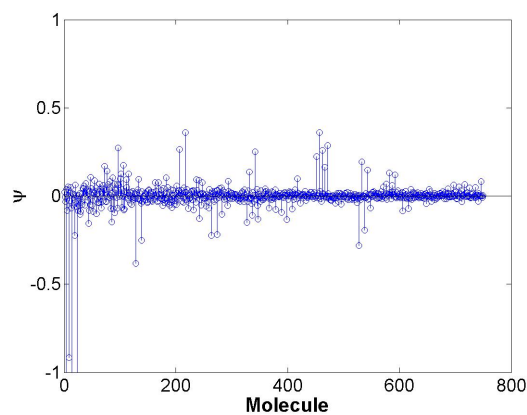
(a) BP result using the reduced plate dictionary.



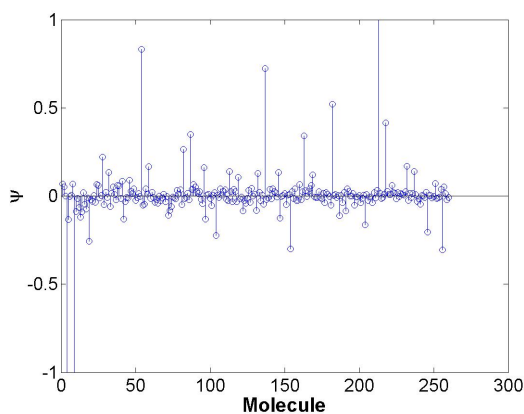
(b) BP result using the reduced dihedral dictionary.



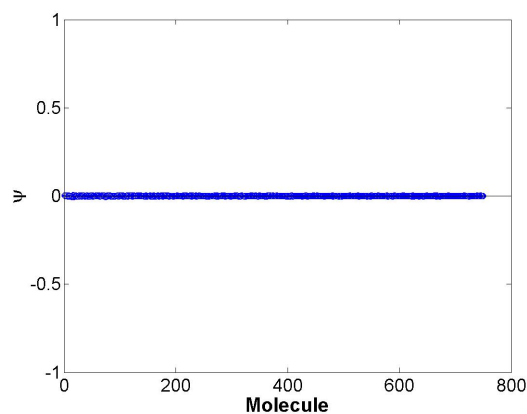
(c) BP result using the reduced trihedral dictionary.



(d) BP result using the reduced sphere dictionary.



(e) BP result using the reduced cylinder dictionary.



(f) BP result using the reduced top-hat dictionary.

Figure 4.11: BP results for each of the reduced shape dictionaries used in the feature extraction problem in scenario 2, example 2.

The maximum coefficient returned by the BP algorithm for each of the shape dictionaries and the sparsities, described by $\|\psi\|_1$, are provided in Table 4.16.

Table 4.16: Maximum coefficients from each shape dictionary along with the ℓ_1 norm (sparsity descriptor) for scenario 2, plate example 2.

Shape	$\max(\psi)$	$\ \psi\ _1$	$(\max(\psi) - \lambda \cdot \ \psi\ _1)$
plate	0.6194	0.8139	0.4566
dihedral	0.0019	0.0351	-0.0051
sphere	0.3602	29.0131	-5.4425
top-hat	0.0041	0.7111	-0.1381
trihedral	4.4132×10^{-4}	0.0213	-0.0038
cylinder	1.0592	19.2665	-2.7941

This method correctly leads to a plate classification. The algorithm incorrectly estimates the y location parameter, but correctly estimates all other parameters, as shown in Table 4.17. The log-likelihood plot for the molecule selected is provided in

Table 4.17: Estimated versus true parameters for scenario 2, plate example 2.

Shape	X	Y	Z	H	L	r	$\tilde{\gamma}$	$\tilde{\theta}$	$\tilde{\phi}$
True plate	0	4	0	2	1	-	0	-30	0
Expected plate	0	5	0	2	1	-	0	-30	0
Estimated plate	0	-5	0	2	1	-	0	-30	0

Figure 4.12. Initially, we assume that the algorithm should choose the plate corresponding to the closest parameter set. Therefore, the expected parameter set would be $\Theta = [0, 5, 0, 2, 1, 0, 0, -30, 0]$. This set corresponds to atom 40 within the molecule depicted in Figure 4.12. The extracted parameter set corresponds to atom 39. Again, the difference in likelihoods are due to a lower LS error between the extracted data and the measured data. The total LS errors given by $\|\mathbf{x} - \mathbf{s}(\Theta_n)\|_2^2$, for $n = [39, 40]$ are provided in Table 4.18. The lowest LS error corresponds to the extracted data set and is equivalent to the largest log-likelihood. Next, we will repeat this process for the z parameter.

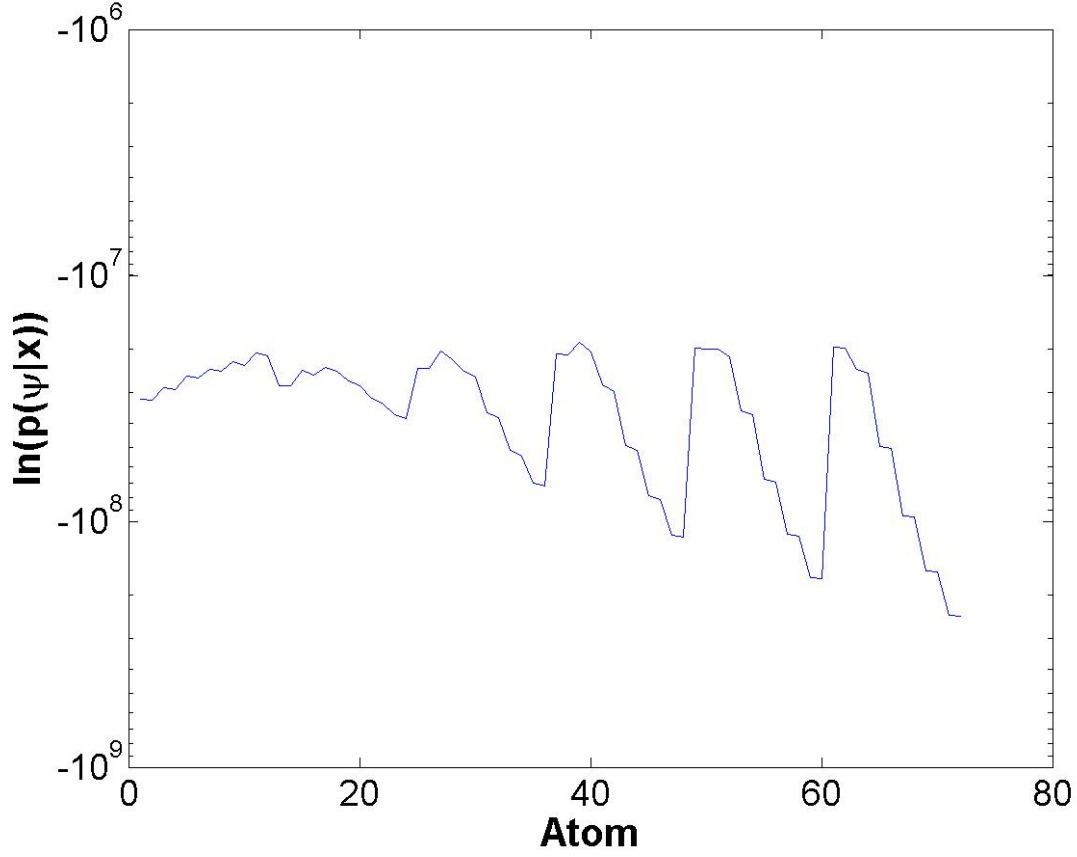


Figure 4.12: Posterior log-likelihood estimates associated with each atom within the selected plate molecule.

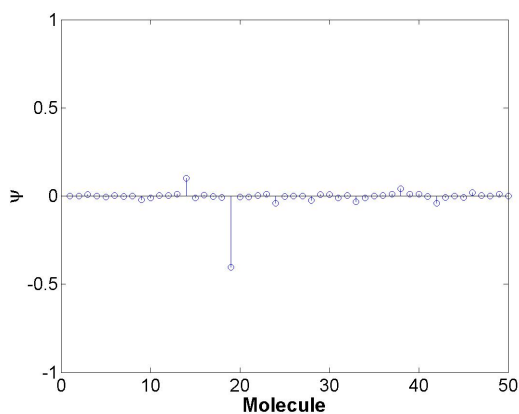
4.3.3 Z Parameter. In this example, we generate a plate target located at $z = 4$ m with an SNR of 30 dB. The plate target is simulated using the parameters listed in Table 4.19. The BP results for each shape are provided in Figure 4.13.

Table 4.18: LS errors for the extracted and hypothesized data sets for scenario 2, plate example 2.

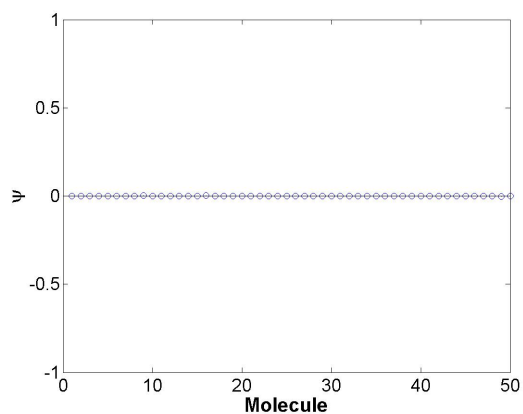
Data	$\ \mathbf{x} - \mathbf{s}(\Theta_n)\ _2^2$
Extracted	2.5269×10^7
Closest	2.7067×10^7

Table 4.19: The parameters used to create the plate target for scenario 2, example 3.

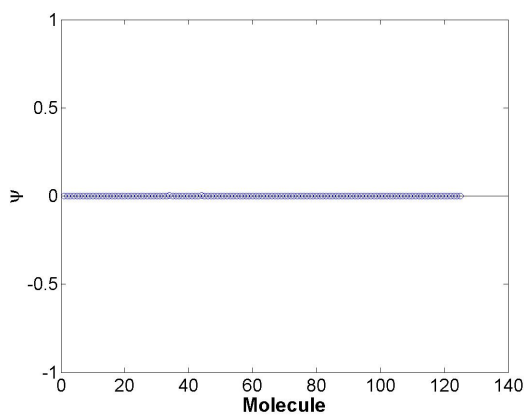
Shape	X	Y	Z	H	L	r	$\tilde{\gamma}$	$\tilde{\theta}$	$\tilde{\phi}$
plate	0	0	4	2	1	-	0	-30	0



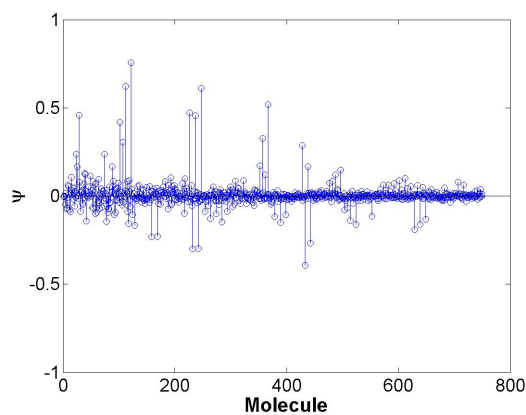
(a) BP result using the reduced plate dictionary.



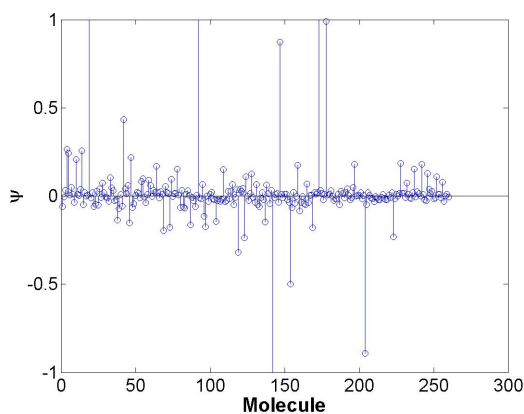
(b) BP result using the reduced dihedral dictionary.



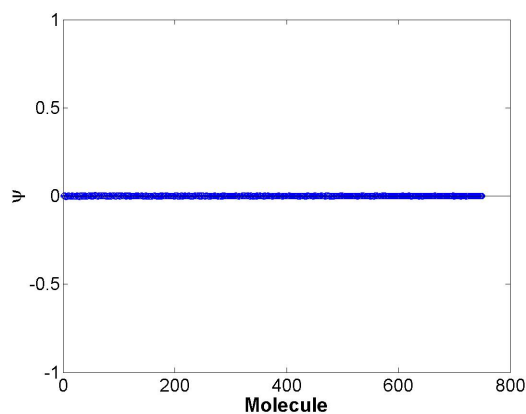
(c) BP result using the reduced trihedral dictionary.



(d) BP result using the reduced sphere dictionary.



(e) BP result using the reduced cylinder dictionary.



(f) BP result using the reduced top-hat dictionary.

Figure 4.13: BP results for the first iteration for each of the reduced shape dictionaries used in the feature extraction problem in scenario 2, plate example 3.

The maximum coefficient returned by the BP algorithm for each of the shape dictionaries and the sparsities, described by $\|\psi\|_1$, are provided in Table 4.20.

Table 4.20: Maximum coefficients from each shape dictionary along with the ℓ_1 norm (sparsity descriptor) for scenario 2, plate example 3.

Shape	$\max(\psi)$	$\ \psi\ _1$	$(\max(\psi) - \lambda \cdot \ \psi\ _1)$
plate	0.1021	0.9386	-0.0856
dihedral	0.0015	0.0300	-0.0046
sphere	0.7549	25.5425	-4.3536
top-hat	0.0042	0.6946	-0.1347
trihedral	0.0030	0.0170	-3.5957×10^{-4}
cylinder	1.6443	20.2092	-2.3975

This method incorrectly classifies the shape as a trihedral. The associated extracted parameter set is provided in Table 4.21. This misclassification is due to the

Table 4.21: Estimated versus true parameters for scenario 2, plate example 3.

Shape	X	Y	Z	H	L	r	$\tilde{\gamma}$	$\tilde{\theta}$	$\tilde{\phi}$
True plate	0	0	4	2	1	-	0	-30	0
Expected plate	0	0	5	2	1	-	0	-30	0
Estimated trihedral	5	5	-5	0.5	-	-	0	0	0

low sparsity value of the trihedral. This may be mitigated by separating shapes based on some threshold on $\max(\psi)$. Once separated, $(\max(\psi) - \lambda \cdot \|\psi\|_1)$ could then be compared for each of the separated shapes. For example, if the threshold was set to 0.1, the plate, sphere and cylinder would be extracted for comparison. In this case, the comparison would lead to a correct classification. Many of the results for the other shape examples misclassify as a trihedral because of this and mitigation techniques should be explored in future research.

The total LS errors for the extracted data versus the hypothesized closest data are provided in Table 4.22.

4.3.4 RCS Parameters. In this section we discuss the results of two example target scenes. Each of the scenes includes a plate that is generated using a length or

Table 4.22: LS errors for the extracted and hypothesized data sets for scenario 2, plate example 3.

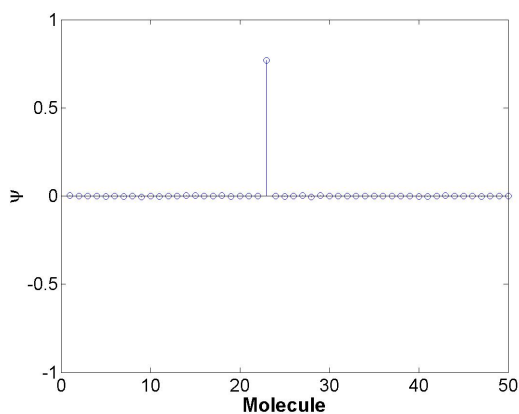
Data	$\ \mathbf{x} - \mathbf{s}(\Theta_n)\ _2^2$
Extracted	1.0110×10^8
Closest	7.4781×10^7

height parameter that falls outside of the dictionary parameter space resolution with an SNR of 30 dB. The dictionary parameter space used for the RCS parameters L , H , r is defined based on a 0.5 m resolution. The plate targets are simulated using the parameters listed in Table 4.23.

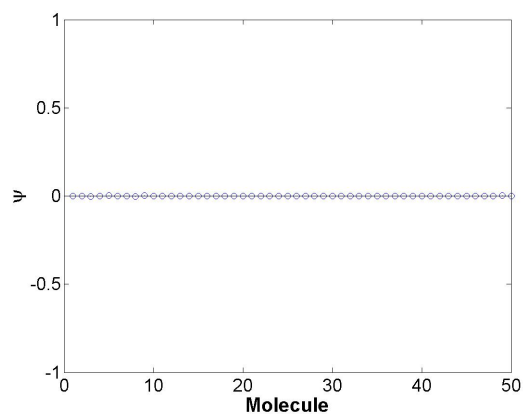
Table 4.23: The parameters used to create the plate target for scenario 2, examples 4 and 5.

Shape	X	Y	Z	H	L	r	$\tilde{\gamma}$	$\tilde{\theta}$	$\tilde{\phi}$
plate 1	0	0	0	2.3	1	-	0	-30	0
plate 2	0	0	0	2	1.3	-	0	-30	0

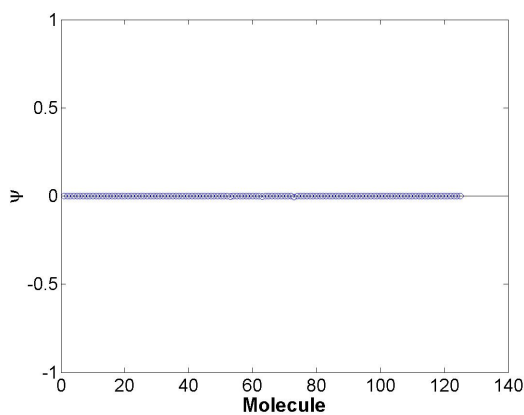
The BP results for each shape are provided in Figure 4.14 and Figure 4.15.



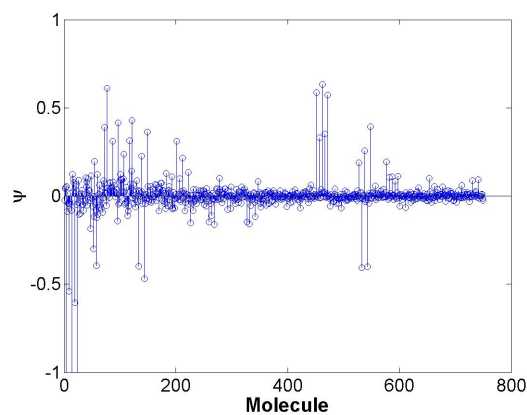
(a) BP result using the reduced plate dictionary.



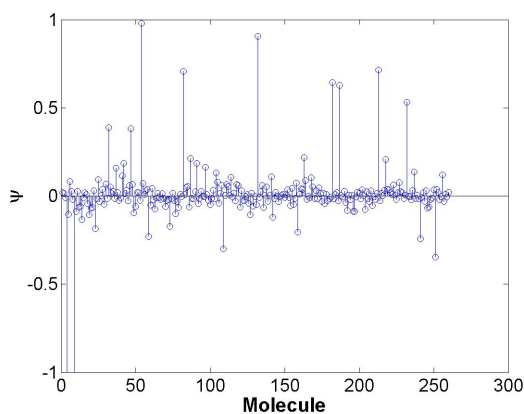
(b) BP result using the reduced dihedral dictionary.



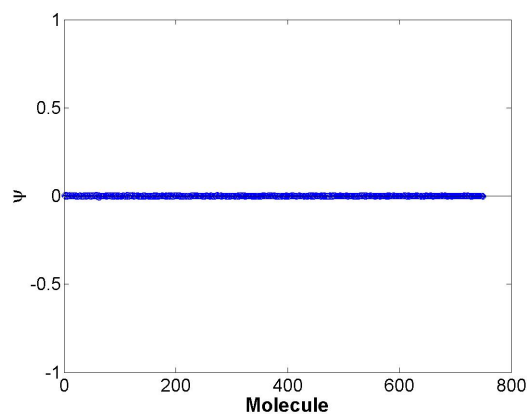
(c) BP result using the reduced trihedral dictionary.



(d) BP result using the reduced sphere dictionary.

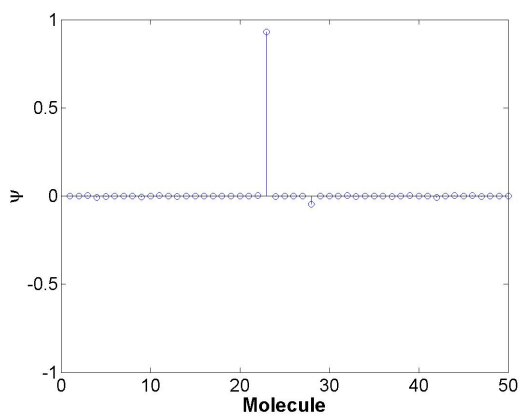


(e) BP result using the reduced cylinder dictionary.

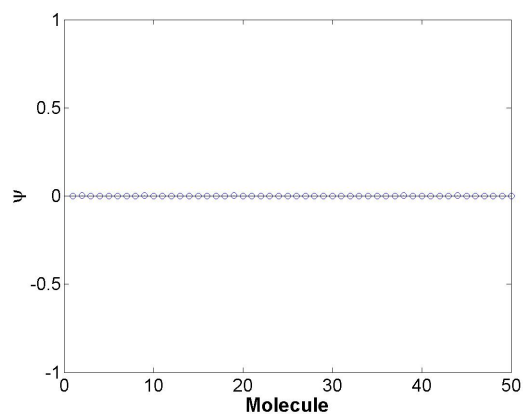


(f) BP result using the reduced tophat dictionary.

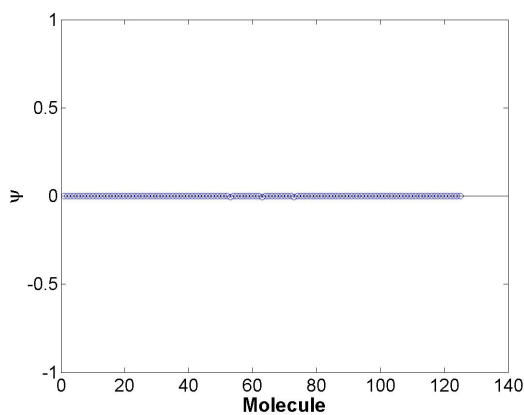
Figure 4.14: BP results for each of the reduced shape dictionaries used in the feature extraction problem in scenario 2, plate example 4.



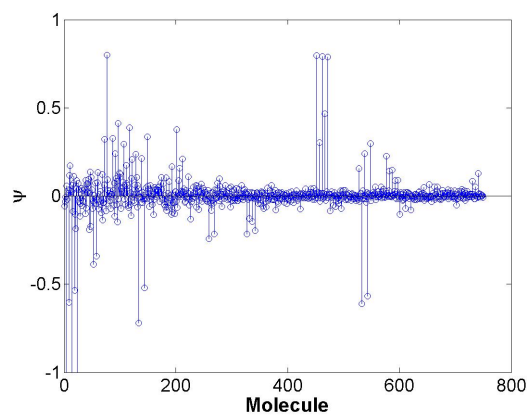
(a) BP result using the reduced plate dictionary.



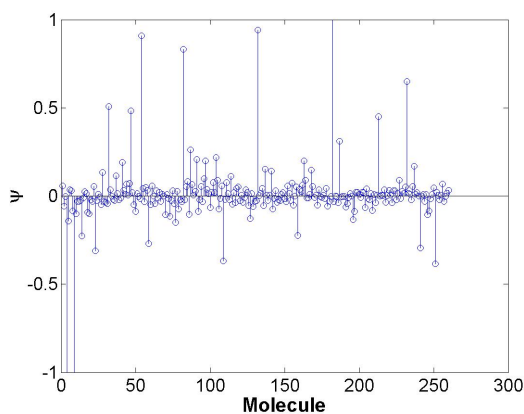
(b) BP result using the reduced dihedral dictionary.



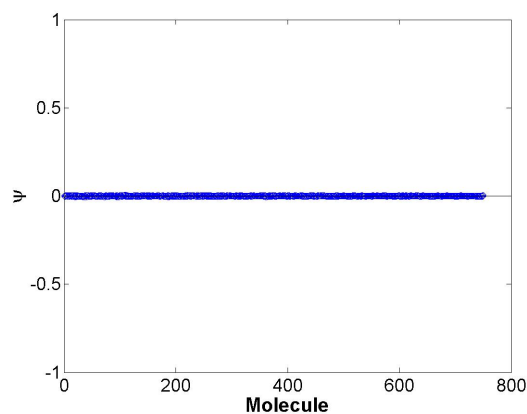
(c) BP result using the reduced trihedral dictionary.



(d) BP result using the reduced sphere dictionary.



(e) BP result using the reduced cylinder dictionary.



(f) BP result using the reduced tophat dictionary.

Figure 4.15: BP results for each of the reduced shape dictionaries used in the feature extraction problem in scenario 2, plate example 5.

The maximum coefficient returned by the BP algorithm for each of the shape dictionaries and the sparsities, described by $\|\psi\|_1$, are provided in Table 4.24 and Table 4.25.

Table 4.24: Maximum coefficients from each shape dictionary along with the ℓ_1 norm (sparsity descriptor) for scenario 2, plate example 4.

Shape	$\max(\psi)$	$\ \psi\ _1$	$(\max(\psi) - \lambda \cdot \ \psi\ _1)$
plate	0.7707	0.8360	0.6035
dihedral	0.0020	0.0330	-0.0046
sphere	0.6326	35.4801	-6.4634
top-hat	0.0054	0.8308	-0.1607
trihedral	3.5983×10^{-4}	0.0240	-0.0044
cylinder	0.9808	21.3668	-3.2926

Table 4.25: Maximum coefficients from each shape dictionary along with the ℓ_1 norm (sparsity descriptor) for scenario 2, plate example 5.

Shape	$\max(\psi)$	$\ \psi\ _1$	$(\psi - \lambda \cdot \ \psi\ _1)$
plate	0.9311	1.0427	0.7226
dihedral	0.0020	0.0334	-0.0047
sphere	0.7985	39.0755	-7.0166
top-hat	0.0048	0.9180	-0.1788
trihedral	5.5256×10^{-4}	0.0310	-0.0056
cylinder	1.1251	23.6112	-3.5972

For both examples, the shape is correctly classified as a plate. The expected parameter set estimations are $\Theta = [0, 0, 0, 2.5, 1, 0, 0, -30, 0]$ and $\Theta = [0, 0, 0, 2, 1.5, 0, 0, -30, 0]$, since these are the closest defined sets. The algorithm successfully estimates the expected parameter sets in both examples, as shown in Table 4.26 and Table 4.27.

Table 4.26: Estimated versus true parameters for scenario 2, plate example 4.

Shape	X	Y	Z	H	L	r	$\tilde{\gamma}$	$\tilde{\theta}$	$\tilde{\phi}$
True plate	0	0	0	2.3	1	-	0	-30	0
Expected plate	0	0	0	2.5	1	-	0	-30	0
Estimated plate	0	0	0	2.5	1	-	0	-30	0

Although the algorithm extracts expected parameter sets for the L and H RCS parameters for the plate. It fails when attempting to extract the radius parameter

Table 4.27: Estimated versus true parameters for scenario 2, plate example 5.

Shape	X	Y	Z	H	L	r	$\tilde{\gamma}$	$\tilde{\theta}$	$\tilde{\phi}$
True plate	0	0	0	2	1.3	-	0	-30	0
Expected plate	0	0	0	2	1.5	-	0	-30	0
Estimated plate	0	0	0	2	1.5	-	0	-30	0

r for the sphere, top-hat and cylinder shapes and has mixed results for the L and H parameters for the other shapes. The results from each of these shapes are included in Appendix C.

4.4 Scenario 3 Results

This section will discuss the extraction and classification results for target scenes containing multiple targets. Each of the targets directly corresponds to a dictionary atom. For simplicity, we present only the results for a target scene containing a plate, dihedral, and top-hat. The results from two other scenes that include combinations of the other shapes, are included in Appendix D. The parameters selected for each shape in this example are given in Table 4.28. The measured data is simulated with

Table 4.28: The parameters used to create scene 3, example 1.

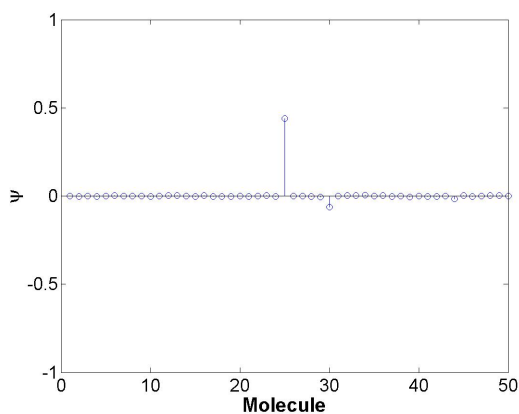
Shape	X	Y	Z	H	L	r	$\tilde{\gamma}$	$\tilde{\theta}$	$\tilde{\phi}$
plate	10	0	0	1	1	-	0	-30	0
dihedral	0	10	5	2	1	-	0	0	0
top-hat	-10	5	0	3	-	1	0	0	0

an SNR of 30 dB. Each of the shapes correspond to atoms within their respective shape dictionaries. This correspondence is provided in Table 4.29.

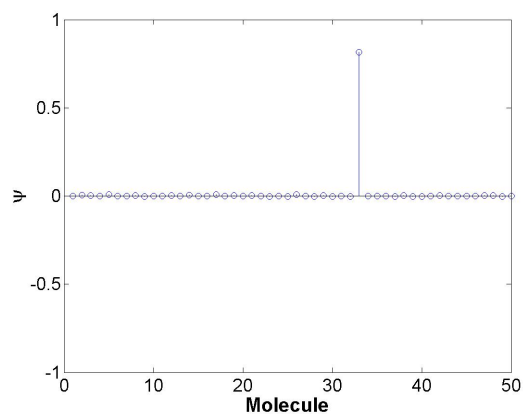
Table 4.29: Correspondence mapping for the measured data and dictionary atoms for scenario 3, example 1.

Shape	Orig. Dict. Atom	Molecule	Molecule Atom
plate	940	25	23
dihedral	2473	33	60
top-hat	1441	191	6

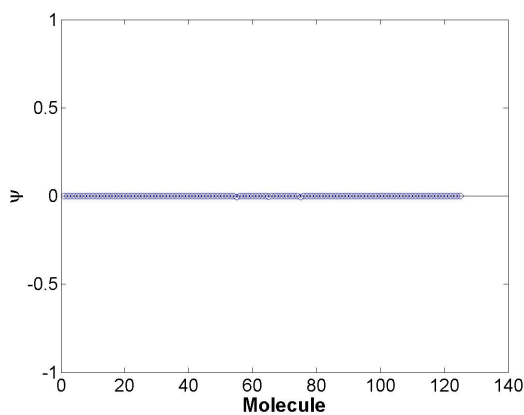
The iterative phase history subtraction process leads to multiple iterations of the BP algorithm when extracting multiple shapes from a target scene. A single shape corresponding to the largest contribution of energy is extracted from each iteration. The BP results for each shape and iteration are provided in Figures 4.16-4.18.



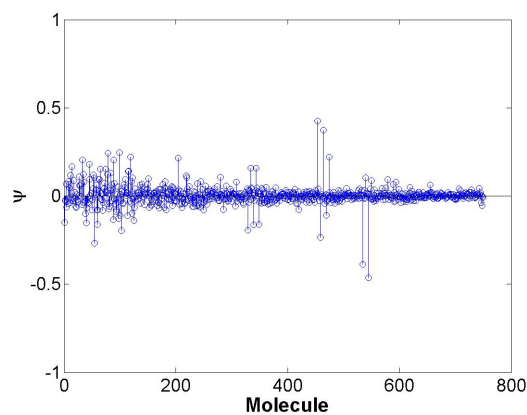
(a) BP result using the reduced plate dictionary.



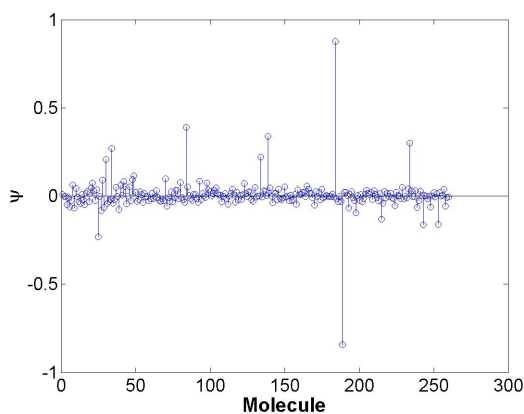
(b) BP result using the reduced dihedral dictionary.



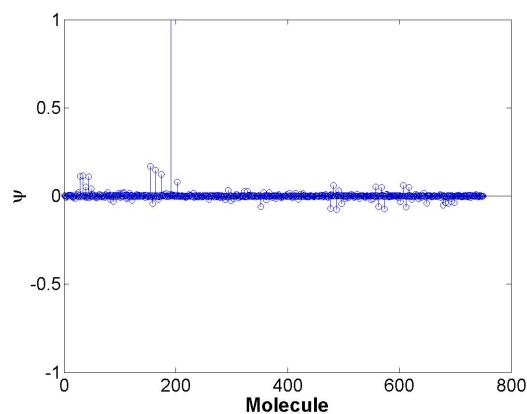
(c) BP result using the reduced trihedral dictionary.



(d) BP result using the reduced sphere dictionary.

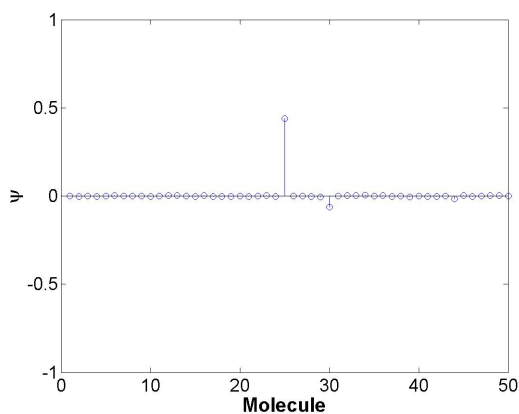


(e) BP result using the reduced cylinder dictionary.

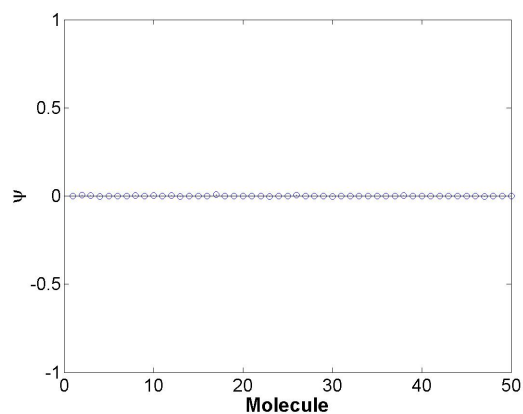


(f) BP result using the reduced top-hat dictionary.

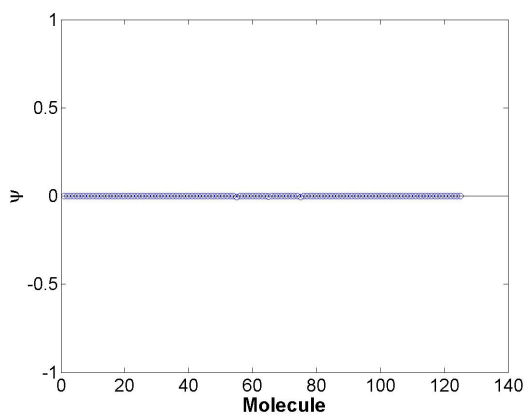
Figure 4.16: BP results for each of the reduced shape dictionaries used in the feature extraction problem in scenario 3, example 1 on the first iteration.



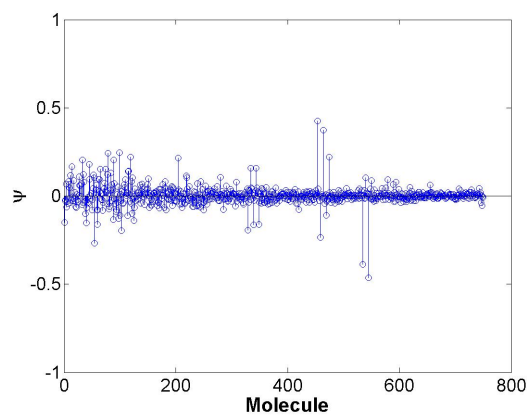
(a) BP result using the reduced plate dictionary.



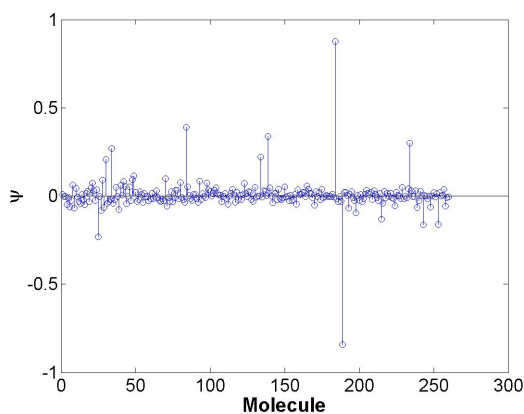
(b) BP result using the reduced dihedral dictionary.



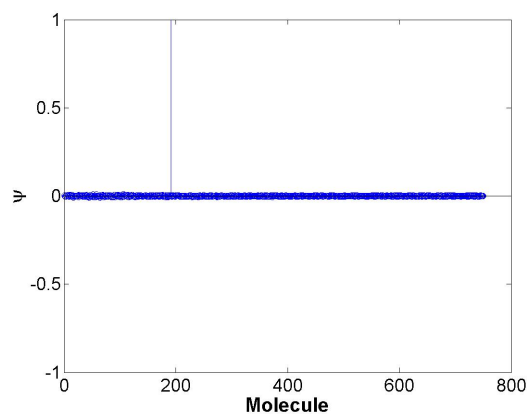
(c) BP result using the reduced trihedral dictionary.



(d) BP result using the reduced sphere dictionary.

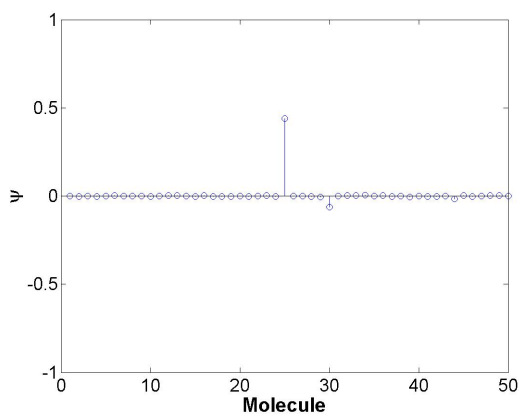


(e) BP result using the reduced cylinder dictionary.

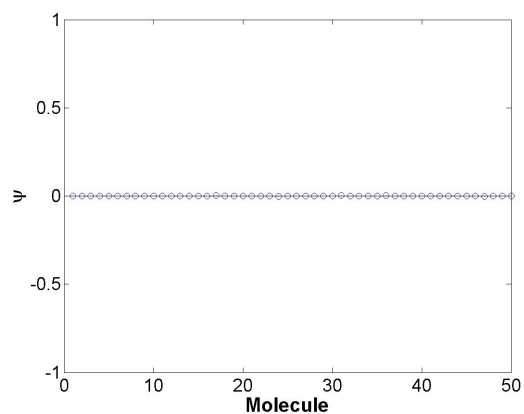


(f) BP result using the reduced top-hat dictionary.

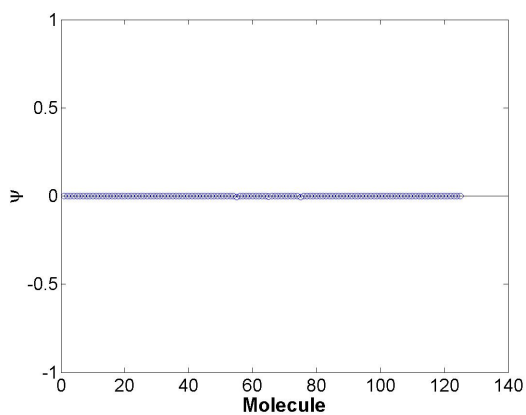
Figure 4.17: BP results for each of the reduced shape dictionaries used in the feature extraction problem in scenario 3, example 1 on the second iteration.



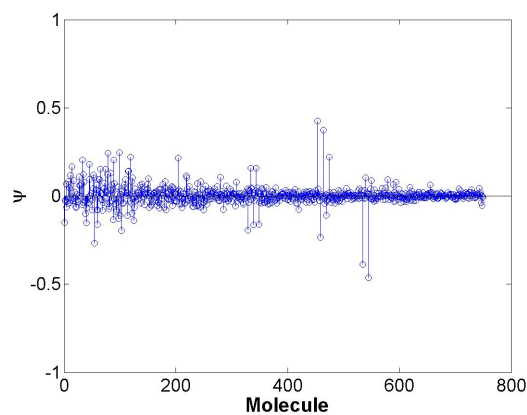
(a) BP result using the reduced plate dictionary.



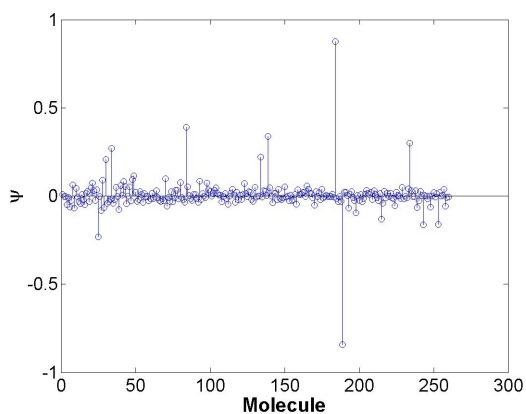
(b) BP result using the reduced dihedral dictionary.



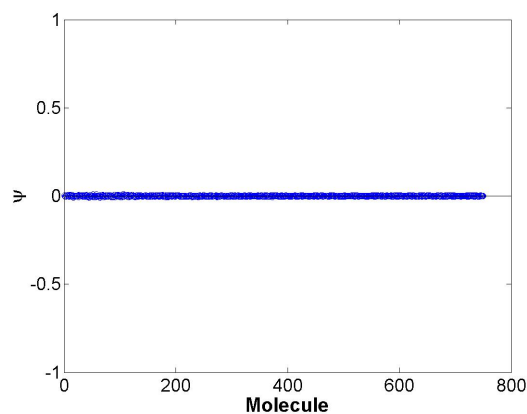
(c) BP result using the reduced trihedral dictionary.



(d) BP result using the reduced sphere dictionary.



(e) BP result using the reduced cylinder dictionary.



(f) BP result using the reduced top-hat dictionary.

Figure 4.18: BP results for each of the reduced shape dictionaries used in the feature extraction problem in scenario 3, example 1 on the final iteration.

The maximum coefficients along with the calculated norms for each iteration are shown in Table 4.30.

Table 4.30: Maximum coefficients from each shape dictionary along with the ℓ_1 norm (sparsity descriptor) for scenario 3, example 1.

Shape	Iteration	$\max(\psi)$	$\ \psi\ _1$	$(\max(\psi) - \lambda \cdot \ \psi\ _1)$
plate	1	0.4396	0.6037	0.3189
	2	0.4396	0.6037	0.3189
	3	0.4396	0.6037	0.3189
dihedral	1	0.8149	0.9083	0.6333
	2	0.0076	0.0651	-0.0054
	3	0.0024	0.0352	-0.0046
sphere	1	0.4269	24.1672	-4.4065
	2	0.4269	24.1672	-4.4065
	3	0.4269	24.1672	-4.4065
top-hat	1	1.7148	6.1812	0.4786
	2	1.7140	2.9059	1.1329
	3	0.0108	1.1921	-0.2276
trihedral	1	3.8552×10^{-4}	0.0255	-0.0047
	2	3.8552×10^{-4}	0.0255	-0.0047
	3	3.8552×10^{-4}	0.0255	-0.0047
cylinder	1	0.8770	10.2192	-1.1668
	2	0.8770	10.2192	-1.1668
	3	0.8770	10.2192	-1.1668

The sparsest solution pertaining to the largest coefficient for each iteration corresponds to a single shape. The shapes returned for each iteration respectively are dihedral, top-hat, and plate which correctly correspond to the shapes within the target scene. The molecules corresponding to each coefficient maximum are selected for parameter estimation.

Estimates of the posterior log-likelihoods are calculated for each atom within each of the three molecules. These estimates are plotted and provided in Figure 4.19. The largest log-likelihoods correspond to the correct atoms as shown by the associated parameters provided in Table 4.31.

The algorithm successfully chose the correct features and parameters. The next section will present comprehensive results for the algorithm.

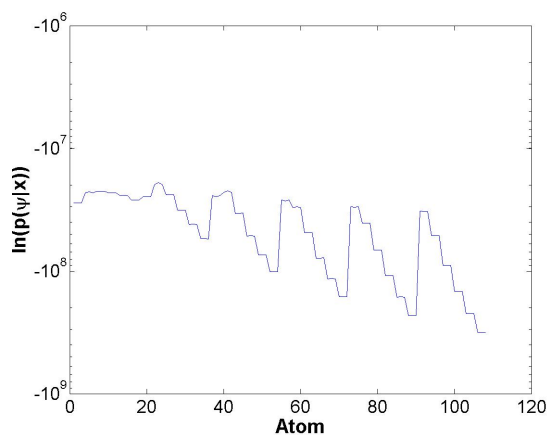
Table 4.31: Extracted parameter sets for each shape compared to truth for scenario 3, example 1.

Shape	X	Y	Z	H	L	r	$\tilde{\gamma}$	$\tilde{\theta}$	$\tilde{\phi}$
True plate	10	0	0	1	1	-	0	-30	0
Estimated plate	10	0	0	1	1	-	0	-30	0
True dihedral	0	10	5	2	1	-	0	0	0
Estimated dihedral	0	10	5	2	1	-	0	0	0
True top-hat	-10	5	0	3	-	1	0	0	0
Estimated top-hat	-10	5	0	3	-	1	0	0	0

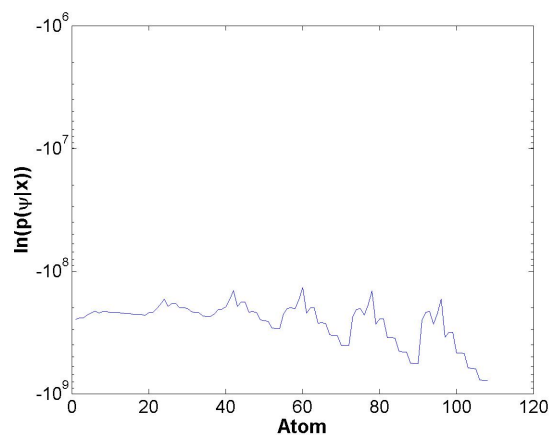
4.5 Comprehensive Results

This section will present comprehensive results for the feature extraction algorithm presented in this thesis. First, we describe the effects of SNR and RCS on target classification and parameter estimation. Second, we analyze several of the miss-classifications resulting from off-dictionary targets tested in scenario 2. Finally, we include summary tables that present the feature extraction results for each of the examples within scenario 2. We concentrate on scenario 2 results since these examples led to incorrect extractions. All targets tested in scenarios 1 and 3, which were simulated from atoms contained within the dictionaries, were successfully extracted.

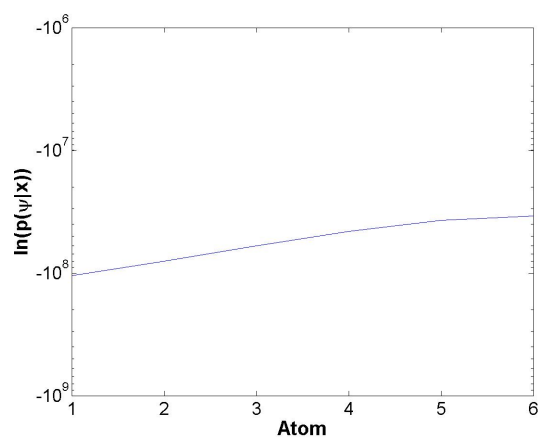
4.5.1 SNR versus RCS. The following SNR data is based on the detection and estimation of a single target. Each data point represents the percentage of correct estimation over 100 iterations. Simulations were run using small, medium, and large RCS targets. The small RCS targets consisted of length, height, and radius parameters from 0.5-3 meters. The medium and large RCS targets consisted of length, height, and radius parameters from 3.5-6 meters and 6.5-9 meters, respectively. Each iteration consists of a new set of additive random noise and a specific dictionary atom. The noise level is determined by the appropriate SNR value. The results for each shape are shown in Figure 4.20.



(a) Posterior log-likelihood estimates associated with each atom within the selected plate molecule.

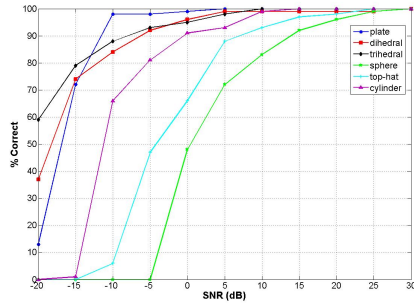


(b) Posterior log-likelihood estimates associated with each atom within the selected dihedral molecule.

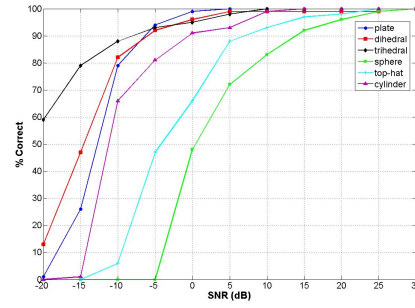


(c) Posterior log-likelihood estimates associated with each atom within the selected top-hat molecule.

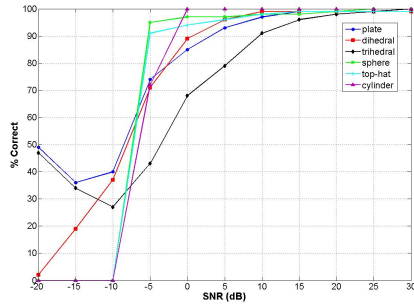
Figure 4.19: Posterior log-likelihood estimates for each shape and iteration for scenario 3, example 1.



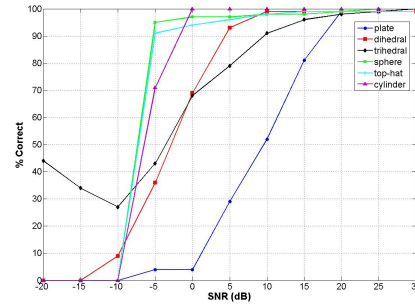
(a) Percentage of correct shape estimation versus SNR for small RCS targets (0.5-3 meter length, height, radius).



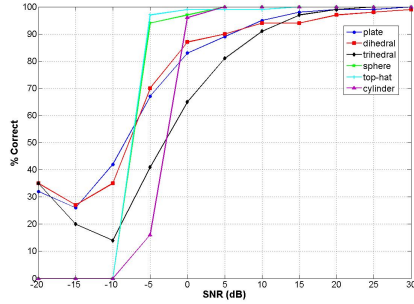
(b) Percentage of correct parameter estimation versus SNR for small RCS targets (0.5-3 meter length, height, radius).



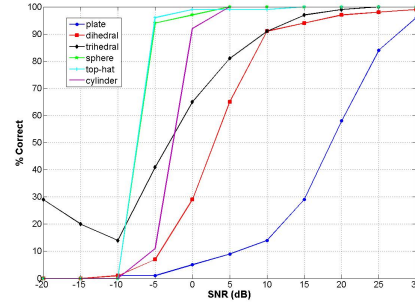
(c) Percentage of correct shape estimation versus SNR for medium RCS targets (3.5-6 meter length, height, radius).



(d) Percentage of correct parameter estimation versus SNR for medium RCS targets (3.5-6 meter length, height, radius).



(e) Percentage of correct shape estimation versus SNR for large RCS targets (6.5-9 meter length, height, radius).



(f) Percentage of correct parameter estimation versus SNR for large RCS targets (6.5-9 meter length, height, radius).

Figure 4.20: Percentage of correct estimation of both shape and parameter set for all shapes versus SNR.

Both shape classification and parameter estimation reached 100% accuracy by 30 dB SNR. The increased RCS simulations show large improvements in both detection and estimation percentage for those shapes with a radial component (i.e. top-hat, sphere, and cylinder). In contrast, the larger RCS values lead to a decrease in both shape classification and parameter estimation accuracy for the plate, trihedral, and dihedral. The larger RCS of the shapes that depend only on L and H parameters may have led to an under-sampled signal. This under-sampling may have caused the decrease in parameter estimation accuracy and the lower SNR values.

4.5.2 Feature Extraction Scenario Summary. The algorithm successfully classifies target shapes and estimates their associated parameter sets whenever the specific target is contained within the defined parameter space and specifically contained within the dictionary. This is evident in the successful feature extraction results in scenarios 1 and 3. In most cases, the algorithm incorrectly extracts a target when the parameter set falls outside the defined parameter space. This is shown by the results from scenario 2. Off-dictionary target locations and radius parameters always led to incorrect feature extractions. The L and H parameters, although outside of the defined parameter space, led to expected feature extractions.

The miss-classifications and incorrect parameter estimations of targets located at X , Y , and Z positions outside of the defined parameter space may be due to the large spatial separations between locations. The step-size between locations is set to 5 m. The L and H parameter steps are set to the actual range resolution of 0.5 m. Higher resolution location definitions may lead to better extraction performance.

In some cases within scenario 2, the algorithm misclassified the target shape as a shape with the wrong polarization response. For example, the algorithm chose a shape with an odd bounce instead of an even bounce response. This is due to the resulting BP coefficients and the defined sparsity constraint. In most cases, the correct shape would have been chosen if a lower cut-off was implemented on the maximum coefficients returned for each shape. Future research should investigate the addition

of a lower threshold to improve these results. This may be shown using the results from plate example 3 in scenario 2.

The maximum coefficients and sparsity values calculated for each shape in this example are provided below in Table 4.32. The correct shape is a plate target. How-

Table 4.32: Maximum coefficients from each shape dictionary along with the ℓ_1 norm (sparsity descriptor) for scenario 2, plate example 3.

Shape	$\max(\psi)$	$\ \psi\ _1$	$(\max(\psi) - \lambda \cdot \ \psi\ _1)$
plate	0.1021	0.9386	-0.0856
dihedral	0.0015	0.0300	-0.0046
sphere	0.7549	25.5425	-4.3536
top-hat	0.0042	0.6946	-0.1347
trihedral	0.0030	0.0170	-3.5957×10^{-4}
cylinder	1.6443	20.2092	-2.3975

ever, the largest $(\max(\psi) - \lambda \cdot \|\psi\|_1)$ value corresponds to the trihedral and leads to an incorrect trihedral classification. If we assign a lower threshold β to $\max(\psi)$ shown by,

$$\max_{\mathbf{r}} (\max(\psi) - \lambda \cdot \|\psi\|_1) \quad \text{s.t.} \quad \beta \leq \max(\psi) \leq \alpha \quad (4.2)$$

we may eliminate the shapes, such as the trihedral, that are chosen based solely on low sparsity. For example, if we set $\beta = 0.1$, then $\max(\psi) \geq 0.1$ and the dihedral, top-hat, and trihedral hypotheses are eliminated, as shown in Table 4.33. The new

Table 4.33: Maximum coefficients from each shape dictionary along with the ℓ_1 norm (sparsity descriptor) for scenario 2, plate example 3, post thresholding.

Shape	$\max(\psi)$	$\ \psi\ _1$	$(\max(\psi) - \lambda \cdot \ \psi\ _1)$
plate	0.1021	0.9386	-0.0856
dihedral	0.0015	0.0300	-0.0046
sphere	0.7549	25.5425	-4.3536
top-hat	0.0042	0.6946	-0.1347
trihedral	0.0030	0.0170	-3.5957×10^{-4}
cylinder	1.6443	20.2092	-2.3975

hypotheses now only include the plate, sphere, and cylinder for comparison. The maximum value of $(\max(\psi) - \lambda \cdot \|\psi\|_1)$ now corresponds to the plate and leads to

a correct shape classification. This thresholding technique may increase extraction performance for off-dictionary targets.

This method may increase shape classification accuracy, but the algorithm may still lead to an incorrect parameter set estimation. This is evident in the results for plate example 2 in scenario 2. The parameter estimation results for this example are shown in Table 4.34. In this example, the algorithm successfully classifies the target

Table 4.34: Estimated versus true parameters for scenario 2, plate example 2.

Shape	X	Y	Z	H	L	r	$\tilde{\gamma}$	$\tilde{\theta}$	$\tilde{\phi}$
True plate	0	4	0	2	1	-	0	-30	0
Expected plate	0	5	0	2	1	-	0	-30	0
Estimated plate	0	-5	0	2	1	-	0	-30	0

as a plate. However, the estimated plate Y location is not as expected. This result is most likely due to phase errors which lead to a lower LS error for the estimated plate, as shown in Table 4.35. The wavelength for the 10 GHz X-band radar simulated is

Table 4.35: LS errors for the extracted and hypothesized data sets for scenario 2, plate example 2.

Data	$\ \mathbf{x} - \mathbf{s}(\boldsymbol{\Theta}_n)\ _2^2$
Extracted	2.5269×10^7
Closest	2.7067×10^7

approximately 3 cm. The difference in Y location from truth to the estimated is 9 m. At this distance the signal is in phase with the true location. However, the 1 m difference in the expected is out of phase and may have been the cause of the larger LS error.

In all scenario 2 examples, the off-dictionary location parameters lead to incorrect parameter estimations. These incorrect estimations are products of the selected parameter spacing and may be mitigated by smart selection of spacing increments. Finer resolution may be required to attain useful feature extraction results for off-dictionary targets. To understand the cause of incorrect extraction, we classify errors as defined by

Table 4.36: Comprehensive results for all shapes in scenario 2, simulated using off-dictionary X locations.

Vary X											
Result	Error Type	Shape	X	Y	Z	H	L	r	$\tilde{\gamma}$	$\tilde{\theta}$	$\tilde{\phi}$
wrong	II	True plate	4	0	0	2	1	-	0	-30	0
		Estimated plate	10	5	-10	3	0.5	-	0	-30	0
wrong	II	True dihedral	4	0	0	2	1	-	0	0	0
		Estimated dihedral	10	-10	10	0.5	0.5	-	0	0	0
wrong	I	True sphere	4	0	0	-	-	2	-	-	-
		Estimated trihedral	0	0	10	0.5	-	-	0	0	0
		Estimated plate	0	0	10	1	0.5	-	0	-30	0
wrong	I	True top-hat	4	0	0	2	-	1	0	0	0
		Estimated dihedral	5	0	0	0.5	0.5	-	0	0	0
wrong	I	True trihedral	4	0	0	2	-	-	0	0	0
		Estimated trihedral	5	-10	0	1	-	-	0	0	0
		Estimated plate	5	10	0	1	1	-	0	-30	0
wrong	I	True cylinder	4	0	0	-	2	1	0	0	0
		Estimated plate	5	-10	0	0.5	0.5	-	0	-30	0

- **Type I:** Incorrect shape classification may be fixed with appropriate threshold on $\max(\psi)$.
- **Type II:** Correct shape classification with incorrect parameter estimation due to LS error.
- **Type III:** Incorrect shape classification or model order estimation which may not be fixed by assigning a threshold on $\max(\psi)$.

The feature extractions for each of the examples within scenario 2 are provided in Tables 4.36-4.39.

The majority of errors causing each of the incorrect feature extractions for scenario 2 are Type I errors. This means that the selection of an appropriate threshold on $\max(\psi)$ would lead to correct shape classifications. The Type II errors were due to phase errors which led to larger LS errors. The phase term for the 3-D signal model

Table 4.37: Comprehensive results for all shapes in scenario 2, simulated using off-dictionary Y locations.

Vary Y											
Result	Error Type	Shape	X	Y	Z	H	L	r	$\tilde{\gamma}$	$\tilde{\theta}$	$\tilde{\phi}$
wrong	II	True plate	0	4	0	2	1	-	0	-30	0
		Estimated plate	0	-5	0	2	1	-	0	-30	0
wrong	II	True dihedral	0	4	0	2	1	-	0	0	0
		Estimated dihedral	0	5	0	0.5	3	-	0	0	0
wrong	I	True sphere	0	4	0	-	-	2	-	-	-
		Estimated plate	5	5	-5	0.5	0.5	-	0	-30	0
wrong	I	True top-hat	0	4	0	2	-	1	0	0	0
		Estimated dihedral	-5	5	10	0.5	0.5	-	0	0	0
wrong	I	True trihedral	0	4	0	2	-	-	0	0	0
		Estimated dihedral	0	-5	5	0.5	0.5	-	0	0	0
		Estimated trihedral	5	-5	-10	0.5	-	-	0	0	0
		Estimated trihedral	-5	10	10	0.5	-	-	0	0	0
wrong	I	True cylinder	0	4	0	-	2	1	0	0	0
		Estimated plate	-5	5	10	0.5	0.5	-	0	-30	0

Table 4.38: Comprehensive results for all shapes in scenario 2, simulated using off-dictionary Z locations.

Vary Z											
Result	Error Type	Shape	X	Y	Z	H	L	r	$\tilde{\gamma}$	$\tilde{\theta}$	$\tilde{\phi}$
wrong	I	True plate	0	0	4	2	1	-	0	-30	0
		Estimated trihedral	5	5	-5	0.5	-	-	0	0	0
wrong	I	True dihedral	0	0	4	2	1	-	0	0	0
		Estimated trihedral	0	-5	-10	0.5	-	-	0	0	0
		Estimated plate	0	-5	-10	1	0.5	-	0	-30	0
wrong	I	True sphere	0	0	4	-	-	2	-	-	-
		Estimated dihedral	-5	-10	10	0.5	0.5	-	0	0	0
wrong	I	True top-hat	0	0	4	2	-	1	0	0	0
		Estimated trihedral	-5	5	-5	0.5	-	-	-	-	-
		Estimated plate	-5	5	-5	1	0.5	-	0	-30	0
wrong	II	True trihedral	0	0	4	2	-	-	0	0	0
		Estimated trihedral	0	-10	5	0.5	-	-	-	-	-
		Estimated plate	5	5	-5	1	1.5	-	0	-30	0
		Estimated plate	5	5	-5	1	1.5	-	0	-30	0
wrong	I	True cylinder	0	0	4	-	2	1	0	0	0
		Estimated trihedral	10	0	-10	0.5	-	-	0	0	0
		Estimated plate	10	0	-10	1	0.5	-	0	-30	0

Table 4.39: Comprehensive results for all shapes in scenario 2, simulated using off-dictionary RCS parameter locations.

Vary RCS parameters											
Result	Error Type	Shape	X	Y	Z	H	L	r	$\tilde{\gamma}$	$\tilde{\theta}$	$\tilde{\phi}$
correct		True plate 1	0	0	0	2.3	1	-	0	-30	0
		Estimated plate	0	0	0	2.5	1	-	0	-30	0
correct		True plate 2	0	0	0	2	1.3	-	0	-30	0
		Estimated plate	0	0	0	2	1.5	-	0	-30	0
correct		True dihedral 1	0	0	0	2.3	1	-	0	0	0
		Estimated dihedral	0	0	0	2.5	1	-	0	0	0
wrong	III	True dihedral 2	0	0	0	2	1.3	-	0	0	0
		Estimated dihedral	0	0	0	1.5	1.5	-	0	0	0
		Estimated dihedral	0	0	0	1	0.5	-	0	0	0
wrong	I	True sphere	0	0	0	-	-	2.3	-	-	-
		Estimated dihedral	-5	-10	10	0.5	0.5	-	0	0	0
correct		True top-hat 1	0	0	0	2.3	-	1	0	0	0
		Estimated top-hat	0	0	0	2.5	-	1	0	0	0
wrong	I	True top-hat 2	0	0	0	2	-	1.3	0	0	0
		Estimated trihedral	5	-5	-10	0.5	-	-	0	0	0
		Estimated plate	5	-5	-10	1	0.5	-	0	-30	0
correct		True trihedral	0	0	0	2.3	-	-	0	0	0
		Estimated trihedral	0	0	0	2.5	-	-	0	0	0
correct		True cylinder 1	0	0	0	-	2.3	1	0	0	0
		Estimated cylinder	0	0	0	-	2.5	1	0	0	0
wrong	I	True cylinder 2	0	0	0	-	2	1.3	0	0	0
		Estimated trihedral	0	-10	0	0.5	-	-	0	0	0
		Estimated plate	0	-10	0	1	0.5	-	0	-30	0

is defined by the differential range ΔR . From Section 2.4,

$$\Delta R(\mathbf{\Lambda}(\tau); \mathbf{\Theta}_m) = \Delta R_0(\mathbf{\Lambda}(\tau); \mathbf{\Theta}_m) + \Delta R_r(\mathbf{\Lambda}(\tau); \mathbf{\Theta}_m) \quad (4.3)$$

where

$$\Delta R_0(\mathbf{\Lambda}(\tau); \mathbf{\Theta}_m) \approx 2x_0 \cos \phi(\tau) \cos \theta(\tau) + 2y_0 \sin \phi(\tau) \cos \theta(\tau) + 2z_0 \sin \theta(\tau) \quad (4.4)$$

and

$$\Delta R_r(\mathbf{\Lambda}(\tau); \mathbf{\Theta}_m) \approx 2x_r \cos \phi(\tau) \cos \theta(\tau) + 2y_r \sin \phi(\tau) \cos \theta(\tau) + 2z_r \sin \theta(\tau) \quad (4.5)$$

Therefore, the phase errors are driven by the spatial extent of the X , Y , and Z location errors.

There are many ways this algorithm may be improved. The results provided in this thesis should guide future dictionary based feature extraction research efforts. In Chapter V, we review the methodology of this thesis, provide conclusions, and summarize several future work possibilities.

V. Conclusions and Future Work

5.1 Chapter Overview

The dictionary based shape classification and feature extraction algorithm proposed in this thesis sets a new framework for target recognition within a SAR scene utilizing the 3-D radar scattering models presented in [1]. In this chapter we will review the objectives, algorithm methodologies, and conclusions. We will end with a list of proposed future development and research areas.

5.2 Review of Objectives and Methodology

The overarching objective of this research was to derive an algorithm, based on results and conclusions from [1, 10], for canonical shape classification and physical parameter estimation. The goal was to develop a process that could lend itself to estimating a confidence metric associated with the extraction results and provide a framework for an efficient dictionary based approach using the 3-D scattering models in [1].

The proposed approach relies on dictionaries populated with simulated SAR phase history data generated using the 3-D radar scattering models derived by Jackson in [1]. Dictionaries are created for various canonical shape hypotheses over a variety of physical parameters. The dictionaries provide a database for comparison to measured data. The feature extraction problem is structured as a sparse signal recovery problem which has been a focus in many research efforts within the compressive sensing community, including [6–8, 15–18] using the BP principle. The BP principle requires low dictionary coherence to provide accurate sparse solutions [7]. Radar collection diversity along with a modified version of the molecule method presented in [7] are used to minimize the dictionary coherence and support the use of the *spgl1* [11] BP algorithm for shape classification. The output of the BP optimization identifies a set of highly correlated atoms which closely resemble the measured data. Posterior log-likelihoods are computed for each of the atoms derived using Bayesian detection and estimation theory from [13, 14]. The largest log-likelihood, equivalent

to the MAP estimate, represents the atom which most closely resembles the measured data set. Finally, the index of this atom is used to extract the associated parameter set.

5.3 Conclusions

The objective of this research was successfully achieved. A Matlab[®] toolbox was created that successfully implements the algorithms proposed in this research. This approach was tested using several target scenes that included an array of target shapes with varying locations and RCS characteristics. The algorithm was able to correctly extract all shapes within the target scenes, most in low SNR (< 30 dB) environments. The algorithm also led to the correct physical parameter estimation of all shapes tested, when the objective parameter set was confined to a dictionary's defined parameter space. These physical characteristics included height, length, radius, and location within a 3-D Cartesian space.

This algorithm requires large computational memory capacity to house the dictionaries. The dictionaries used in the simulations presented in this research were coarsely sampled and covered only a small piece of the operationally possible parameter space. Prior knowledge of the target scene is required to efficiently utilize this algorithm. Prior target knowledge will drive the parameter space selected for dictionary creation.

This research also presented the need for a diverse radar collection profile. Accurate extraction and estimation relies on minimized dictionary coherence. Therefore, SAR data should be collected over multiple radar frequencies, polarizations, and varying aspect angles.

5.4 Future Development and Research

The algorithm developed in this research sets up a framework on which to build upon. Improvements in algorithm efficiency along with developments in dictionary

creation may lead to improved classification. The proposed research topics listed below are derived from observations made during the development and implementation of this algorithm. Future work includes:

- Derive a prior pdf that promotes the tractable integration of the denominator $p(\mathbf{Y})$ needed to calculate an accurate posterior probability $p(\psi_m|\mathbf{Y})$. Specifically, see Carin's work on the hierarchical prior described in [18].
- Investigate the use of more efficient compressive sensing algorithms, as described by Carin in [18].
- Implement algorithm on the multi-node HPC network to promote finer resolution dictionaries that can encompass a larger parameter space.
- Compare results over multiple target scenarios with results from the LS algorithm used in [1].
- Attempt classification using algorithm on simulated complex target (such as a tank) that is comprised of multiple canonical shapes.
- Attempt classification using algorithm on actual measured phase history data for single shapes using RCS lab.
- Develop thresholding technique to improve classification performance for off-dictionary parameter sets.
- Modify algorithm to create dictionary data as needed and characterize gains and losses in computation memory and processing efficiency.

Appendix A. Dictionary Coherence Reduction

This appendix includes the dictionary coherence reductions described in Section 3.5. Specifically, we show the confusion maps illustrating the correlation reductions for the plate, sphere, top-hat, trihedral, and cylinder dictionaries. The figures included show the decreases in atom redundancy obtained through increased radar collection diversity and the implementation of the molecule method.

A.1 Plate Dictionary

The confuser map for the baseline plate dictionary, created using 1 frequency, HH polarization and linear flight path, is provided in Figure A.1. The coherence reductions from increasing the radar collection parameter diversities are shown in Figure A.2.

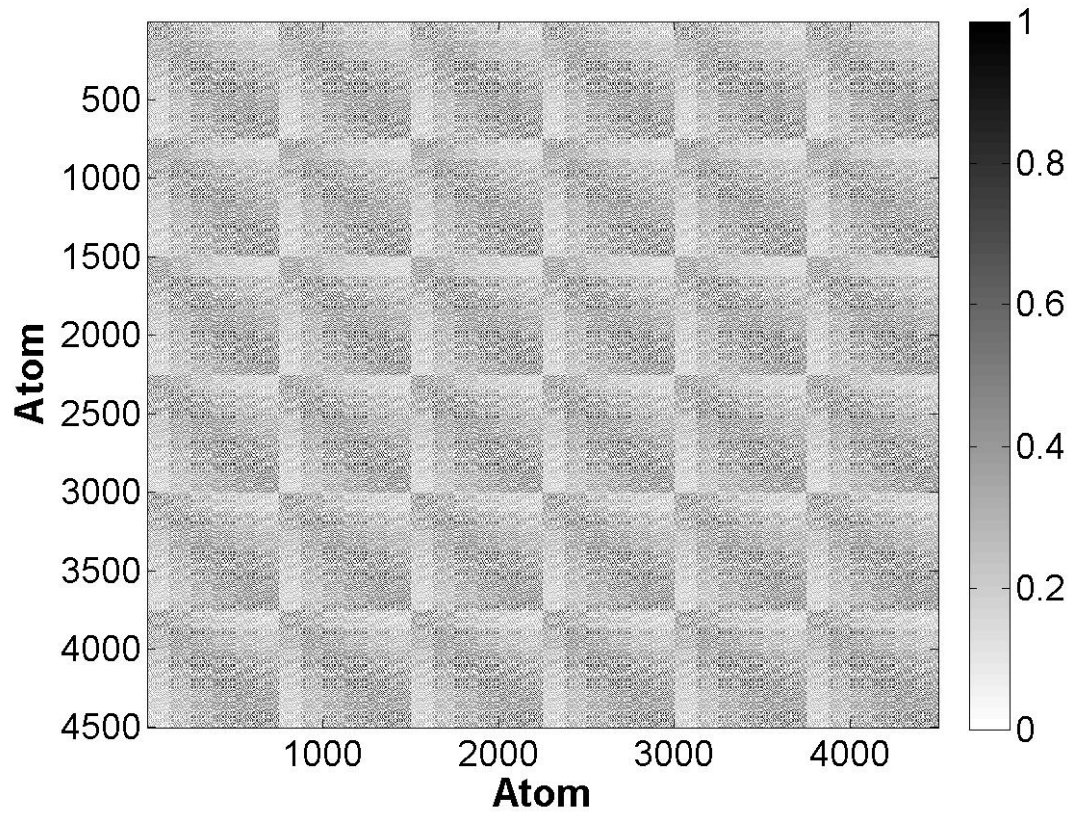
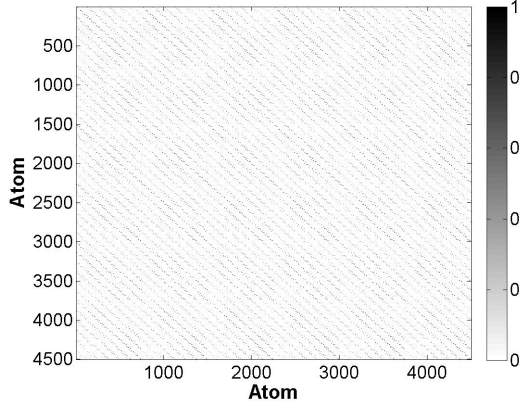
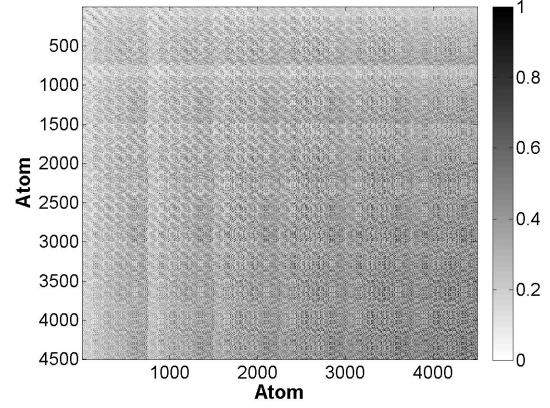


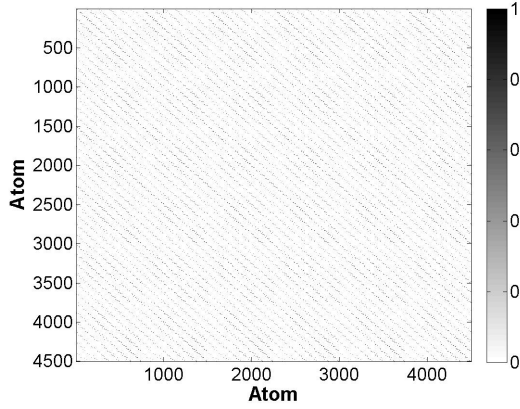
Figure A.1: Correlation map corresponding to $\mathbf{D}_{\Gamma_{\text{plate}}}$ generated using a linear flight path, HH polarization, and 1 frequency.



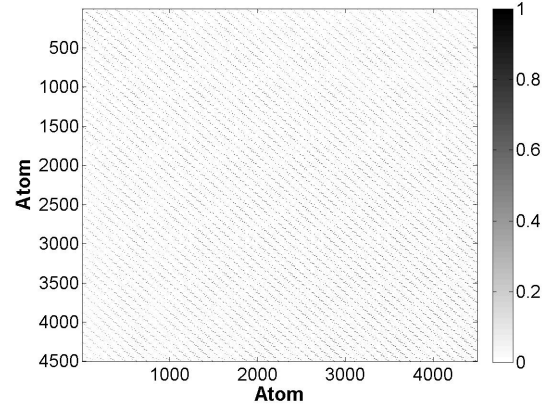
(a) Correlation map corresponding to $\mathbf{D}_{\Gamma_{\text{plate}}}$ generated using a linear flight path, HH polarization, and 125 frequencies.



(b) Correlation map corresponding to $\mathbf{D}_{\Gamma_{\text{plate}}}$ generated using a nonlinear flight path, HH polarization, and 1 frequency.

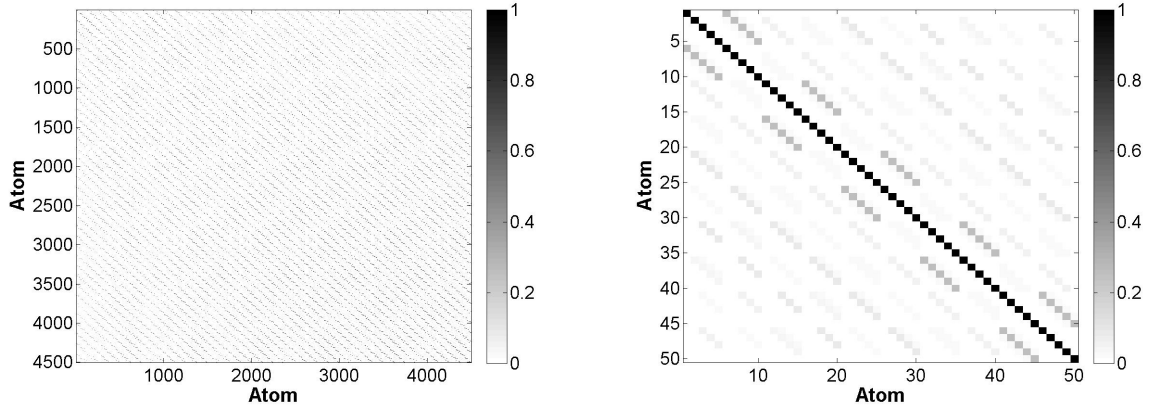


(c) Correlation map corresponding to $\mathbf{D}_{\Gamma_{\text{plate}}}$ generated using a linear flight path, HH, HV, and VV polarizations, and 125 frequencies.



(d) Correlation map corresponding to $\mathbf{D}_{\Gamma_{\text{dihedral}}}$ generated using a nonlinear flight path, HH, HV, and VV polarizations, and 125 frequencies.

Figure A.2: Reduction in correlation due to increased aspect and frequency diversity for $\mathbf{D}_{\Gamma_{\text{plate}}}$.



(a) Correlation map corresponding to $\mathbf{D}_{\Gamma_{\text{plate}}}$ generated using a nonlinear flight path, HH, HV, and VV polarizations, and 125 frequencies before clustering.

(b) Correlation map corresponding to $\mathbf{D}_{\Gamma_{\text{plate}}}$ generated using a nonlinear flight path, HH, HV, and VV polarizations, and 125 frequencies after implementing molecule method.

Figure A.3: Reduction in correlation due to molecule clustering algorithm.

The reduction in coherence and dictionary size due to the molecule method is shown in Figure A.3.

A.2 Sphere Dictionary

The confuser map for the baseline Sphere dictionary, created using 1 frequency, HH polarization and linear flight path, is provided in Figure A.4. The coherence reductions from increasing the radar collection parameter diversities are shown in Figure A.5.

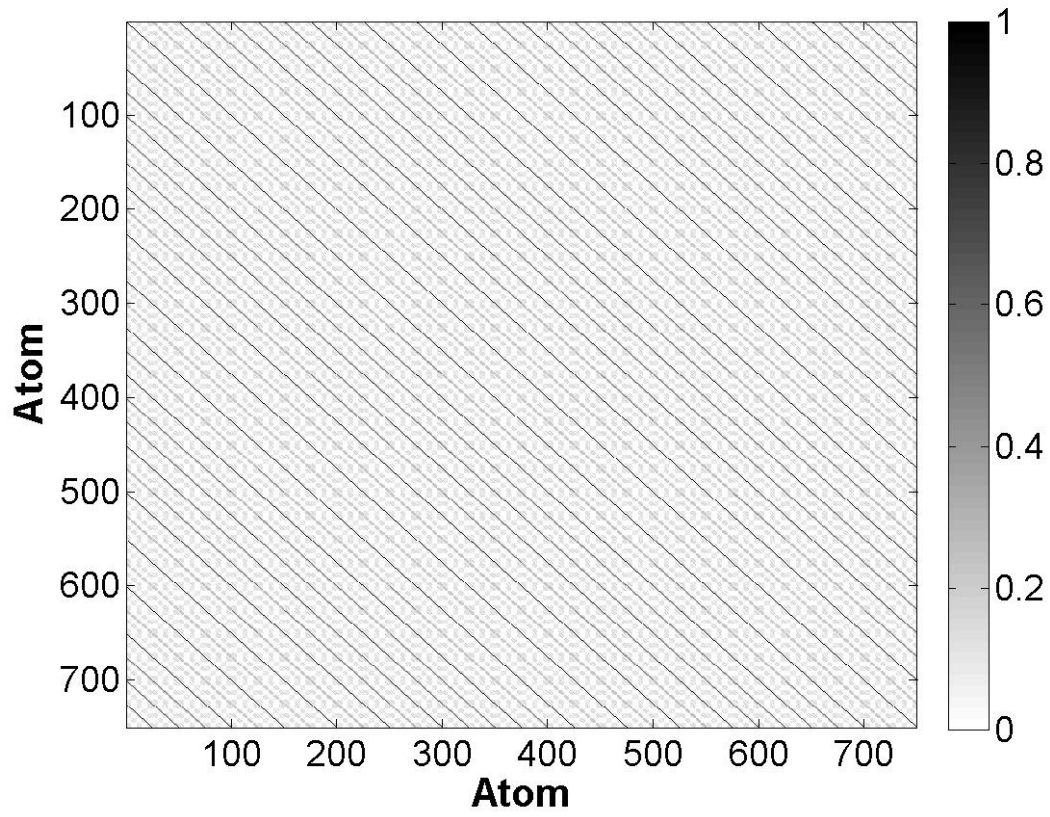
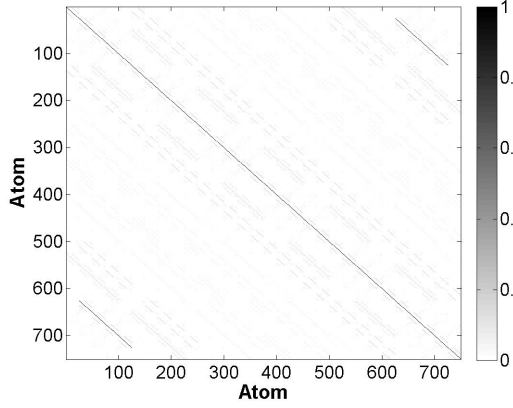
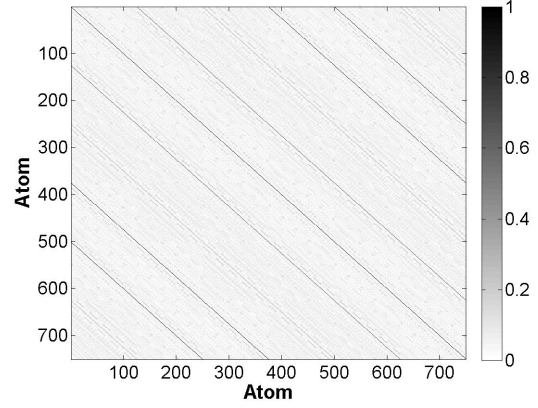


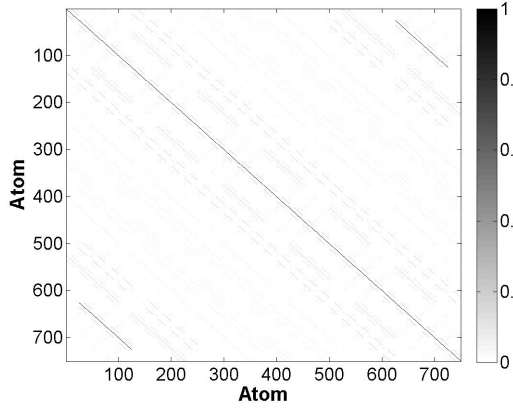
Figure A.4: Correlation map corresponding to $\mathbf{D}_{\Gamma_{\text{sphere}}}$ generated using a linear flight path, HH polarization, and 1 frequency.



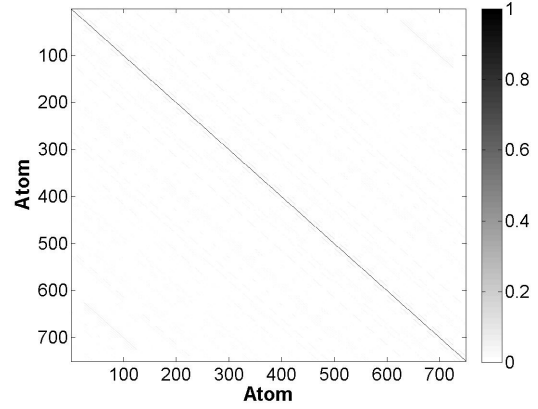
(a) Correlation map corresponding to $\mathbf{D}_{\Gamma_{\text{sphere}}}$ generated using a linear flight path, HH polarization, and 125 frequencies.



(b) Correlation map corresponding to $\mathbf{D}_{\Gamma_{\text{sphere}}}$ generated using a nonlinear flight path, HH polarization, and 1 frequency.

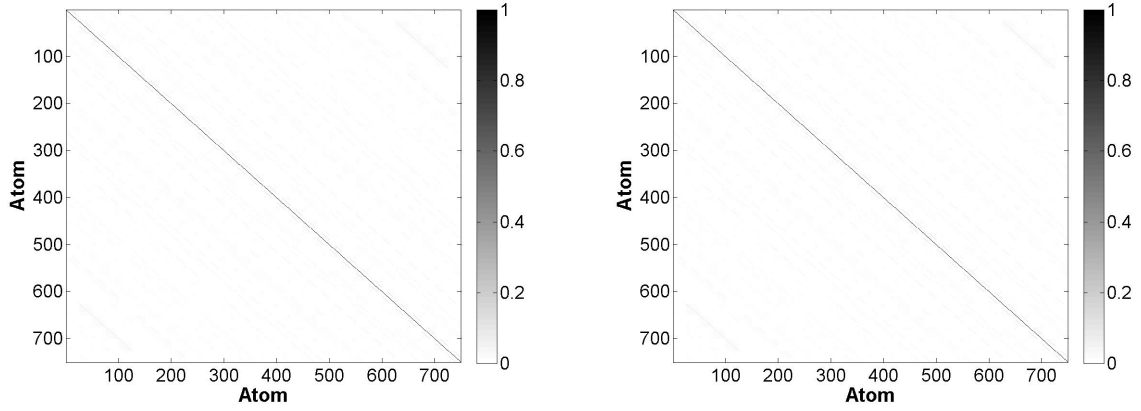


(c) Correlation map corresponding to $\mathbf{D}_{\Gamma_{\text{sphere}}}$ generated using a linear flight path, HH, HV, and VV polarizations, and 125 frequencies.



(d) Correlation map corresponding to $\mathbf{D}_{\Gamma_{\text{sphere}}}$ generated using a nonlinear flight path, HH, HV, and VV polarizations, and 125 frequencies.

Figure A.5: Reduction in correlation due to increased aspect and frequency diversity for $\mathbf{D}_{\Gamma_{\text{sphere}}}$.



(a) Correlation map corresponding to $\mathbf{D}_{\Gamma_{\text{sphere}}}$ generated using a nonlinear flight path, HH, HV, and VV polarizations, and 125 frequencies before clustering.

(b) Correlation map corresponding to $\mathbf{D}_{\Gamma_{\text{sphere}}}$ generated using a nonlinear flight path, HH, HV, and VV polarizations, and 125 frequencies after implementing molecule method.

Figure A.6: Reduction in correlation due to molecule clustering algorithm.

The reduction in coherence and dictionary size due to the molecule method is shown in Figure A.6.

A.3 Top-Hat Dictionary

The confuser map for the baseline top-hat dictionary, created using 1 frequency, HH polarization and linear flight path, is provided in Figure A.7. The coherence reductions from increasing the radar collection parameter diversities are shown in Figure A.8.

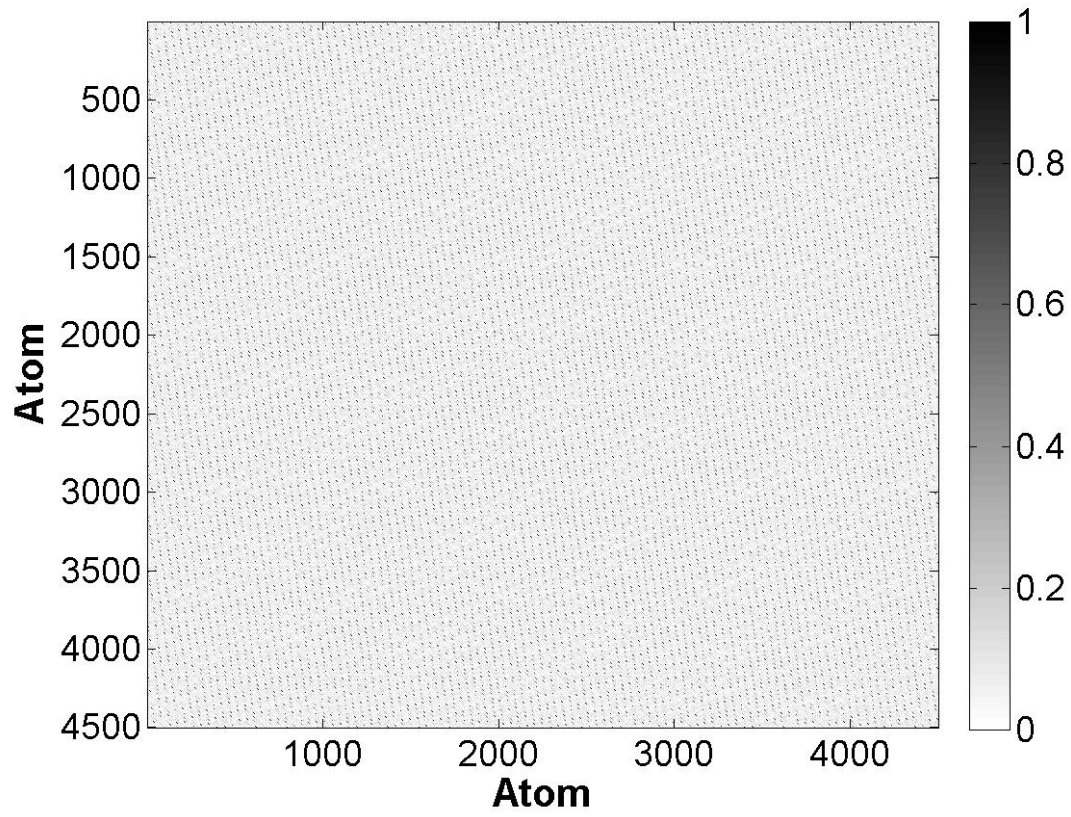
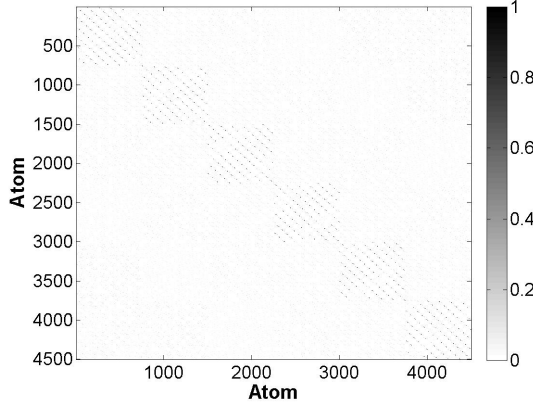
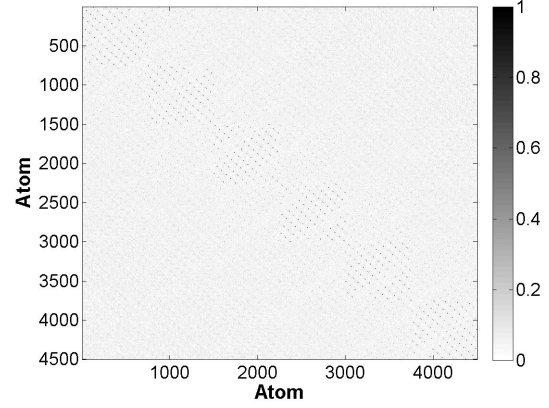


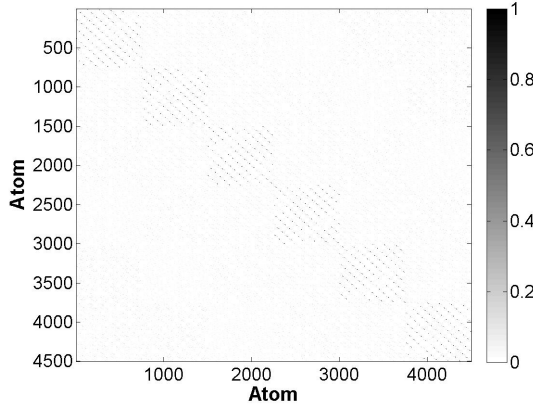
Figure A.7: Correlation map corresponding to $\mathbf{D}_{\Gamma_{\text{top-hat}}}$ generated using a linear flight path, HH polarization, and 1 frequency.



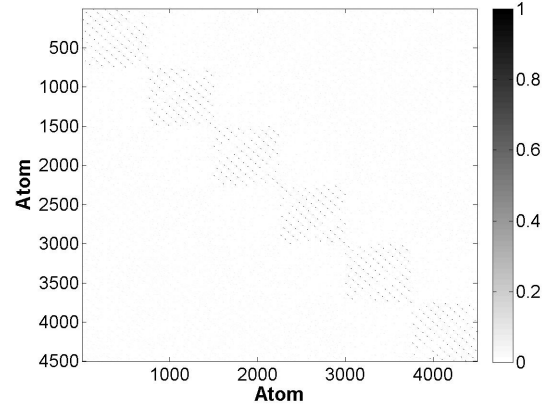
(a) Correlation map corresponding to $\mathbf{D}_{\Gamma_{\text{top-hat}}}$ generated using a linear flight path, HH polarization, and 125 frequencies.



(b) Correlation map corresponding to $\mathbf{D}_{\Gamma_{\text{top-hat}}}$ generated using a nonlinear flight path, HH polarization, and 1 frequency.



(c) Correlation map corresponding to $\mathbf{D}_{\Gamma_{\text{top-hat}}}$ generated using a linear flight path, HH, HV, and VV polarizations, and 125 frequencies.



(d) Correlation map corresponding to $\mathbf{D}_{\Gamma_{\text{top-hat}}}$ generated using a nonlinear flight path, HH, HV, and VV polarizations, and 125 frequencies.

Figure A.8: Reduction in correlation due to increased aspect and frequency diversity for $\mathbf{D}_{\Gamma_{\text{top-hat}}}$.

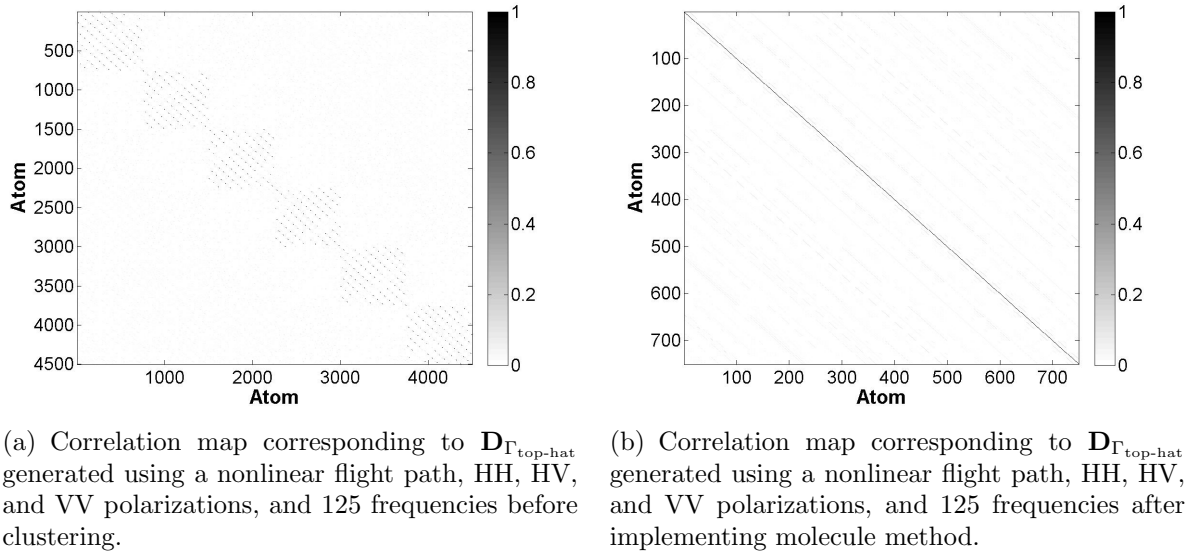


Figure A.9: Reduction in correlation due to molecule clustering algorithm.

The reduction in coherence and dictionary size due to the molecule method is shown in Figure A.9.

A.4 Trihedral Dictionary

The confuser map for the baseline trihedral dictionary, created using 1 frequency, HH polarization and linear flight path, is provided in Figure A.10. The coherence reductions from increasing the radar collection parameter diversities are shown in Figure A.11.

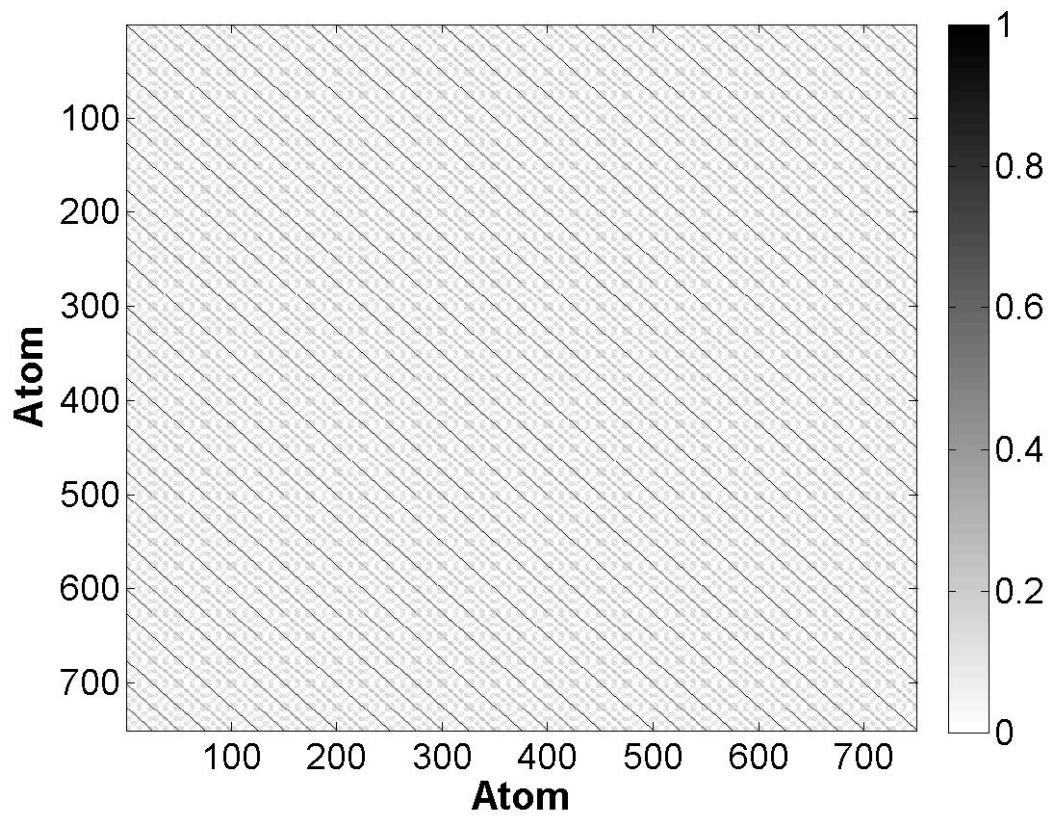
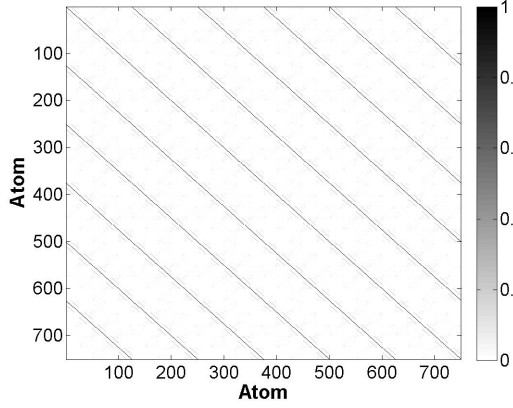
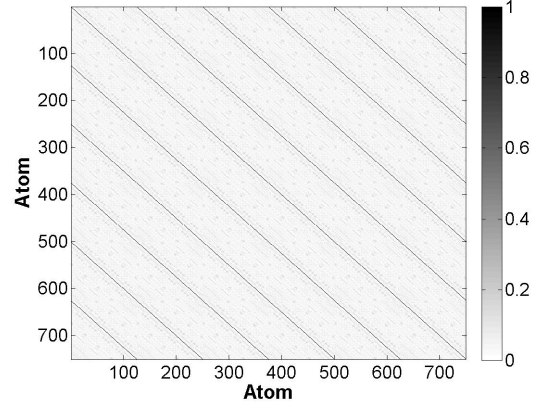


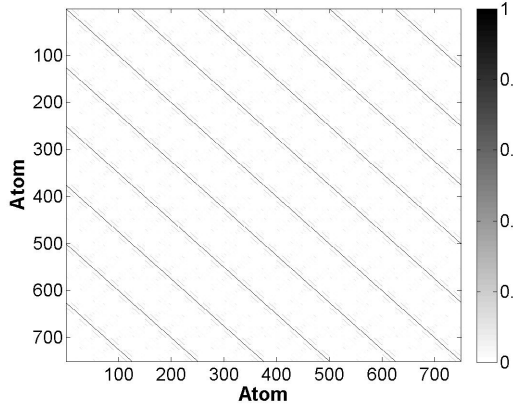
Figure A.10: Correlation map corresponding to $\mathbf{D}_{\Gamma_{\text{trihedral}}}$ generated using a linear flight path, HH polarization, and 1 frequency.



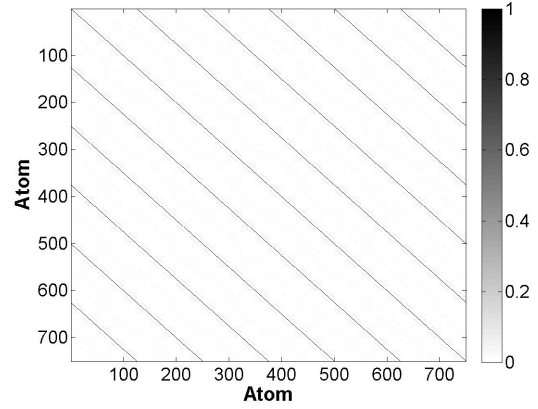
(a) Correlation map corresponding to $\mathbf{D}_{\Gamma_{\text{trihedral}}}$ generated using a linear flight path, HH polarization, and 125 frequencies.



(b) Correlation map corresponding to $\mathbf{D}_{\Gamma_{\text{trihedral}}}$ generated using a nonlinear flight path, HH polarization, and 1 frequency.

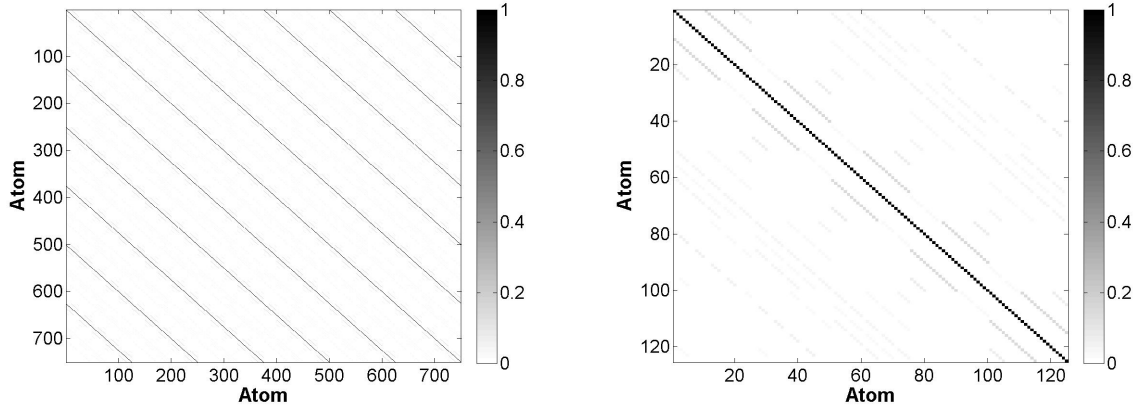


(c) Correlation map corresponding to $\mathbf{D}_{\Gamma_{\text{trihedral}}}$ generated using a linear flight path, HH, HV, and VV polarizations, and 125 frequencies.



(d) Correlation map corresponding to $\mathbf{D}_{\Gamma_{\text{trihedral}}}$ generated using a nonlinear flight path, HH, HV, and VV polarizations, and 125 frequencies.

Figure A.11: Reduction in correlation due to increased aspect and frequency diversity for $\mathbf{D}_{\Gamma_{\text{trihedral}}}$.



(a) Correlation map corresponding to $\mathbf{D}_{\Gamma_{\text{trihedral}}}$ generated using a nonlinear flight path, HH, HV, and VV polarizations, and 125 frequencies before clustering.

(b) Correlation map corresponding to $\mathbf{D}_{\Gamma_{\text{trihedral}}}$ generated using a nonlinear flight path, HH, HV, and VV polarizations, and 125 frequencies after implementing molecule method.

Figure A.12: Reduction in correlation due to molecule clustering algorithm.

The reduction in coherence and dictionary size due to the molecule method is shown in Figure A.12.

A.5 *Cylinder Dictionary*

The confuser map for the baseline cylinder dictionary, created using 1 frequency, HH polarization and linear flight path, is provided in Figure A.13. The coherence reductions from increasing the radar collection parameter diversities are shown in Figure A.14.

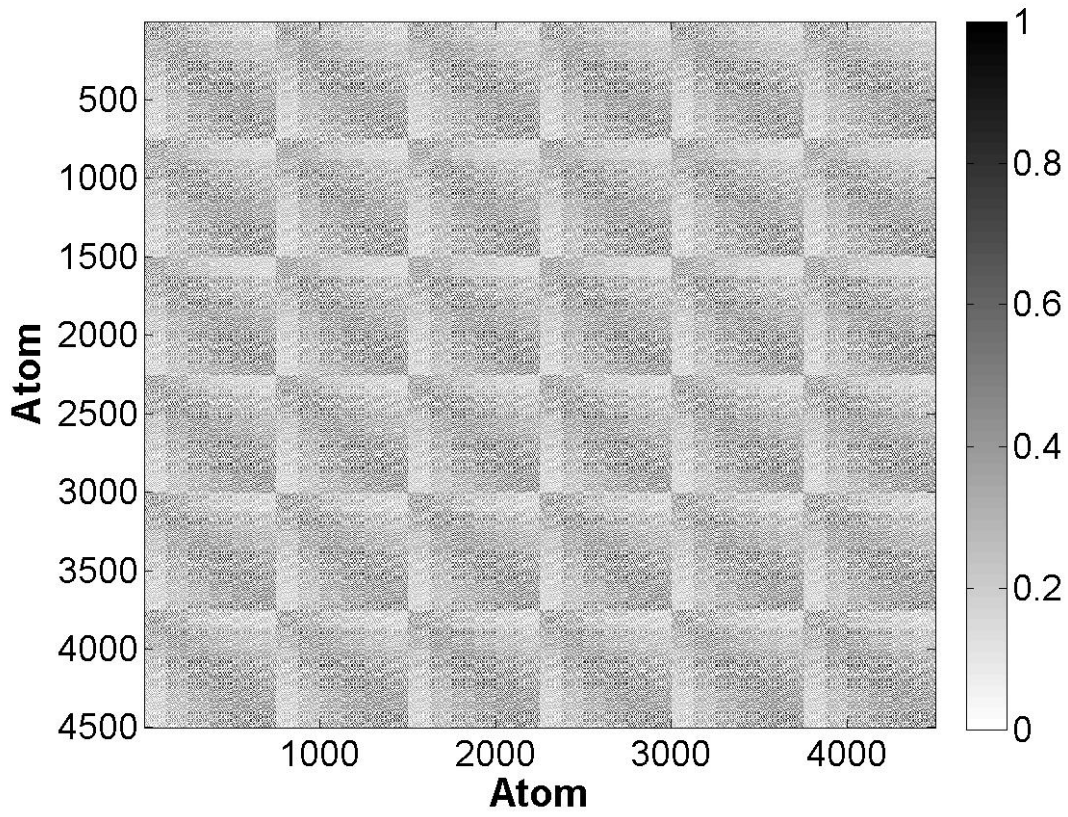
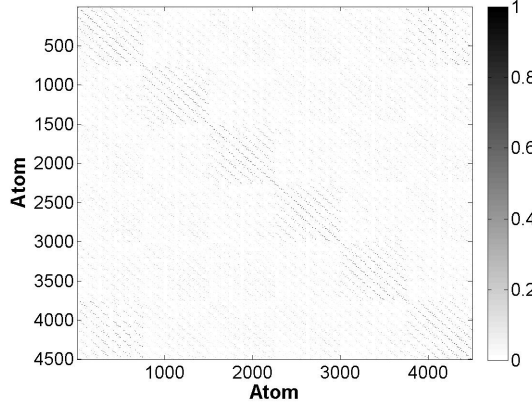
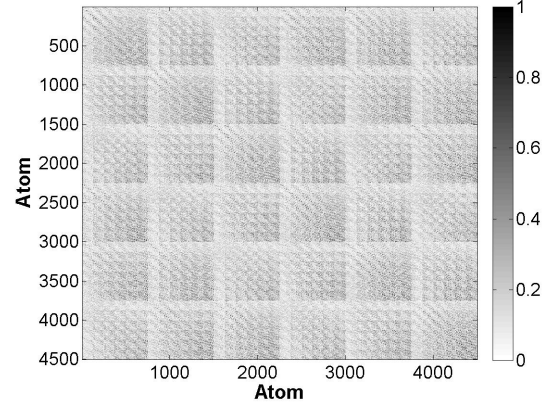


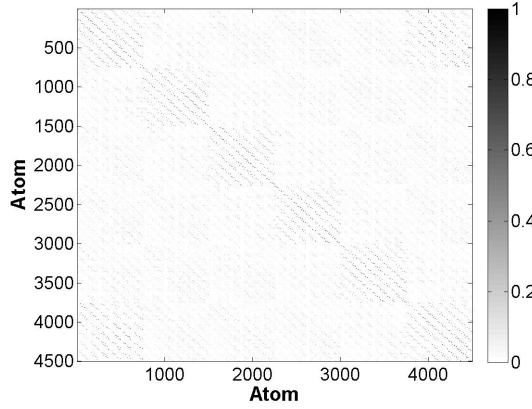
Figure A.13: Correlation map corresponding to $\mathbf{D}_{\Gamma_{\text{cylinder}}}$ generated using a linear flight path, HH polarization, and 1 frequency.



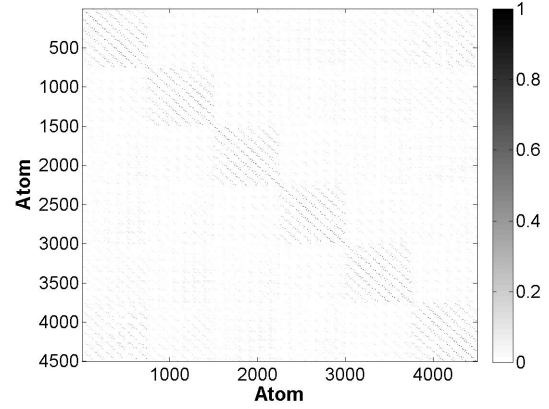
(a) Correlation map corresponding to $\mathbf{D}_{\Gamma_{\text{cylinder}}}$ generated using a linear flight path, HH polarization, and 125 frequencies.



(b) Correlation map corresponding to $\mathbf{D}_{\Gamma_{\text{cylinder}}}$ generated using a nonlinear flight path, HH polarization, and 1 frequency.



(c) Correlation map corresponding to $\mathbf{D}_{\Gamma_{\text{cylinder}}}$ generated using a linear flight path, HH, HV, and VV polarizations, and 125 frequencies.



(d) Correlation map corresponding to $\mathbf{D}_{\Gamma_{\text{cylinder}}}$ generated using a nonlinear flight path, HH, HV, and VV polarizations, and 125 frequencies.

Figure A.14: Reduction in correlation due to increased aspect and frequency diversity for $\mathbf{D}_{\Gamma_{\text{cylinder}}}$.

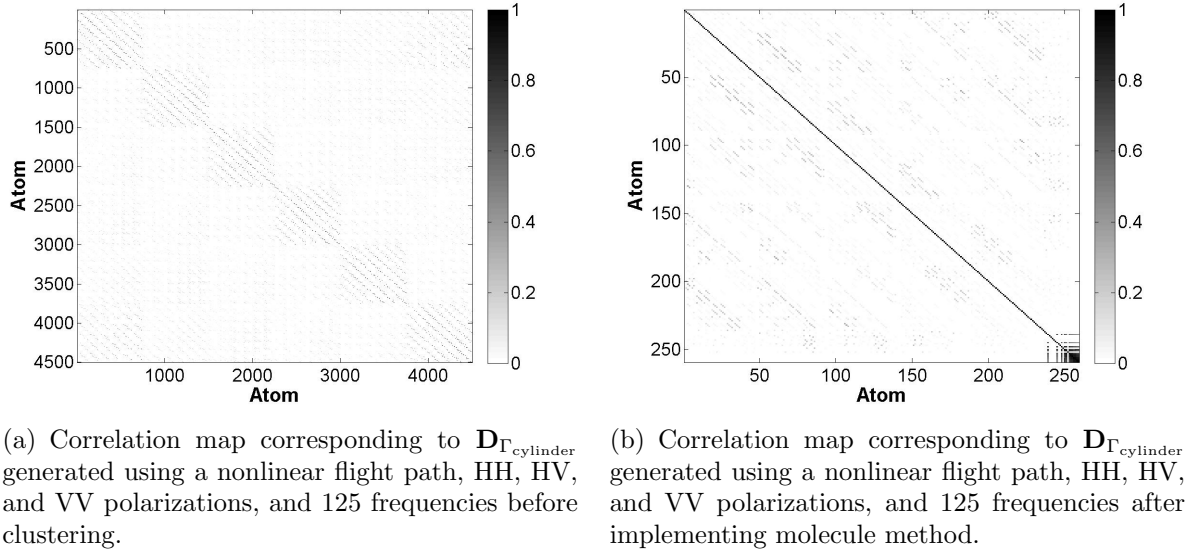
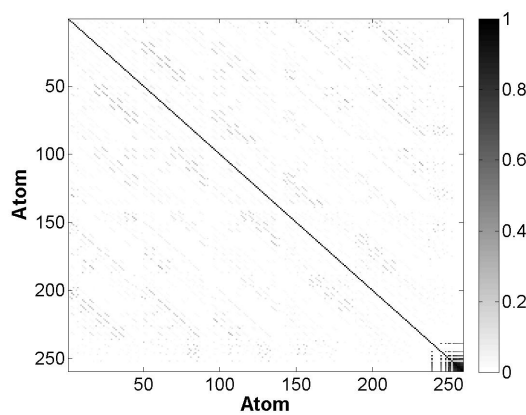
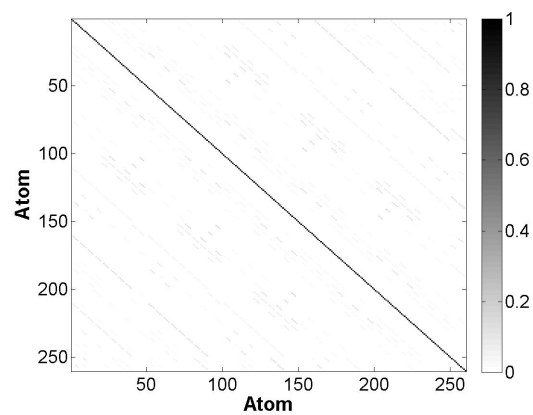


Figure A.15: Reduction in correlation due to molecule clustering algorithm.

The reduction in coherence and dictionary size due to the molecule method is shown in Figure A.15. The large coherence in the bottom right-hand corner of Figure A.15 is due to correlations between the representative means. This shape is the only shape that led to significant coherence between replaced atoms. These correlations lead to the degradation in parameter estimation performance shown in the original SNR plots. For this shape, the molecule method is modified to replace correlated atoms with the single atom corresponding to the current index instead of the mean of the atoms. The method leads to the successful classification and estimation of the cylinder and a diagonalized Gram-Matrix. The reduction in coherence is shown in Figure A.16.



(a) Correlation map corresponding to $\mathbf{D}_{\Gamma_{\text{cylinder}}}$ generated using a nonlinear flight path, HH, HV, and VV polarizations, and 125 frequencies after implementing original molecule method.



(b) Correlation map corresponding to $\mathbf{D}_{\Gamma_{\text{cylinder}}}$ generated using a nonlinear flight path, HH, HV, and VV polarizations, and 125 frequencies after implementing modified molecule method.

Figure A.16: Reduction in correlation due to modified molecule clustering algorithm.

Appendix B. Scenario 1 Results

This appendix includes the scenario 1 results for target scenes containing a single plate, sphere, top-hat, or trihedral.

B.1 Plate Target

The plate target scene is simulated using atom 2501 from the plate dictionary. The specific parameters used to create the plate are shown in Table B.1.

Table B.1: The parameters used to create the plate for scenario 1.

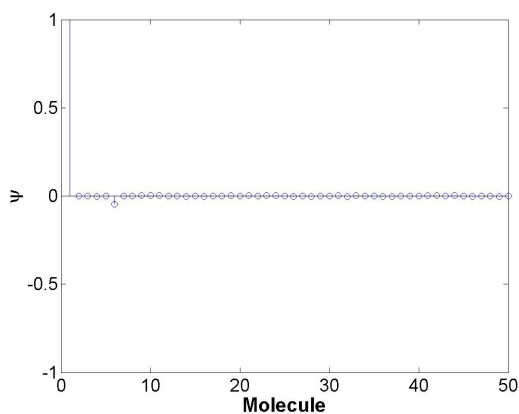
Shape	X	Y	Z	H	L	r	$\tilde{\gamma}$	$\tilde{\theta}$	$\tilde{\phi}$
plate	-10	-10	-10	2	1.5	-	0	-30	0

The atom and molecule correspondences are provided in Table B.2. The six

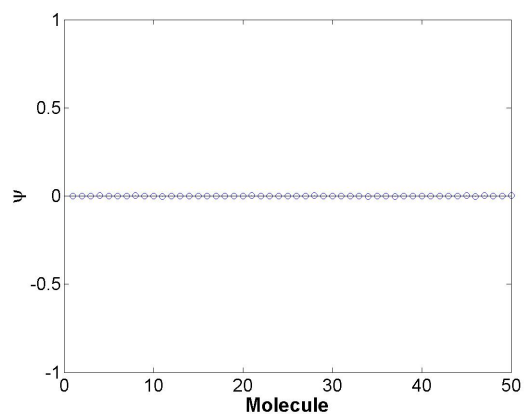
Table B.2: Atom correspondence for measured shape.

Shape	Orig. Dict. Atom	Molecule	Molecule Atom
plate	2501	1	61

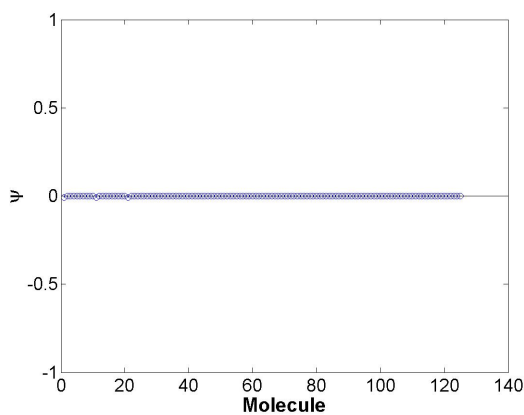
resulting coefficient plots, separated by shape, are provided in Figure B.1.



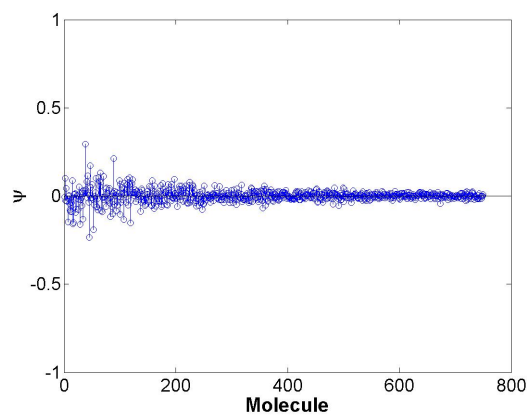
(a) BP result using the reduced plate dictionary.



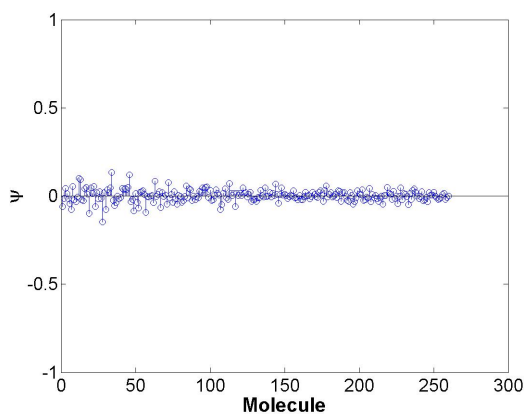
(b) BP result using the reduced dihedral dictionary.



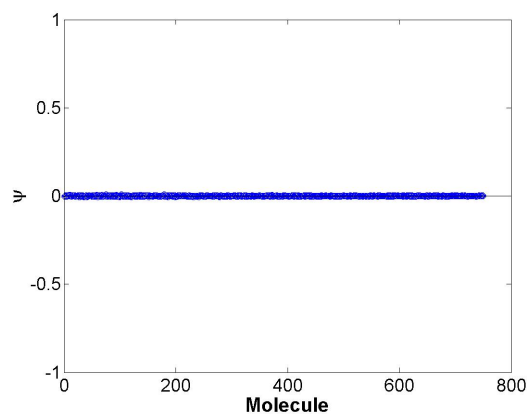
(c) BP result using the reduced trihedral dictionary.



(d) BP result using the reduced sphere dictionary.



(e) BP result using the reduced cylinder dictionary.



(f) BP result using the reduced top-hat dictionary.

Figure B.1: BP results for each of the reduced shape dictionaries used in the feature extraction problem in scenario 1 for the plate target scene.

The maximum coefficient returned by the BP algorithm for each of the shape dictionaries and the sparsities, described by $\|\psi\|_1$, are provided in Table B.3.

Table B.3: Maximum coefficients from each shape dictionary along with the ℓ_1 norm (sparsity descriptor) for scenario 1, plate example.

Shape	$\max(\psi)$	$\ \psi\ _1$	$(\psi - \lambda \cdot \ \psi\ _1)$
plate	1.0662	1.1840	0.8293
dihedral	0.0023	0.0434	-0.0064
sphere	0.2947	18.1124	-3.3278
top-hat	0.0090	1.0522	-0.2014
triangular	2.5678×10^{-4}	0.0335	-0.0064
cylinder	0.1330	6.4715	-1.1613

This method correctly leads to a plate classification. The plate dictionary molecule corresponding to the largest coefficient within ψ is chosen as the “sub-dictionary” used for parameter estimation via the MAP estimator. This largest coefficient correctly corresponds to molecule 1.

Estimates of the posterior log-likelihoods are calculated for each atom within this molecule. These estimates are plotted and provided in Figure B.2. The largest log-likelihood corresponds to the correct atom (atom 61) as shown by the associated parameters provided in Table B.4.

Table B.4: Estimated versus true parameters for scenario 1, plate example.

Shape	X	Y	Z	H	L	r	$\tilde{\gamma}$	$\tilde{\theta}$	$\tilde{\phi}$
True plate	-10	-10	-10	2	1.5	-	0	-30	0
Estimated plate	-10	-10	-10	2	1.5	-	0	-30	0

B.2 Sphere Target

The sphere target scene is simulated using atom 700 from the sphere dictionary. The specific parameters used to create the sphere are shown in Table B.5.

The sphere dictionary coherence was already minimized prior to implementing the molecule clustering. Therefore, only the BP method is used to select the appro-

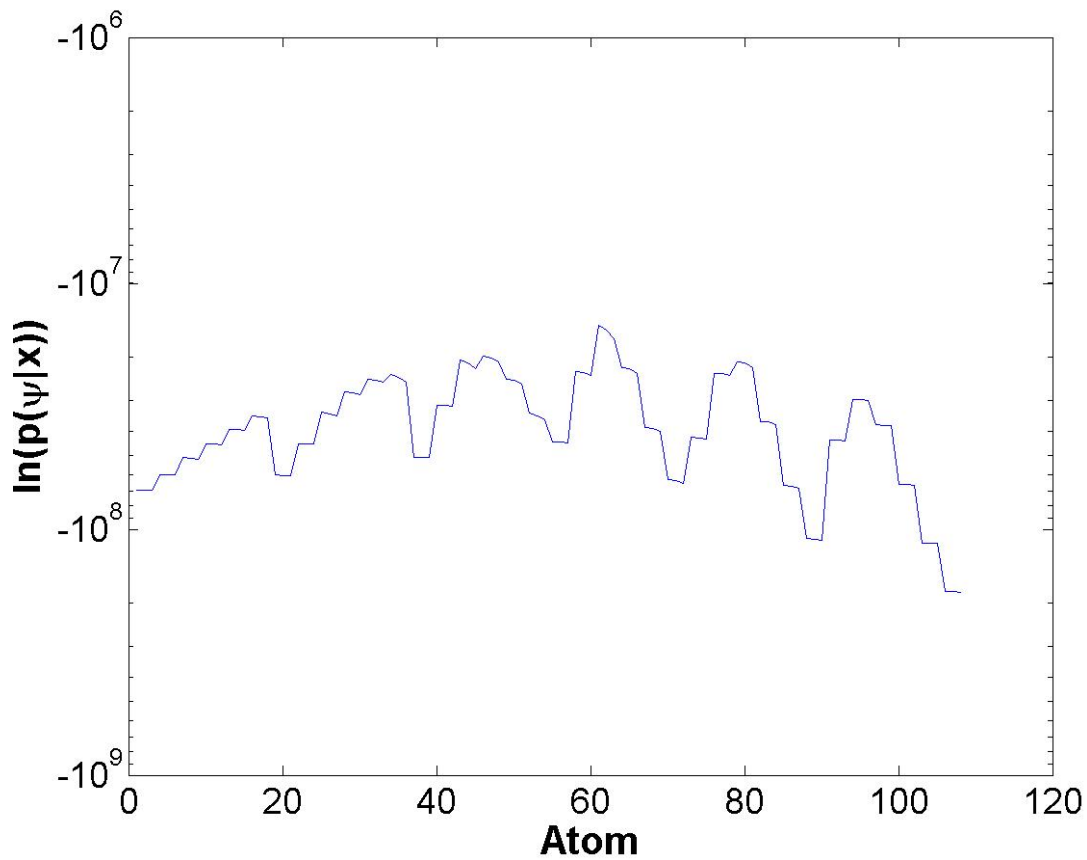
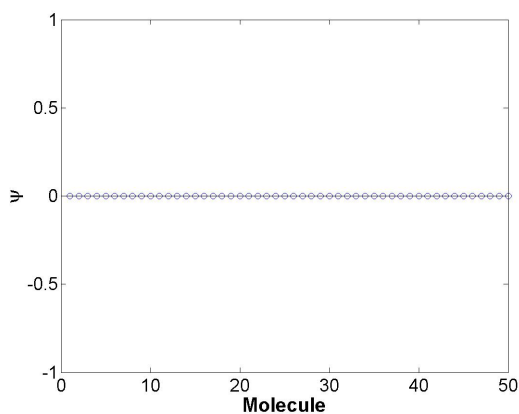


Figure B.2: Posterior log-likelihood estimates associated with each atom within the selected plate molecule (True Atom = 61).

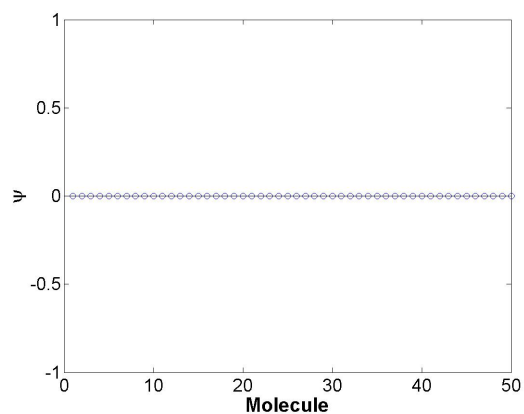
Table B.5: The parameters used to create the sphere for scenario 1.

Shape	X	Y	Z	H	L	r	$\tilde{\gamma}$	$\tilde{\theta}$	$\tilde{\phi}$
sphere	10	10	0	-	-	3	0	0	0

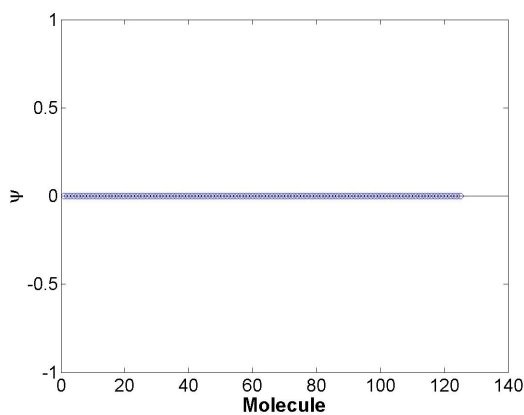
priate atom. The six resulting coefficient plots, separated by shape, are provided in Figure B.3.



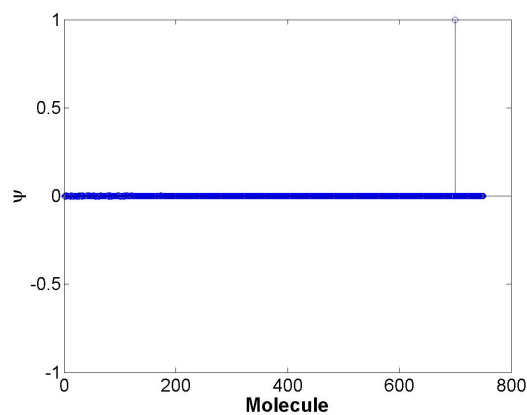
(a) BP result using the reduced plate dictionary.



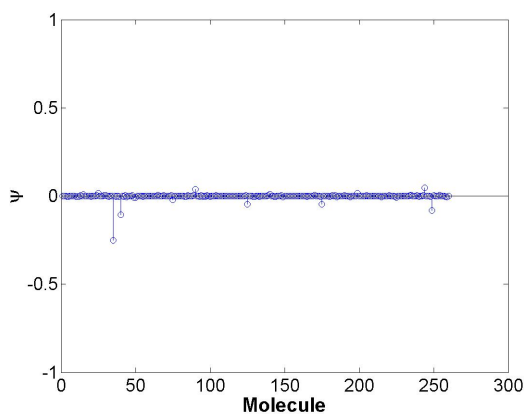
(b) BP result using the reduced dihedral dictionary.



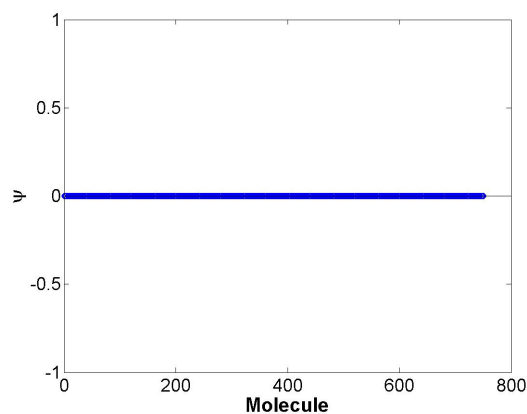
(c) BP result using the reduced trihedral dictionary.



(d) BP result using the reduced sphere dictionary.



(e) BP result using the reduced cylinder dictionary.



(f) BP result using the reduced top-hat dictionary.

Figure B.3: BP results for each of the reduced shape dictionaries used in the feature extraction problem in scenario 1 for the sphere target scene.

The maximum coefficient returned by the BP algorithm for each of the shape dictionaries and the sparsities, described by $\|\psi\|_1$, are provided in Table B.6.

Table B.6: Maximum coefficients from each shape dictionary along with the ℓ_1 norm (sparsity descriptor) for scenario 1, sphere example.

Shape	$\max(\psi)$	$\ \psi\ _1$	$(\psi - \lambda \cdot \ \psi\ _1)$
plate	5.7913×10^{-4}	0.0045	-3.2081×10^{-4}
dihedral	3.1978×10^{-5}	5.7225×10^{-4}	-8.2743×10^{-5}
sphere	0.9999	1.2553	0.7489
top-hat	1.0751×10^{-4}	0.0150	-0.0029
triangular	3.5184×10^{-4}	0.0018	-1.3389×10^{-6}
cylinder	0.0473	0.9931	-1.1513

This method correctly leads to a sphere classification. The sphere dictionary atom corresponding to the largest coefficient within ψ is chosen as the index for parameter estimation. This index corresponds to the correct atom (atom 700) as shown by the associated parameters provided in Table B.7.

Table B.7: Estimated versus true parameters for scenario 1, sphere example.

Shape	X	Y	Z	H	L	r	$\tilde{\gamma}$	$\tilde{\theta}$	$\tilde{\phi}$
True sphere	10	10	0	-	-	3	0	0	0
Estimated sphere	10	10	0	-	-	3	0	0	0

B.3 Top-hat Target

The top-hat target scene is simulated using atom 2563 from the top-hat dictionary. The specific parameters used to create the plate are shown in Table B.8.

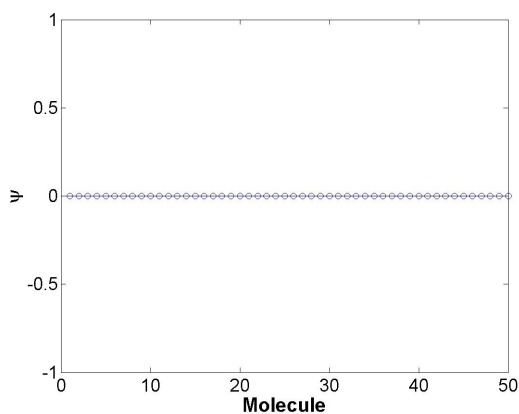
Table B.8: The parameters used to create the top-hat for scenario 1.

Shape	X	Y	Z	H	L	r	$\tilde{\gamma}$	$\tilde{\theta}$	$\tilde{\phi}$
top-hat	0	0	0	1.5	-	2	0	0	0

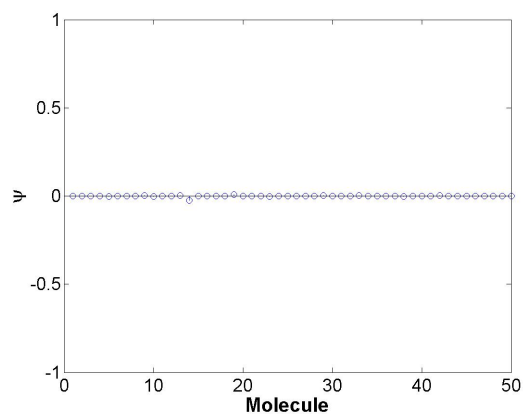
The atom and molecule correspondences are provided in Table B.9. The six resulting coefficient plots, separated by shape, are provided in Figure B.4.

Table B.9: Atom correspondence for measured shape.

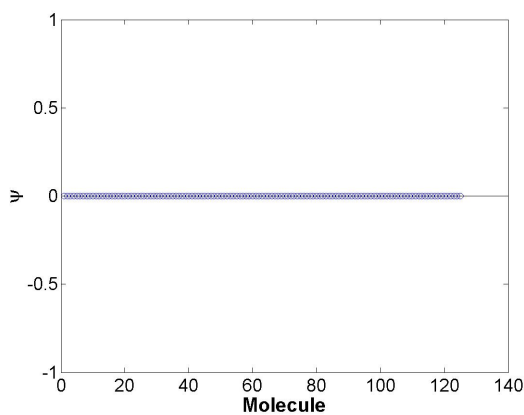
Shape	Orig. Dict. Atom	Molecule	Molecule Atom
top-hat	2563	438	3



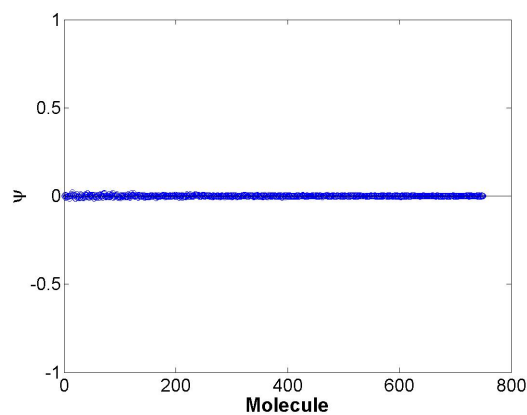
(a) BP result using the reduced plate dictionary.



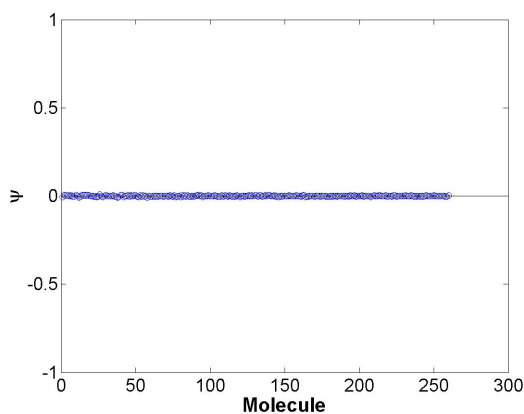
(b) BP result using the reduced dihedral dictionary.



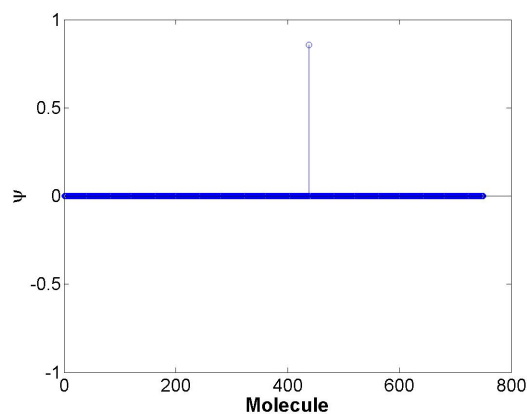
(c) BP result using the reduced trihedral dictionary.



(d) BP result using the reduced sphere dictionary.



(e) BP result using the reduced cylinder dictionary.



(f) BP result using the reduced top-hat dictionary.

Figure B.4: BP results for each of the reduced shape dictionaries used in the feature extraction problem in scenario 1 for the top-hat target scene.

The maximum coefficient returned by the BP algorithm for each of the shape dictionaries and the sparsities, described by $\|\psi\|_1$, are provided in Table B.10.

Table B.10: Maximum coefficients from each shape dictionary along with the ℓ_1 norm (sparsity descriptor) for scenario 1, top-hat example.

Shape	$\max(\psi)$	$\ \psi\ _1$	$(\psi - \lambda \cdot \ \psi\ _1)$
plate	3.7997×10^{-4}	0.0067	-9.5520×10^{-4}
dihedral	0.0094	0.0670	-0.0040
sphere	0.0191	1.7713	-0.3352
top-hat	0.8570	0.9742	0.6621
trihedral	2.3507×10^{-5}	0.0010	-1.7903×10^{-4}
cylinder	0.0071	0.4928	-0.0914

This method correctly leads to a top-hat classification. The top-hat dictionary molecule corresponding to the largest coefficient within ψ is chosen as the “sub-dictionary” used for parameter estimation via the MAP estimator. This largest coefficient correctly corresponds to molecule 438.

Estimates of the posterior log-likelihoods are calculated for each atom within this molecule. These estimates are plotted and provided in Figure B.5. The largest log-likelihood corresponds to the correct atom (atom 3) as shown by the associated parameters provided in Table B.11.

Table B.11: Estimated versus true parameters for scenario 1, top-hat example.

Shape	X	Y	Z	H	L	r	$\tilde{\gamma}$	$\tilde{\theta}$	$\tilde{\phi}$
True top-hat	0	0	0	1.5	-	2	0	0	0
Estimated top-hat	0	0	0	1.5	-	2	0	0	0

B.4 Trihedral Target

The trihedral target scene is simulated using atom 725 from the trihedral dictionary. The specific parameters used to create the plate are shown in Table B.12.

The atom and molecule correspondences are provided in Table B.13. The six resulting coefficient plots, separated by shape, are provided in Figure B.6.

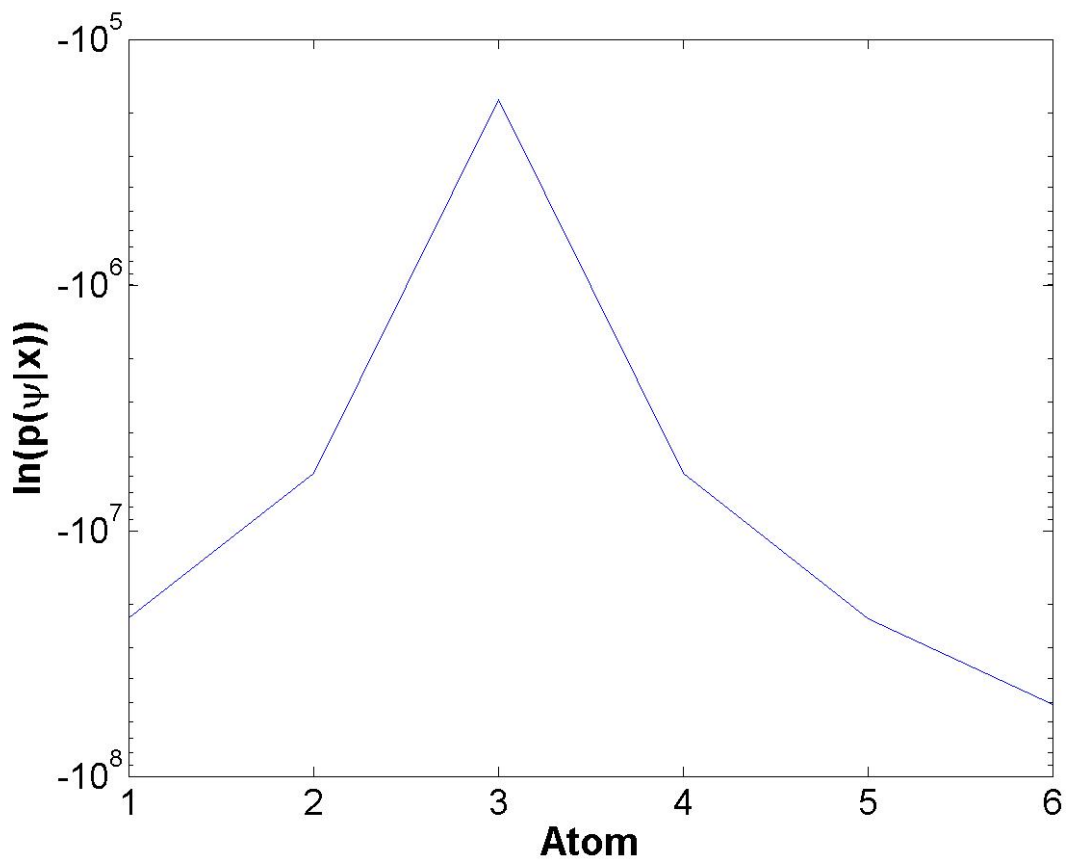


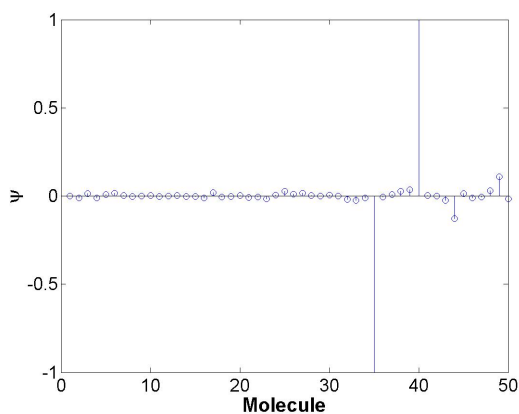
Figure B.5: Posterior log-likelihood estimates associated with each atom within the selected top-hat molecule (True Atom = 3).

Table B.12: The parameters used to create the trihedral for scenario 1.

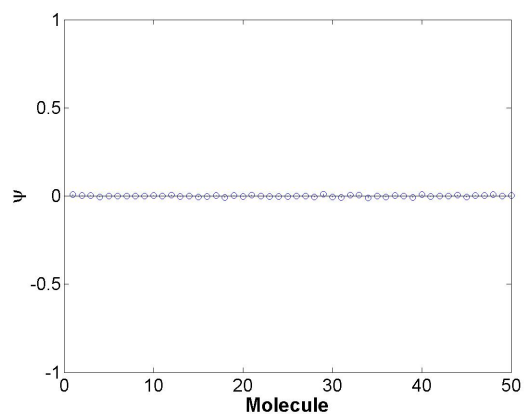
Shape	X	Y	Z	H	L	r	$\tilde{\gamma}$	$\tilde{\theta}$	$\tilde{\phi}$
trihedral	10	10	5	3	-	-	0	0	0

Table B.13: Atom correspondence for measured shape.

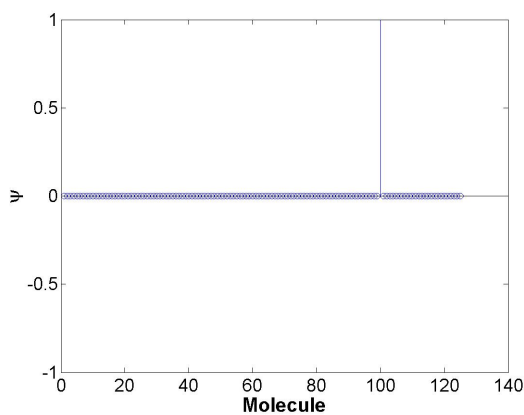
Shape	Orig. Dict. Atom	Molecule	Molecule Atom
trihedral	725	100	6



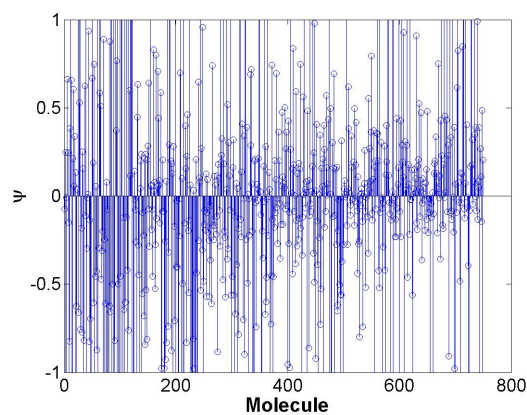
(a) BP result using the reduced plate dictionary.



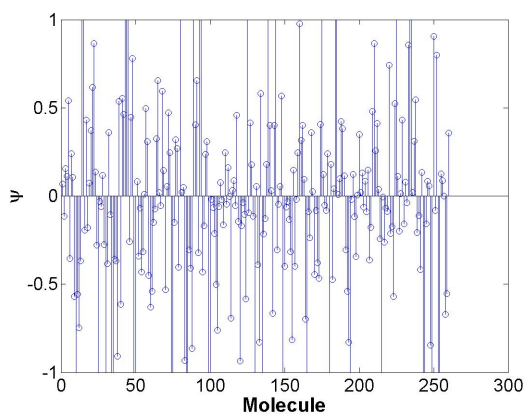
(b) BP result using the reduced dihedral dictionary.



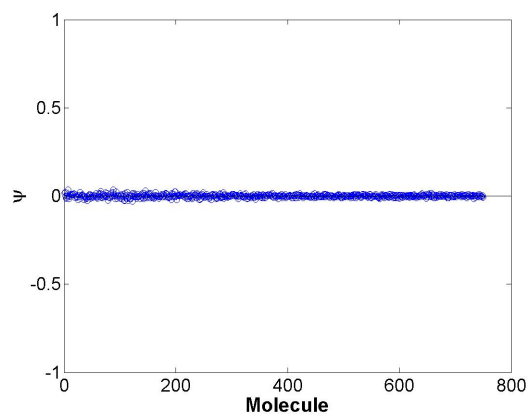
(c) BP result using the reduced trihedral dictionary.



(d) BP result using the reduced sphere dictionary.



(e) BP result using the reduced cylinder dictionary.



(f) BP result using the reduced top-hat dictionary.

Figure B.6: BP results for each of the reduced shape dictionaries used in the feature extraction problem in scenario 1 for the trihedral target scene.

The maximum coefficient returned by the BP algorithm for each of the shape dictionaries and the sparsities, described by $\|\psi\|_1$, are provided in Table B.14.

Table B.14: Maximum coefficients from each shape dictionary along with the ℓ_1 norm (sparsity descriptor) for scenario 1, trihedral example.

Shape	$\max(\psi)$	$\ \psi\ _1$	$(\psi - \lambda \cdot \ \psi\ _1)$
plate	1.2445	8.7238	-0.5003
dihedral	0.0104	0.1822	-0.0260
sphere	48.3599	1.2343×10^3	-198.5060
top-hat	0.0363	4.7410	-0.9119
trihedral	2.3736	2.4128	1.8910
cylinder	18.0406	323.6352	-46.6864

This method correctly leads to a trihedral classification. The trihedral dictionary molecule corresponding to the largest coefficient within ψ is chosen as the “sub-dictionary” used for parameter estimation via the MAP estimator. This largest coefficient correctly corresponds to molecule 100.

Estimates of the posterior log-likelihoods are calculated for each atom within this molecule. These estimates are plotted and provided in Figure B.7. The largest log-likelihood corresponds to the correct atom (atom 6) as shown by the associated parameters provided in Table B.15.

Table B.15: Estimated versus true parameters for scenario 1, trihedral example.

Shape	X	Y	Z	H	L	r	$\tilde{\gamma}$	$\tilde{\theta}$	$\tilde{\phi}$
True trihedral	10	10	5	3	-	-	0	0	0
Estimated trihedral	10	10	5	3	-	-	0	0	0

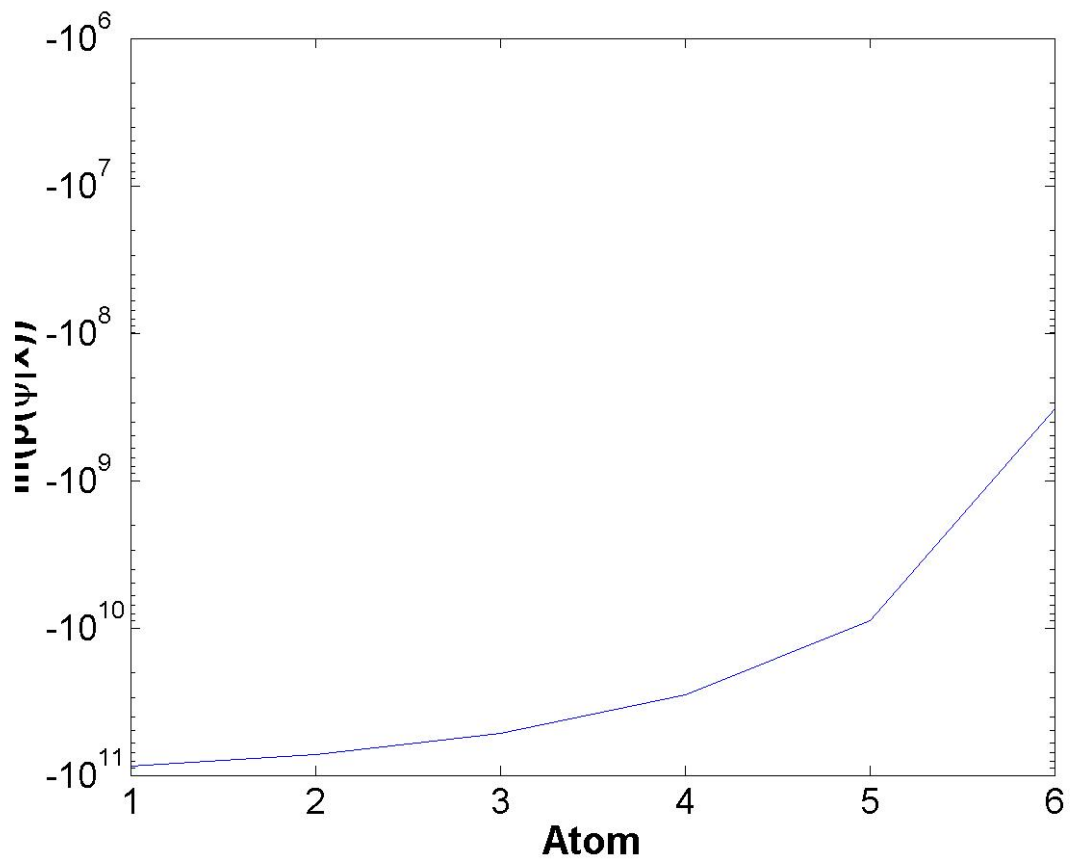


Figure B.7: Posterior log-likelihood estimates associated with each atom within the selected trihedral molecule (True Atom = 3).

Appendix C. Scenario 2 Results

C.1 Dihedral Results

C.1.1 X Parameter. In this example, we generate a dihedral target located at $x = 4$ m with an SNR of 30 dB. The dihedral target is simulated using the parameters listed in Table C.1. The BP results for each shape are provided in Figure C.1.

Table C.1: The parameters used to create the dihedral target for scenario 2, example 1.

Shape	X	Y	Z	H	L	r	$\tilde{\gamma}$	$\tilde{\theta}$	$\tilde{\phi}$
dihedral	4	0	0	2	1	-	0	0	0

The maximum coefficient returned by the BP algorithm for each of the shape dictionaries and the sparsities, described by $\|\psi\|_1$, are provided in Table C.2. This

Table C.2: Maximum coefficients from each shape dictionary along with ℓ_1 norm (sparsity descriptor).

Shape	$\max(\psi)$	$\ \psi\ _1$	$(\max(\psi) - \lambda \cdot \ \psi\ _1)$
plate	0.0021	0.0396	-0.0058
dihedral	0.1833	0.4004	0.1033
sphere	0.1245	10.2423	-1.9239
top-hat	0.0873	3.5333	-0.6193
trihedral	1.8667×10^{-4}	0.0055	-9.1924×10^{-4}
cylinder	0.0540	2.8144	-0.5089

method correctly leads to a dihedral classification. However, the algorithm incorrectly estimates both the size and location parameters, as shown in Table C.3.

Table C.3: Estimated versus true parameters for scenario 2, dihedral example 1.

Shape	X	Y	Z	H	L	r	$\tilde{\gamma}$	$\tilde{\theta}$	$\tilde{\phi}$
True dihedral	4	0	0	2	1	-	0	0	0
Expected dihedral	5	0	0	2	1	-	0	0	0
Estimated dihedral	10	-10	-10	0.5	0.5	-	0	0	0

Initially, we make the hypothesis that the parameter set extracted should be the closest dictionary contained representative parameter set, $\Theta = [5, 0, 0, 2, 1, 0, 0, 0, 0]$

(atom 2439). Although this atom seems closer, the range profile provided in Figure C.2 shows that the extracted parameter set, $\Theta = [10, -10, -10, 0.5, 0.5, 0, 0, 0, 0]$ (atom 3770) is more representative in the range, or x dimension. This range error may have led to a larger LS error and the incorrect parameter set estimation. The LS errors are provided in Table C.4. The minimum LS error is equivalent to the MAP estimates, Table C.4: LS errors for the extracted and hypothesized data sets for scenario 2, dihedral example 1.

Data	$\ \mathbf{x} - \mathbf{s}(\Theta_n)\ _2^2$
Extracted	1.3989×10^8
Closest	2.7285×10^8

as described in Chapter II.

C.1.2 Y Parameter. In this example, we generate a dihedral target located at $y = 4$ m with an SNR of 30 dB. The dihedral target is simulated using the parameters listed in Table C.5.

Table C.5: The parameters used to create the dihedral target for scenario 2, example 2.

Shape	X	Y	Z	H	L	r	$\tilde{\gamma}$	$\tilde{\theta}$	$\tilde{\phi}$
dihedral	0	4	0	2	1	-	0	0	0

The BP results for each shape are provided in Figure C.3.

The maximum coefficient returned by the BP algorithm for each of the shape dictionaries and the sparsities, described by $\|\psi\|_1$, are provided in Table C.6.

This method correctly leads to a dihedral classification. The algorithm estimates the closest y location parameter, but incorrectly estimates the RCS parameters L and H , as shown in Table C.7.

Initially, we assume that the algorithm should choose the dihedral corresponding to the closest parameter set. Therefore, the expected parameter set would be $\Theta = [0, 5, 0, 2, 1, 0, 0, 0, 0]$. The extracted parameter set corresponds to atom 12. The

Table C.6: Maximum coefficients from each shape dictionary along with the ℓ_1 norm (sparsity descriptor) for scenario 2, dihedral example 2.

Shape	$\max(\psi)$	$\ \psi\ _1$	$(\max(\psi) - \lambda \cdot \ \psi\ _1)$
plate	0.0015	0.0395	-0.0064
dihedral	0.4116	0.6430	0.2830
sphere	0.1197	11.0668	-2.0936
top-hat	0.0674	2.9651	-0.5257
trihedral	1.7573×10^{-4}	0.0060	-0.0010
cylinder	0.0486	2.7934	-0.5101

Table C.7: Estimated versus true parameters for scenario 2, dihedral example 2.

Shape	X	Y	Z	H	L	r	$\tilde{\gamma}$	$\tilde{\theta}$	$\tilde{\phi}$
True dihedral	0	4	0	2	1	-	0	0	0
Expected dihedral	0	5	0	2	1	-	0	0	0
Estimated dihedral	0	5	0	0.5	3	-	0	0	0

total LS-errors are provided in Table C.8. The lowest LS error corresponds to the extracted data set and is equivalent to the largest log-likelihood. Next, we will repeat this process for the z parameter.

C.1.3 Z Parameter. In this example, we generate a dihedral target located at $z = 4$ m with an SNR of 30 dB. The dihedral target is simulated using the parameters listed in Table C.9.

The BP results for each shape are provided in Figures C.4-C.5.

The maximum coefficient returned by the BP algorithm for each of the shape dictionaries and the sparsities, described by $\|\psi\|_1$, are provided in Table C.2.

This method incorrectly classifies the shape as a combination of a trihedral and a plate. The associated extracted parameter set is provided in Table C.11.

Table C.8: LS errors for the extracted and hypothesized data sets for scenario 2, dihedral example 2.

Data	$\ \mathbf{x} - \mathbf{s}(\Theta_n)\ _2^2$
Extracted	1.0190×10^8
Closest	2.7791×10^8

Table C.9: The parameters used to create the dihedral target for scenario 2, example 3.

Shape	X	Y	Z	H	L	r	$\tilde{\gamma}$	$\tilde{\theta}$	$\tilde{\phi}$
dihedral	0	0	4	2	1	-	0	0	0

Table C.10: Maximum coefficients from each shape dictionary along with the ℓ_1 norm (sparsity descriptor) for scenario 2, dihedral example 3.

Shape	Iteration	$\max(\psi)$	$\ \psi\ _1$	$(\max(\psi) - \lambda \cdot \ \psi\ _1)$
plate	1	0.0017	0.0382	-0.0060
	2	0.1916	0.2863	0.1344
dihedral	1	0.0170	0.6365	-0.1103
	2	0.0170	0.6365	-0.1103
sphere	1	0.1163	10.4378	-1.9713
	2	3.2425	50.6746	-6.8924
top-hat	1	0.1327	3.6546	-0.5982
	2	0.1327	3.6546	-0.5982
trihedral	1	1.5837×10^{-4}	0.0071	-0.0013
	2	1.2568×10^{-4}	0.0727	-0.0144
cylinder	1	0.0626	2.9127	-0.5199
	2	0.5477	8.5697	-1.1662

The total LS errors for the extracted data versus the hypothesized closest data are provided in Table C.12.

C.1.4 RCS Parameters. In this section we discuss the results of two example target scenes. Each of the scenes includes a dihedral that is generated using a length or height parameter that falls outside of the dictionary parameter space resolution with an SNR of 30 dB. The dihedral targets are simulated using the parameters listed in Table C.13.

Table C.11: Estimated versus true parameters for scenario 2, dihedral example 3.

Shape	X	Y	Z	H	L	r	$\tilde{\gamma}$	$\tilde{\theta}$	$\tilde{\phi}$
True dihedral	0	0	4	2	1	-	0	0	0
Expected dihedral	0	0	5	2	1	-	0	0	0
Estimated trihedral	0	-5	-10	0.5	-	-	0	0	0
Estimated plate	0	-5	-10	1	0.5	-	0	-30	0

Table C.12: LS errors for the extracted and hypothesized data sets for scenario 2, dihedral example 3.

Data	$\ \mathbf{x} - \mathbf{s}(\Theta_n)\ _2^2$
Extracted	2.0210×10^8
Closest	2.8090×10^8

Table C.13: The parameters used to create the dihedral target for scenario 2, examples 4 and 5.

Shape	X	Y	Z	H	L	r	$\tilde{\gamma}$	$\tilde{\theta}$	$\tilde{\phi}$
dihedral 1	0	0	0	2.3	1	-	0	0	0
dihedral 2	0	0	0	2	1.3	-	0	0	0

The BP results for each shape are provided in Figures C.6-C.8.

The maximum coefficient returned by the BP algorithm for each of the shape dictionaries and the sparsities, described by $\|\psi\|_1$, are provided in Table C.14 and Table C.15.

Table C.14: Maximum coefficients from each shape dictionary along with the ℓ_1 norm (sparsity descriptor) for scenario 2, dihedral example 4.

Shape	$\max(\psi)$	$\ \psi\ _1$	$(\max(\psi) - \lambda \cdot \ \psi\ _1)$
plate	0.0022	0.0491	-0.0076
dihedral	0.9535	1.0159	0.7503
sphere	0.1284	12.6538	-2.4024
top-hat	0.1849	4.4749	-0.7101
trihedral	1.7732×10^{-4}	0.0064	-0.0011
cylinder	0.0459	3.3130	-0.6167

For both examples, the shape is correctly classified as a dihedral. The expected parameter set estimations are $\Theta = [0, 0, 0, 2.5, 1, 0, 0, 0, 0]$ and $\Theta = [0, 0, 0, 2, 1.5, 0, 0, 0, 0]$, since these are the closest defined sets. The algorithm successfully estimates the expected parameter set in example 4, but fails to estimation the expected set for example 5. In example 5, the algorithm overestimates the model order. These results are provided in Table C.16 and Table C.17.

Table C.15: Maximum coefficients from each shape dictionary along with the ℓ_1 norm (sparsity descriptor) for scenario 2, dihedral example 5.

Shape	Iteration	$\max(\psi)$	$\ \psi\ _1$	$(\max(\psi) - \lambda \cdot \ \psi\ _1)$
plate	1	0.0034	0.0500	-0.0066
	2	0.0034	0.0500	-0.0066
dihedral	1	1.0202	1.0891	0.8024
	2	0.1672	0.2053	0.1261
sphere	1	0.2000	14.9725	-2.7946
	2	0.2000	14.9725	-2.7946
top-hat	1	0.1891	4.4130	-0.6935
	2	0.0661	2.3852	-0.4110
trihedral	1	2.3260×10^{-4}	0.0073	-0.0012
	2	2.3260×10^{-4}	0.0073	-0.0012
cylinder	1	0.0843	3.5878	-0.6332
	2	0.0843	3.5878	-0.6332

Table C.16: Estimated versus true parameters for scenario 2, dihedral example 4.

Shape	X	Y	Z	H	L	r	$\tilde{\gamma}$	$\tilde{\theta}$	$\tilde{\phi}$
True dihedral	0	0	0	2.3	1	-	0	0	0
Expected dihedral	0	0	0	2.5	1	-	0	0	0
Estimated dihedral	0	0	0	2.5	1	-	0	0	0

C.2 Sphere Results

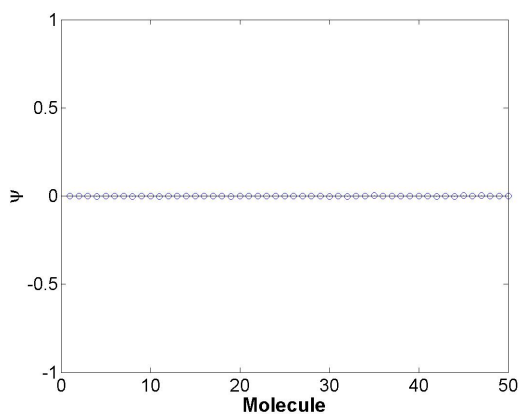
C.2.1 X Parameter. In this example, we generate a sphere target located at $x = 4$ m with an SNR of 30 dB. The sphere target is simulated using the parameters listed in Table C.18. The BP results for each shape are provided in Figures C.9-C.10.

Table C.17: Estimated versus true parameters for scenario 2, dihedral example 5.

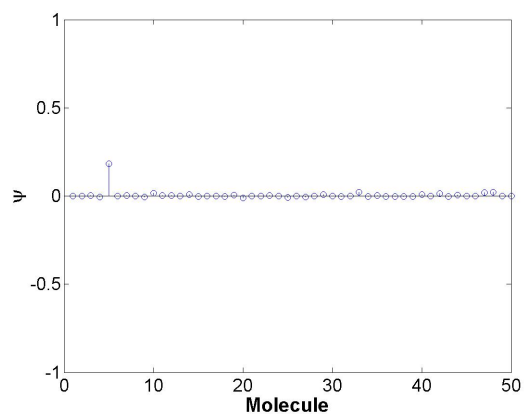
Shape	X	Y	Z	H	L	r	$\tilde{\gamma}$	$\tilde{\theta}$	$\tilde{\phi}$
True dihedral	0	0	0	2	1.3	-	0	0	0
Expected dihedral	0	0	0	2	1.5	-	0	0	0
Estimated dihedral 1	0	0	0	1.5	1.5	-	0	0	0
Estimated dihedral 2	0	0	0	1	0.5	-	0	0	0

Table C.18: The parameters used to create the sphere target for scenario 2, example 1.

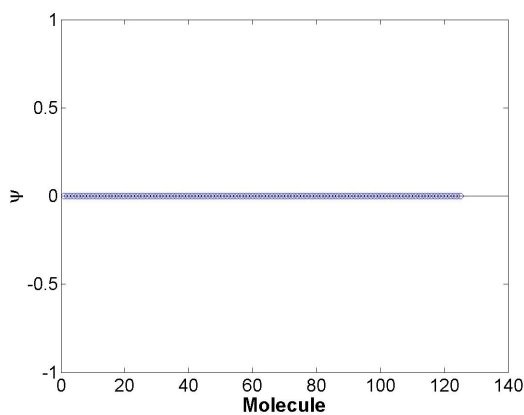
Shape	X	Y	Z	H	L	r	$\tilde{\gamma}$	$\tilde{\theta}$	$\tilde{\phi}$
sphere	4	0	0	-	-	2	-	-	-



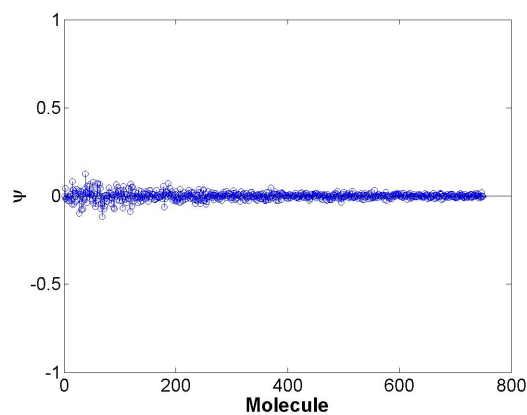
(a) BP result using the reduced plate dictionary.



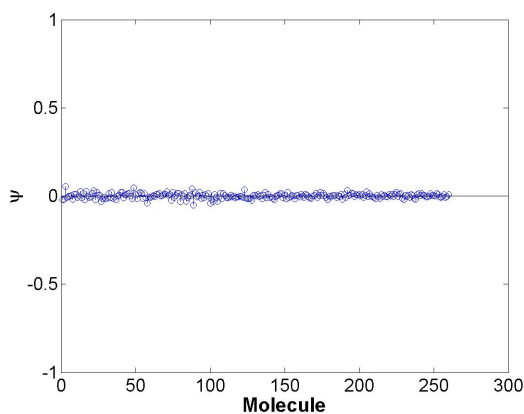
(b) BP result using the reduced dihedral dictionary.



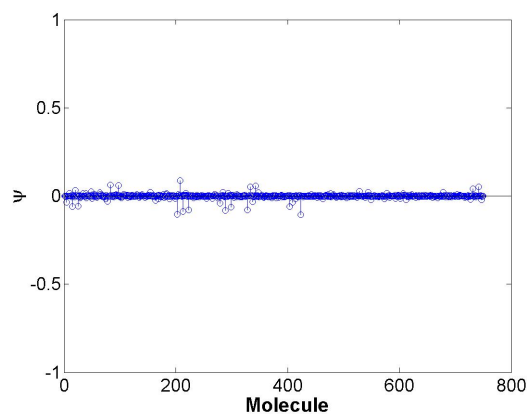
(c) BP result using the reduced trihedral dictionary.



(d) BP result using the reduced sphere dictionary.



(e) BP result using the reduced cylinder dictionary.



(f) BP result using the reduced top-hat dictionary.

Figure C.1: BP results for each of the reduced shape dictionaries used in the feature extraction problem in scenario 2, dihedral example 1.

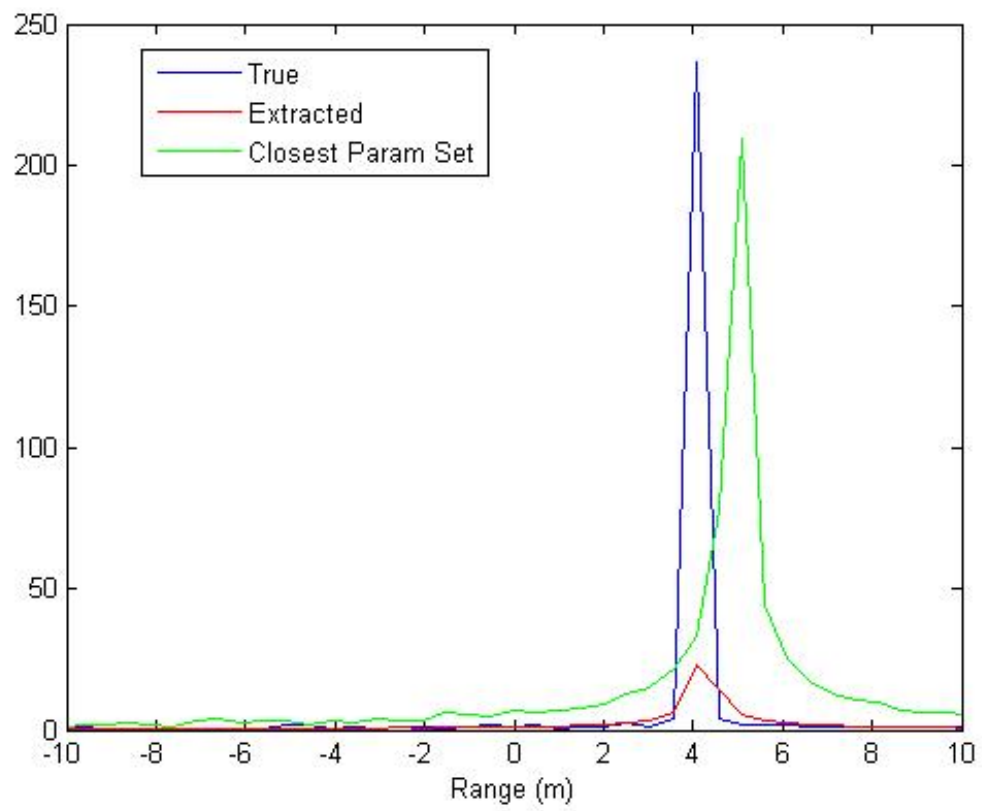
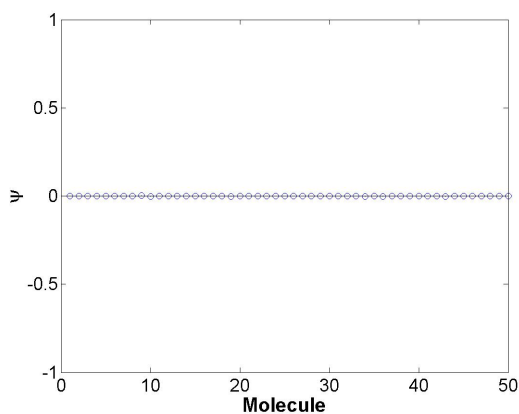
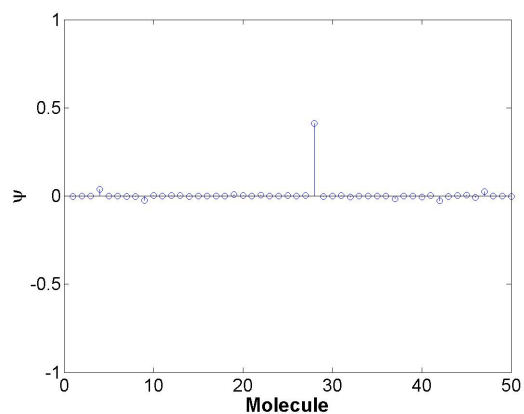


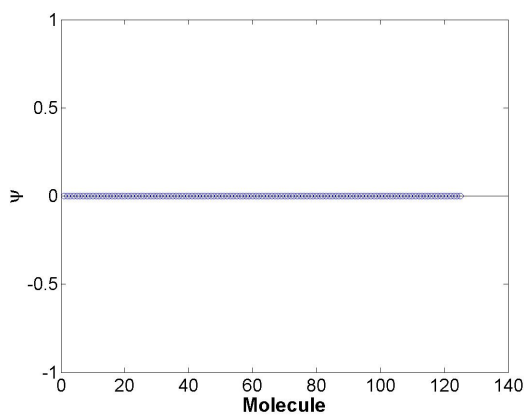
Figure C.2: Range profile for the true, extracted, and close simulated dihedral targets.



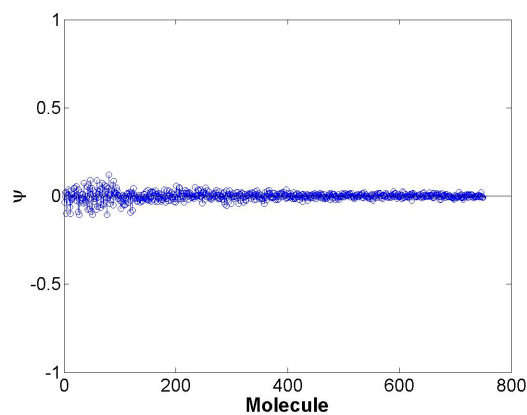
(a) BP result using the reduced plate dictionary.



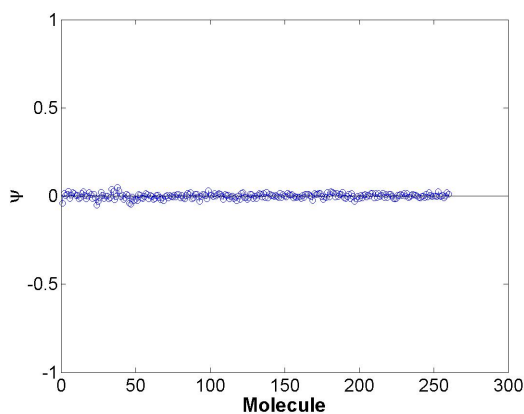
(b) BP result using the reduced dihedral dictionary.



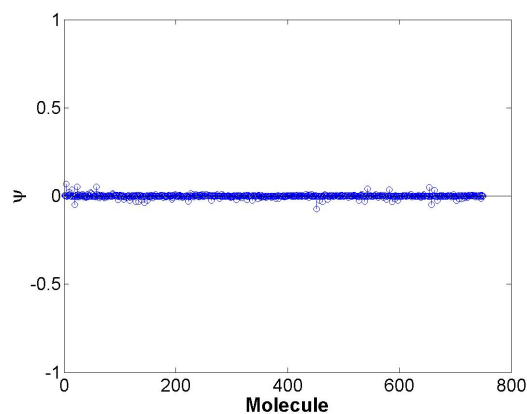
(c) BP result using the reduced trihedral dictionary.



(d) BP result using the reduced sphere dictionary.

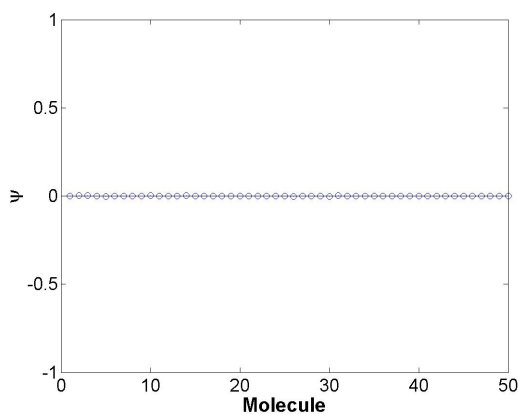


(e) BP result using the reduced cylinder dictionary.

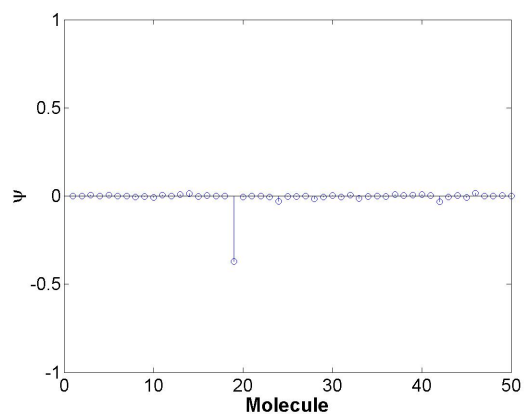


(f) BP result using the reduced top-hat dictionary.

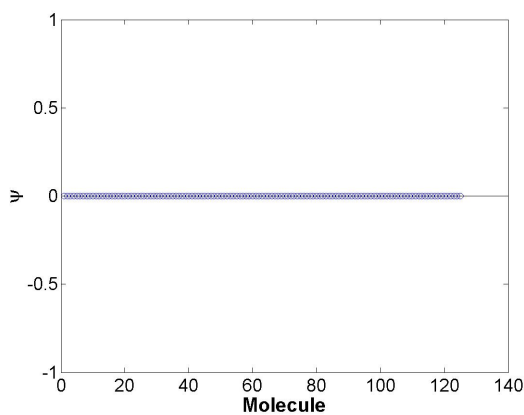
Figure C.3: BP results for each of the reduced shape dictionaries used in the feature extraction problem in scenario 2, dihedral example 2.



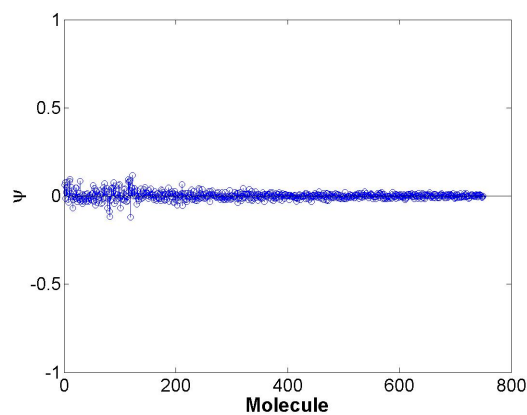
(a) BP result using the reduced plate dictionary.



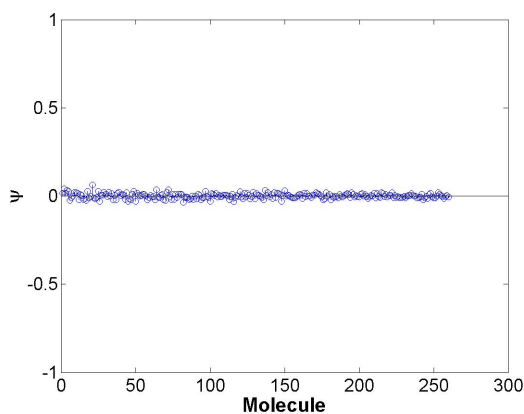
(b) BP result using the reduced dihedral dictionary.



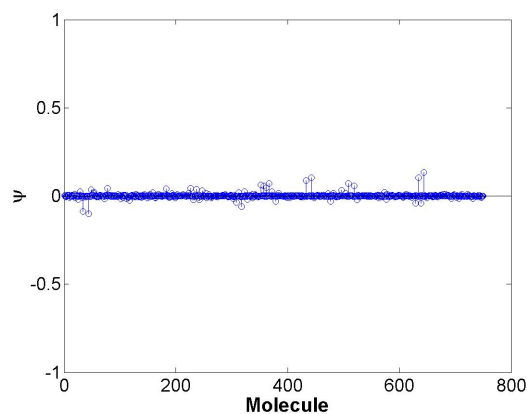
(c) BP result using the reduced trihedral dictionary.



(d) BP result using the reduced sphere dictionary.

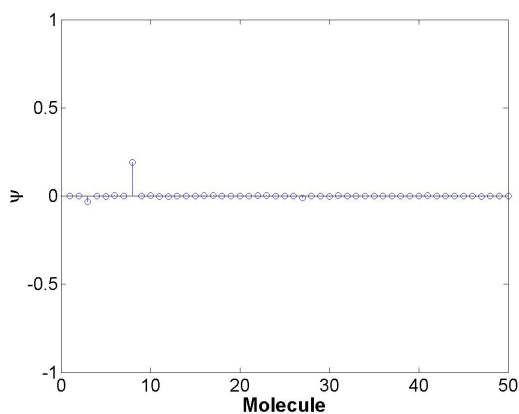


(e) BP result using the reduced cylinder dictionary.

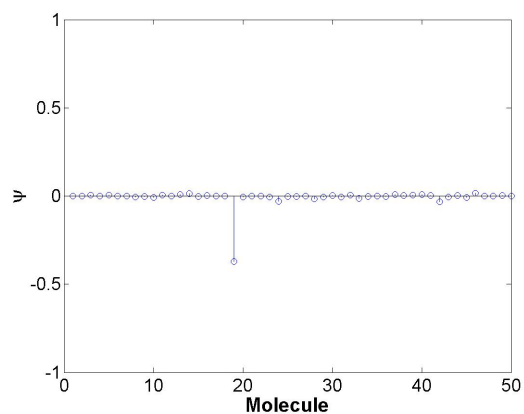


(f) BP result using the reduced top-hat dictionary.

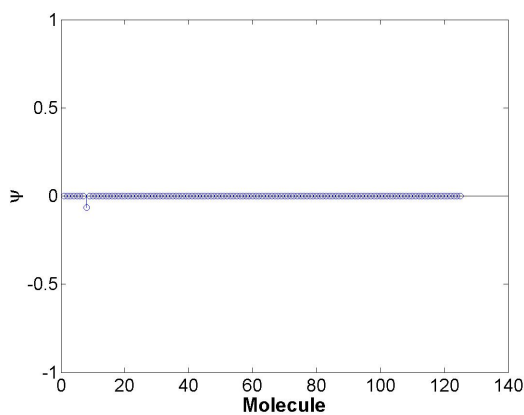
Figure C.4: BP results for the first iteration for each of the reduced shape dictionaries used in the feature extraction problem in scenario 2, dihedral example 3.



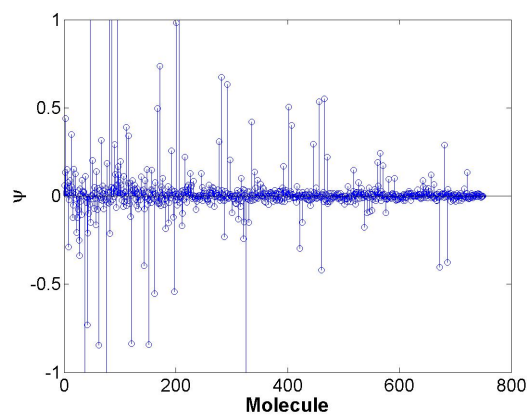
(a) BP result using the reduced plate dictionary.



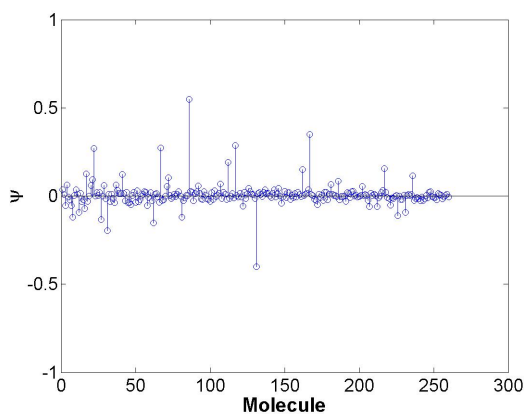
(b) BP result using the reduced dihedral dictionary.



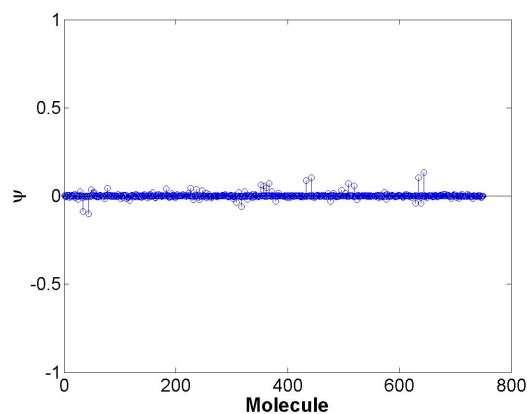
(c) BP result using the reduced trihedral dictionary.



(d) BP result using the reduced sphere dictionary.

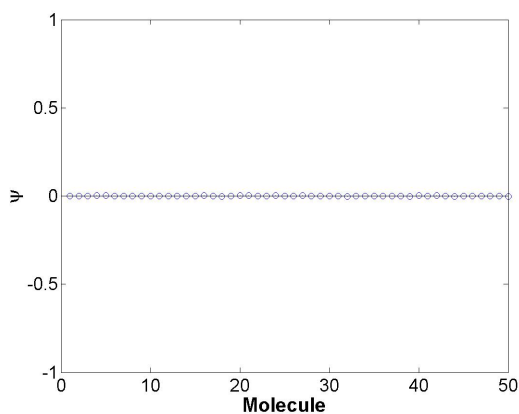


(e) BP result using the reduced cylinder dictionary.

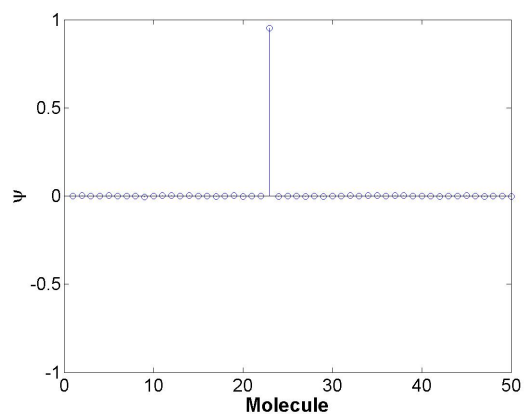


(f) BP result using the reduced top-hat dictionary.

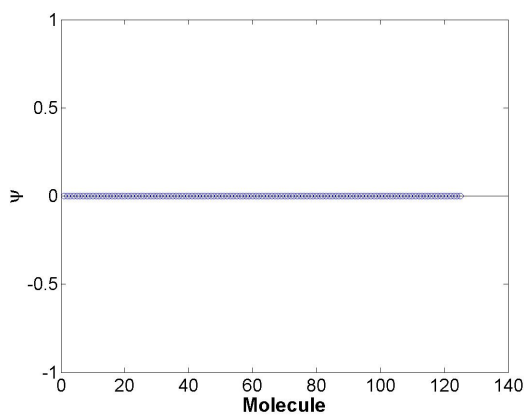
Figure C.5: BP results for the final iteration for each of the reduced shape dictionaries used in the feature extraction problem in scenario 2, dihedral example 3.



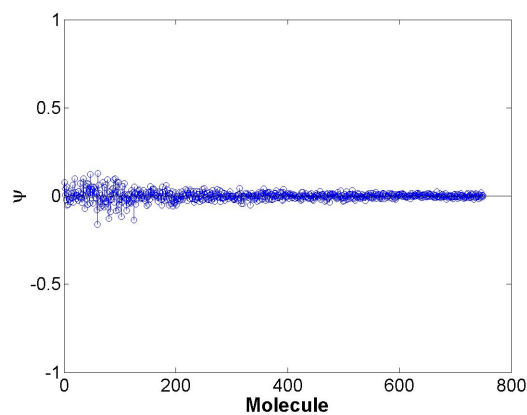
(a) BP result using the reduced plate dictionary.



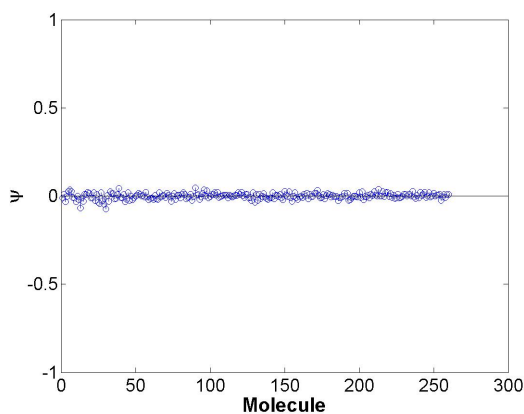
(b) BP result using the reduced dihedral dictionary.



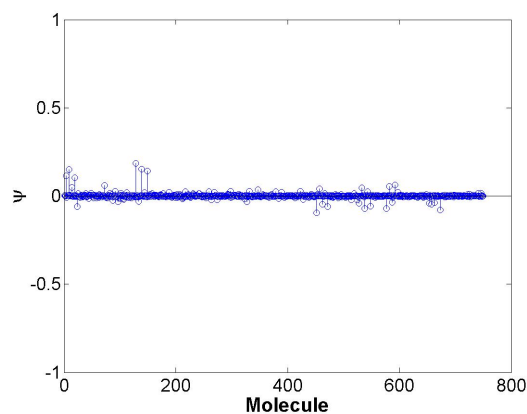
(c) BP result using the reduced trihedral dictionary.



(d) BP result using the reduced sphere dictionary.

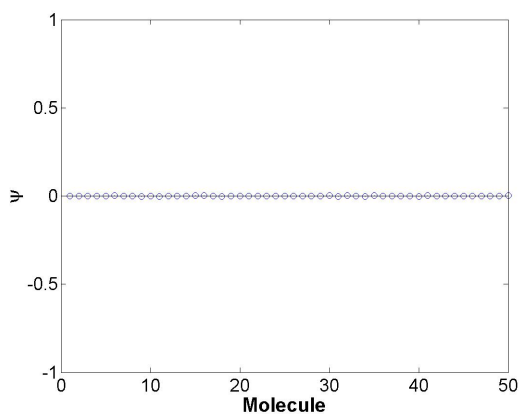


(e) BP result using the reduced cylinder dictionary.

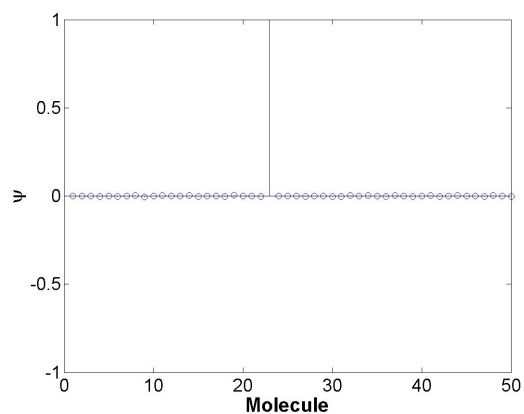


(f) BP result using the reduced top-hat dictionary.

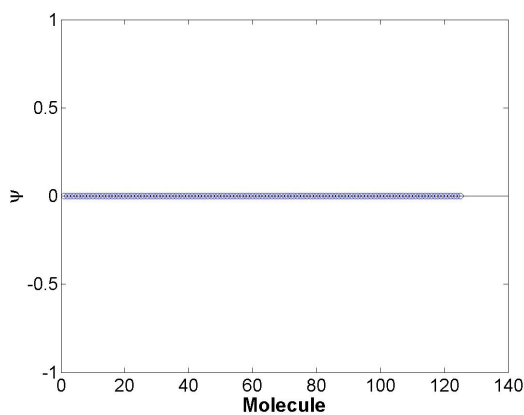
Figure C.6: BP results for each of the reduced shape dictionaries used in the feature extraction problem in scenario 2, dihedral example 4.



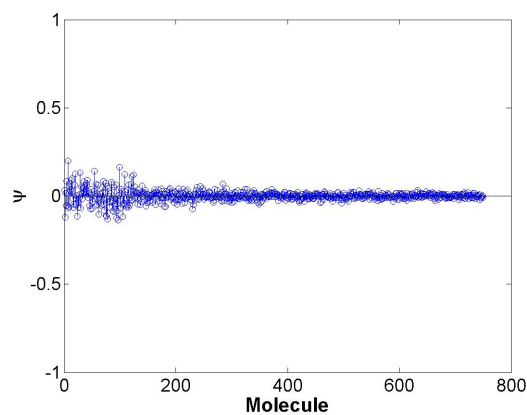
(a) BP result using the reduced plate dictionary.



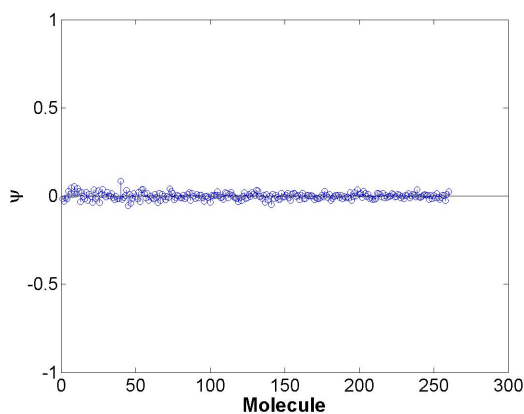
(b) BP result using the reduced dihedral dictionary.



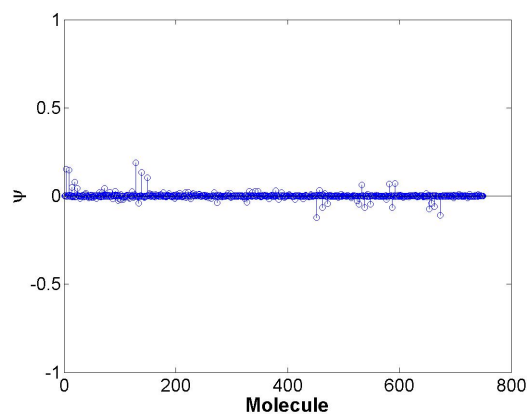
(c) BP result using the reduced trihedral dictionary.



(d) BP result using the reduced sphere dictionary.

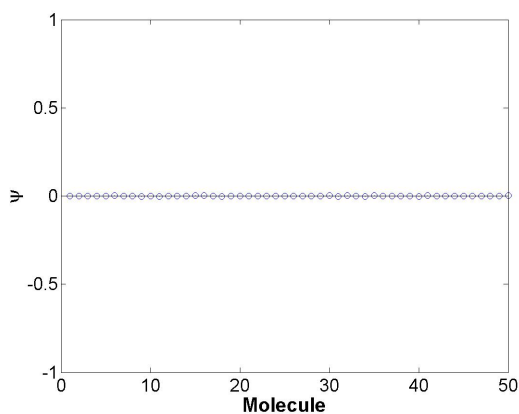


(e) BP result using the reduced cylinder dictionary.

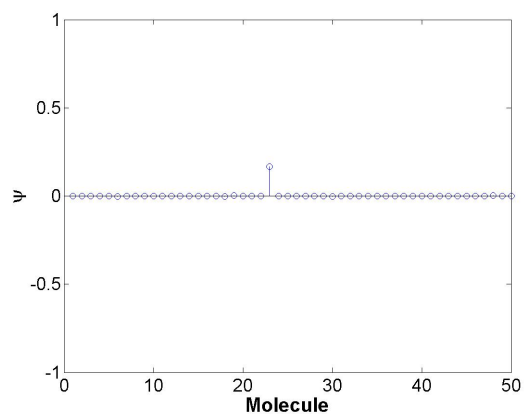


(f) BP result using the reduced top-hat dictionary.

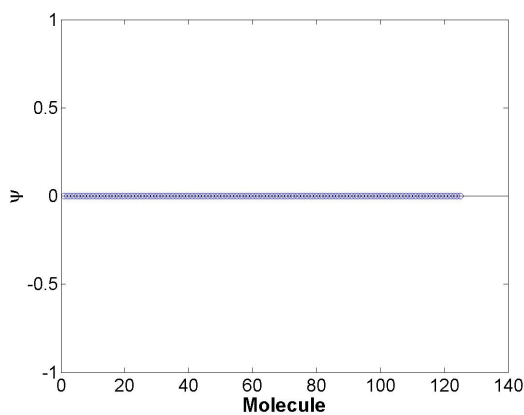
Figure C.7: BP results for the first iteration for each of the reduced shape dictionaries used in the feature extraction problem in scenario 2, dihedral example 5.



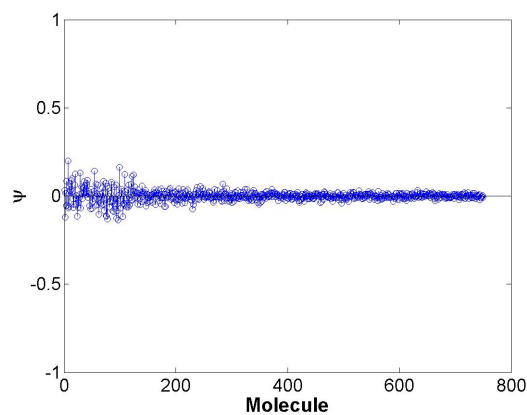
(a) BP result using the reduced plate dictionary.



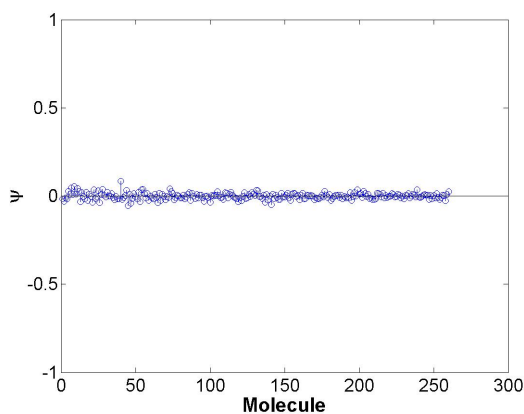
(b) BP result using the reduced dihedral dictionary.



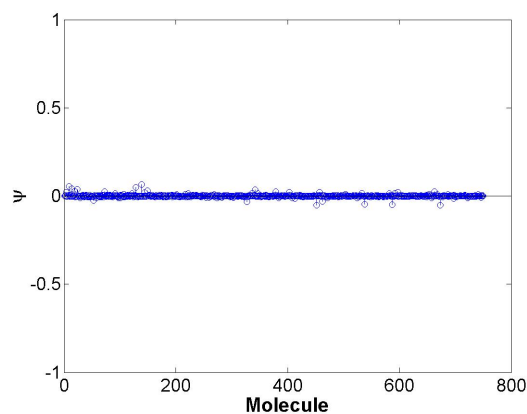
(c) BP result using the reduced trihedral dictionary.



(d) BP result using the reduced sphere dictionary.

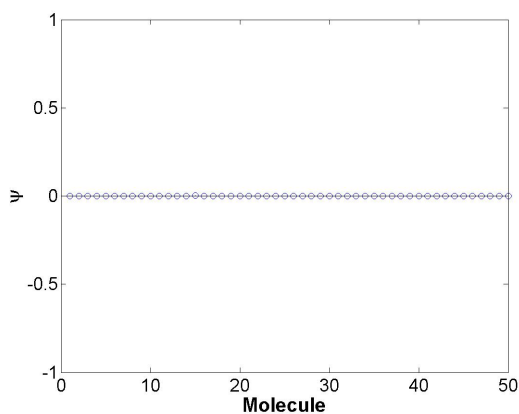


(e) BP result using the reduced cylinder dictionary.

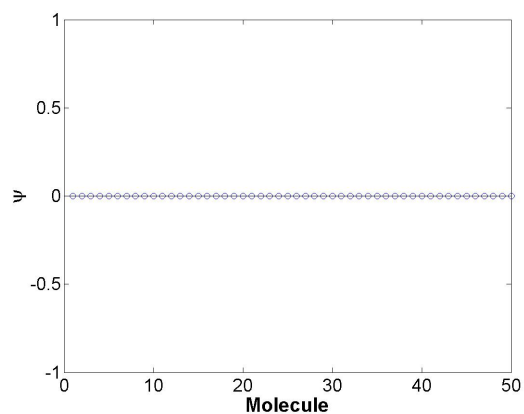


(f) BP result using the reduced top-hat dictionary.

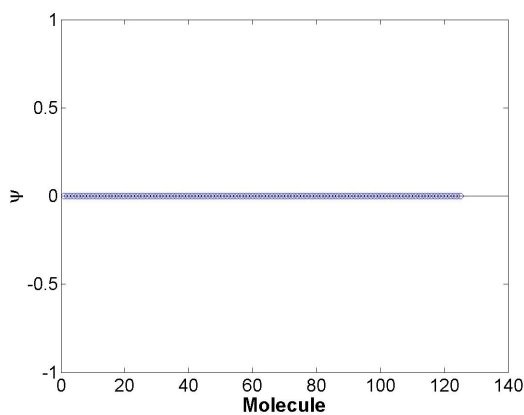
Figure C.8: BP results for the final iteration for each of the reduced shape dictionaries used in the feature extraction problem in scenario 2, dihedral example 5.



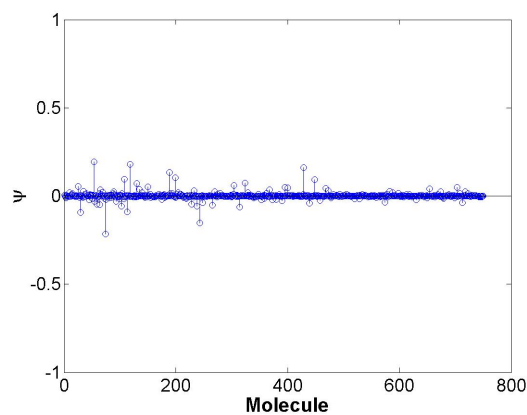
(a) BP result using the reduced plate dictionary.



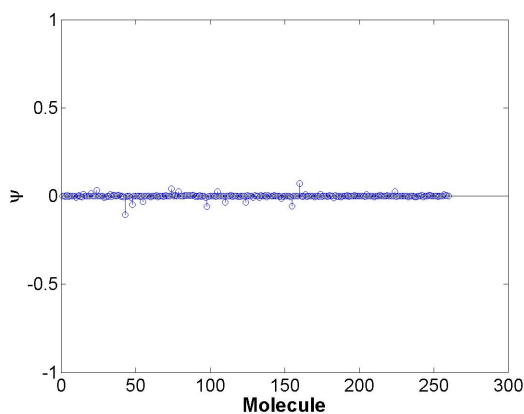
(b) BP result using the reduced dihedral dictionary.



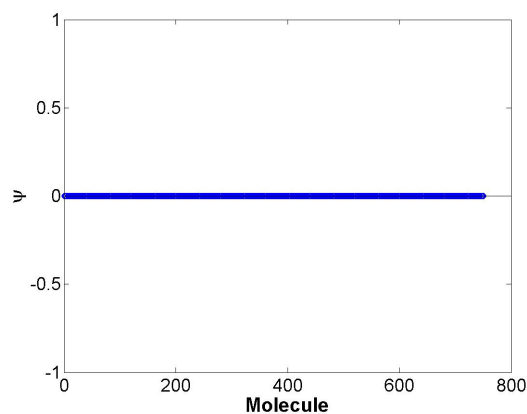
(c) BP result using the reduced trihedral dictionary.



(d) BP result using the reduced sphere dictionary.

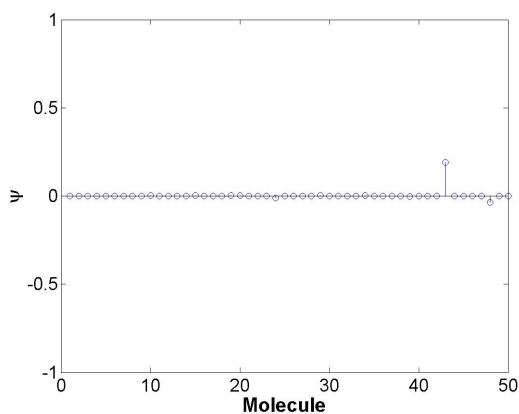


(e) BP result using the reduced cylinder dictionary.

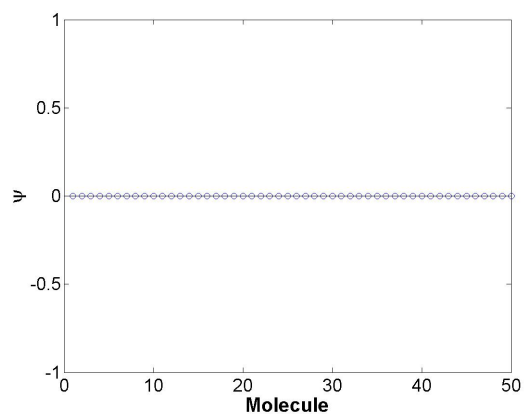


(f) BP result using the reduced top-hat dictionary.

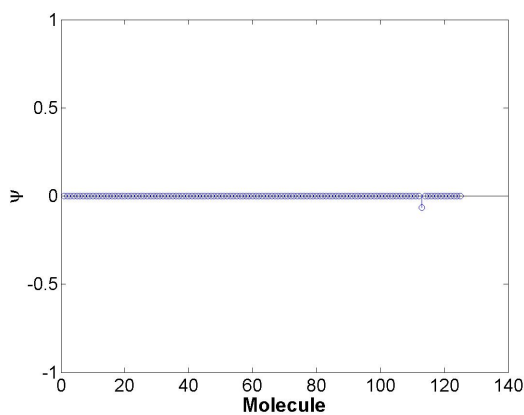
Figure C.9: BP results for the first iteration for each of the reduced shape dictionaries used in the feature extraction problem in scenario 2, sphere example 1.



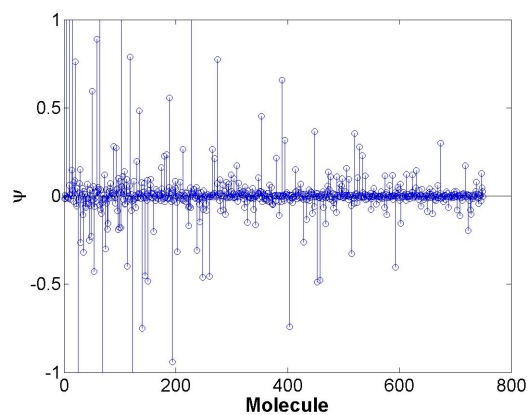
(a) BP result using the reduced plate dictionary.



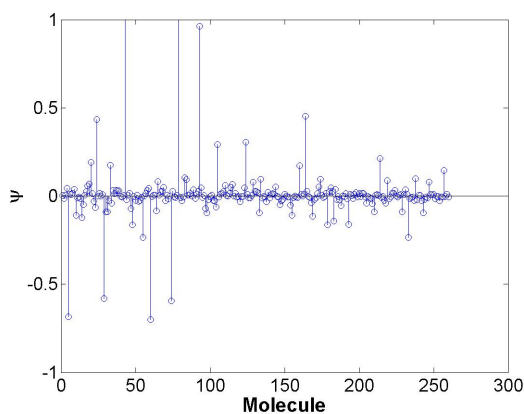
(b) BP result using the reduced dihedral dictionary.



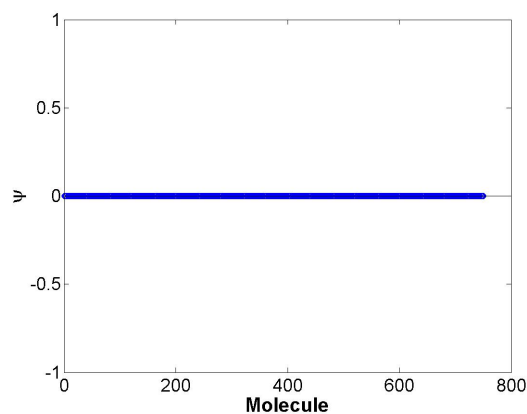
(c) BP result using the reduced trihedral dictionary.



(d) BP result using the reduced sphere dictionary.



(e) BP result using the reduced cylinder dictionary.



(f) BP result using the reduced top-hat dictionary.

Figure C.10: BP results for the final iteration for each of the reduced shape dictionaries used in the feature extraction problem in scenario 2, sphere example 1.

The maximum coefficient returned by the BP algorithm for each of the shape dictionaries and the sparsities, described by $\|\psi\|_1$, are provided in Table C.19. This

Table C.19: Maximum coefficients from each shape dictionary along with the ℓ_1 norm (sparsity descriptor) for scenario 2, sphere example 1.

Shape	Iteration	$\max(\psi)$	$\ \psi\ _1$	$(\max(\psi) - \lambda \cdot \ \psi\ _1)$
plate	1	0.0015	0.0111	-6.9248×10^{-4}
	2	0.1913	0.2704	0.1372
dihedral	1	2.1916×10^{-5}	3.8250×10^{-4}	-5.4583×10^{-5}
	2	2.1916×10^{-5}	3.8250×10^{-4}	-5.4583×10^{-5}
sphere	1	0.1928	4.9376	-0.7947
	2	3.3469	53.9532	-7.4437
top-hat	1	6.0841×10^{-5}	0.0107	-0.0021
	2	6.0841×10^{-5}	0.0107	-0.0021
trihedral	1	5.0893×10^{-4}	0.0026	-6.5790×10^{-6}
	2	1.9959×10^{-4}	0.0675	-0.0133
cylinder	1	0.0702	1.0799	-0.1458
	2	1.6847	15.4521	-1.4058

method incorrectly leads to a trihedral and plate classification. The extracted shapes along with their associated parameter sets are provided in Table C.20.

Table C.20: Estimated versus true parameters for scenario 2, sphere example 1.

Shape	X	Y	Z	H	L	r	$\tilde{\gamma}$	$\tilde{\theta}$	$\tilde{\phi}$
True sphere	4	0	0	-	-	2	-	-	-
Expected sphere	5	0	0	-	-	2	-	-	-
Estimated trihedral	0	0	10	0.5	-	-	0	0	0
Estimated plate	0	0	10	1	0.5	-	0	-30	0

Initially, we make the hypothesis that the parameter set extracted should be the closest dictionary contained representative parameter set, $\Theta = [5, 0, 0, 2]$ (atom 438). The LS errors given by are provided in Table C.21. In this example, the hypothesized

Table C.21: LS errors for the extracted and hypothesized data sets for scenario 2, sphere example 1.

Data	$\ \mathbf{x} - \mathbf{s}(\Theta_n)\ _2^2$
Extracted	6.1206×10^7
Closest	9.6771×10^5

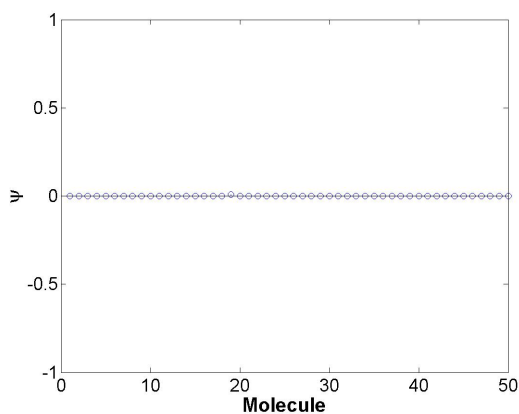
data leads to a lower LS error. However, the algorithm still chooses the two other shapes. This is most likely due to the sparsity constraint. The sphere coefficient vector is much less sparse as shown in Table C.19.

C.2.2 Y Parameter. In this example, we generate a sphere target located at $y = 4$ m with an SNR of 30 dB. The sphere target is simulated using the parameters listed in Table C.22.

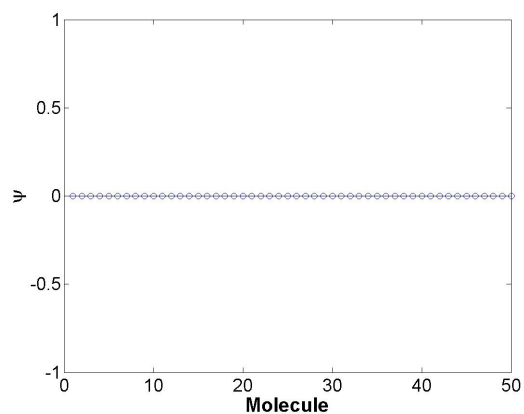
Table C.22: The parameters used to create the sphere target for scenario 2, example 2.

Shape	X	Y	Z	H	L	r	$\tilde{\gamma}$	$\tilde{\theta}$	$\tilde{\phi}$
sphere	0	4	0	-	-	2	-	-	-

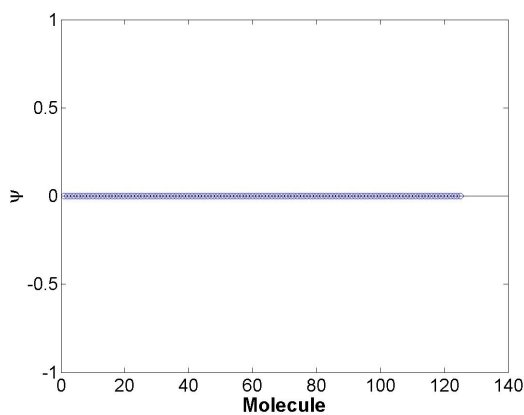
The BP results for each shape are provided in Figure C.11.



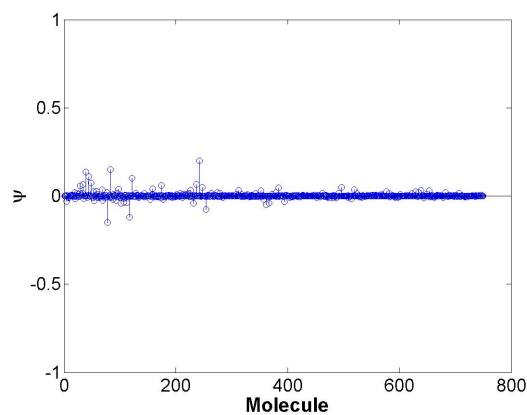
(a) BP result using the reduced plate dictionary.



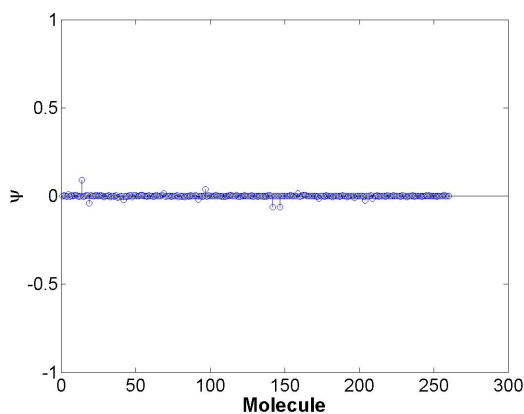
(b) BP result using the reduced dihedral dictionary.



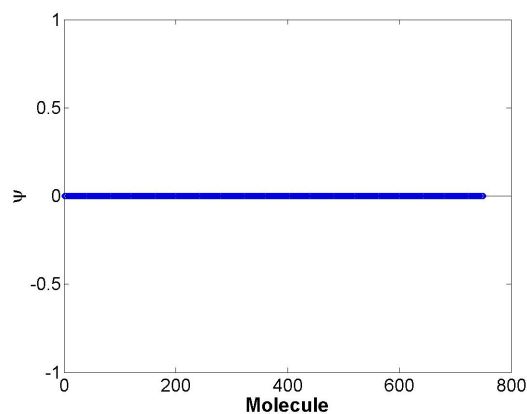
(c) BP result using the reduced trihedral dictionary.



(d) BP result using the reduced sphere dictionary.



(e) BP result using the reduced cylinder dictionary.



(f) BP result using the reduced top-hat dictionary.

Figure C.11: BP results for each of the reduced shape dictionaries used in the feature extraction problem in scenario 2, sphere example 2.

The maximum coefficient returned by the BP algorithm for each of the shape dictionaries and the sparsities, described by $\|\psi\|_1$, are provided in Table C.23.

Table C.23: Maximum coefficients from each shape dictionary along with the ℓ_1 norm (sparsity descriptor) for scenario 2, sphere example 2.

Shape	$\max(\psi)$	$\ \psi\ _1$	$(\max(\psi) - \lambda \cdot \ \psi\ _1)$
plate	0.0093	0.0176	0.0058
dihedral	2.4215×10^{-5}	3.4927×10^{-4}	-4.5639×10^{-5}
sphere	0.1985	4.1117	-0.6239
top-hat	6.2936×10^{-5}	0.0106	-0.0021
trihedral	3.3194×10^{-4}	0.0025	-1.6731×10^{-4}
cylinder	0.0895	0.8079	-0.0720

This method incorrectly leads to a plate classification. The associated extracted parameter set is provided in Table C.24.

Table C.24: Estimated versus true parameters for scenario 2, sphere example 2.

Shape	X	Y	Z	H	L	r	$\tilde{\gamma}$	$\tilde{\theta}$	$\tilde{\phi}$
True sphere	0	4	0	-	-	2	-	-	-
Expected sphere	0	5	0	-	-	2	-	-	-
Estimated plate	5	5	-5	0.5	0.5	-	0	-30	0

Initially, we assume that the algorithm should choose the sphere corresponding to the closest parameter set. Therefore, the expected parameter set would be $\Theta = [0, 5, 0, 2]$. This set corresponds to atom 443 within the sphere dictionary. The extracted parameter set corresponds to atom 113 within the plate dictionary. The total LS errors for the extracted data versus the hypothesized closest data are provided in Table C.25. As with the sphere example 1, the extracted error is greater

Table C.25: LS errors for the extracted and hypothesized data sets for scenario 2, sphere example 2.

Data	$\ \mathbf{x} - \mathbf{s}(\Theta_n)\ _2^2$
Extracted	2.8232×10^6
Closest	9.4698×10^5

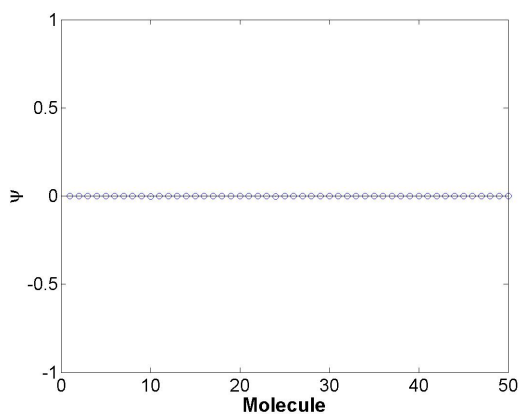
than the hypothesis data. However, the sparsity of the extracted coefficient vector is much less, as shown in Table C.23.

C.2.3 Z Parameter. In this example, we generate a sphere target located at $z = 4$ m with an SNR of 30 dB. The sphere target is simulated using the parameters listed in Table C.26.

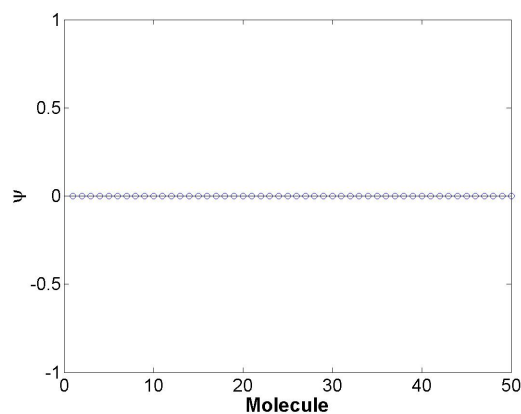
Table C.26: The parameters used to create the sphere target for scenario 2, example 3.

Shape	X	Y	Z	H	L	r	$\tilde{\gamma}$	$\tilde{\theta}$	$\tilde{\phi}$
sphere	0	0	4	-	-	2	-	-	-

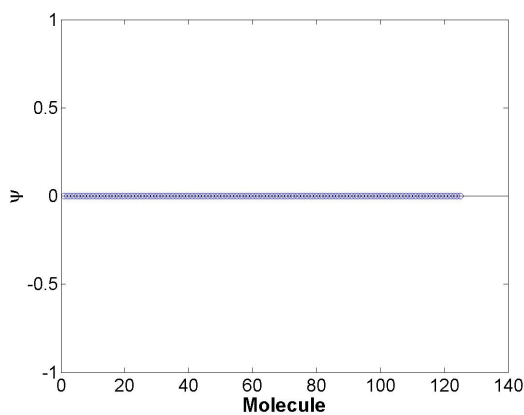
The BP results for each shape are provided in Figure C.12.



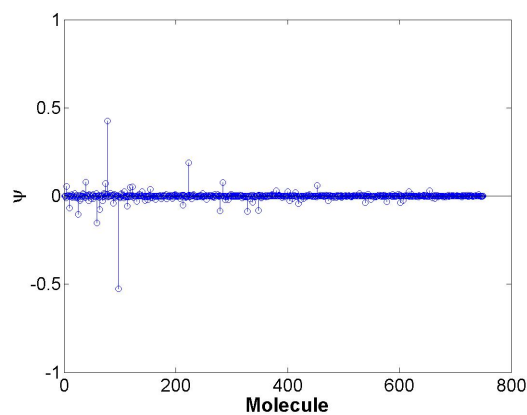
(a) BP result using the reduced plate dictionary.



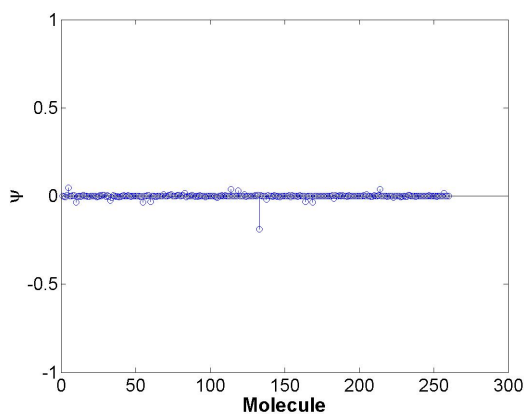
(b) BP result using the reduced dihedral dictionary.



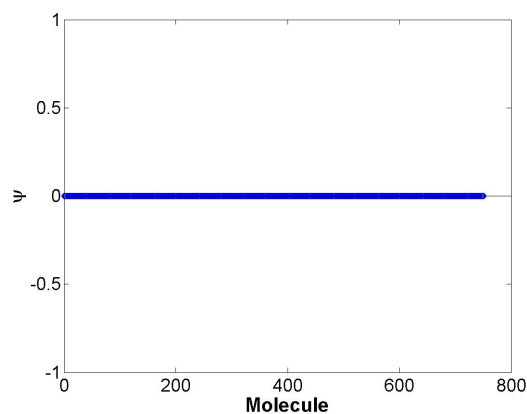
(c) BP result using the reduced trihedral dictionary.



(d) BP result using the reduced sphere dictionary.



(e) BP result using the reduced cylinder dictionary.



(f) BP result using the reduced top-hat dictionary.

Figure C.12: BP results for each of the reduced shape dictionaries used in the feature extraction problem in scenario 2, sphere example 3.

The maximum coefficient returned by the BP algorithm for each of the shape dictionaries and the sparsities, described by $\|\psi\|_1$, are provided in Table C.27.

Table C.27: Maximum coefficients from each shape dictionary along with the ℓ_1 norm (sparsity descriptor) for scenario 2, sphere example 3.

Shape	$\max(\psi)$	$\ \psi\ _1$	$(\max(\psi) - \lambda \cdot \ \psi\ _1)$
plate	8.9865×10^{-4}	0.0129	-0.0017
dihedral	2.9631×10^{-5}	5.0004×10^{-4}	-7.0376×10^{-5}
sphere	0.4259	4.8113	-0.5364
top-hat	7.9184×10^{-5}	0.0105	-0.0020
trihedral	3.2449×10^{-4}	0.0024	-1.5230×10^{-4}
cylinder	0.0475	0.9930	-0.1511

This method incorrectly leads to a dihedral classification. The associated extracted parameter set is provided in Table C.28.

Table C.28: Estimated versus true parameters for scenario 2, sphere example 3.

Shape	X	Y	Z	H	L	r	$\tilde{\gamma}$	$\tilde{\theta}$	$\tilde{\phi}$
True sphere	0	4	0	-	-	2	-	-	-
Expected sphere	0	5	0	-	-	2	-	-	-
Estimated dihedral	-5	-10	10	0.5	0.5	-	0	0	0

Initially, we assume that the algorithm should choose the sphere corresponding to the closest parameter set. Therefore, the expected parameter set would be $\Theta = [0, 0, 5, 2]$. This set corresponds to atom 463 within the sphere dictionary. The extracted parameter set corresponds to atom 102 within the dihedral dictionary. The total LS errors for the extracted data versus the hypothesized closest data are provided in Table C.29. As with the sphere example 1 and 2, the extracted error is greater than the hypothesis data. However, the sparsity of the extracted coefficient vector is much less, as shown in Table C.27.

Table C.29: LS errors for the extracted and hypothesized data sets for scenario 2, sphere example 3.

Data	$\ \mathbf{x} - \mathbf{s}(\Theta_n)\ _2^2$
Extracted	4.6663×10^6
Closest	9.4191×10^5

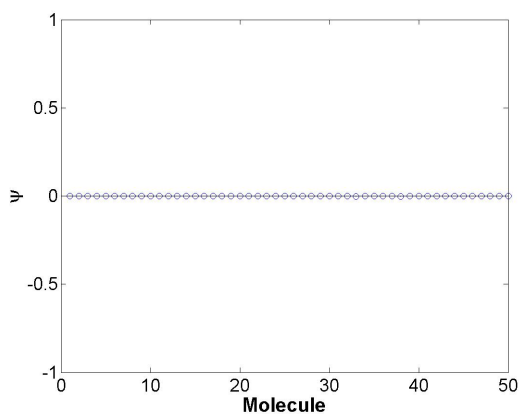
greater than the hypothesis data. However, the sparsity of the extracted coefficient vector is much less, as shown in Table C.27.

C.2.4 RCS Parameters. In this example, we generate a sphere target with RCS parameter $r = 2.3$ m with an SNR of 30 dB. The sphere target is simulated using the parameters listed in Table C.30.

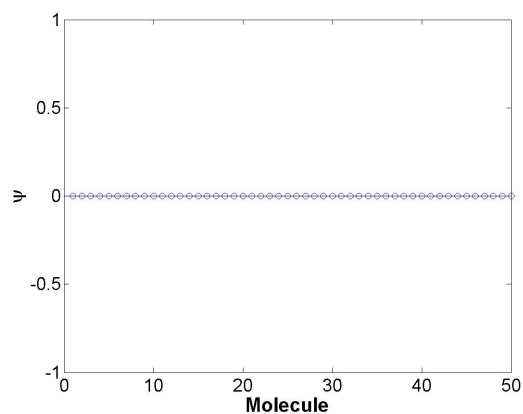
Table C.30: The parameters used to create the sphere target for scenario 2, example 4.

Shape	X	Y	Z	H	L	r	$\tilde{\gamma}$	$\tilde{\theta}$	$\tilde{\phi}$
sphere	0	0	0	-	-	2.3	-	-	-

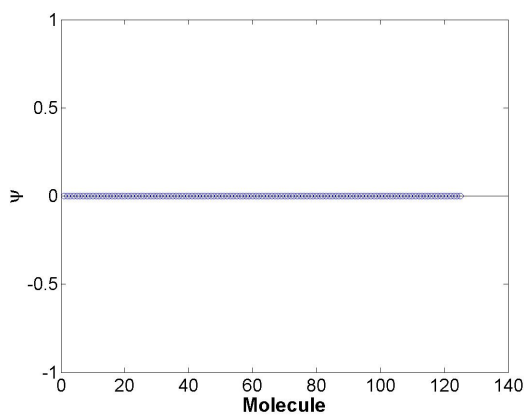
The BP results for each shape are provided in Figure C.13.



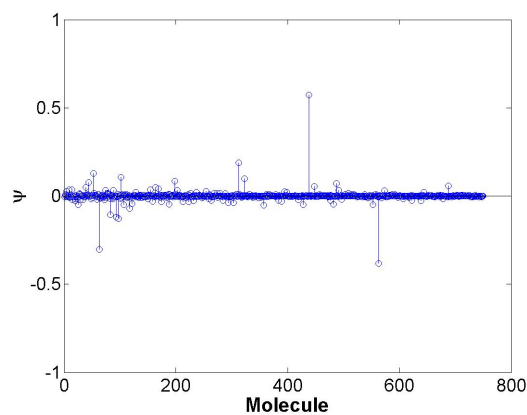
(a) BP result using the reduced plate dictionary.



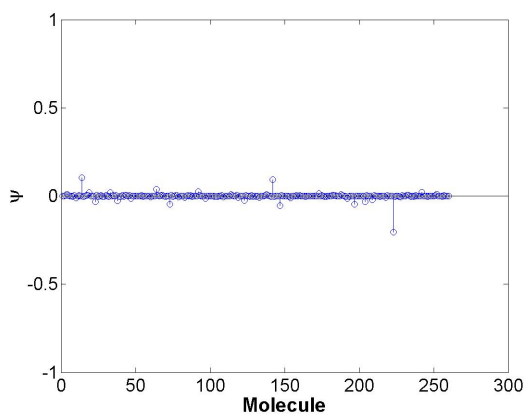
(b) BP result using the reduced dihedral dictionary.



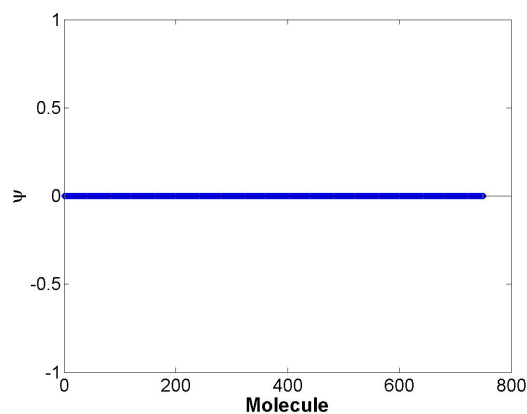
(c) BP result using the reduced trihedral dictionary.



(d) BP result using the reduced sphere dictionary.



(e) BP result using the reduced cylinder dictionary.



(f) BP result using the reduced top-hat dictionary.

Figure C.13: BP results for each of the reduced shape dictionaries used in the feature extraction problem in scenario 2, sphere example 4.

The maximum coefficient returned by the BP algorithm for each of the shape dictionaries and the sparsities, described by $\|\psi\|_1$, are provided in Table C.31.

Table C.31: Maximum coefficients from each shape dictionary along with the ℓ_1 norm (sparsity descriptor) for scenario 2, sphere example 4.

Shape	$\max(\psi)$	$\ \psi\ _1$	$(\max(\psi) - \lambda \cdot \ \psi\ _1)$
plate	9.0017×10^{-4}	0.0114	-0.0014
dihedral	1.6933×10^{-5}	4.0114×10^{-4}	-6.3294×10^{-5}
sphere	0.5731	6.0040	-0.6277
top-hat	9.2781×10^{-5}	0.0112	-0.0021
triangular	2.5944×10^{-4}	0.0029	-3.2844×10^{-4}
cylinder	0.1040	1.2727	-0.1506

For this example, the shape is incorrectly classified as a dihedral. The expected parameter set estimation is $\Theta = [0, 0, 0, 2.5]$. The extracted parameter set is provided in Table C.32.

Table C.32: Estimated versus true parameters for scenario 2, sphere example 4.

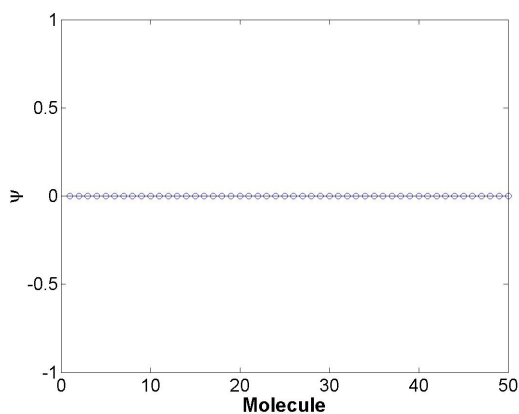
Shape	X	Y	Z	H	L	r	$\tilde{\gamma}$	$\tilde{\theta}$	$\tilde{\phi}$
True sphere	0	0	0	-	-	2.3	-	-	-
Expected sphere	0	0	0	-	-	2.5	-	-	-
Estimated dihedral	-5	-10	10	0.5	0.5	-	0	0	0

C.3 Top-Hat Results

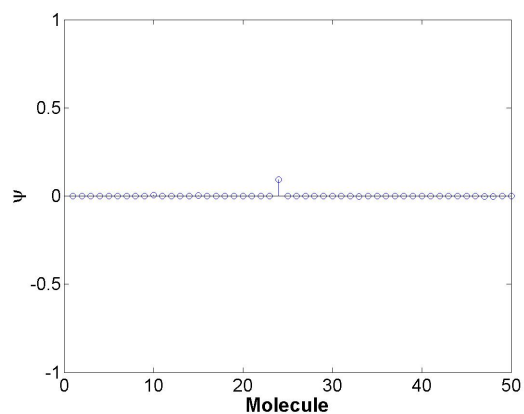
C.3.1 X Parameter. In this example, we generate a top-hat target located at $x = 4$ m with an SNR of 30 dB. The top-hat target is simulated using the parameters listed in Table C.33. The BP results for each shape are provided in Figure C.14.

Table C.33: The parameters used to create the top-hat target for scenario 2, example 1.

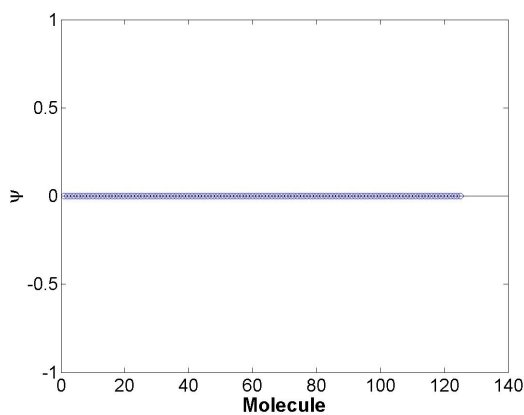
Shape	X	Y	Z	H	L	r	$\tilde{\gamma}$	$\tilde{\theta}$	$\tilde{\phi}$
top-hat	4	0	0	2	-	1	0	0	0



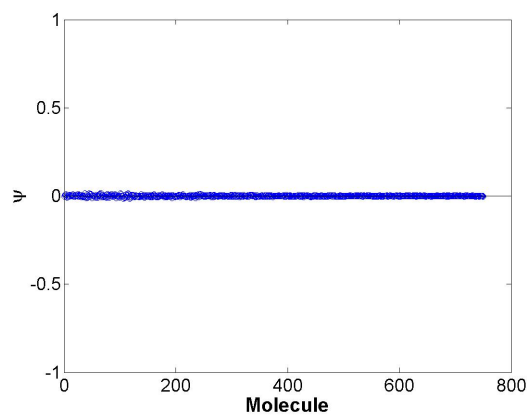
(a) BP result using the reduced plate dictionary.



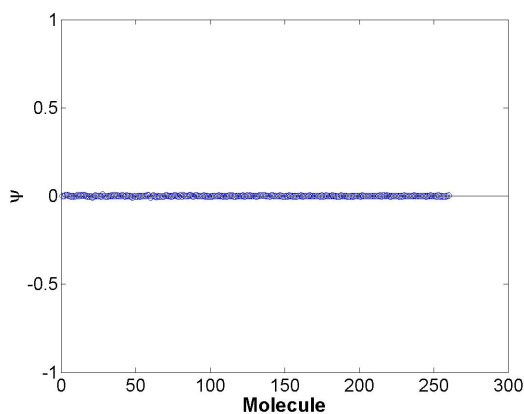
(b) BP result using the reduced dihedral dictionary.



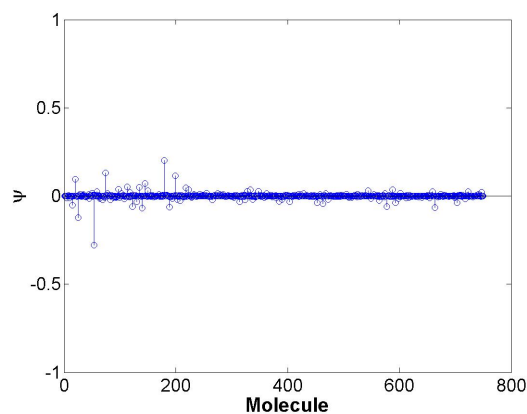
(c) BP result using the reduced trihedral dictionary.



(d) BP result using the reduced sphere dictionary.



(e) BP result using the reduced cylinder dictionary.



(f) BP result using the reduced top-hat dictionary.

Figure C.14: BP results for the first iteration for each of the reduced shape dictionaries used in the feature extraction problem in scenario 2, top-hat example 1.

The maximum coefficient returned by the BP algorithm for each of the shape dictionaries and the sparsities, described by $\|\psi\|_1$, are provided in Table C.34. This

Table C.34: Maximum coefficients from each shape dictionary along with the ℓ_1 norm (sparsity descriptor) for scenario 2, top-hat example 1.

Shape	$\max(\psi)$	$\ \psi\ _1$	$(\max(\psi) - \lambda \cdot \ \psi\ _1)$
plate	2.8102×10^{-4}	0.0057	-8.6823×10^{-4}
dihedral	0.0938	0.1217	0.0694
sphere	0.0166	1.6821	-0.3199
top-hat	0.2010	3.7888	-0.5567
triangular	3.1400×10^{-5}	0.0010	-1.7440×10^{-4}
cylinder	0.0087	0.4364	-0.0786

method incorrectly leads to a dihedral classification. The extracted shape along with its associated parameter set is provided in Table C.35.

Table C.35: Estimated versus true parameters for scenario 2, top-hat example 1.

Shape	X	Y	Z	H	L	r	$\tilde{\gamma}$	$\tilde{\theta}$	$\tilde{\phi}$
True top-hat	4	0	0	2	-	1	0	0	0
Expected top-hat	5	0	0	2	-	1	0	0	0
Estimated dihedral	5	0	0	0.5	0.5	-	0	0	0

Initially, we make the hypothesis that the parameter set extracted should be the closest dictionary contained representative parameter set, $\Theta = [5, 0, 0, 2, 0, 1, 0, 0, 0]$ (atom 1189). As with the plate example presented in Section 4.3, the misclassification is caused by the lower sparsity term computed for the dihedral. Again, if we modified the algorithm to separate shapes based on a threshold $\max(\psi)$ 0.1, we would have achieved the correct top-hat classification. The LS errors are provided in Table C.36.

Table C.36: LS errors for the extracted and hypothesized data sets for scenario 2, top-hat example 1.

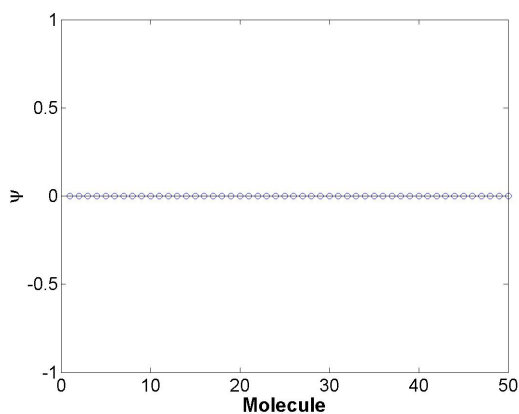
Data	$\ \mathbf{x} - \mathbf{s}(\Theta_n)\ _2^2$
Extracted	4.2135×10^7
Closest	9.2129×10^7

C.3.2 Y Parameter. In this example, we generate a top-hat target located at $y = 4$ m with an SNR of 30 dB. The top-hat target is simulated using the parameters listed in Table C.37.

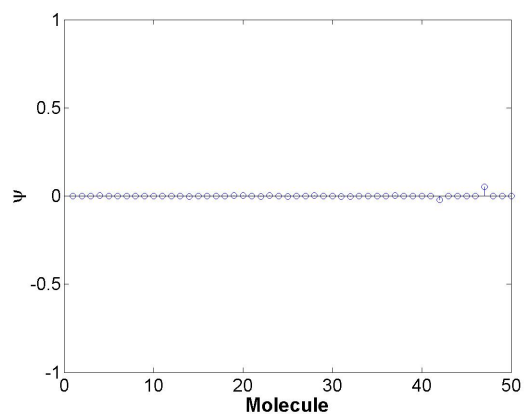
Table C.37: The parameters used to create the top-hat target for scenario 2, example 2.

Shape	X	Y	Z	H	L	r	$\tilde{\gamma}$	$\tilde{\theta}$	$\tilde{\phi}$
top-hat	0	4	0	2	-	1	0	0	0

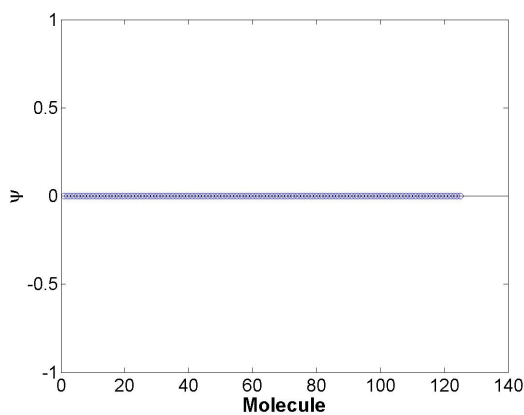
The BP results for each shape are provided in Figure C.15.



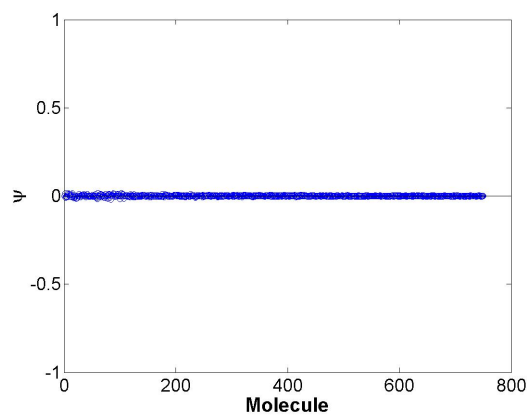
(a) BP result using the reduced plate dictionary.



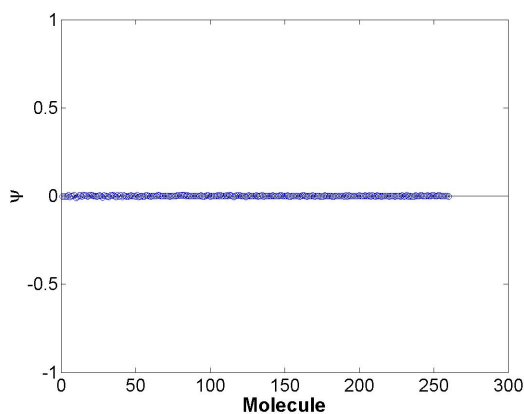
(b) BP result using the reduced dihedral dictionary.



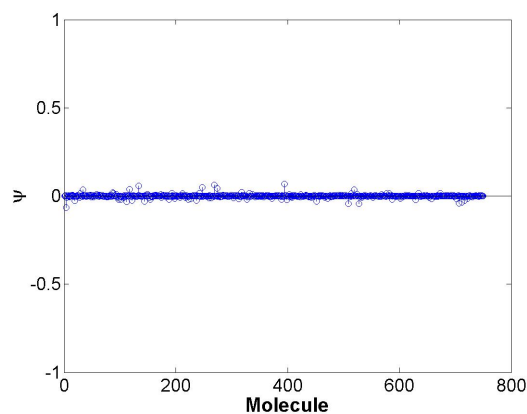
(c) BP result using the reduced trihedral dictionary.



(d) BP result using the reduced sphere dictionary.



(e) BP result using the reduced cylinder dictionary.



(f) BP result using the reduced top-hat dictionary.

Figure C.15: BP results for each of the reduced shape dictionaries used in the feature extraction problem in scenario 2, top-hat example 2.

The maximum coefficient returned by the BP algorithm for each of the shape dictionaries and the sparsities, described by $\|\psi\|_1$, are provided in Table C.38.

Table C.38: Maximum coefficients from each shape dictionary along with the ℓ_1 norm (sparsity descriptor) for scenario 2, top-hat example 2.

Shape	$\max(\psi)$	$\ \psi\ _1$	$(\max(\psi) - \lambda \cdot \ \psi\ _1)$
plate	4.7940×10^{-4}	0.0076	-0.0010
dihedral	0.0525	0.1144	0.0296
sphere	0.0176	1.7032	-0.3230
top-hat	0.0695	2.4489	-0.4203
triangular	2.5039×10^{-5}	7.9156×10^{-4}	-1.3327×10^{-4}
cylinder	0.0066	0.4665	-0.0867

This method incorrectly leads to a dihedral classification. The associated extracted parameter set is provided in Table C.39.

Table C.39: Estimated versus true parameters for scenario 2, top-hat example 2.

Shape	X	Y	Z	H	L	r	$\tilde{\gamma}$	$\tilde{\theta}$	$\tilde{\phi}$
True top-hat	0	4	0	-	-	2	0	0	0
Expected top-hat	0	5	0	-	-	2	0	0	0
Estimated dihedral	-5	5	10	0.5	0.5	-	0	0	0

Initially, we assume that the algorithm should choose the top-hat corresponding to the closest parameter set. Therefore, the expected parameter set would be $\Theta = [0, 5, 0, 2, 0, 1, 0, 0, 0]$. This set corresponds to atom 1193 within the top-hat dictionary. The extracted parameter set corresponds to atom 117 within the dihedral dictionary. The total LS errors for the extracted data versus the hypothesized closest data are provided in Table C.40.

Table C.40: LS errors for the extracted and hypothesized data sets for scenario 2, top-hat example 2.

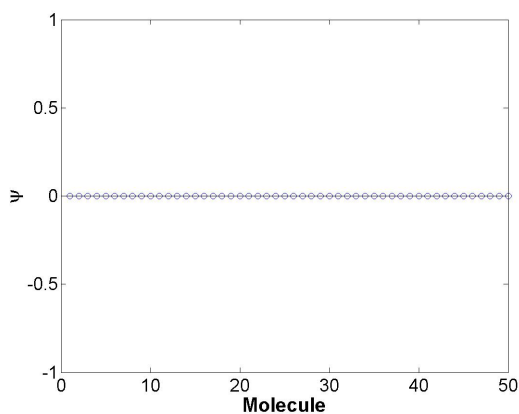
Data	$\ \mathbf{x} - \mathbf{s}(\Theta_n)\ _2^2$
Extracted	4.8717×10^7
Closest	9.0342×10^7

C.3.3 Z Parameter. In this example, we generate a top-hat target located at $z = 4$ m with an SNR of 30 dB. The top-hat target is simulated using the parameters listed in Table C.41.

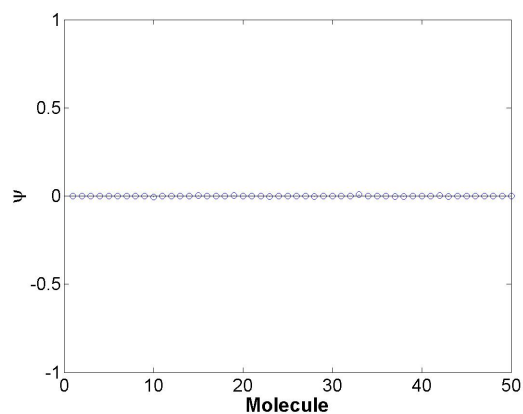
Table C.41: The parameters used to create the top-hat target for scenario 2, example 3.

Shape	X	Y	Z	H	L	r	$\tilde{\gamma}$	$\tilde{\theta}$	$\tilde{\phi}$
top-hat	0	0	4	2	-	1	0	0	0

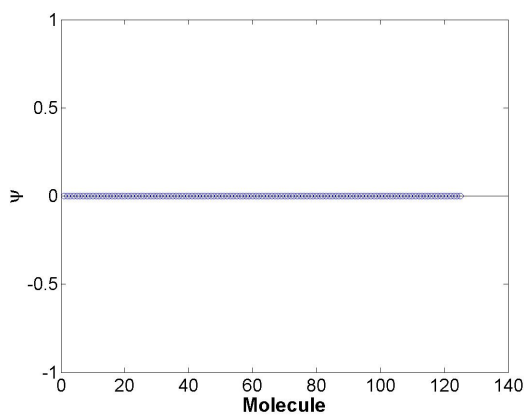
The BP results for each shape are provided in Figures C.16-C.17.



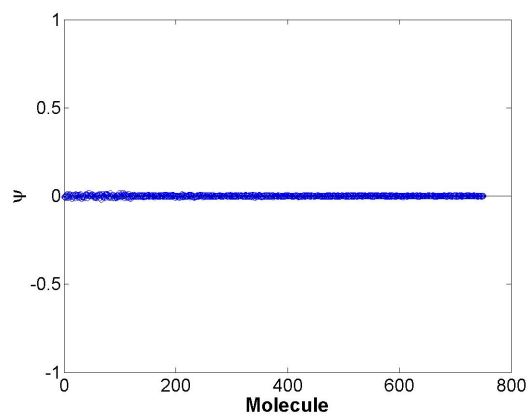
(a) BP result using the reduced plate dictionary.



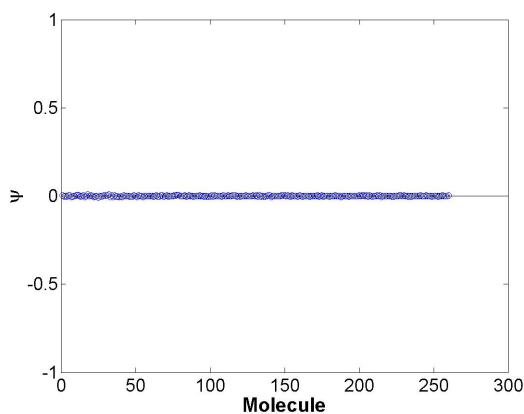
(b) BP result using the reduced dihedral dictionary.



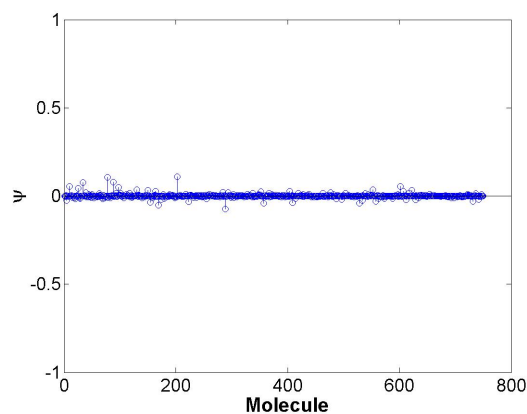
(c) BP result using the reduced trihedral dictionary.



(d) BP result using the reduced sphere dictionary.

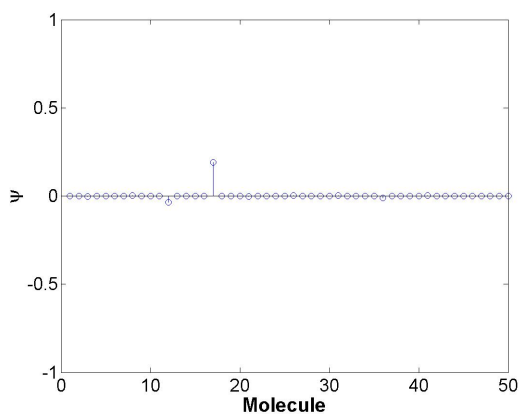


(e) BP result using the reduced cylinder dictionary.

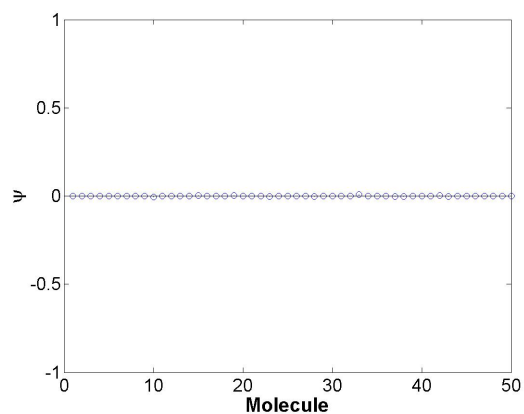


(f) BP result using the reduced top-hat dictionary.

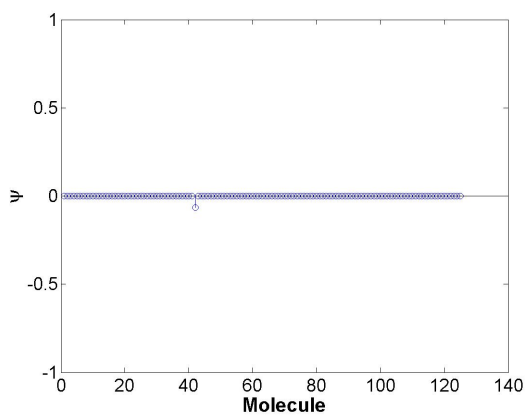
Figure C.16: BP results for the first iteration for each of the reduced shape dictionaries used in the feature extraction problem in scenario 2, top-hat example 3.



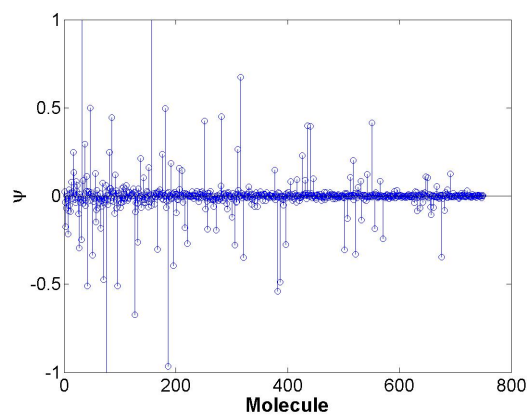
(a) BP result using the reduced plate dictionary.



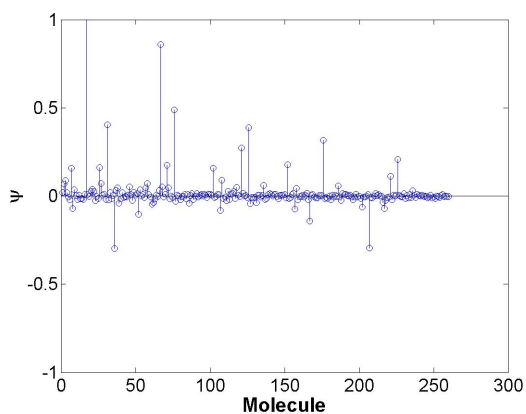
(b) BP result using the reduced dihedral dictionary.



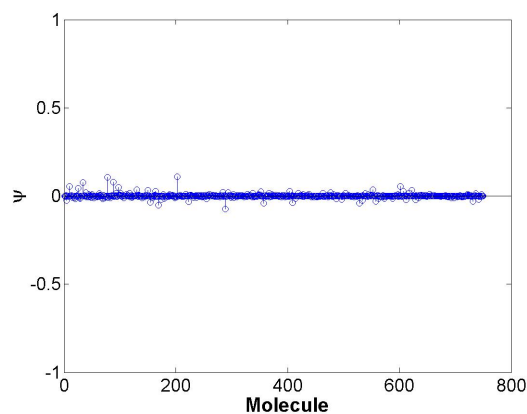
(c) BP result using the reduced trihedral dictionary.



(d) BP result using the reduced sphere dictionary.



(e) BP result using the reduced cylinder dictionary.



(f) BP result using the reduced top-hat dictionary.

Figure C.17: BP results for the final iteration for each of the reduced shape dictionaries used in the feature extraction problem in scenario 2, top-hat example 3.

The maximum coefficient returned by the BP algorithm for each of the shape dictionaries and the sparsities, described by $\|\psi\|_1$, are provided in Table C.34.

Table C.42: Maximum coefficients from each shape dictionary along with the ℓ_1 norm (sparsity descriptor) for scenario 2, top-hat example 3.

Shape	Iteration	$\max(\psi)$	$\ \psi\ _1$	$(\max(\psi) - \lambda \cdot \ \psi\ _1)$
plate	1	3.1801×10^{-4}	0.0062	-9.3117×10^{-4}
	2	0.1905	0.2641	0.1377
dihedral	1	0.0069	0.0512	-0.0034
	2	0.0069	0.0512	-0.0034
sphere	1	0.0156	1.6928	-0.3230
	2	1.3527	31.9828	-5.0438
top-hat	1	0.1095	3.0124	-0.4930
	2	0.1095	3.0124	-0.4930
trihedral	1	2.1498×10^{-5}	9.1958×10^{-4}	-1.6242×10^{-4}
	2	2.1424×10^{-5}	0.0668	-0.0133
cylinder	1	0.0083	0.4255	-0.0768
	2	1.6771	10.0025	-0.3234

This method incorrectly classifies the shape as a combination of a trihedral and a plate. The associated extracted parameter set is provided in Table C.43.

Table C.43: Estimated versus true parameters for scenario 2, top-hat example 3.

Shape	X	Y	Z	H	L	r	$\tilde{\gamma}$	$\tilde{\theta}$	$\tilde{\phi}$
True top-hat	0	0	4	2	-	1	0	0	0
Expected top-hat	0	0	5	2	-	1	0	0	0
Estimated trihedral	-5	5	-5	0.5	-	-	0	0	0
Estimated plate	-5	5	-5	1	0.5	-	0	-30	0

Initially, we assume that the algorithm should choose the top-hat corresponding to the closest parameter set. Therefore, the expected parameter set would be $\Theta = [0, 0, 5, 2, 0, 1, 0, 0, 0]$. This set corresponds to atom 1213 within the top-hat dictionary. The extracted parameter sets correspond to atom 42 within the trihedral dictionary and atom 792 within the plate dictionary. The total LS errors for the extracted data versus the hypothesized closest data are provided in Table C.44. The extracted error, for this example, is greater than the hypothesis data. This is due to the incorrect shape

Table C.44: LS errors for the extracted and hypothesized data sets for scenario 2, top-hat example 3.

Data	$\ \mathbf{x} - \mathbf{s}(\mathbf{\Theta}_n)\ _2^2$
Extracted	1.0707×10^8
Closest	8.9945×10^7

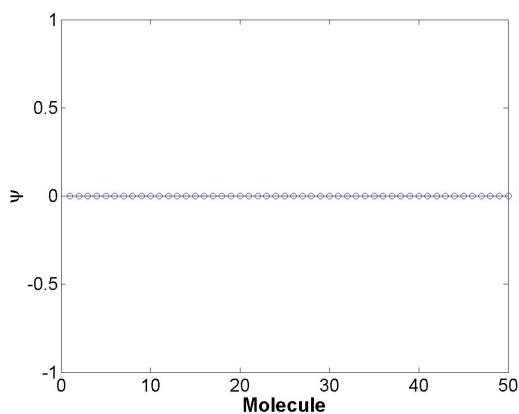
classification and model order estimation. Future research should include adding a threshold, $\max(\psi) 0.1$ to the algorithm.

C.3.4 RCS Parameters. In this section we discuss the results of two example target scenes. Each of the scenes includes a top-hat that is generated using a height or radius parameter that falls outside of the dictionary parameter space resolution with an SNR of 30 dB. The top-hat targets are simulated using the parameters listed in Table C.45.

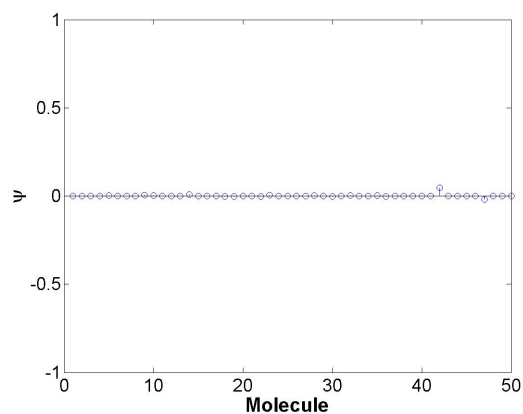
Table C.45: The parameters used to create the top-hat target for scenario 2, examples 4 and 5.

Shape	X	Y	Z	H	L	r	$\tilde{\gamma}$	$\tilde{\theta}$	$\tilde{\phi}$
top-hat 1	0	0	0	2.3	-	1	0	0	0
top-hat 2	0	0	0	2	-	1.3	0	0	0

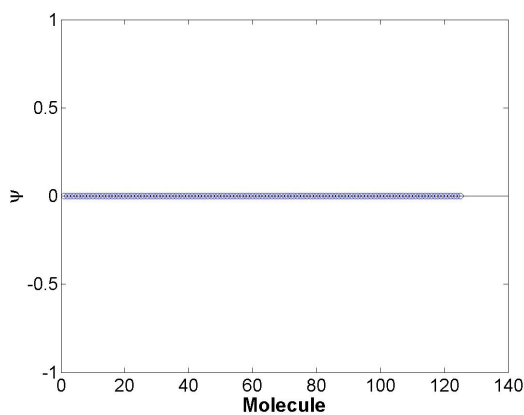
The BP results for each shape are provided in Figures C.18-C.20.



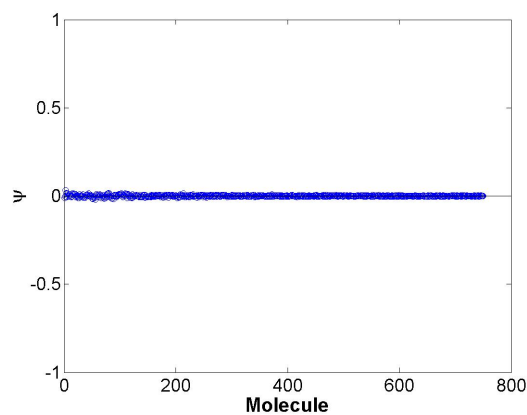
(a) BP result using the reduced plate dictionary.



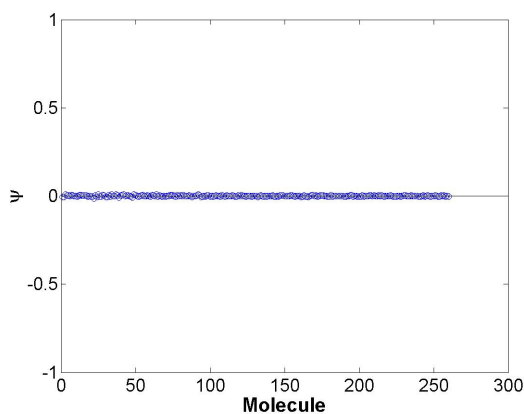
(b) BP result using the reduced dihedral dictionary.



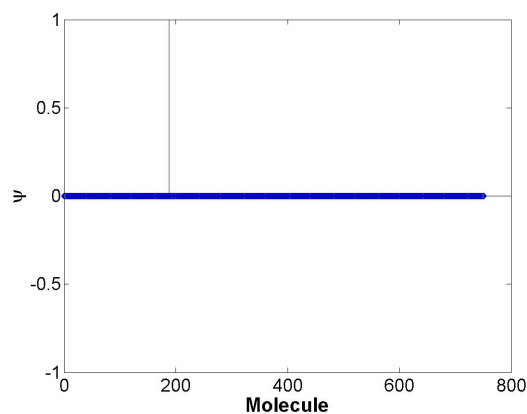
(c) BP result using the reduced trihedral dictionary.



(d) BP result using the reduced sphere dictionary.

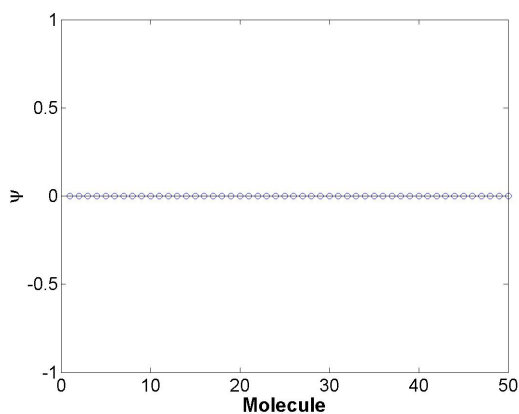


(e) BP result using the reduced cylinder dictionary.

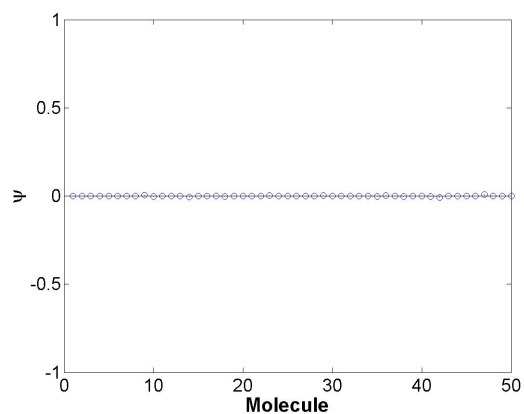


(f) BP result using the reduced top-hat dictionary.

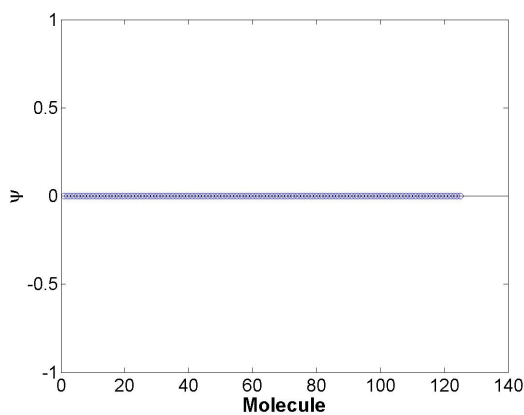
Figure C.18: BP results for each of the reduced shape dictionaries used in the feature extraction problem in scenario 2, top-hat example 4.



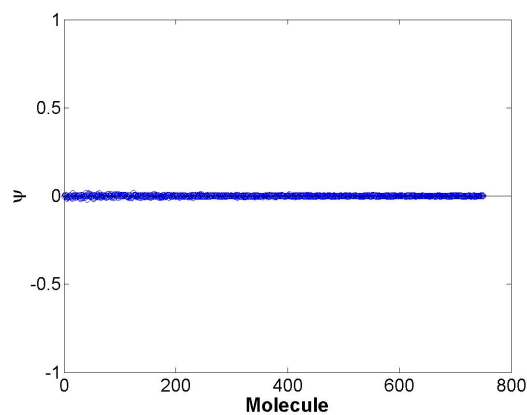
(a) BP result using the reduced plate dictionary.



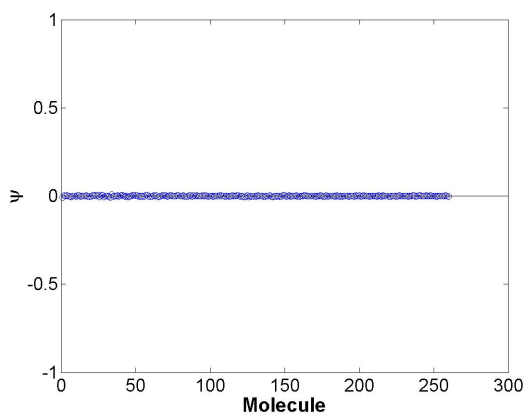
(b) BP result using the reduced dihedral dictionary.



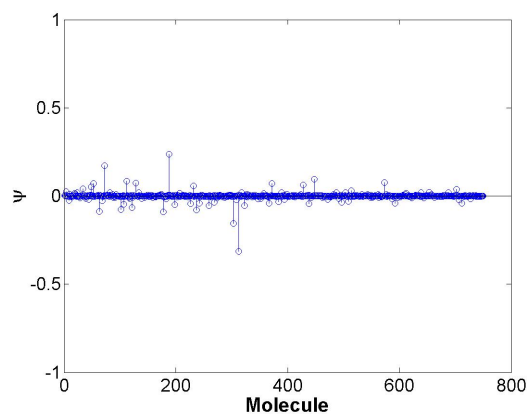
(c) BP result using the reduced trihedral dictionary.



(d) BP result using the reduced sphere dictionary.

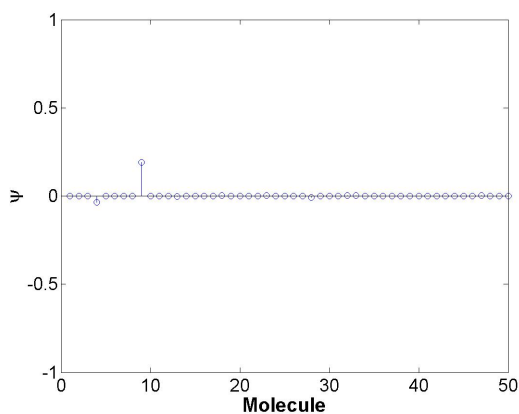


(e) BP result using the reduced cylinder dictionary.

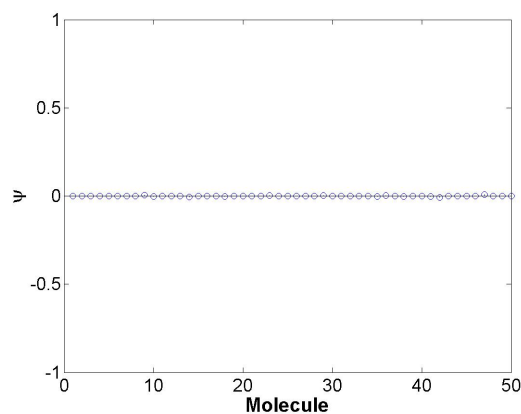


(f) BP result using the reduced top-hat dictionary.

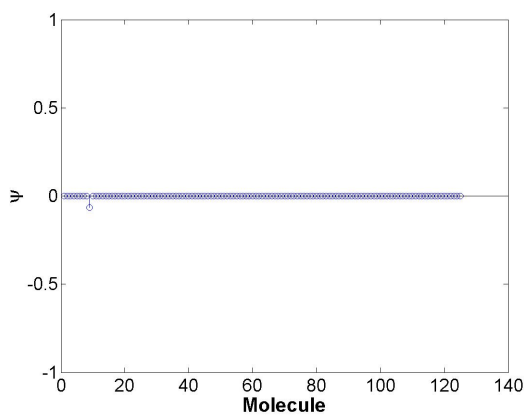
Figure C.19: BP results for the first iteration for each of the reduced shape dictionaries used in the feature extraction problem in scenario 2, top-hat example 5.



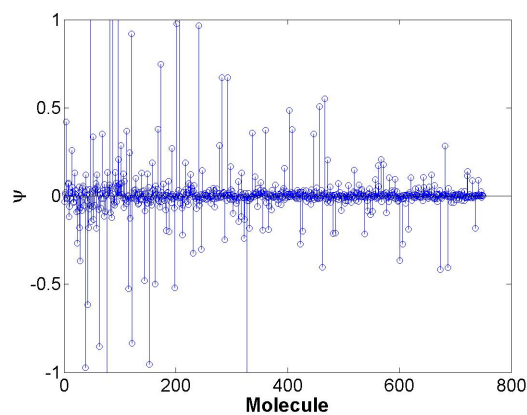
(a) BP result using the reduced plate dictionary.



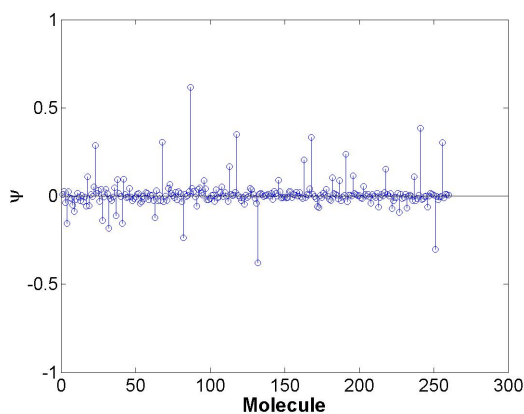
(b) BP result using the reduced dihedral dictionary.



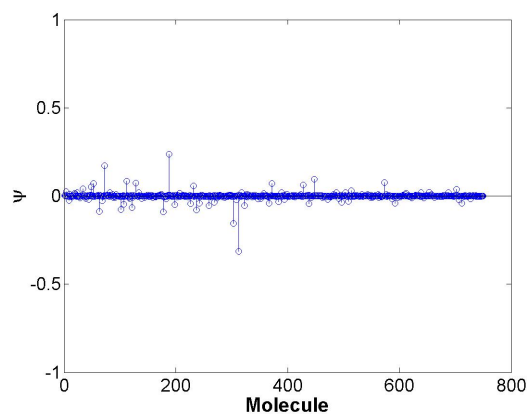
(c) BP result using the reduced trihedral dictionary.



(d) BP result using the reduced sphere dictionary.



(e) BP result using the reduced cylinder dictionary.



(f) BP result using the reduced top-hat dictionary.

Figure C.20: BP results for the second iteration for each of the reduced shape dictionaries used in the feature extraction problem in scenario 2, top-hat example 5.

The maximum coefficient returned by the BP algorithm for each of the shape dictionaries and the sparsities, described by $\|\psi\|_1$, are provided in Table C.46 and Table C.47.

Table C.46: Maximum coefficients from each shape dictionary along with the ℓ_1 norm (sparsity descriptor) for scenario 2, top-hat example 4.

Shape	$\max(\psi)$	$\ \psi\ _1$	$(\max(\psi) - \lambda \cdot \ \psi\ _1)$
plate	4.4934×10^{-4}	0.0080	-0.0011
dihedral	0.0472	0.1212	0.0230
sphere	0.0320	2.0478	-0.3776
top-hat	1.3139	1.4430	1.0253
trihedral	3.0412×10^{-5}	0.0010	-1.7378×10^{-4}
cylinder	0.0089	0.5709	-0.1052

Table C.47: Maximum coefficients from each shape dictionary along with the ℓ_1 norm (sparsity descriptor) for scenario 2, top-hat example 5.

Shape	Iteration	$\max(\psi)$	$\ \psi\ _1$	$(\max(\psi) - \lambda \cdot \ \psi\ _1)$
plate	1	3.5777×10^{-4}	0.0078	-0.0012
	2	0.1906	0.2591	0.1388
dihedral	1	0.0088	0.0592	-0.0030
	2	0.0088	0.0592	-0.0030
sphere	1	0.0163	1.7751	-0.3387
	2	3.3965	54.1462	-7.4328
top-hat	1	0.2370	4.3769	-0.6383
	2	0.2370	4.3769	-0.6383
trihedral	1	2.8690×10^{-5}	0.0010	-1.7189×10^{-4}
	2	2.8038×10^{-5}	0.0669	-0.0133
cylinder	1	0.0075	0.4848	-0.0895
	2	0.6154	10.1761	-1.4198

In the first example, the closest parameter set contained within the top-hat dictionary corresponds to $\Theta = [0, 0, 0, 2.5, 1, 0, 0, 0, 0]$. The algorithm successfully classifies the target as a top-hat. The estimated parameter set also corresponds to the closest set. In the second example, the closest parameter set is $\Theta = [0, 0, 0, 2, 1.5, 0, 0, 0, 0]$. The algorithm incorrectly estimates the model order as 2 and classifies the target a plate and a trihedral. The resulting parameter set estimations are provided in Table C.48 and Table C.49.

Table C.48: Estimated versus true parameters for scenario 2, top-hat example 4.

Shape	X	Y	Z	H	L	r	$\tilde{\gamma}$	$\tilde{\theta}$	$\tilde{\phi}$
True top-hat	0	0	0	2.3	-	1	0	0	0
Expected top-hat	0	0	0	2.5	-	1	0	0	0
Estimated top-hat	0	0	0	2.5	-	1	0	0	0

Table C.49: Estimated versus true parameters for scenario 2, top-hat example 5.

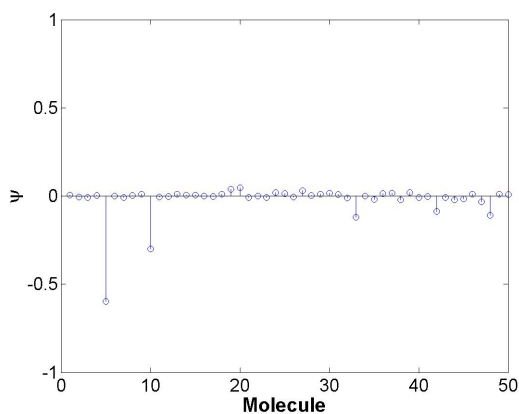
Shape	X	Y	Z	H	L	r	$\tilde{\gamma}$	$\tilde{\theta}$	$\tilde{\phi}$
True top-hat	0	0	0	2	-	1.3	0	0	0
Expected top-hat	0	0	0	2	-	1.5	0	0	0
Estimated trihedral	5	-5	-10	0.5	-	-	0	0	0
Estimated plate	5	-5	-10	1	0.5	-	0	-30	0

C.4 Trihedral Results

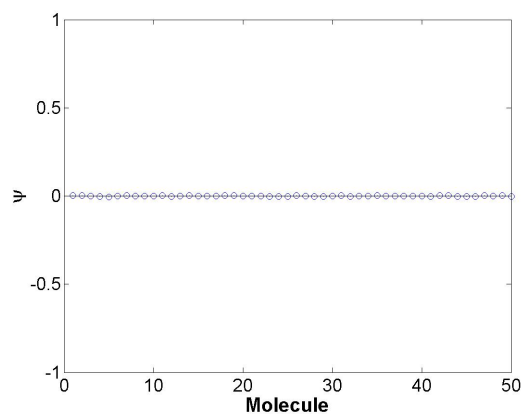
C.4.1 X Parameter. In this example, we generate a trihedral target located at $x = 4$ m with an SNR of 30 dB. The trihedral target is simulated using the parameters listed in Table C.50. The BP results for each shape are provided in Table C.50: The parameters used to create the trihedral target for scenario 2, example 1.

Shape	X	Y	Z	H	L	r	$\tilde{\gamma}$	$\tilde{\theta}$	$\tilde{\phi}$
trihedral	4	0	0	2	-	-	0	0	0

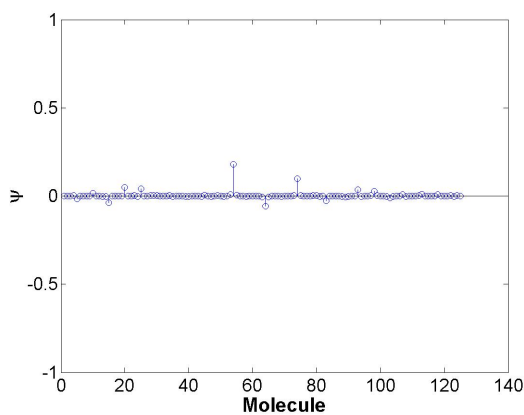
Figures C.21-C.22.



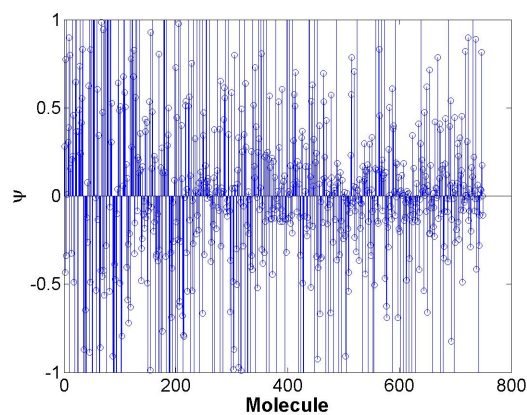
(a) BP result using the reduced plate dictionary.



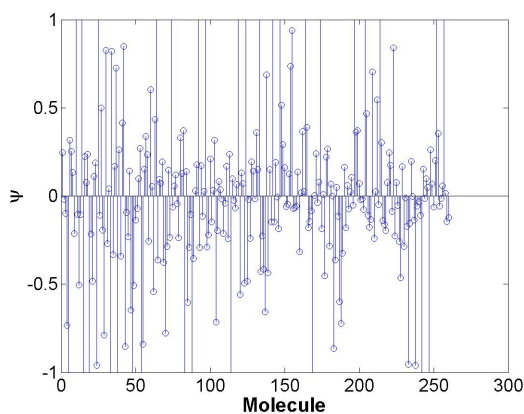
(b) BP result using the reduced dihedral dictionary.



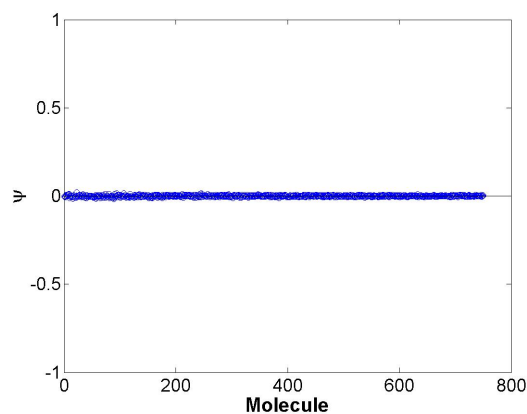
(c) BP result using the reduced trihedral dictionary.



(d) BP result using the reduced sphere dictionary.

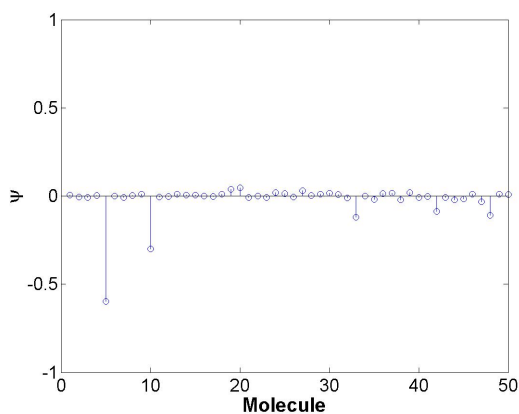


(e) BP result using the reduced cylinder dictionary.

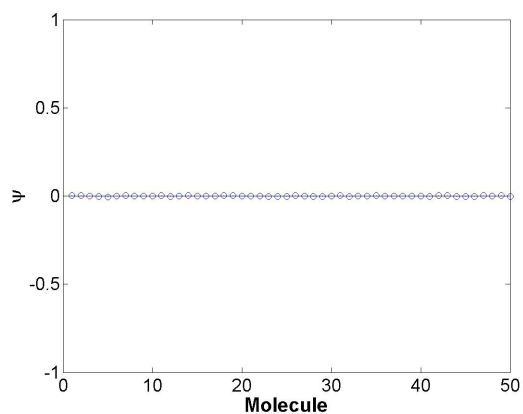


(f) BP result using the reduced top-hat dictionary.

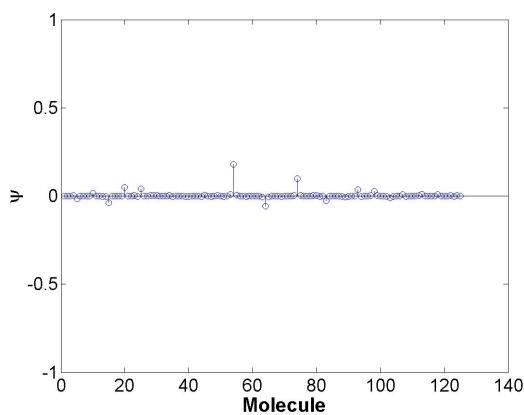
Figure C.21: BP results for the first iteration for each of the reduced shape dictionaries used in the feature extraction problem in scenario 2, trihedral example 1.



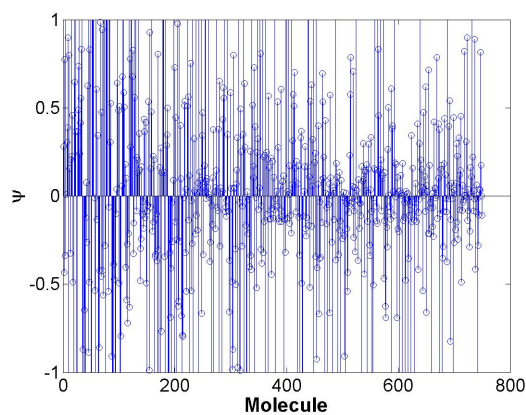
(a) BP result using the reduced plate dictionary.



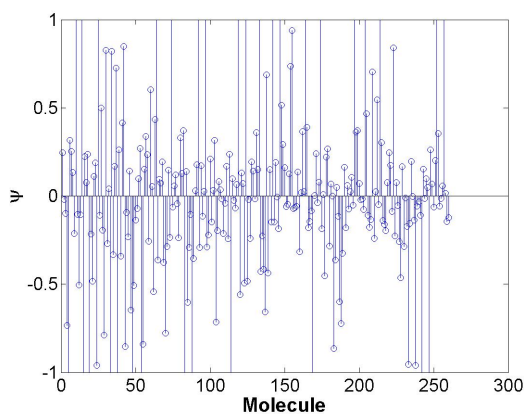
(b) BP result using the reduced dihedral dictionary.



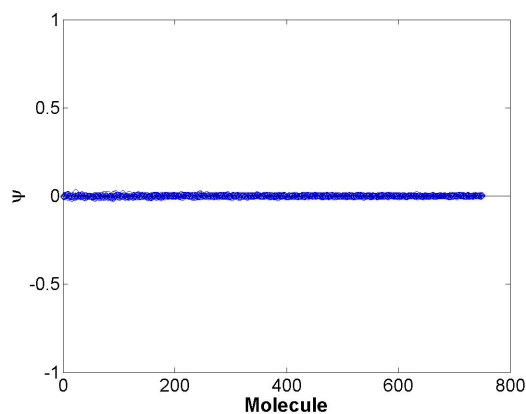
(c) BP result using the reduced trihedral dictionary.



(d) BP result using the reduced sphere dictionary.



(e) BP result using the reduced cylinder dictionary.



(f) BP result using the reduced top-hat dictionary.

Figure C.22: BP results for the final iteration for each of the reduced shape dictionaries used in the feature extraction problem in scenario 2, trihedral example 1.

The maximum coefficient returned by the BP algorithm for each of the shape dictionaries and the sparsities, described by $\|\psi\|_1$, are provided in Table C.51. This

Table C.51: Maximum coefficients from each shape dictionary along with the ℓ_1 norm (sparsity descriptor) for scenario 2, trihedral example 1.

Shape	Iteration	$\max(\psi)$	$\ \psi\ _1$	$(\max(\psi) - \lambda \cdot \ \psi\ _1)$
plate	1	0.0452	1.7269	-0.3002
	2	0.7814	2.6540	0.2506
dihedral	1	0.0037	0.0895	-0.0142
	2	0.0037	0.0895	-0.0142
sphere	1	36.7881	936.0928	-150.4304
	2	34.9225	962.5994	-157.5973
top-hat	1	0.0178	2.2200	-0.4262
	2	0.0178	2.2200	-0.4262
trihedral	1	0.1814	0.7681	0.0278
	2	0.0991	0.6689	-0.0347
cylinder	1	12.8528	208.3579	-28.8188
	2	12.4624	209.5427	-29.4462

method overestimates the model order and incorrectly leads to a trihedral and a plate classification. The extracted shapes along with their associated parameter sets are provided in Table C.52.

Table C.52: Estimated versus true parameters for scenario 2, trihedral example 1.

Shape	X	Y	Z	H	L	r	$\tilde{\gamma}$	$\tilde{\theta}$	$\tilde{\phi}$
True trihedral	4	0	0	2	-	-	0	0	0
Expected trihedral	5	0	0	2	-	-	0	0	0
Estimated trihedral	5	-10	0	1	-	-	0	0	0
Estimated plate	5	10	0	1	1	-	0	-30	0

Initially, we make the hypothesis that the parameter set extracted should be the closest dictionary contained parameter set, $\Theta = [5, 0, 0, 2, 0, 0, 0, 0, 0]$ (atom 439). The LS errors are provided in Table C.53.

C.4.2 Y Parameter. In this example, we generate a trihedral target located at $y = 4$ m with an SNR of 30 dB. The trihedral target is simulated using the parameters listed in Table C.54.

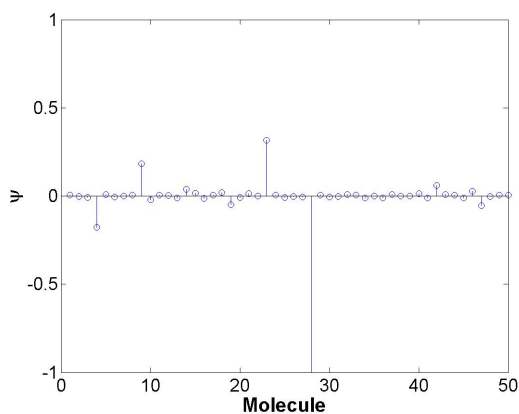
Table C.53: LS errors for the extracted and hypothesized data sets for scenario 2, trihedral example 1.

Data	$\ \mathbf{x} - \mathbf{s}(\Theta_n)\ _2^2$
Extracted	1.7642×10^{10}
Closest	3.6814×10^{10}

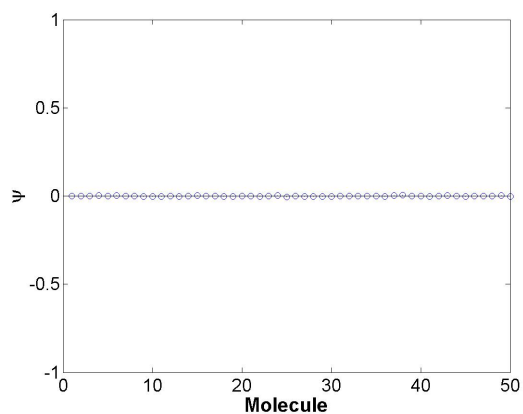
Table C.54: The parameters used to create the trihedral target for scenario 2, example 2.

Shape	X	Y	Z	H	L	r	$\tilde{\gamma}$	$\tilde{\theta}$	$\tilde{\phi}$
trihedral	0	4	0	2	-	-	0	0	0

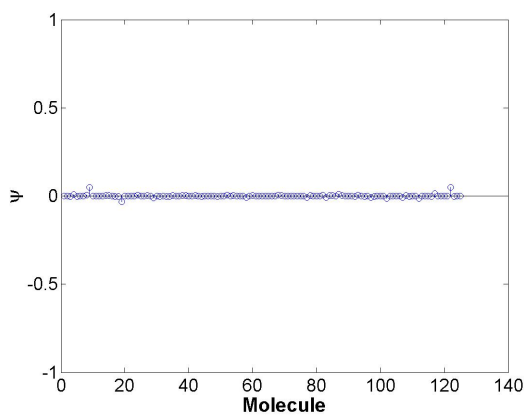
The BP results for each shape are provided in Figures C.23-C.25.



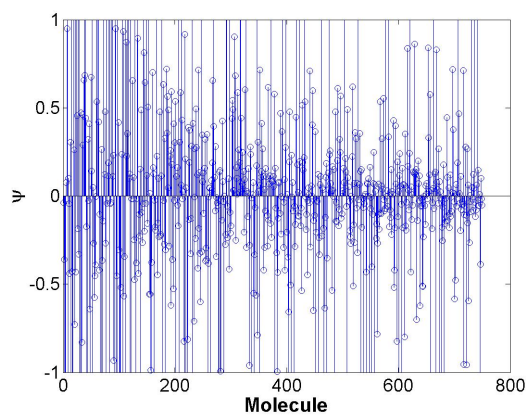
(a) BP result using the reduced plate dictionary.



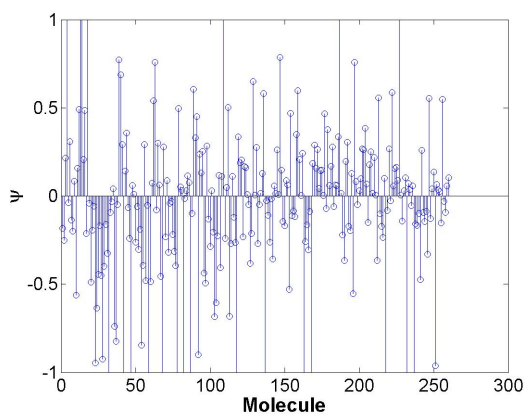
(b) BP result using the reduced dihedral dictionary.



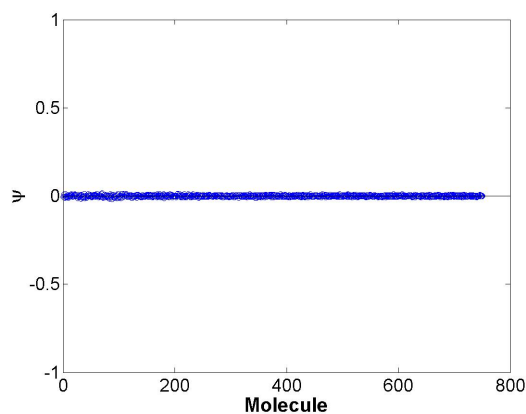
(c) BP result using the reduced trihedral dictionary.



(d) BP result using the reduced sphere dictionary.

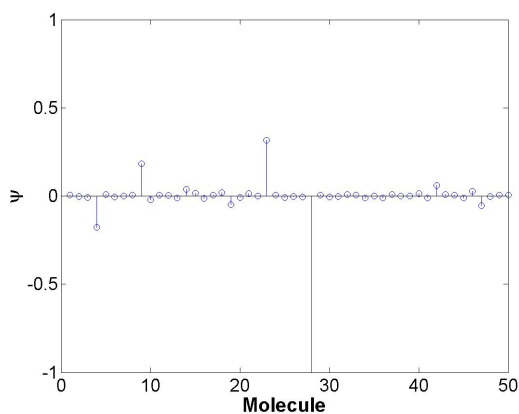


(e) BP result using the reduced cylinder dictionary.

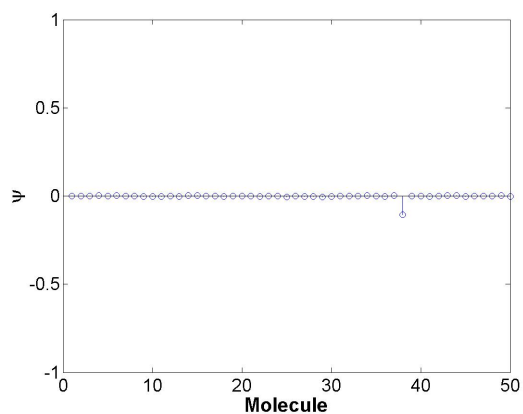


(f) BP result using the reduced top-hat dictionary.

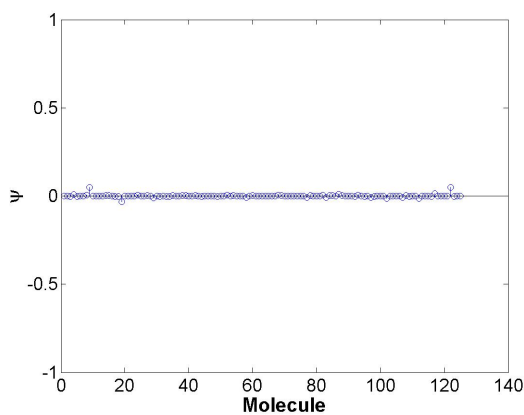
Figure C.23: BP results for the first iteration for each of the reduced shape dictionaries used in the feature extraction problem in scenario 2, trihedral example 2.



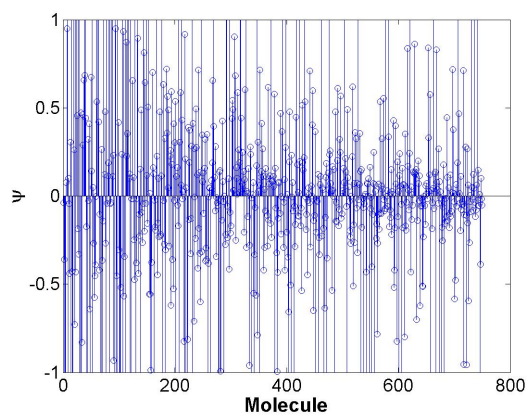
(a) BP result using the reduced plate dictionary.



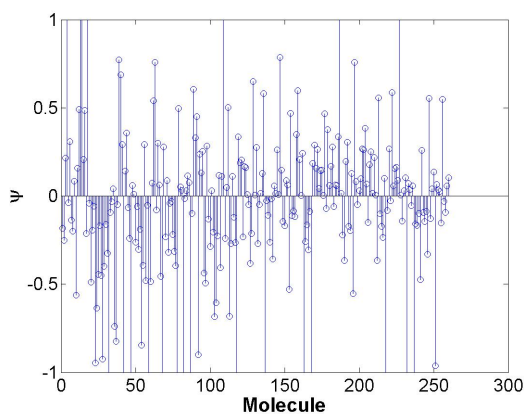
(b) BP result using the reduced dihedral dictionary.



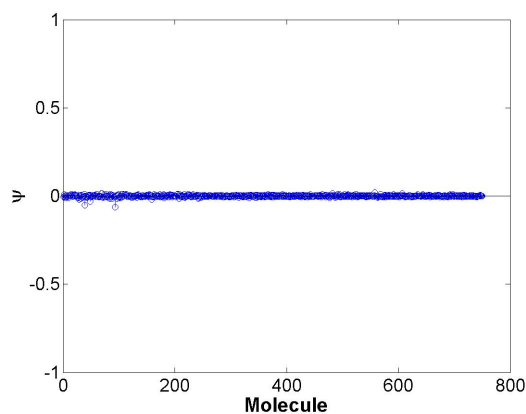
(c) BP result using the reduced trihedral dictionary.



(d) BP result using the reduced sphere dictionary.

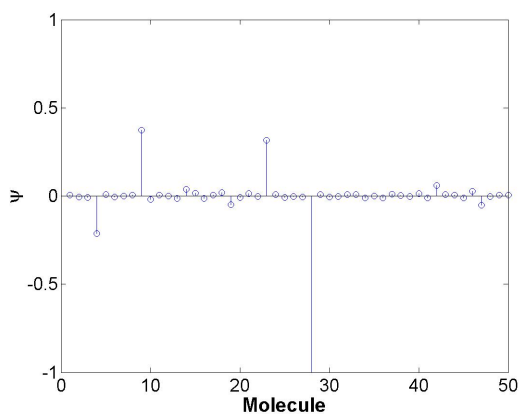


(e) BP result using the reduced cylinder dictionary.

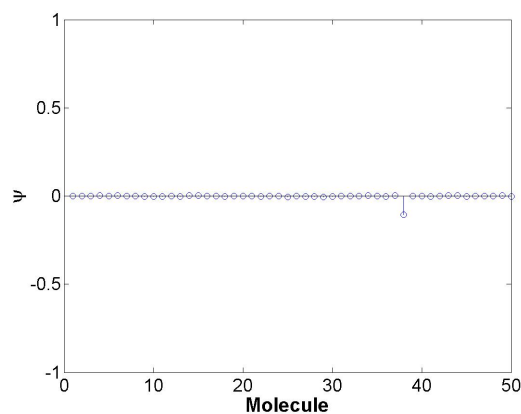


(f) BP result using the reduced top-hat dictionary.

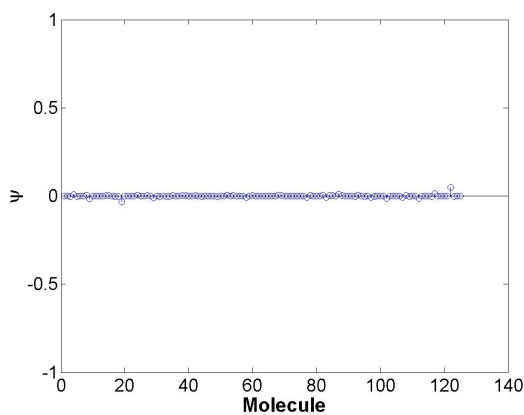
Figure C.24: BP results for the second iteration for each of the reduced shape dictionaries used in the feature extraction problem in scenario 2, trihedral example 2.



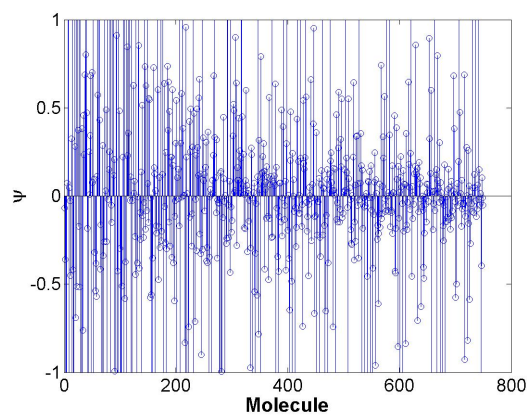
(a) BP result using the reduced plate dictionary.



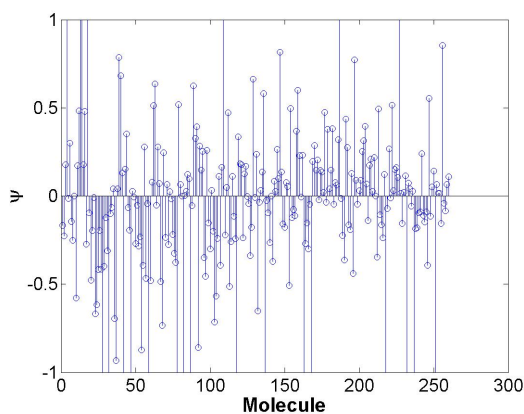
(b) BP result using the reduced dihedral dictionary.



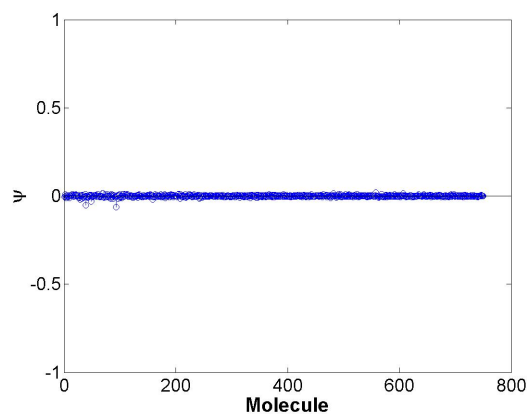
(c) BP result using the reduced trihedral dictionary.



(d) BP result using the reduced sphere dictionary.



(e) BP result using the reduced cylinder dictionary.



(f) BP result using the reduced top-hat dictionary.

Figure C.25: BP results for the final iteration for each of the reduced shape dictionaries used in the feature extraction problem in scenario 2, trihedral example 2.

The maximum coefficient returned by the BP algorithm for each of the shape dictionaries and the sparsities, described by $\|\psi\|_1$, are provided in Table C.55.

Table C.55: Maximum coefficients from each shape dictionary along with the ℓ_1 norm (sparsity descriptor) for scenario 2, trihedral example 2.

Shape	Iteration	$\max(\psi)$	$\ \psi\ _1$	$(\max(\psi) - \lambda \cdot \ \psi\ _1)$
plate	1	0.3154	3.5692	-0.3985
	2	0.3154	3.5692	-0.3985
	3	0.3727	3.8158	-0.3905
dihedral	1	0.0042	0.0762	-0.0110
	2	0.0037	0.1820	-0.0327
	3	0.0037	0.1820	-0.0327
sphere	1	29.3667	682.7459	-107.1825
	2	29.3667	682.7459	-107.1825
	3	29.0975	685.6160	108.0257
top-hat	1	0.0130	2.1260	-0.4122
	2	0.0189	2.5048	-0.4821
	3	0.0189	2.5048	-0.4821
trihedral	1	0.0485	0.3774	-0.0270
	2	0.0485	0.3774	-0.0270
	3	0.0482	0.3463	-0.0211
cylinder	1	5.1166	129.7189	-20.8272
	2	5.1166	129.7189	-20.8272
	3	4.9592	127.4049	-20.5218

This method overestimates the model order and incorrectly leads to shape classifications including two trihedrals and a dihedral. The associated extracted parameter sets are provided in Table C.56.

Table C.56: Estimated versus true parameters for scenario 2, trihedral example 2.

Shape	X	Y	Z	H	L	r	$\tilde{\gamma}$	$\tilde{\theta}$	$\tilde{\phi}$
True trihedral	0	4	0	2	-	-	0	0	0
Expected trihedral	0	5	0	2	-	-	0	0	0
Estimated dihedral	0	-5	5	0.5	0.5	-	0	0	0
Estimated trihedral 1	5	-5	-10	0.5	-	-	0	0	0
Estimated trihedral 2	-5	10	10	0.5	-	-	0	0	0

Initially, we assume that the algorithm should choose the trihedral corresponding to the closest parameter set. Therefore, the expected parameter set would be

$\Theta = [0, 5, 0, 2, 0, 0, 0, 0, 0]$. The total LS errors for the extracted data versus the hypothesized closest data are provided in Table C.57.

Table C.57: LS errors for the extracted and hypothesized data sets for scenario 2, trihedral example 2.

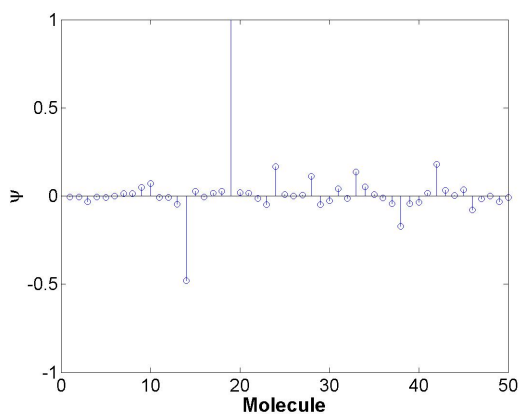
Data	$\ \mathbf{x} - \mathbf{s}(\Theta_n)\ _2^2$
Extracted	1.8090×10^{10}
Closest	3.6082×10^{10}

C.4.3 Z Parameter. In this example, we generate a trihedral target located at $z = 4$ m with an SNR of 30 dB. The trihedral target is simulated using the parameters listed in Table C.58.

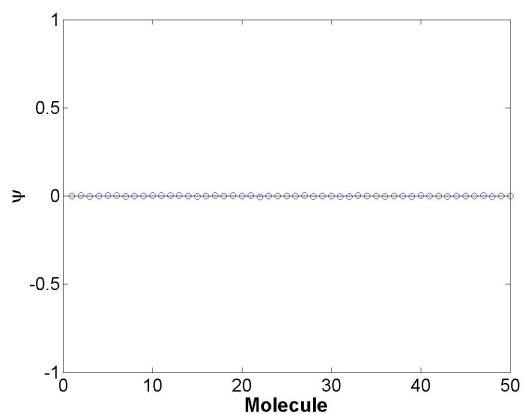
Table C.58: The parameters used to create the trihedral target for scenario 2, example 3.

Shape	X	Y	Z	H	L	r	$\tilde{\gamma}$	$\tilde{\theta}$	$\tilde{\phi}$
trihedral	0	0	4	2	-	-	0	0	0

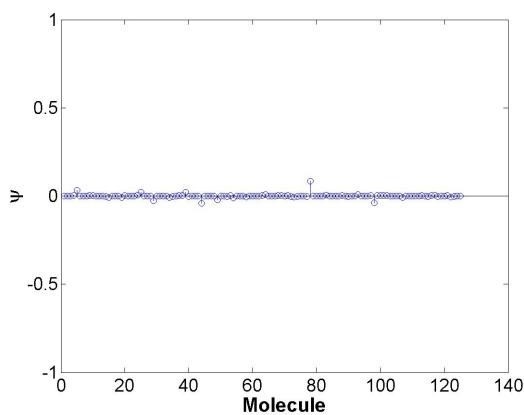
The BP results for each shape are provided in Figures C.26-C.28.



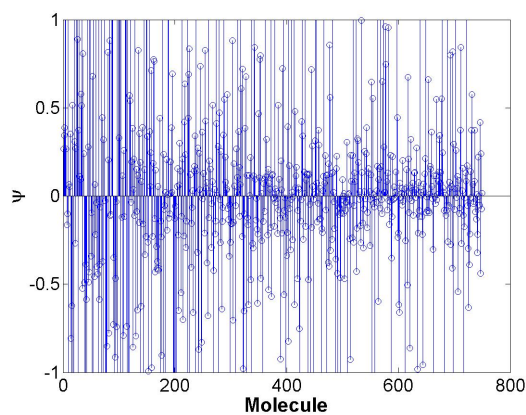
(a) BP result using the reduced plate dictionary.



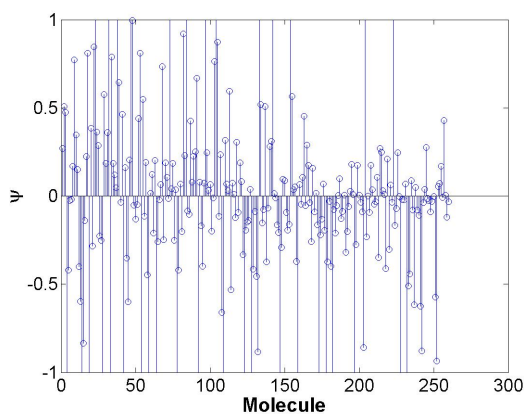
(b) BP result using the reduced dihedral dictionary.



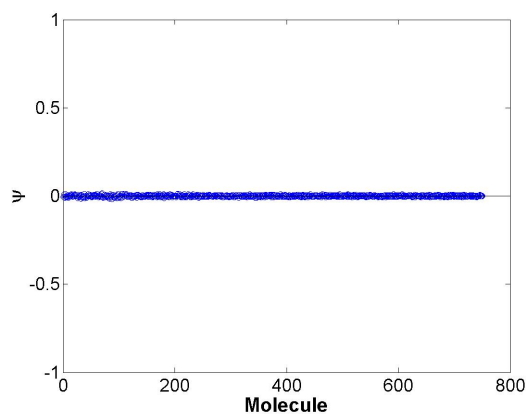
(c) BP result using the reduced trihedral dictionary.



(d) BP result using the reduced sphere dictionary.

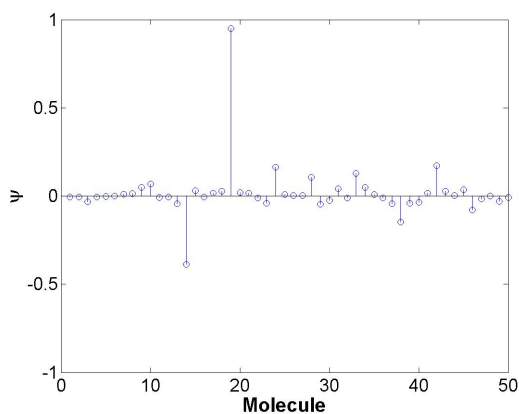


(e) BP result using the reduced cylinder dictionary.

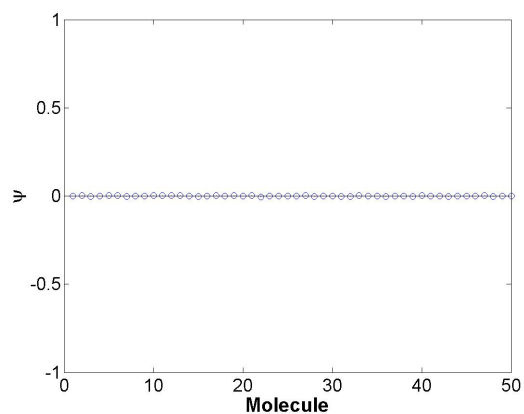


(f) BP result using the reduced top-hat dictionary.

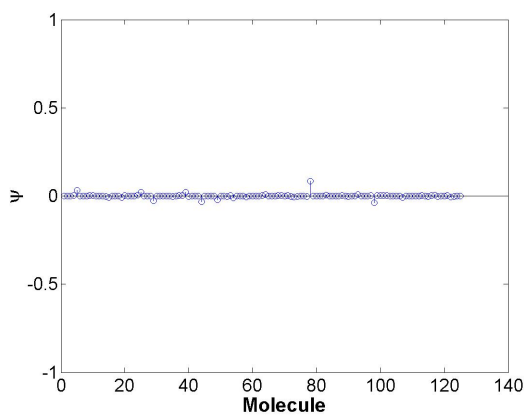
Figure C.26: BP results for the first iteration for each of the reduced shape dictionaries used in the feature extraction problem in scenario 2, trihedral example 3.



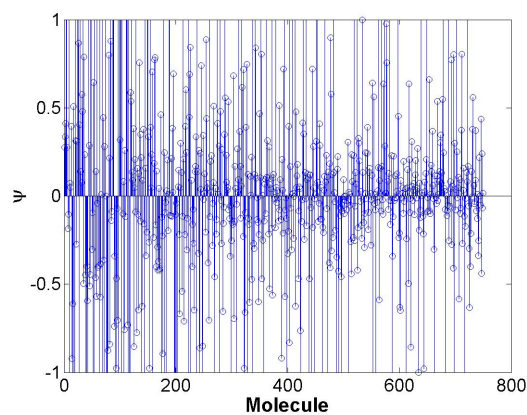
(a) BP result using the reduced plate dictionary.



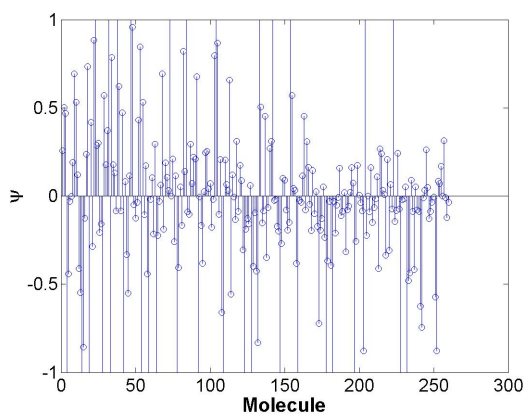
(b) BP result using the reduced dihedral dictionary.



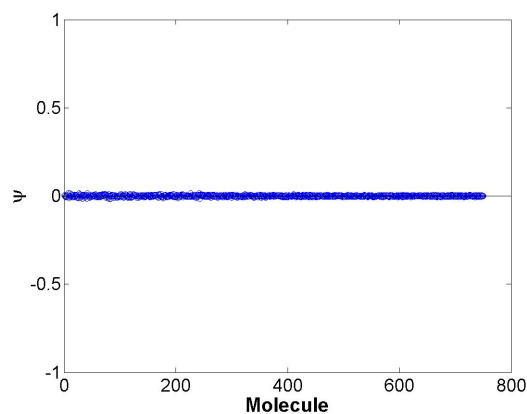
(c) BP result using the reduced trihedral dictionary.



(d) BP result using the reduced sphere dictionary.

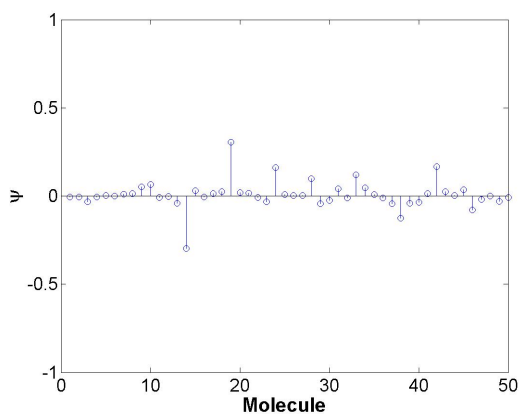


(e) BP result using the reduced cylinder dictionary.

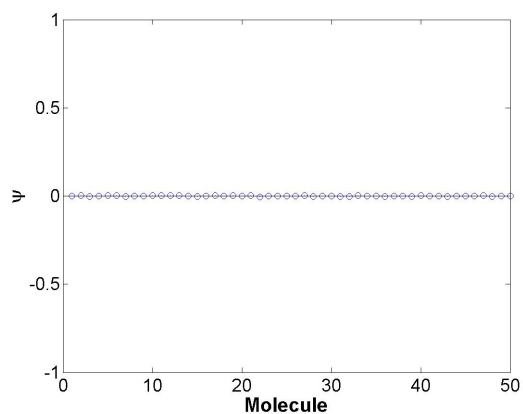


(f) BP result using the reduced top-hat dictionary.

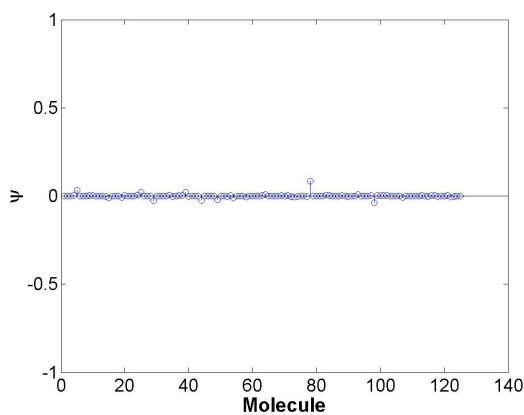
Figure C.27: BP results for the second iteration for each of the reduced shape dictionaries used in the feature extraction problem in scenario 2, trihedral example 3.



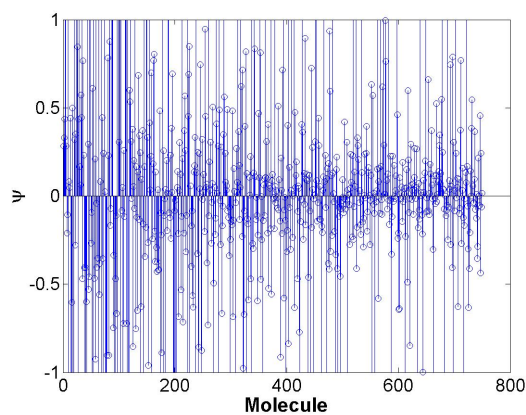
(a) BP result using the reduced plate dictionary.



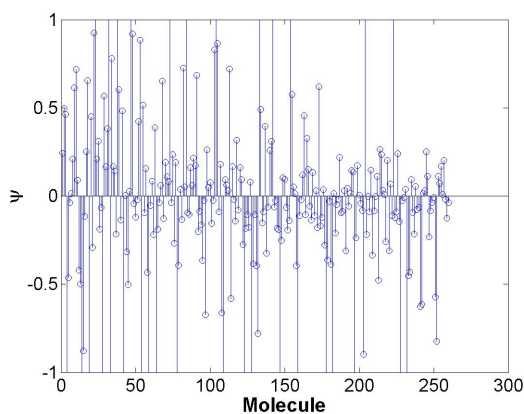
(b) BP result using the reduced dihedral dictionary.



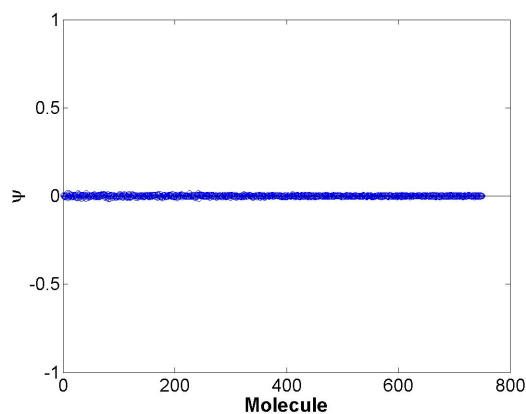
(c) BP result using the reduced trihedral dictionary.



(d) BP result using the reduced sphere dictionary.



(e) BP result using the reduced cylinder dictionary.



(f) BP result using the reduced top-hat dictionary.

Figure C.28: BP results for the final iteration for each of the reduced shape dictionaries used in the feature extraction problem in scenario 2, trihedral example 3.

The maximum coefficient returned by the BP algorithm for each of the shape dictionaries and the sparsities, described by $\|\psi\|_1$, are provided in Table C.59.

Table C.59: Maximum coefficients from each shape dictionary along with the ℓ_1 norm (sparsity descriptor) for scenario 2, trihedral example 3.

Shape	Iteration	$\max(\psi)$	$\ \psi\ _1$	$(\max(\psi) - \lambda \cdot \ \psi\ _1)$
plate	1	1.5926	3.8507	0.8224
	2	0.9492	3.0205	0.3451
	3	0.3059	2.1984	-0.1338
dihedral	1	0.0039	0.0752	-0.0112
	2	0.0039	0.0752	-0.0112
	3	0.0039	0.0752	-0.0112
sphere	1	46.1615	917.5072	-137.3399
	2	45.9706	918.6691	-137.7632
	3	45.7797	921.2261	-138.4655
top-hat	1	0.0147	2.2082	-0.4270
	2	0.0147	2.2082	-0.4270
	3	0.0147	2.2082	-0.4270
trihedral	1	0.0853	0.4977	-0.0143
	2	0.0851	0.4801	-0.0109
	3	0.0850	0.4755	-0.0101
cylinder	1	13.9106	181.4277	-22.3749
	2	13.8515	176.4864	-21.4457
	3	13.7924	175.0444	-21.2164

This method overestimates the model order and incorrectly leads to shape classifications including two plates and a trihedral. The associated extracted parameter sets are provided in Table C.60.

Table C.60: Estimated versus true parameters for scenario 2, trihedral example 3.

Shape	X	Y	Z	H	L	r	$\tilde{\gamma}$	$\tilde{\theta}$	$\tilde{\phi}$
True trihedral	0	0	4	2	-	-	0	0	0
Expected trihedral	0	0	5	2	-	-	0	0	0
Estimated trihedral	0	-10	5	0.5	-	-	0	0	0
Estimated plate 1	5	5	-5	1	1.5	-	0	-30	0
Estimated plate 2	5	5	-5	1	1.5	-	0	-30	0

Initially, we assume that the algorithm should choose the trihedral corresponding to the closest parameter set. Therefore, the expected parameter set would be

$\Theta = [0, 0, 5, 2, 0, 0, 0, 0, 0]$. The total LS errors for the extracted data versus the hypothesized closest data are provided in Table C.61.

Table C.61: LS errors for the extracted and hypothesized data sets for scenario 2, trihedral example 3.

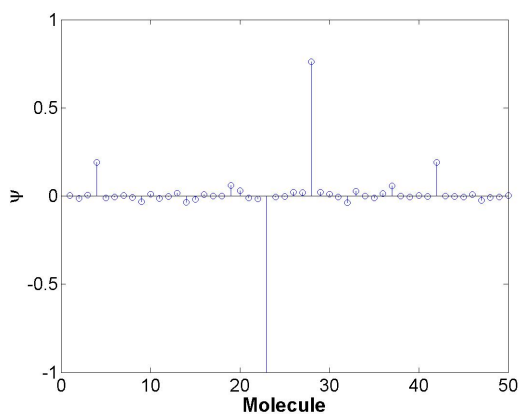
Data	$\ \mathbf{x} - \mathbf{s}(\Theta_n)\ _2^2$
Extracted	1.7839×10^{10}
Closest	3.5890×10^{10}

C.4.4 RCS Parameters. In this example, we generate a trihedral target with RCS parameter $h = 2.3$ m with an SNR of 30 dB. The trihedral target is simulated using the parameters listed in Table C.62.

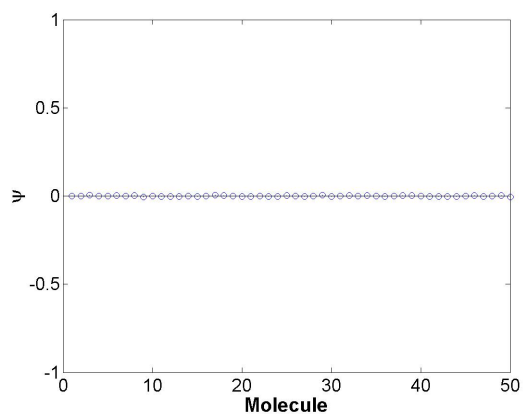
Table C.62: The parameters used to create the trihedral target for scenario 2, example 4.

Shape	X	Y	Z	H	L	r	$\tilde{\gamma}$	$\tilde{\theta}$	$\tilde{\phi}$
trihedral	0	0	0	2.3	-	-	0	0	0

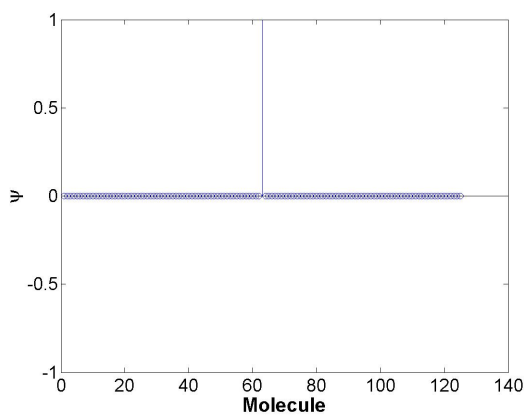
The BP results for each shape are provided in Figure C.29.



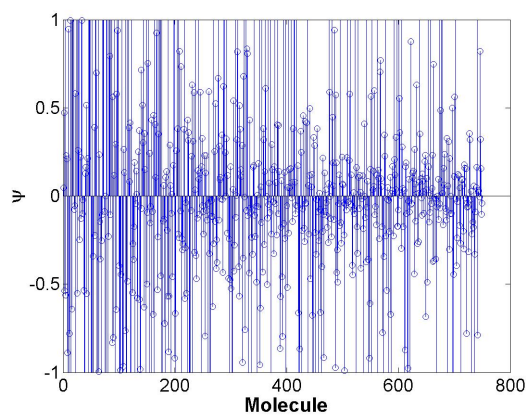
(a) BP result using the reduced plate dictionary.



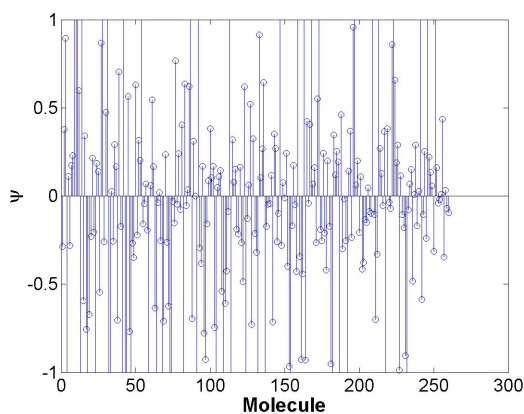
(b) BP result using the reduced dihedral dictionary.



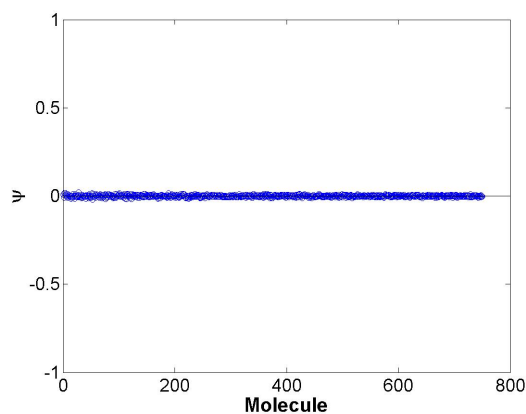
(c) BP result using the reduced trihedral dictionary.



(d) BP result using the reduced sphere dictionary.



(e) BP result using the reduced cylinder dictionary.



(f) BP result using the reduced top-hat dictionary.

Figure C.29: BP results for each of the reduced shape dictionaries used in the feature extraction problem in scenario 2, trihedral example 4.

The maximum coefficient returned by the BP algorithm for each of the shape dictionaries and the sparsities, described by $\|\psi\|_1$, are provided in Table C.63.

Table C.63: Maximum coefficients from each shape dictionary along with the ℓ_1 norm (sparsity descriptor) for scenario 2, trihedral example 4.

Shape	$\max(\psi)$	$\ \psi\ _1$	$(\max(\psi) - \lambda \cdot \ \psi\ _1)$
plate	0.7625	5.8507	0.1819
dihedral	0.0061	0.1041	-0.0043
sphere	45.3260	1.0681×10^3	-61.4793
top-hat	0.0192	2.8672	-0.2675
trihedral	1.3949	1.4189	1.2530
cylinder	12.1820	309.4477	-18.7628

For this example, the shape is correctly classified as a trihedral. The expected parameter set estimation is $\Theta = [0, 0, 0, 2.5, 0, 0, 0, 0, 0]$. The extracted parameter set is provided in Table C.64.

Table C.64: Estimated versus true parameters for scenario 2, trihedral example 4.

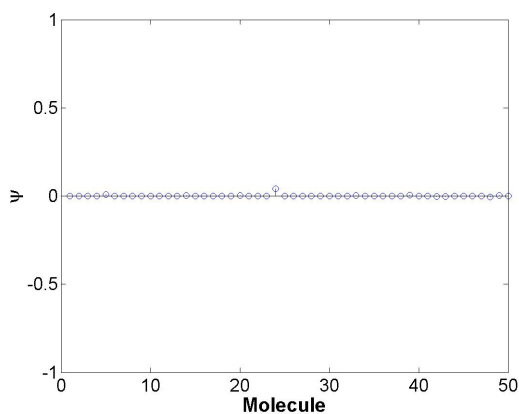
Shape	X	Y	Z	H	L	r	$\tilde{\gamma}$	$\tilde{\theta}$	$\tilde{\phi}$
True trihedral	0	0	0	2.3	-	-	0	0	0
Expected trihedral	0	0	0	2.5	-	-	0	0	0
Estimated trihedral	0	0	0	2.5	-	-	0	0	0

C.5 Cylinder Results

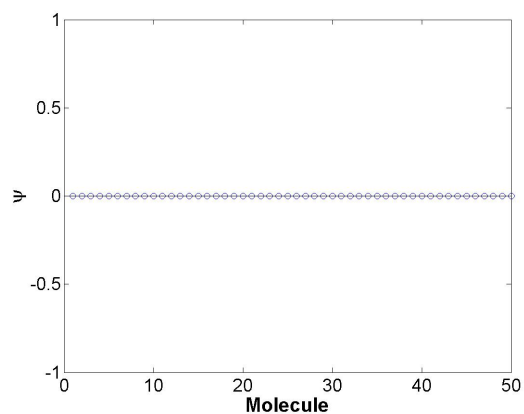
C.5.1 X Parameter. In this example, we generate a cylinder target located at $x = 4$ m with an SNR of 30 dB. The cylinder target is simulated using the parameters listed in Table C.65. The BP results for each shape are provided in Figure C.30.

Table C.65: The parameters used to create the cylinder target for this scene.

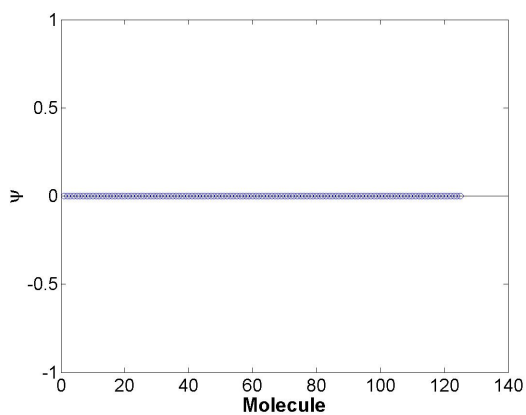
Shape	X	Y	Z	H	L	r	$\tilde{\gamma}$	$\tilde{\theta}$	$\tilde{\phi}$
cylinder	4	0	0	-	2	1	0	0	0



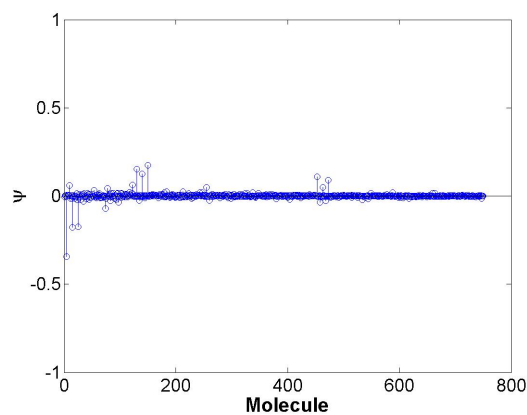
(a) BP result using the reduced plate dictionary.



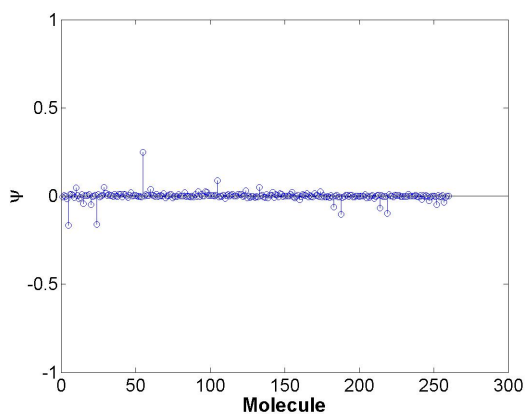
(b) BP result using the reduced dihedral dictionary.



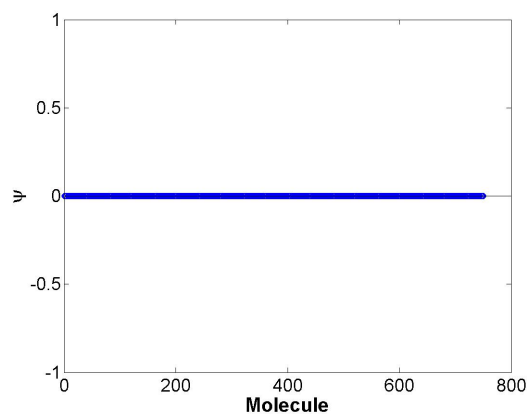
(c) BP result using the reduced trihedral dictionary.



(d) BP result using the reduced sphere dictionary.



(e) BP result using the reduced cylinder dictionary.



(f) BP result using the reduced top-hat dictionary.

Figure C.30: BP results for the first iteration for each of the reduced shape dictionaries used in the feature extraction problem in scenario 2, cylinder example 1.

The maximum coefficient returned by the BP algorithm for each of the shape dictionaries and the sparsities, described by $\|\psi\|_1$, are provided in Table C.66. This

Table C.66: Maximum coefficients from each shape dictionary along with the ℓ_1 norm (sparsity descriptor) for scenario 2, cylinder example 1.

Shape	$\max(\psi)$	$\ \psi\ _1$	$(\max(\psi) - \lambda \cdot \ \psi\ _1)$
plate	0.0405	0.0862	0.0233
dihedral	2.1546×10^{-4}	0.0040	-5.8105×10^{-4}
sphere	0.1759	4.5267	-0.7294
top-hat	5.2297×10^{-4}	0.0820	-0.0159
trihedral	2.2578×10^{-4}	0.0024	-2.4537×10^{-4}
cylinder	0.2494	2.6869	-0.2880

method incorrectly leads to a plate classification. The extracted shape along with its associated parameter set is provided in Table C.67.

Table C.67: Estimated versus true parameters for scenario 2, cylinder example 1.

Shape	X	Y	Z	H	L	r	$\tilde{\gamma}$	$\tilde{\theta}$	$\tilde{\phi}$
True cylinder	4	0	0	-	2	1	0	0	0
Expected cylinder	5	0	0	-	2	1	0	0	0
Estimated plate	5	-10	0	0.5	0.5	-	0	-30	0

Initially, we make the hypothesis that the parameter set extracted should be the closest dictionary contained representative parameter set, $\Theta = [5, 0, 0, 0, 2, 1, 0, 0, 0]$. The LS errors are provided in Table C.68.

Table C.68: LS errors for the extracted and hypothesized data sets for scenario 2, cylinder example 1.

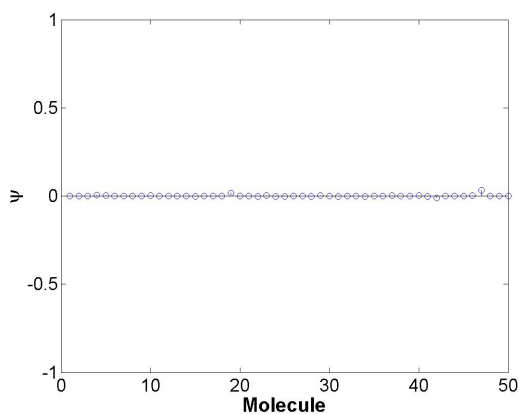
Dictionary Atom	$\ \mathbf{x} - \mathbf{s}(\Theta_n)\ _2^2$
Extracted	3.1414×10^6
Closest	2.2627×10^6

C.5.2 Y Parameter. In this example, we generate a cylinder target located at $y = 4$ m with an SNR of 30 dB. The cylinder target is simulated using the parameters listed in Table C.69.

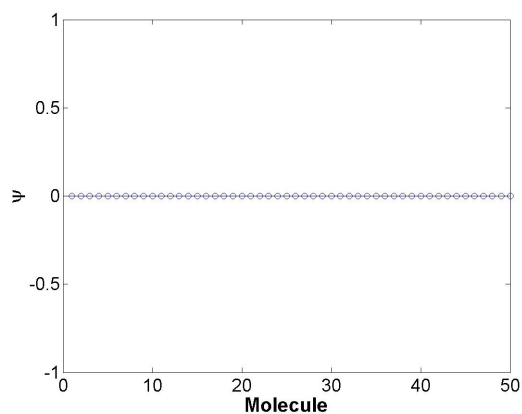
The BP results for each shape are provided in Figure C.31.

Table C.69: The parameters used to create the cylinder target for scenario 2, example 2.

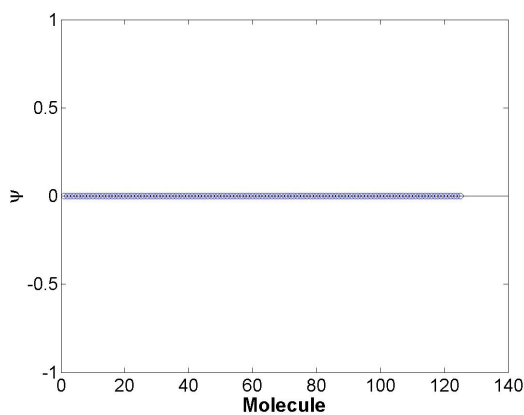
Shape	X	Y	Z	H	L	r	$\tilde{\gamma}$	$\tilde{\theta}$	$\tilde{\phi}$
cylinder	0	4	0	-	2	1	0	0	0



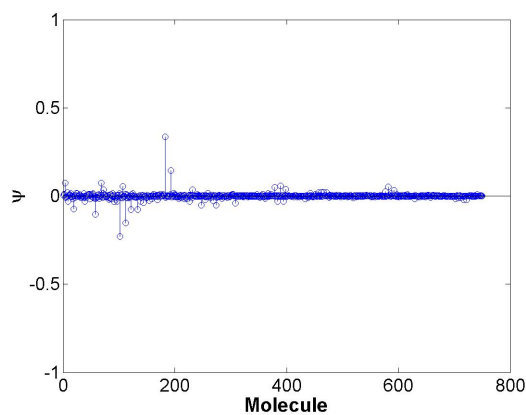
(a) BP result using the reduced plate dictionary.



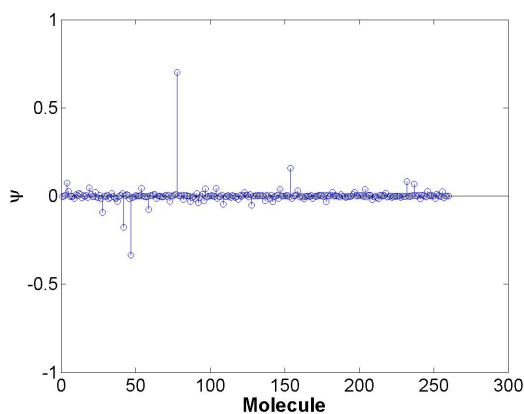
(b) BP result using the reduced dihedral dictionary.



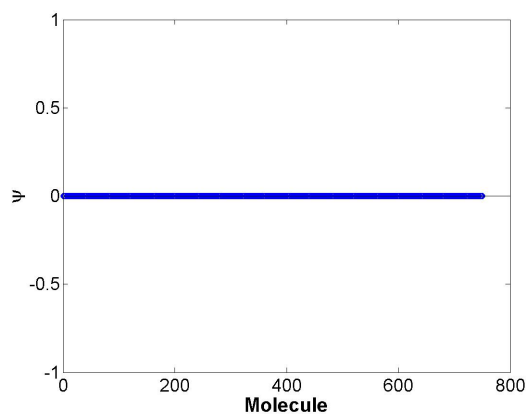
(c) BP result using the reduced trihedral dictionary.



(d) BP result using the reduced sphere dictionary.



(e) BP result using the reduced cylinder dictionary.



(f) BP result using the reduced top-hat dictionary.

Figure C.31: BP results for each of the reduced shape dictionaries used in the feature extraction problem in scenario 2, cylinder example 2.

The maximum coefficient returned by the BP algorithm for each of the shape dictionaries and the sparsities, described by $\|\psi\|_1$, are provided in Table C.70.

Table C.70: Maximum coefficients from each shape dictionary along with the ℓ_1 norm (sparsity descriptor) for scenario 2, cylinder example 2.

Shape	$\max(\psi)$	$\ \psi\ _1$	$(\max(\psi) - \lambda \cdot \ \psi\ _1)$
plate	0.0316	0.1141	0.0088
dihedral	1.4602×10^{-4}	0.0036	-5.7679×10^{-4}
sphere	0.3354	4.7249	-0.6096
top-hat	5.9643×10^{-4}	0.0852	-0.0164
trihedral	2.9651×10^{-4}	0.0024	-1.8896×10^{-4}
cylinder	0.7025	3.6024	-0.0179

This method incorrectly leads to a plate classification. However, the BP optimization results for the cylinder dictionary identified the correct molecule containing the closes parameter set, $\Theta = [0, 5, 0, 0, 2, 1, 0, 0, 0]$. The algorithm failed to choose this molecule because the largest $(\psi - \lambda \cdot \|\psi\|_1)$, shown in Table C.70, corresponded to the plate dictionary. The extracted parameter set is provided in Table C.71. The

Table C.71: Estimated versus true parameters for scenario 2, cylinder example 2.

Shape	X	Y	Z	H	L	r	$\tilde{\gamma}$	$\tilde{\theta}$	$\tilde{\phi}$
True cylinder	0	4	0	-	2	1	0	0	0
Expected cylinder	0	5	0	-	2	1	0	0	0
Estimated plate	-5	5	10	0.5	0.5	-	0	-30	0

expected cylinder also leads to a lower LS error, as shown in Table C.72.

Table C.72: LS errors for the extracted and hypothesized data sets for scenario 2, cylinder example 2.

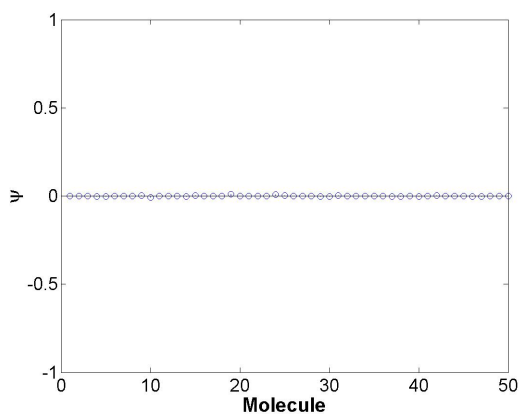
Data	$\ \mathbf{x} - \mathbf{s}(\Theta_n)\ _2^2$
Extracted	3.1518×10^6
Closest	1.2202×10^6

C.5.3 Z Parameter. In this example, we generate a cylinder target located at $z = 4$ m with an SNR of 30 dB. The cylinder target is simulated using the parameters listed in Table C.73.

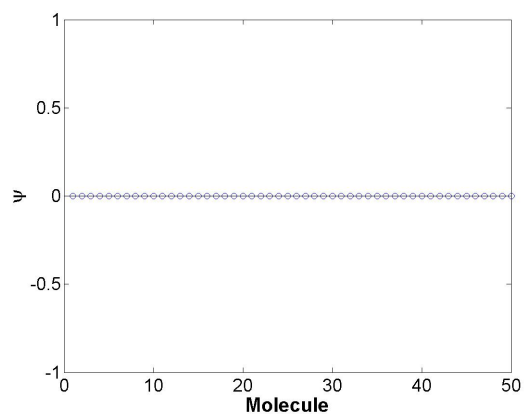
Table C.73: The parameters used to create the cylinder target for scenario 2, example 3.

Shape	X	Y	Z	H	L	r	$\tilde{\gamma}$	$\tilde{\theta}$	$\tilde{\phi}$
cylinder	0	0	4	-	2	1	0	0	0

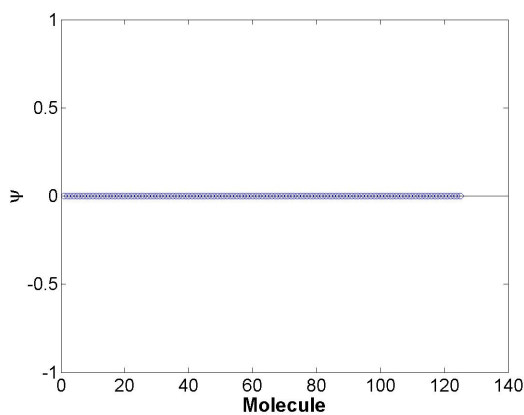
The BP results for each shape are provided in Figures C.32-C.33.



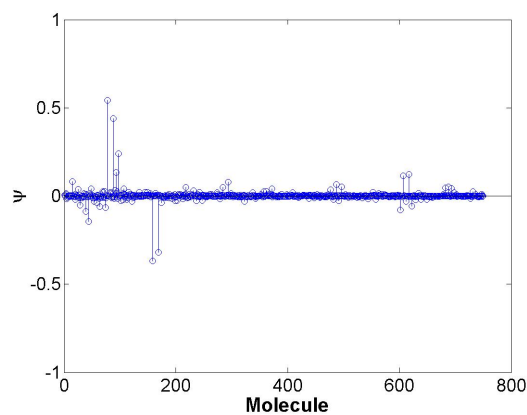
(a) BP result using the reduced plate dictionary.



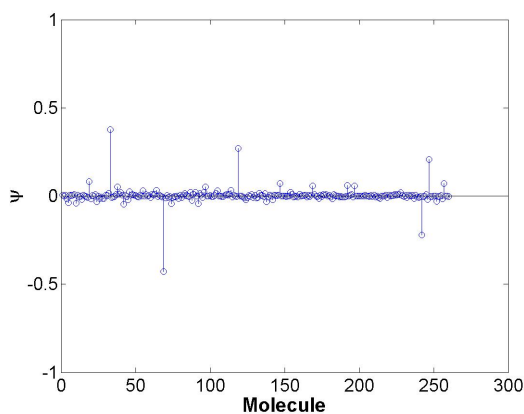
(b) BP result using the reduced dihedral dictionary.



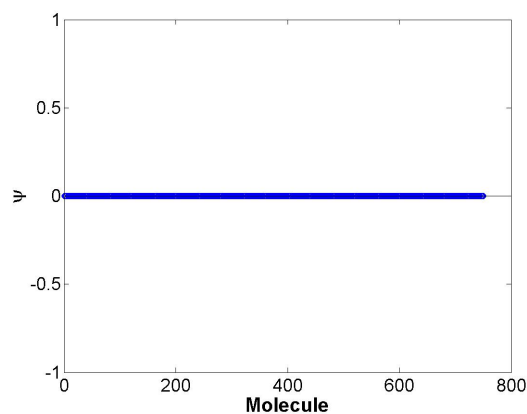
(c) BP result using the reduced trihedral dictionary.



(d) BP result using the reduced sphere dictionary.

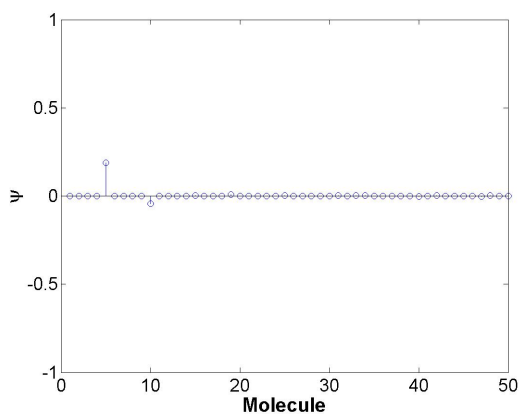


(e) BP result using the reduced cylinder dictionary.

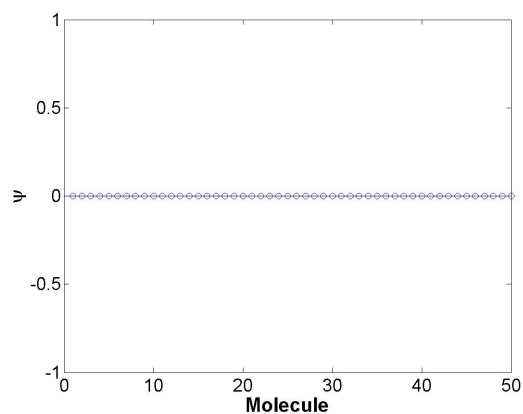


(f) BP result using the reduced top-hat dictionary.

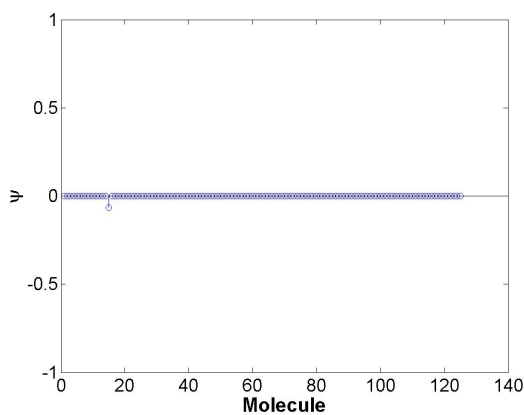
Figure C.32: BP results for the first iteration for each of the reduced shape dictionaries used in the feature extraction problem in scenario 2, cylinder example 3.



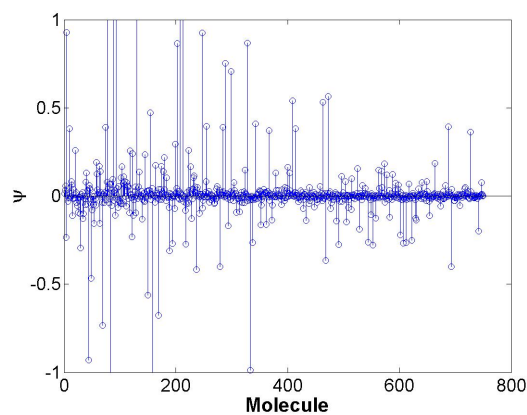
(a) BP result using the reduced plate dictionary.



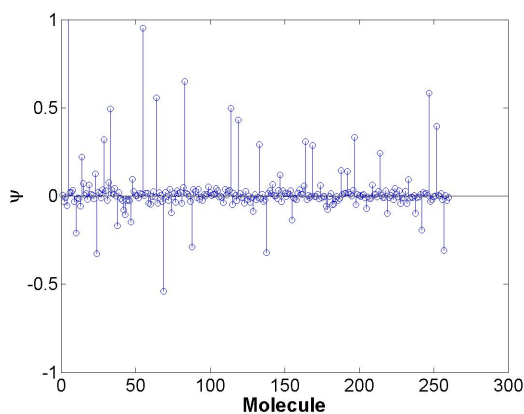
(b) BP result using the reduced dihedral dictionary.



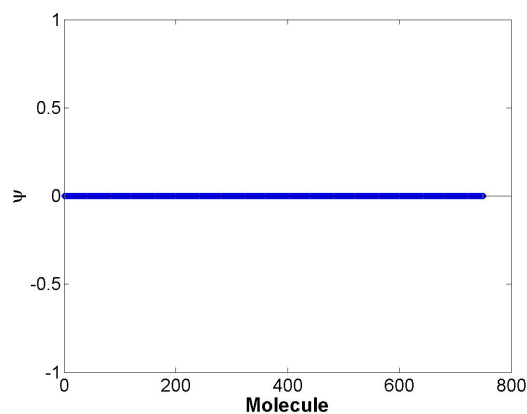
(c) BP result using the reduced trihedral dictionary.



(d) BP result using the reduced sphere dictionary.



(e) BP result using the reduced cylinder dictionary.



(f) BP result using the reduced top-hat dictionary.

Figure C.33: BP results for the final iteration for each of the reduced shape dictionaries used in the feature extraction problem in scenario 2, cylinder example 3.

The maximum coefficient returned by the BP algorithm for each of the shape dictionaries and the sparsities, described by $\|\psi\|_1$, are provided in Table C.74.

Table C.74: Maximum coefficients from each shape dictionary along with the ℓ_1 norm (sparsity descriptor) for scenario 2, cylinder example 3.

Shape	Iteration	$\max(\psi)$	$\ \psi\ _1$	$(\max(\psi) - \lambda \cdot \ \psi\ _1)$
plate	1	0.0113	0.0698	-0.0026
	2	0.1890	0.2763	0.1338
dihedral	1	2.2883×10^{-4}	0.0035	-4.7581×10^{-4}
	2	2.2883×10^{-4}	0.0035	-4.7581×10^{-4}
sphere	1	0.5424	6.6633	-0.7902
	2	3.5947	55.2898	-7.4632
top-hat	1	4.6976×10^{-4}	0.0828	-0.0160
	2	4.6976×10^{-4}	0.0828	-0.0161
trihedral	1	7.8412×10^{-5}	0.0022	-3.5624×10^{-4}
	2	7.0216×10^{-5}	0.0680	-0.0135
cylinder	1	0.3756	3.7915	-0.3827
	2	1.6222	16.4810	-1.6739

This method incorrectly classifies the shape as a combination of a trihedral and a plate. The associated extracted parameter set is provided in Table C.75.

Table C.75: Estimated versus true parameters for scenario 2, cylinder example 3.

Shape	X	Y	Z	H	L	r	$\tilde{\gamma}$	$\tilde{\theta}$	$\tilde{\phi}$
True cylinder	0	0	4	-	2	1	0	0	0
Expected cylinder	0	0	5	-	2	1	0	0	0
Estimated trihedral	10	0	-10	0.5	-	-	0	0	0
Estimated plate	10	0	-10	1	0.5	-	0	-30	0

The total LS errors for the extracted data versus the hypothesized closest data are provided in Table C.76.

Table C.76: LS errors for the extracted and hypothesized data sets for scenario 2, cylinder example 3.

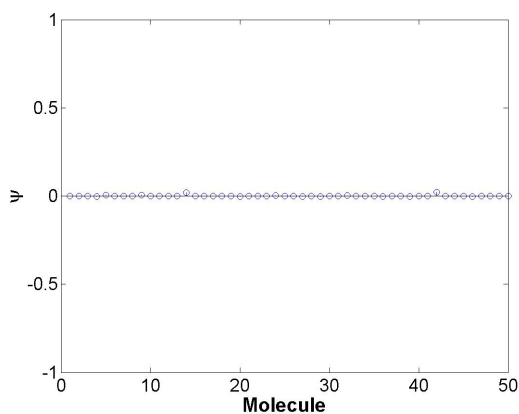
Data	$\ \mathbf{x} - \mathbf{s}(\Theta_n)\ _2^2$
Extracted	6.2758×10^7
Closest	2.2399×10^6

C.5.4 RCS Parameters. In this section we discuss the results of two example target scenes. Each of the scenes includes a cylinder that is generated using a length or radius parameter that falls outside of the dictionary parameter space resolution with an SNR of 30 dB. The cylinder targets are simulated using the parameters listed in Table C.77.

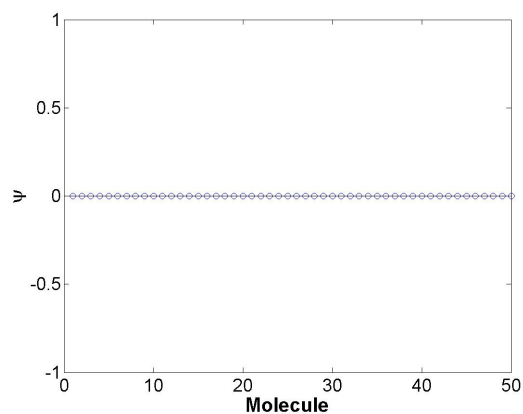
Table C.77: The parameters used to create the cylinder target for scenario 2, examples 4 and 5.

Shape	X	Y	Z	H	L	r	$\tilde{\gamma}$	$\tilde{\theta}$	$\tilde{\phi}$
cylinder 1	0	0	0	-	2.3	1	0	0	0
cylinder 2	0	0	0	-	2	1.3	0	0	0

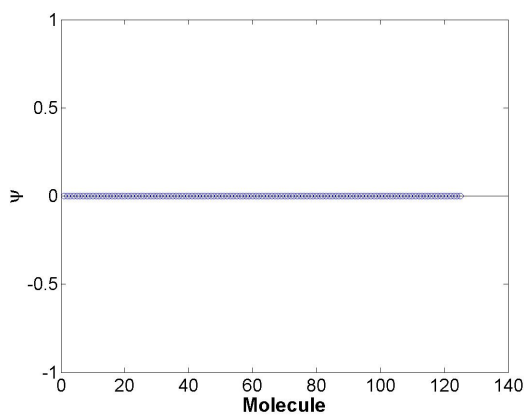
The BP results for each shape are provided in Figures C.34-C.36.



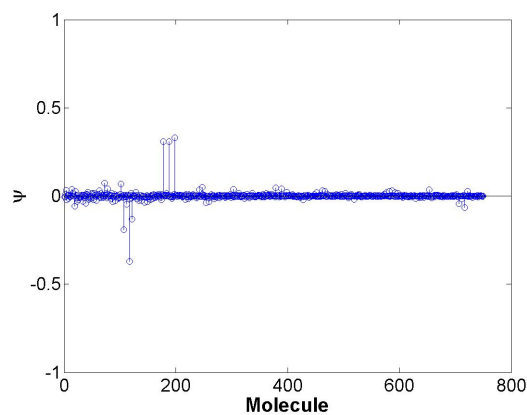
(a) BP result using the reduced plate dictionary.



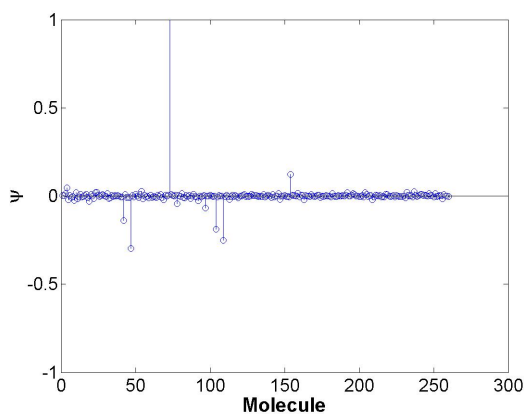
(b) BP result using the reduced dihedral dictionary.



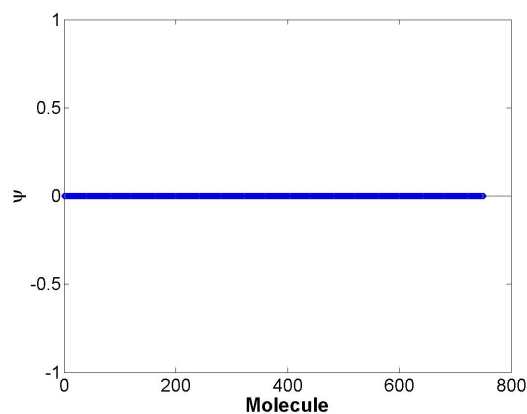
(c) BP result using the reduced trihedral dictionary.



(d) BP result using the reduced sphere dictionary.

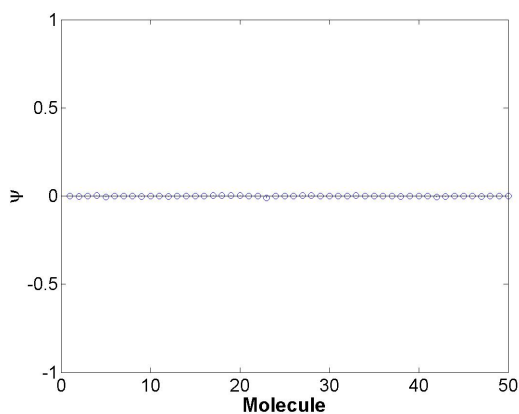


(e) BP result using the reduced cylinder dictionary.

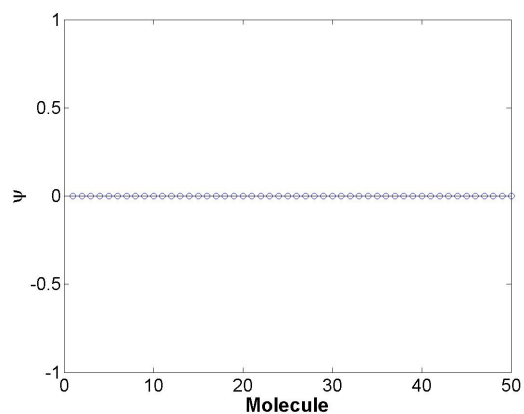


(f) BP result using the reduced top-hat dictionary.

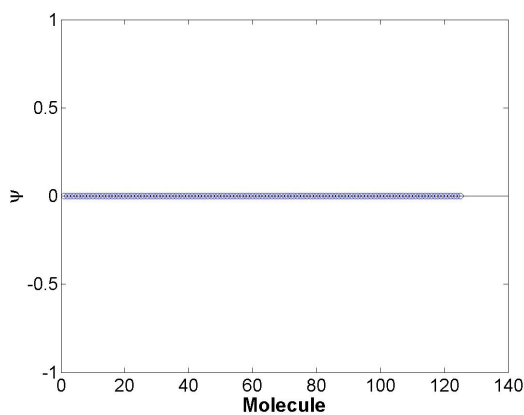
Figure C.34: BP results for each of the reduced shape dictionaries used in the feature extraction problem in scenario 2, cylinder example 4.



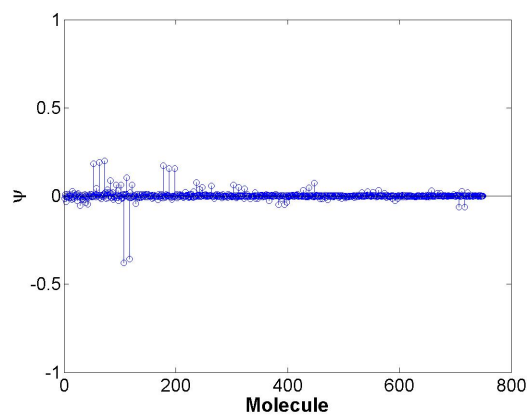
(a) BP result using the reduced plate dictionary.



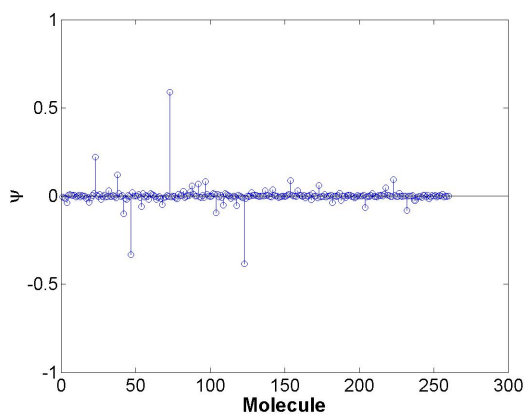
(b) BP result using the reduced dihedral dictionary.



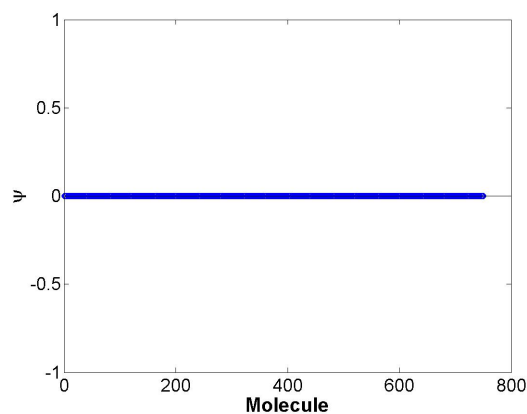
(c) BP result using the reduced trihedral dictionary.



(d) BP result using the reduced sphere dictionary.

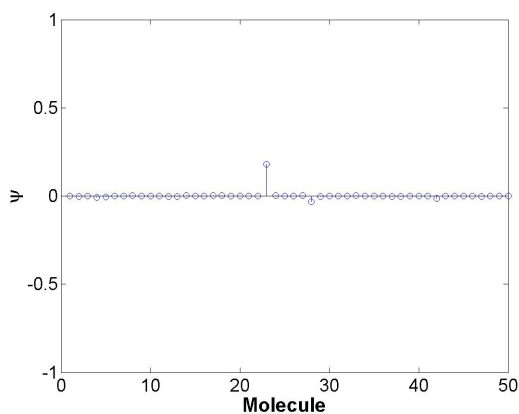


(e) BP result using the reduced cylinder dictionary.

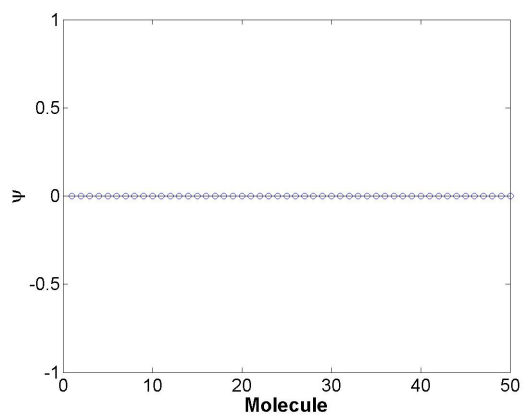


(f) BP result using the reduced top-hat dictionary.

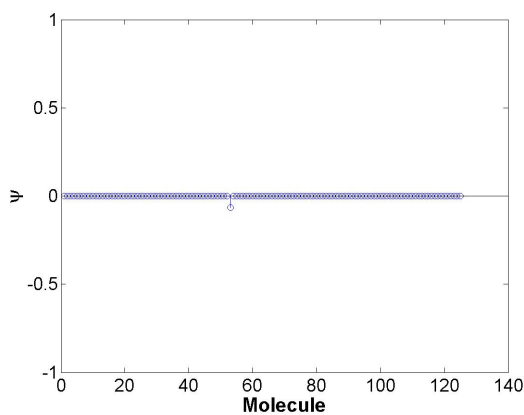
Figure C.35: BP results for the first iteration for each of the reduced shape dictionaries used in the feature extraction problem in scenario 2, cylinder example 5.



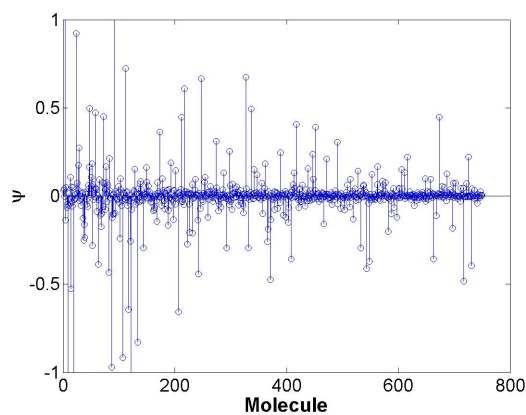
(a) BP result using the reduced plate dictionary.



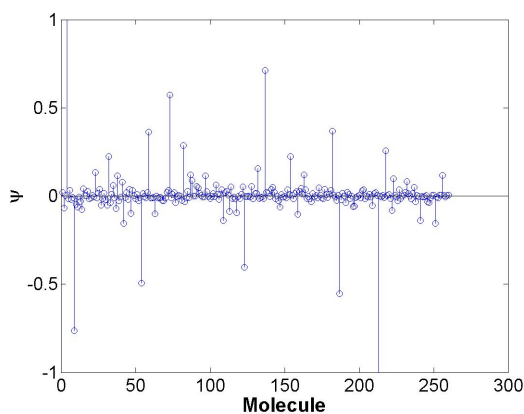
(b) BP result using the reduced dihedral dictionary.



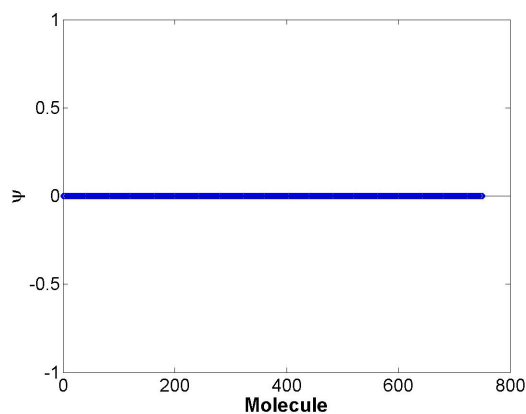
(c) BP result using the reduced trihedral dictionary.



(d) BP result using the reduced sphere dictionary.



(e) BP result using the reduced cylinder dictionary.



(f) BP result using the reduced top-hat dictionary.

Figure C.36: BP results for the final iteration for each of the reduced shape dictionaries used in the feature extraction problem in scenario 2, cylinder example 5.

The maximum coefficient returned by the BP algorithm for each of the shape dictionaries and the sparsities, described by $\|\psi\|_1$, are provided in Table C.78 and Table C.79.

Table C.78: Maximum coefficients from each shape dictionary along with the ℓ_1 norm (sparsity descriptor) for scenario 2, cylinder example 4.

Shape	$\max(\psi)$	$\ \psi\ _1$	$(\max(\psi) - \lambda \cdot \ \psi\ _1)$
plate	0.0221	0.0888	0.0043
dihedral	2.5921×10^{-4}	0.0036	-4.5178×10^{-4}
sphere	0.3315	5.5452	-0.7775
top-hat	7.0102×10^{-4}	0.0914	-0.0176
trihedral	4.5497×10^{-5}	0.0020	-3.5471×10^{-4}
cylinder	1.0207	3.6033	0.3000

Table C.79: Maximum coefficients from each shape dictionary along with the ℓ_1 norm (sparsity descriptor) for scenario 2, cylinder example 5.

Shape	Iteration	$\max(\psi)$	$\ \psi\ _1$	$(\max(\psi) - \lambda \cdot \ \psi\ _1)$
plate	1	0.0039	0.0696	-0.0100
	2	0.1792	0.2891	0.1214
dihedral	1	1.6101×10^{-4}	0.0031	-4.6081×10^{-4}
	2	1.6101×10^{-4}	0.0031	-4.6081×10^{-4}
sphere	1	0.1994	6.1876	-1.0381
	2	3.1234	53.0549	-7.4876
top-hat	1	6.7742×10^{-4}	0.0932	-0.0180
	2	6.7742×10^{-4}	0.0932	-0.0180
trihedral	1	1.2960×10^{-4}	0.0021	-2.9104×10^{-4}
	2	1.2196×10^{-4}	0.0678	-0.0134
cylinder	1	0.5900	4.2337	-0.2567
	2	1.0662	13.9655	-1.7269

In the first example, the closest parameter set contained within the cylinder dictionary corresponds to $\Theta = [0, 0, 0, 0, 2.5, 1, 0, 0, 0]$. The algorithm successfully classifies the target as a cylinder. The estimated parameter set also corresponds to the closest set. In the second example, the closest parameter set is $\Theta = [0, 0, 0, 0, 2, 1.5, 0, 0, 0]$. The algorithm incorrectly overestimates the model order and classifies the target a plate and a trihedral. The resulting parameter set estimations are provided in Table C.80 and Table C.81.

Table C.80: Estimated versus true parameters for scenario 2, cylinder example 4.

Shape	X	Y	Z	H	L	r	$\tilde{\gamma}$	$\tilde{\theta}$	$\tilde{\phi}$
True cylinder	0	0	0	-	2.3	1	0	0	0
Expected cylinder	0	0	0	-	2.5	1	0	0	0
Estimated cylinder	0	0	0	-	2.5	1	0	0	0

Table C.81: Estimated versus true parameters for scenario 2, cylinder example 5.

Shape	X	Y	Z	H	L	r	$\tilde{\gamma}$	$\tilde{\theta}$	$\tilde{\phi}$
True cylinder	0	0	0	-	2	1.3	0	0	0
Expected cylinder	0	0	0	-	2	1.5	0	0	0
Estimated trihedral	0	-10	0	0.5	-	-	0	0	0
Estimated plate	0	-10	0	1	0.5	-	0	-30	0

Appendix D. Scenario 3 Results

D.1 Dihedral, Trihedral, and Top-hat Target Scene

This section will discuss the extraction and classification results for a target scene containing multiple targets that include a dihedral, trihedral and a top-hat. Each of the targets directly corresponds to a dictionary atom. The parameters selected for each shape in this example are given in Table D.1. The measured data is simulated

Table D.1: The parameters used to create scene 3, example 2.

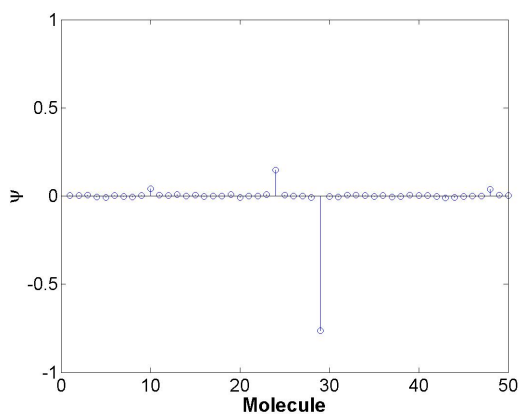
Shape	X	Y	Z	H	L	r	$\tilde{\gamma}$	$\tilde{\theta}$	$\tilde{\phi}$
dihedral	0	10	0	2	2	-	0	0	0
trihedral	5	-5	0	1	-	-	0	0	0
top-hat	0	0	5	2	-	1	0	0	0

with an SNR of 30 dB. Each of the shapes correspond to atoms within their respective shape dictionaries. This correspondence is provided in Table D.2.

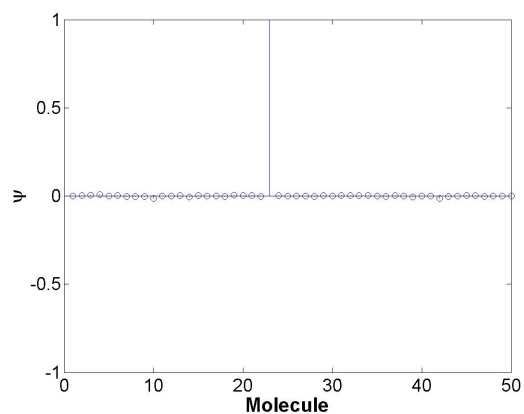
Table D.2: The correspondence mapping for the measured data and dictionary atoms for scenario 3, example 2.

Shape	Orig. Dict. Atom	Molecule	Molecule Atom
dihedral	2698	23	66
trihedral	184	59	2
top-hat	1213	213	4

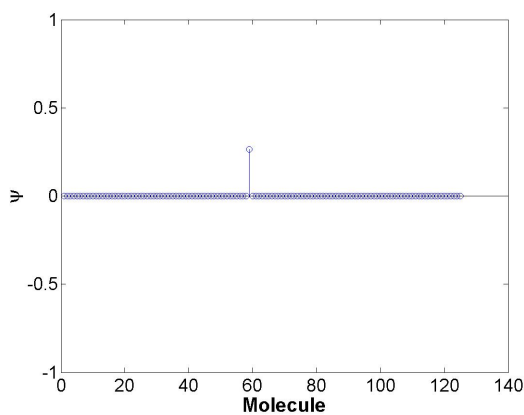
The iterative PH subtraction process leads to multiple iterations of the BP algorithm when extracting multiple shapes from a target scene. A single shape corresponding to the largest contribution of energy is extracted from each iteration. The BP results for each shape and iteration are provided in Figures D.1-D.3.



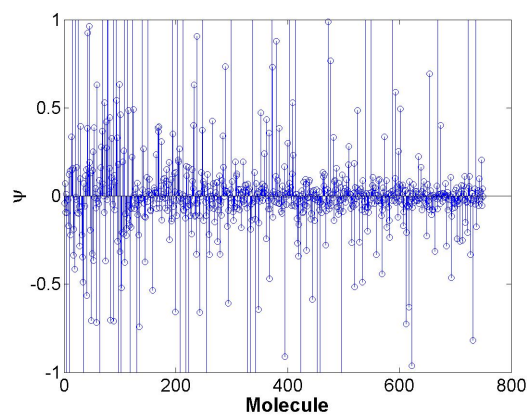
(a) BP result using the reduced plate dictionary.



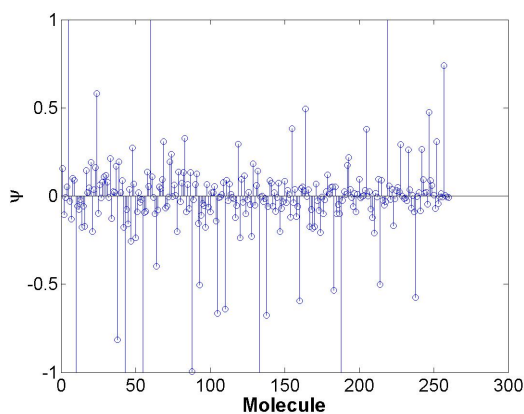
(b) BP result using the reduced dihedral dictionary.



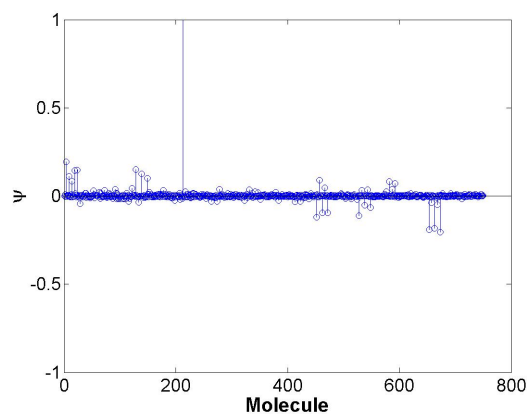
(c) BP result using the reduced trihedral dictionary.



(d) BP result using the reduced sphere dictionary.

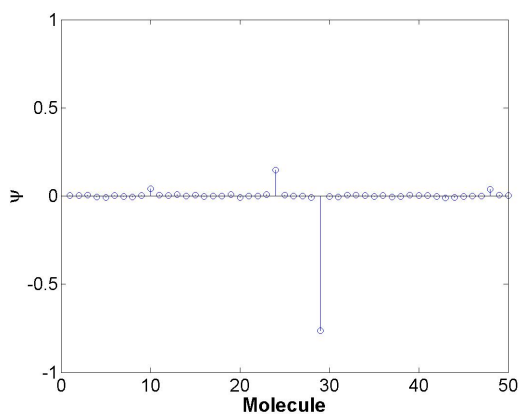


(e) BP result using the reduced cylinder dictionary.

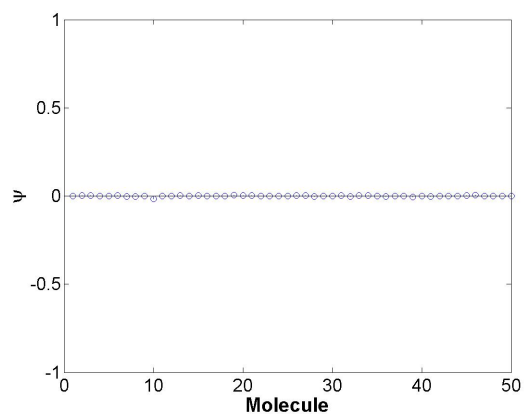


(f) BP result using the reduced top-hat dictionary.

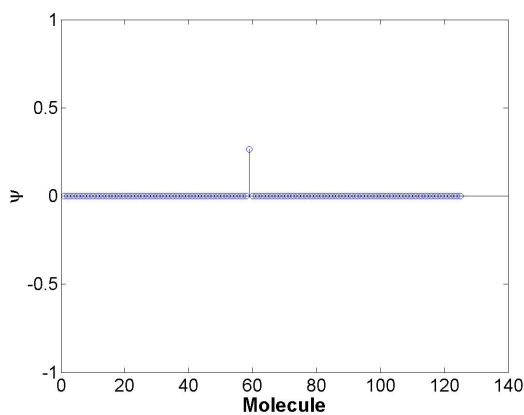
Figure D.1: BP results for each of the reduced shape dictionaries used in the feature extraction problem in scenario 3, example 2 on the first iteration.



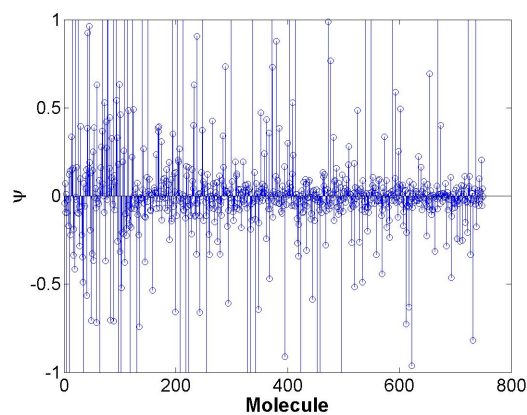
(a) BP result using the reduced plate dictionary.



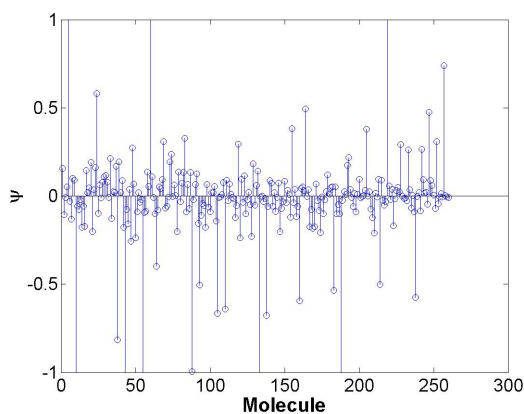
(b) BP result using the reduced dihedral dictionary.



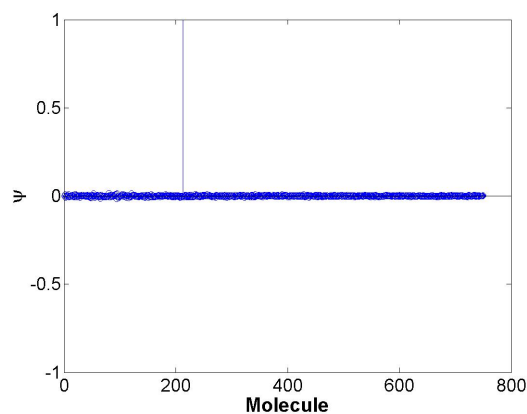
(c) BP result using the reduced trihedral dictionary.



(d) BP result using the reduced sphere dictionary.

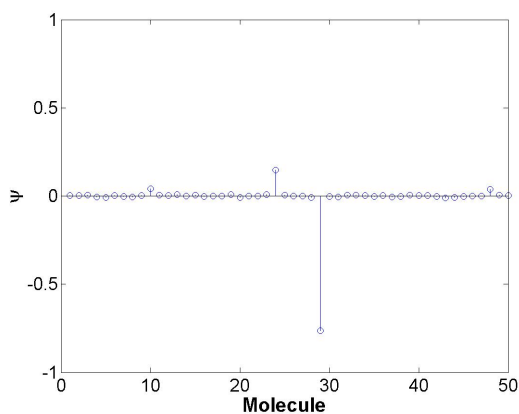


(e) BP result using the reduced cylinder dictionary.

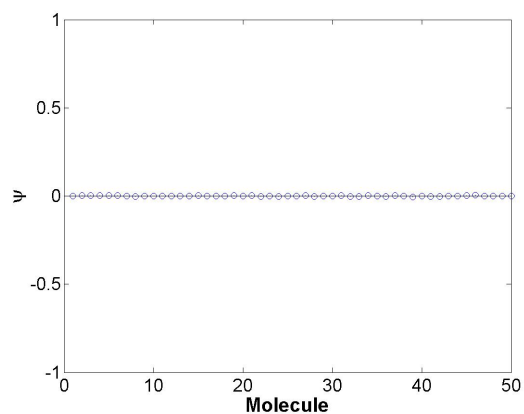


(f) BP result using the reduced top-hat dictionary.

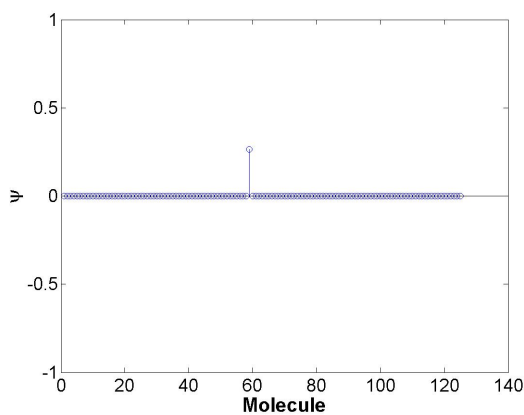
Figure D.2: BP results for each of the reduced shape dictionaries used in the feature extraction problem in scenario 3, example 2 on the second iteration.



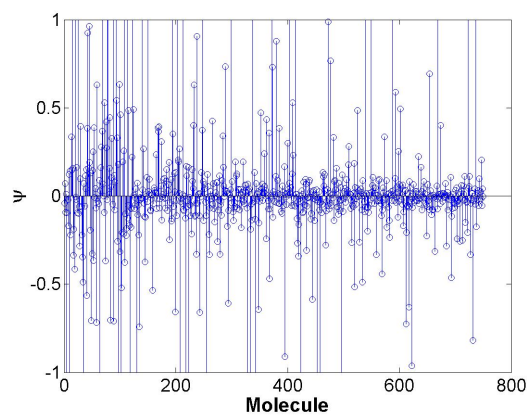
(a) BP result using the reduced plate dictionary.



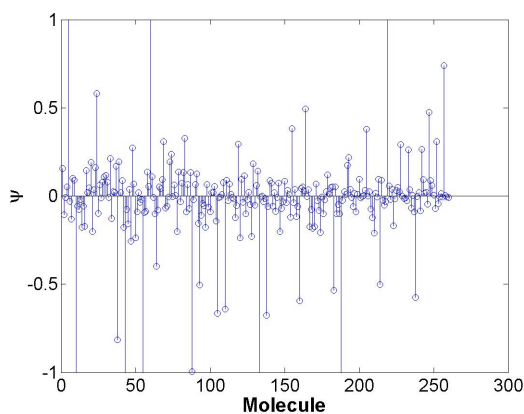
(b) BP result using the reduced dihedral dictionary.



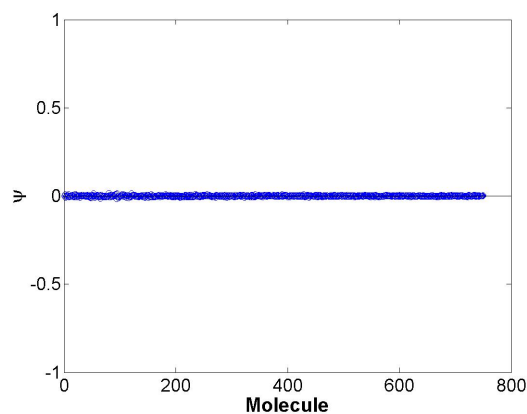
(c) BP result using the reduced trihedral dictionary.



(d) BP result using the reduced sphere dictionary.



(e) BP result using the reduced cylinder dictionary.



(f) BP result using the reduced top-hat dictionary.

Figure D.3: BP results for each of the reduced shape dictionaries used in the feature extraction problem in scenario 3, example 2 on the final iteration.

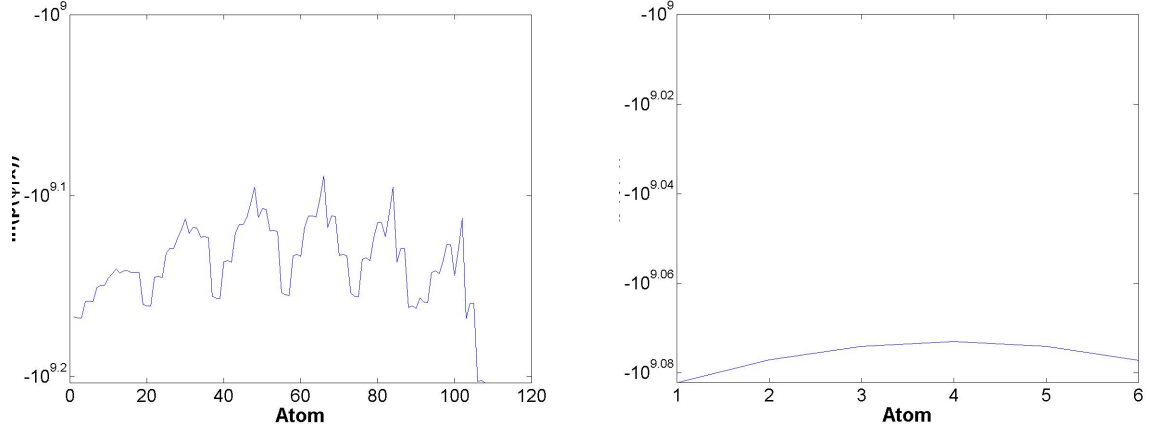
The maximum coefficients along with the calculated norms for each iteration are shown in Table D.3.

Table D.3: Maximum coefficients from each shape dictionary along with the ℓ_1 norm (sparsity descriptor) for scenario 3, example 2.

Shape	Iteration	$\max(\psi)$	$\ \psi\ _1$	$(\max(\psi) - \lambda \cdot \ \psi\ _1)$
plate	1	0.4364	0.5858	0.3193
	2	0.4364	0.5858	0.3193
	3	0.4364	0.5858	0.3193
dihedral	1	0.8154	0.9200	0.6314
	2	0.0082	0.9200	-0.1758
	3	0.0040	0.9200	-0.1800
sphere	1	0.4254	24.3958	-4.4538
	2	0.4254	24.3958	-4.4538
	3	0.4254	24.3958	-4.4538
top-hat	1	1.7119	6.2231	0.4672
	2	1.7111	6.2231	0.4665
	3	0.0078	6.2231	-1.2368
trihedral	1	2.9×10^{-4}	0.0255	-0.0048
	2	2.9×10^{-4}	0.0255	-0.0048
	3	2.9×10^{-4}	0.0255	-0.0048
cylinder	1	0.6091	9.7637	-1.3437
	2	0.6091	9.7637	-1.3437
	3	0.6091	9.7637	-1.3437

The sparsest solution pertaining to the largest coefficient for each iteration corresponds to a single shape. The shapes returned for each iteration respectively are dihedral, top-hat, and trihedral which correctly correspond to the shapes within the target scene. The molecules corresponding to each coefficient maximum are selected for parameter estimation.

Estimates of the posterior log-likelihoods are calculated for each atom within each of the dihedral and top-hat molecules. The BP results are used for determining the sphere parameters, since the dictionary was reduced prior to implementing the molecule method. The estimates for the dihedral and top-hat molecules are plotted and provided in Figure D.4. The largest log-likelihoods, along with the BP results for



(a) Posterior log-likelihood estimates associated with each atom within the selected dihedral molecule.

(b) Posterior log-likelihood estimates associated with each atom within the selected top-hat molecule.

Figure D.4: Posterior log-likelihood estimates for each shape and iteration for scenario 3, example 2.

the sphere, correspond to the correct atoms as shown by the associated parameters provided in Table D.4.

Table D.4: Extracted parameter sets for each shape compared to truth for scenario 3, example 2.

Shape	X	Y	Z	H	L	r	$\tilde{\gamma}$	$\tilde{\theta}$	$\tilde{\phi}$
True dihedral	0	10	0	2	2	-	0	0	0
Estimated dihedral	0	10	0	2	2	-	0	0	0
True trihedral	5	-5	0	1	-	-	0	0	0
Estimated trihedral	5	-5	0	1	-	-	0	0	0
True top-hat	0	0	5	2	-	1	0	0	0
Estimated top-hat	0	0	5	2	-	1	0	0	0

The algorithm successfully extracted the correct features and parameters.

D.2 Sphere, Top-hat, and Cylinder Target Scene

This section will discuss the extraction and classification results for a target scene containing multiple targets that include a sphere, top-hat and a cylinder. Each of the targets directly corresponds to a dictionary atom. The parameters selected for each shape in this example are given in Table D.5. The measured data is simulated

Table D.5: The parameters used to create scene 3, example 3.

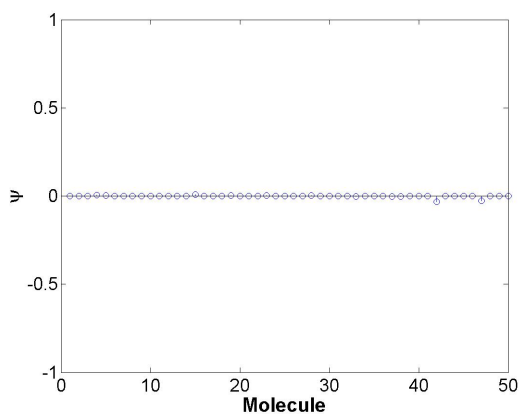
Shape	X	Y	Z	H	L	r	$\tilde{\gamma}$	$\tilde{\theta}$	$\tilde{\phi}$
sphere	5	0	0	-	-	2	0	0	0
top-hat	-5	5	0	1	-	3	0	0	0
cylinder	0	-5	0	-	3	0.5	0	0	0

with an SNR of 30 dB. Each of the shapes correspond to atoms within their respective shape dictionaries. This correspondence is provided in Table D.6.

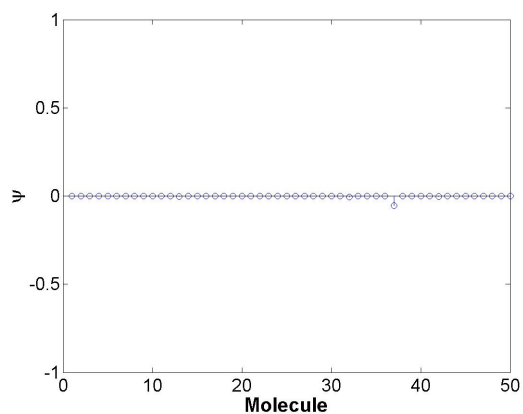
Table D.6: The correspondence mapping for the measured data and dictionary atoms for scenario 3, example 3.

Shape	Orig. Dict. Atom	Molecule	Molecule Atom
sphere	439	-	-
top-hat	3942	692	2
cylinder	683	28	11

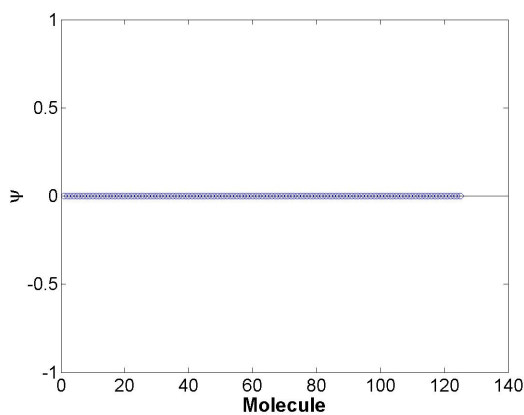
The iterative PH subtraction process leads to multiple iterations of the BP algorithm when extracting multiple shapes from a target scene. A single shape corresponding to the largest contribution of energy is extracted from each iteration. The BP results for each shape and iteration are provided in Figures D.5-D.7.



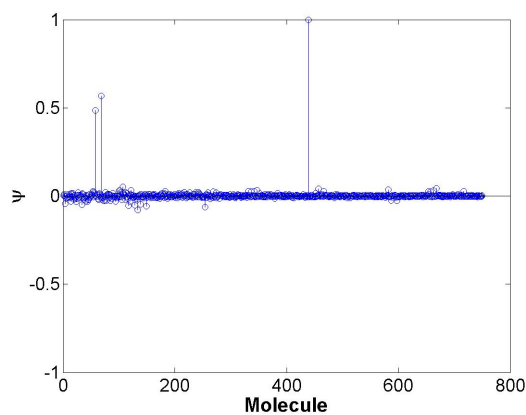
(a) BP result using the reduced plate dictionary.



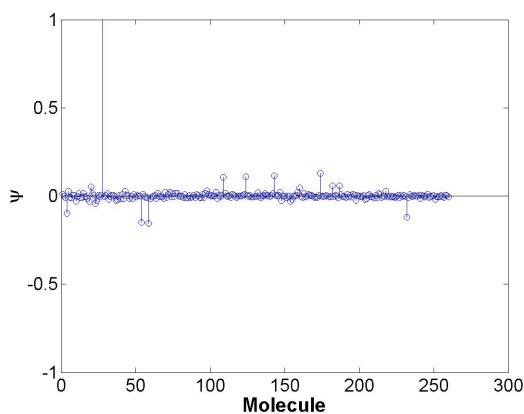
(b) BP result using the reduced dihedral dictionary.



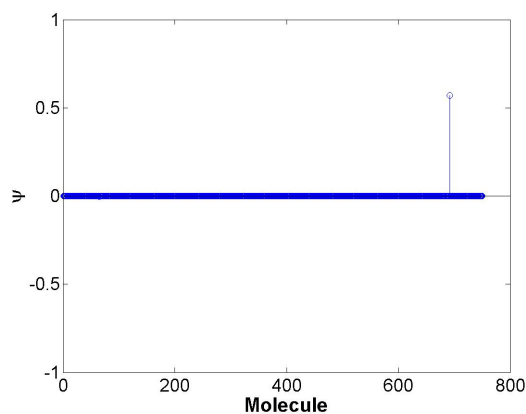
(c) BP result using the reduced trihedral dictionary.



(d) BP result using the reduced sphere dictionary.

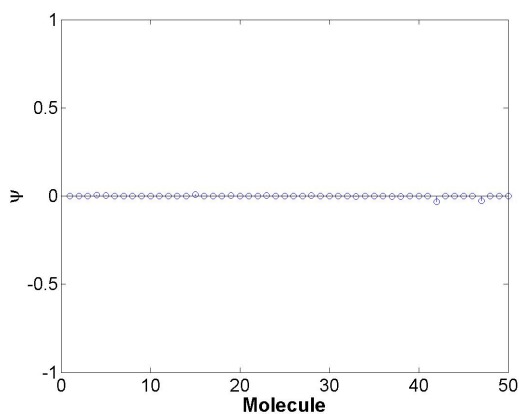


(e) BP result using the reduced cylinder dictionary.

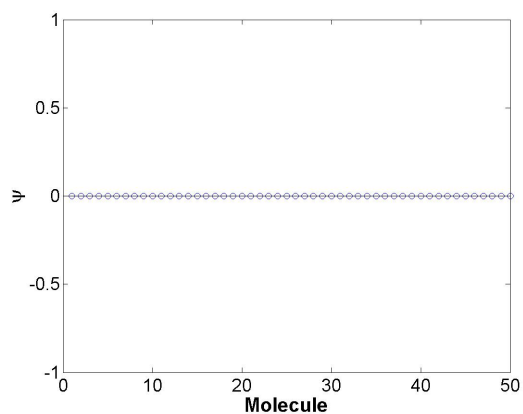


(f) BP result using the reduced top-hat dictionary.

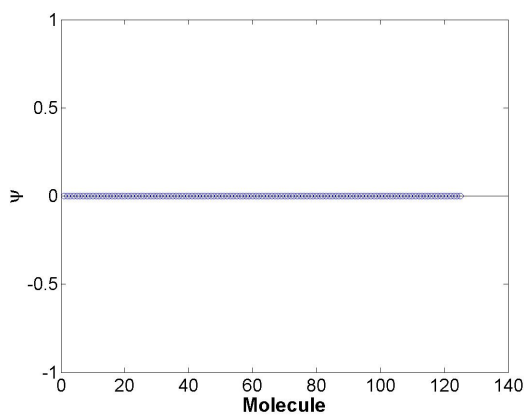
Figure D.5: BP results for each of the reduced shape dictionaries used in the feature extraction problem in scenario 3, example 3 on the first iteration.



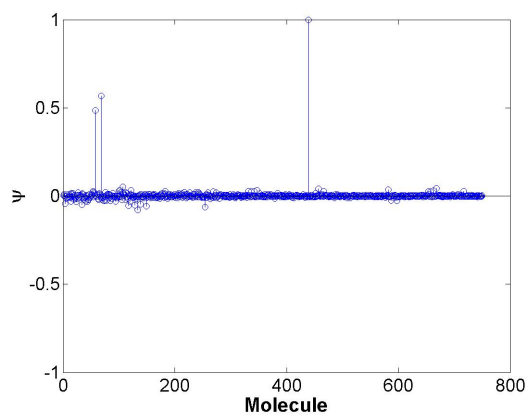
(a) BP result using the reduced plate dictionary.



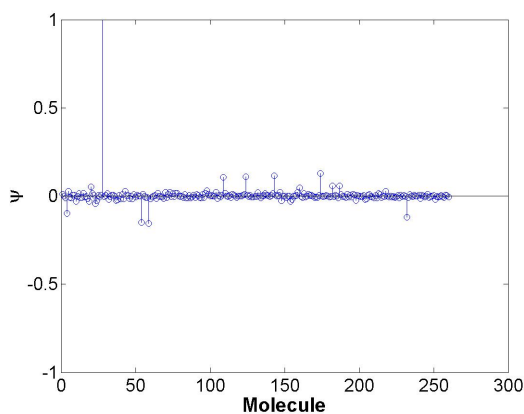
(b) BP result using the reduced dihedral dictionary.



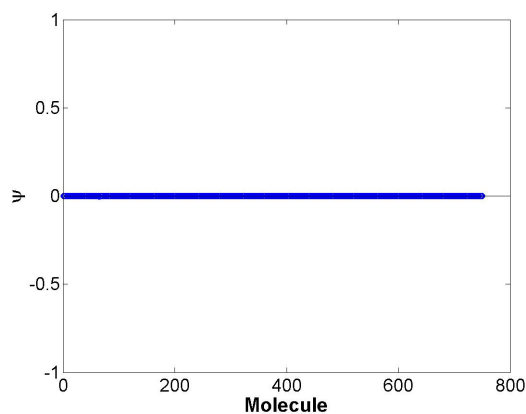
(c) BP result using the reduced trihedral dictionary.



(d) BP result using the reduced sphere dictionary.

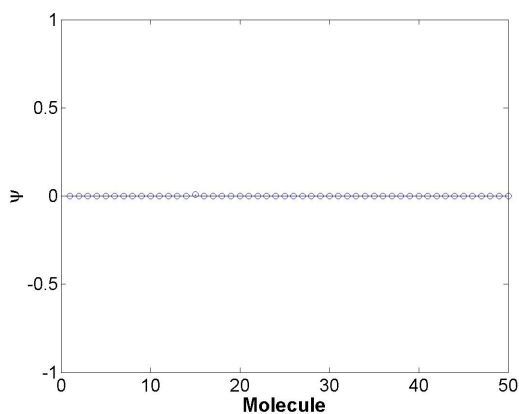


(e) BP result using the reduced cylinder dictionary.

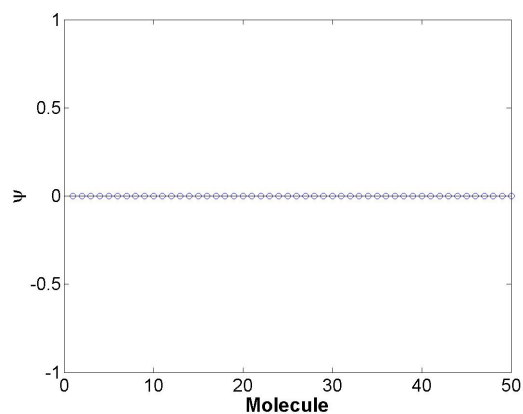


(f) BP result using the reduced top-hat dictionary.

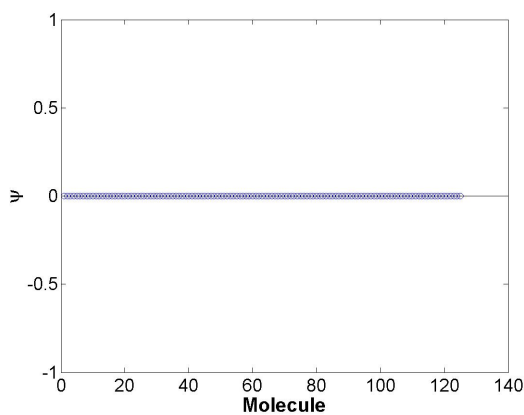
Figure D.6: BP results for each of the reduced shape dictionaries used in the feature extraction problem in scenario 3, example 3 on the second iteration.



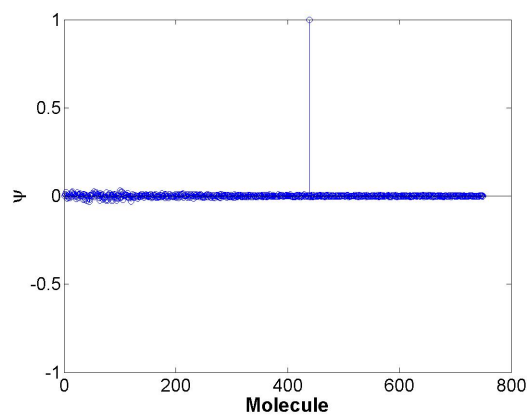
(a) BP result using the reduced plate dictionary.



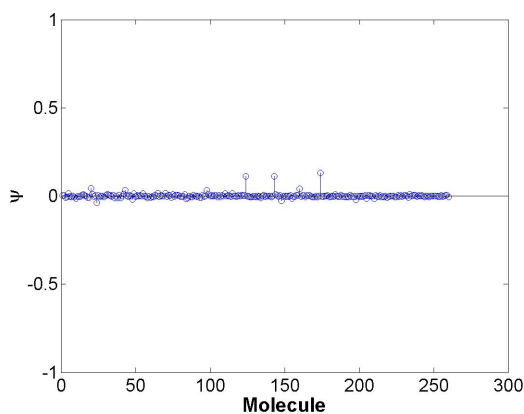
(b) BP result using the reduced dihedral dictionary.



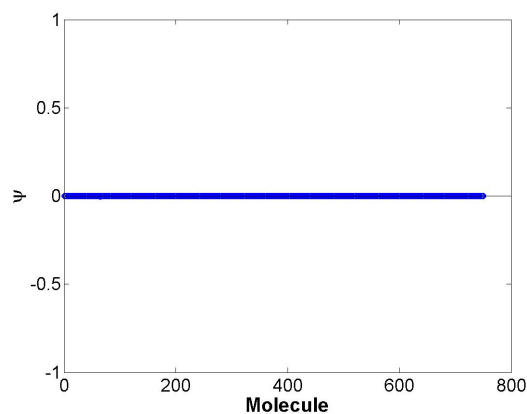
(c) BP result using the reduced trihedral dictionary.



(d) BP result using the reduced sphere dictionary.



(e) BP result using the reduced cylinder dictionary.



(f) BP result using the reduced top-hat dictionary.

Figure D.7: BP results for each of the reduced shape dictionaries used in the feature extraction problem in scenario 3, example 3 on the final iteration.

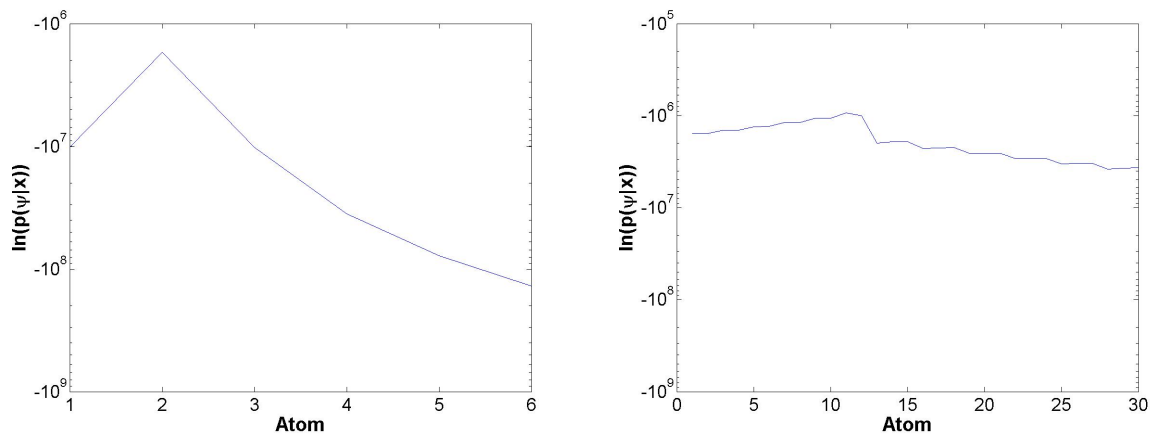
The maximum coefficients along with the calculated norms for each iteration are shown in Table D.7.

Table D.7: Maximum coefficients from each shape dictionary along with the ℓ_1 norm (sparsity descriptor) for scenario 3, example 3.

Shape	Iteration	$\max(\psi)$	$\ \psi\ _1$	$(\max(\psi) - \lambda \cdot \ \psi\ _1)$
plate	1	0.4364	0.5858	0.3193
	2	0.4364	0.5858	0.3193
	3	0.4364	0.5858	0.3193
dihedral	1	0.8154	0.9200	0.6314
	2	0.0082	0.9200	-0.1758
	3	0.0040	0.9200	-0.1800
sphere	1	0.4254	24.3958	-4.4538
	2	0.4254	24.3958	-4.4538
	3	0.4254	24.3958	-4.4538
top-hat	1	1.7119	6.2231	0.4672
	2	1.7111	6.2231	0.4665
	3	0.0078	6.2231	-1.2368
trihedral	1	2.9×10^{-4}	0.0255	-0.0048
	2	2.9×10^{-4}	0.0255	-0.0048
	3	2.9×10^{-4}	0.0255	-0.0048
cylinder	1	0.6091	9.7637	-1.3437
	2	0.6091	9.7637	-1.3437
	3	0.6091	9.7637	-1.3437

The sparsest solution pertaining to the largest coefficient for each iteration corresponds to a single shape. The shapes returned for each iteration respectively are top-hat, cylinder, and sphere which correctly correspond to the shapes within the target scene. The molecules corresponding to each coefficient maximum are selected for parameter estimation.

Estimates of the posterior log-likelihoods are calculated for each atom within the top-hat and cylinder molecules. As in example 2, the BP results are used for determining the sphere parameters. The estimates for the top-hat and cylinder molecules are plotted and provided in Figure D.4. The largest log-likelihoods, along with the BP results for the sphere, correspond to the correct atoms as shown by the associated parameters provided in Table D.8.



(a) Posterior log-likelihood estimates associated with each atom within the selected top-hat molecule.

(b) Posterior log-likelihood estimates associated with each atom within the selected cylinder molecule.

Figure D.8: Posterior log-likelihood estimates for each shape and iteration for scenario 3, example 3.

Table D.8: Extracted parameter sets for each shape compared to truth for scenario 3, example 3.

Shape	X	Y	Z	H	L	r	$\tilde{\gamma}$	$\tilde{\theta}$	$\tilde{\phi}$
True sphere	5	0	0	-	-	2	0	0	0
Estimated sphere	5	0	0	-	-	2	0	0	0
True top-hat	-5	5	0	1	-	3	0	0	0
Estimated top-hat	-5	5	0	1	-	3	0	0	0
True cylinder	0	-5	0	-	3	0.5	0	0	0
Estimated cylinder	0	-5	0	-	3	0.5	0	0	0

The algorithm successfully extracted the correct features and parameters.

Bibliography

1. J.A. Jackson, *Three-Dimensional Feature Models for Synthetic Aperture Radar and Experiments in Feature Extraction*, Ph.D. Dissertation, The Ohio State University, 2009.
2. H. Chiang, R.L. Moses, and L.C. Potter, “Model-based classification of radar images,” *IEEE Transactions of Information Theory*, vol. 46, pp. 1842–1854, 2000.
3. B. Krishnapuram, J. Sichina, and L. Carin, “Physics-based detection of targets in SAR imagery using support vector machines,” *IEEE Sensors Journal*, vol. 3, no. 2, pp. 147 – 157, Apr. 2003.
4. M.R. McClure and L. Carin, “Matching pursuits with a wave-based dictionary,” *IEEE Transactions on Signal Processing*, vol. 45, no. 12, pp. 2912 –2927, Dec. 1997.
5. P.K. Bharadwaj, P.R. Runkle, and L. Carin, “Target identification with wave-based matched pursuits and hidden markov models,” *IEEE Transactions on Antennas and Propagation*, vol. 47, no. 10, pp. 1543 –1554, Oct. 1999.
6. C.D. Austin, J.N. Ash, and R.L. Moses, “Parameter estimation using sparse reconstruction with dynamic dictionaries,” in *Proc. IEEE Int. Conf. on Acoustics, Speech, and Signal Processing (ICASSP)*, Prague, Czech Republic, May 22 – 27 2011.
7. P. Jost, P. Vandergheynst, and P. Frossard, “Tree-based pursuit: Algorithm and properties,” *IEEE Transactions on Signal Processing*, vol. 54, no. 12, pp. 4685–4697, Dec. 2006.
8. S.S. Chen, D.L. Donoho, and M.A. Saunders, “Atomic decomposition by basis pursuit,” *SIAM REVIEW*, vol. 43, pp. 129–159, 2001.
9. J.A. Tropp, “Greed is good: algorithmic results for sparse approximation,” *IEEE Transactions on Information Theory*, vol. 50, no. 10, pp. 2231 – 2242, Oct. 2004.
10. J.A. Jackson, B.D. Rigling, and R.L. Moses, “Canonical scattering feature models for 3D and bistatic SAR,” *IEEE Transactions on Aerospace and Electronic Systems*, vol. 46, no. 2, pp. 525–541, Apr. 2010.
11. E. van den Berg and M.P. Friedlander, “Probing the pareto frontier for basis pursuit solutions,” 2008.
12. S.M. Kay, *Fundamentals of Statistical Signal Processing: Estimation Theory*, vol. I of *signal processing*, Prentice Hall PTR, 1993.
13. H.L. Van Trees, *Detection, Estimation, and Modulation Theory: Part 1*, Wiley-Interscience, 2001.
14. D.G.T. Denison, C.C. Holmes, B.K. Mallick, and A.F.M. Smith, *Bayesian Method for Nonlinear Classification and Regression*, John Wiley and Sons, LTD, 2002.

15. E. Candes, J. Romberg, and T. Tao, “Stable signal recovery from incomplete and inaccurate measurements,” *Comm. Pure Appl. Math.*, vol. 59, no. 8, pp. 1207–1223, 2006.
16. D.L. Donoho and M. Elad, “Optimally sparse representation in general (nonorthogonal) dictionaries via ℓ_1 minimization,” in *Proceedings of the National Academy of Sciences*. March 2003, pp. 2197–2202, printed online before print at www.pnas.org/cgi/doi/10.1073/pnas.0437847100.
17. Y. Tsaig and D.L. Donoho, “Compressed sensing,” *IEEE Trans. Inform. Theory*, vol. 52, pp. 1289–1306, 2006.
18. S. Ji and L. Carin, “Bayesian compressive sensing and projection optimization,” in *Proceedings of the 24th International Conference on Machine Learning*, New York, NY, USA, 2007, ICML ’07, pp. 377–384, ACM.

REPORT DOCUMENTATION PAGE					<i>Form Approved</i> OMB No. 0704-0188	
The public reporting burden for this collection of information is estimated to average 1 hour per response, including the time for reviewing instructions, searching existing data sources, gathering and maintaining the data needed, and completing and reviewing the collection of information. Send comments regarding this burden estimate or any other aspect of this collection of information, including suggestions for reducing this burden to Department of Defense, Washington Headquarters Services, Directorate for Information Operations and Reports (0704-0188), 1215 Jefferson Davis Highway, Suite 1204, Arlington, VA 22202-4302. Respondents should be aware that notwithstanding any other provision of law, no person shall be subject to any penalty for failing to comply with a collection of information if it does not display a currently valid OMB control number. PLEASE DO NOT RETURN YOUR FORM TO THE ABOVE ADDRESS.						
1. REPORT DATE (DD-MM-YYYY) 22-03-2012		2. REPORT TYPE Master's Thesis			3. DATES COVERED (From — To) Aug 2010 — Mar 2012	
4. TITLE AND SUBTITLE Target Classification of Canonical Scatterers Using Classical Estimation and Dictionary Based Techniques				5a. CONTRACT NUMBER		
				5b. GRANT NUMBER		
				5c. PROGRAM ELEMENT NUMBER		
6. AUTHOR(S) G. Barry Hammond II, Capt, USAF				5d. PROJECT NUMBER		
				5e. TASK NUMBER		
				5f. WORK UNIT NUMBER		
7. PERFORMING ORGANIZATION NAME(S) AND ADDRESS(ES) Air Force Institute of Technology Graduate School of Engineering and Management (AFIT/EN) 2950 Hobson Way WPAFB OH 45433-7765					8. PERFORMING ORGANIZATION REPORT NUMBER AFIT/GE/ENG/12-19	
9. SPONSORING / MONITORING AGENCY NAME(S) AND ADDRESS(ES) Intentionally left blank					10. SPONSOR/MONITOR'S ACRONYM(S)	
					11. SPONSOR/MONITOR'S REPORT NUMBER(S)	
12. DISTRIBUTION / AVAILABILITY STATEMENT APPROVED FOR PUBLIC RELEASE; DISTRIBUTION UNLIMITED.						
13. SUPPLEMENTARY NOTES This material is declared a work of the U.S. Government and is not subject to copyright protection in the United States.						
14. ABSTRACT This research effort will utilize a hierarchical dictionary-based approach for canonical shape classification within measured synthetic aperture radar (SAR) phase history data. This primary goal of this research is to develop an efficient framework for dictionary based SAR feature extraction using modified 3-D radar scattering models. Previous work in this area relies on maximum likelihood (ML) estimation and similar approaches to extract shapes using 2-D signal models. We include characterizations of shape model redundancies caused by similar shape scattering responses. Simulated SAR collection methods, including frequency, elevation aspect, and polarization diversities, are modeled to show reductions in inter-atom correlation. A "molecule" method is used to combine highly correlated atoms to support a basis pursuit (BP) method of feature identification. Finally, a Bayesian approach is used to determine a maximum <i>a posteriori</i> (MAP) estimate for each atom, leading to feature classification and parameter identification.						
15. SUBJECT TERMS Feature Extraction, Synthetic Aperture Radar, Automatic Target Recognition						
16. SECURITY CLASSIFICATION OF:			17. LIMITATION OF ABSTRACT	18. NUMBER OF PAGES	19a. NAME OF RESPONSIBLE PERSON	
a. REPORT	b. ABSTRACT	c. THIS PAGE			Julie A. Jackson, PhD (ENG)	
U	U	U	UU	221	19b. TELEPHONE NUMBER (include area code) (937) 255-3636 x4678; julie.jackson@afit.edu	